DEVOLATILIZATION OF COAL BY RAPID HEATING

M. Mentser, H. J. O'Donnell, S. Ergun and R. A. Friedel

Pittsburgh Energy Research Center, Bureau of Mines
U. S. Department of the Interior
4800 Forbes Avenue, Pittsburgh, Pennsylvania 15213

INTRODUCTION

Coal has been used mainly for the generation of electric power to the present time. Now that critical shortages exist in the supply of natural gas for residential heating and industrial usage, a broad effort is being made by industry and government to develop processes for gasifying coal.[1-2] When these processes are fully developed, they will represent a second major source of coal utilization.

In both combustion and gasification, coal is heated to elevated temperatures, and therefore it inevitably sustains some degree of decomposition prior to or concurrently with other chemical reactions. In the Bureau of Mines' Synthane process,[3-4] for example, pretreated coal enters the upper, carbonizing section of the gasifier where it undergoes extensive thermal degradation to form char. The reaction products formed at this stage in the process make an important contribution to the overall performance of the gasifier.

For these reasons, research on the devolatilization of coal by rapid heating has been a part of the Bureau's program on gasification. The results presented in this paper represent a continuation of preliminary work that was reported earlier.[5]

EXPERIMENTAL

Single pulses of electrical current provide high-speed heating that is needed to measure the thermophysical properties of solids at elevated temperatures,[6] and of metals in particular.[7-8] This technique, termed pulse heating, was adopted for devolatilizing coal in the present study. Coal samples were decomposed in vacuo in order to collect and identify the gaseous products. Quantitative measurements of the resultant weight loss of sample after rapid heating, served as a measure of the total volatiles evolved from the coal.

The reaction vessel was essentially a 29/42 tapered ground glass joint sealed on to a pumping system. Suitable vacuum gages, manometers, gas sampling and storage bulbs were attached to the reactor. Total volume of the reactor, including the sampling bulb, amounted to 418 $cm.^3$ Number 10 copper wires entered the reactor through Kovar-pyrex seals. These copper electrodes terminated in spring clamps which supported the heating element containing the coal sample. Resistive heating elements were made in the form of long, thin cylinders by wrapping 400 mesh stainless steel screen on a mandril. Dimensions of the cylinders were 6 cm in length and 1.2 mm in diameter. In preparation for pulsing, the open ends of the cylinder were completely closed, and the flattened ends inserted into the jaws of the spring clamps.

Current was supplied to the wire screen heating elements by a current controller. This device was an electronic circuit designed to set the initial current flow at a desired value and to allow the current to increase in a predetermined way. Shaping of the current pulse was necessary to compensate for increase in electrical resistance

of the wire and also for radiant heat losses at high temperatures. Typical current values were in the range 15-20 A. The current controller was triggered by a preselected pulse coming from a General Radio unit pulse generator, and current flow continued only for the duration of the timing pulse. Pulse times extended from 65 to 155 msec. A 0.1 Ω resistor in the current controller converted the current pulse to a voltage pulse which was displayed on a storage-type oscilloscope. Precise values of current and time were measured from the oscilloscope trace.

Coal samples were prepared by cutting out vitrains from lumps of coal. Further upgrading of the vitrains was accomplished by microscopic examination in which coal particles with adhering mineral matter were discarded. Vitrains were chosen for study because they constitute the most abundant and homogeneous component of coal and because they are also low in mineral matter.[9/] It is seen from table 1 that the ash content was less than 2 percent in the Pittsburgh coal and less than 1 percent in the other coals used. A low mineral matter content in the vitrains was desired to avoid ambiguities in the data from possible pyrolysis of mineral matter. The vitrains were ground to a particle size range of 44-53 μm for use in the experiments.

Coals were selected to encompass a rather wide range of rank and volatile matter. Bituminous coals ranged in rank from hvCb to lvb; one subbituminous coal was also studied. Their proximate analyses are given in table 1.

Table 1.--Proximate analyses of vitrains.

Coal source	Rank	Proximate analysis, percent (mf)		
		Fixed carbon	Volatile matter	Ash
Pocahontas No. 3, W. Va.	lvb	82.4	16.8	0.8
Lower Kittanning, Pa.	mvb	73.8	25.3	0.9
Pittsburgh, Pa.	hvAb	63.1	35.1	1.8
Colchester Illinois No. 2, Ill.	hvCb	51.1	48.0	0.9
Rock Springs No. 7-1/2, Wyo.	Sub A	61.7	37.7	0.6

The temperature attained by the wire screen heating elements was related to the time of current flow by a calibration method. Trial and error determinations were made of the times required to melt pure metal powders of like particle size and amounts as the coal. A number of calibration points were thus established, and it was shown that the temperature at the end of the current pulse was proportional to the time of current flow in the region to 1450° C. The heating rate was therefore constant, and it was determined to be 8250° C/sec.

The experimental procedure for devolatilizing coal samples may now be described. A new (unheated) screen cylinder, containing no coal, was pulsed to 900° C in the reactor which had previously been evacuated. Pre-firing of the screen cylinders is essential because they undergo significant weight losses when they are heated for the first time. Such losses would interfere with measurements made on the coals. However, after the initial heating of a screen cylinder, its weight remains demonstrably constant in further tests. A prefired screen was weighed precisely on a Cahn RG microbalance; approximately 250 µg of coal were inserted into the cylinder, and the combined weight of the screen cylinder and coal sample was again determined precisely on the balance. The weighed coal sample and heating element were placed in the reactor and pumped until the system pressure was reduced to 10^{-3} torr. When this reduced pressure was attained, the coal sample was pulse heated to a given temperature. After devolatilization occurred, the coal residue and screen were removed from the reactor and reweighed.

The volume of gases generated during devolatilization was determined from the pressure increase in the reactor. Mass spectrometric analyses of the gases were made at many, but not all, of the different test conditions. In this way, the weight of the gases produced by rapid devolatilization of coal was ascertained.

RESULTS AND DISCUSSION

The devolatilization behavior of bituminous coals under rapid heating conditions is shown in figure 1. This figure presents the weight-loss curves of four bituminous coals of different rank over a temperature region from 400° to 1150° C. All of the weight-loss curves have a characteristic shape in common, although they differ in detail. For most of the coals the reaction threshold occurs at 400° C, followed by very rapid decomposition to 600° C. Production of volatile reaction products reaches a peak at relatively low temperatures of 700° to 900°, a finding that should be of considerable importance to those engaged in design of coal gasification equipment. At still higher temperatures the declining trend in the formation of volatiles reverses, and starts to increase again at the highest temperatures of this study.

Some discussion of the low temperature peak in volatile production from bituminous coals is merited because this phenomenon does not occur during slow heating. In the latter case the weight loss increases monotonically with temperature.[10] The broadest peak is exhibited by the Illinois hvCb coal which has the highest volatile matter content among the coals studied (see table 1). With regard to the higher rank bituminous coals, the peaks become progressively less intense with increase in rank, and the peak position shifts to higher temperatures. In all instances the volatile yield corresponding to the peak in the weight-loss curves was greater than the volatile matter in the coal determined by the ASTM standard method of analysis. These results are demonstrated by the data in table 2, which show that the yield of total volatiles may be increased as much as 36 percent by rapid heating. Supportive evidence for increased yields of volatiles is found in other rapid heating studies.[11-12]

Consideration of the cited studies in conjunction with our own leads to the conclusion that the ratio of total volatiles from rapid heating to ASTM volatile content depends not only on the rank of coal, as shown in table 2, but also on the magnitude of the heating rate. One suggested explanation for the appearance of maxima in the weight-loss curves is that of competitive reactions. For example, the bond-breaking reactions that occur in the coal structure and give rise to initial decomposition fragments may well have different temperature dependencies from those of recombination reactions that may form molecules more stable than the parent coal.

Table 2.--Increased volatiles from rapid pyrolysis.

Coal source	Volatile matter content by ASTM analysis	Volatile matter content from peak weight loss	Increase factor
	%	%	
Pocahontas No. 3	16.8	18.5	1.10
Lower Kittanning	25.3	30.8	1.22
Pittsburgh	35.1	47.9	1.36
Colchester Ill. No. 2	48.0	55.8	1.16
Rock Springs No. 7-1/2	37.7	42.4 (plateau)	1.12

In contrast to the results obtained with bituminous coals, the weight-loss curve of subbituminous coal exhibited no peak; instead, it reached what might be called a plateau in figure 2. From 800° to 1000° C the volatile yield remained level at about 42 weight percent of the coal. Beyond this region the production of volatiles increased sharply. The fact that the devolatilization curve of subbituminous A coal differs distinctly from those of bituminous coals indicates a need for more work with other subbituminous coals and lignites. Low rank materials such as these are of interest in coal gasification because their reserves are abundant and because they are situated in deposits with shallow ground cover.

The gases arising from rapid pyrolysis of coal vitrains have been examined by mass spectrometric analysis. The major components in the gas are H_2, CH_4 and CO. Lesser amounts of CO_2 and the higher molecular weight hydrocarbons (up to C_6) are also present. Hydrocarbons are present as both saturates and unsaturates with the notable exception of acetylene. Traces of aromatics such as benzene, toluene and xylene are found as well as sulfur in the form of H_2S. The absence of acetylene, which has been found in appreciable quantity in some rapid heating processes[13-14], is most likely due to the lower temperatures and lower heating rate employed in our experiments.

Temperature profiles of the individual gases from pyrolysis of Pittsburgh vitrain are shown in figure 3. Here it is seen that the molar percentages of CO_2, CH_4 and the C_2-C_4 hydrocarbons decrease with increasing reaction temperature. The functional dependence of H_2 and CO on temperature is more complex. H_2 production starts at 31.5 mole percent at 700° C and increases to a maximum value of 67.0 percent at 990° C. Further increase in temperature causes a small but real decrease in its concentration. CO concentration changes in an opposite manner to H_2. A minimum CO value of 12.0 mole percent is achieved at about the same temperature at which the maximum H_2 concentration occurred. The gas composition data are given on a H_2O-O_2-N_2-free basis.

In addition to the gases produced by rapid devolatilization of coal, heavier products, referred to as tar, also form. This material condenses on the walls of the reactor and is visible as brown stain on the glass. Because the quantity of tar from a single experiment is so small, it has not been measured nor has it been chemically analyzed. However, the quantity of tar can be obtained indirectly by subtracting the weight of the gases from the total volatiles, i.e. the weight loss of the coal. Results of such calculations for Pittsburgh vitrain are shown in figure 4 in which the experimentally determined curves for "total volatiles" and for "gas" have first been drawn. The curve for "tar" is of course determined by the difference calculation. The curves show that tar formation is favored by low decomposition temperatures and that tar is in fact the main product at all temperatures up to 1000° C. Above 1000° the amount of gas exceeds the amount of tar even though the total volatile yield is still below the peak yield obtained at 700° C. Further correlations of product yields with rank and temperature parameters have been made and will be published later.

REFERENCES

1. Forney, A. J. and W. P. Haynes. The Am. Soc. Mech. Engrs., Paper No. 72-WA/APC-3, New York, N. Y., Nov. 26-30, 1972.

2. Henry, J. P. and B. M. Louks. Chem. Tech., 1, 238, (1971).

3. Forney, A. J., S. J. Gasior, W. P. Haynes, and S. Kattel. BuMines Tech. Prog. Report 24, 1970, 6 pp.

4. Forney, A. J., W. P. Haynes, J. J. Elliott and R. F. Kenny. BuMines Tech. Prog. Rept. 48, 1972, 6 pp.

5. Mentser, M., H. J. O'Donnell and S. Ergun. Am. Chem. Soc., Div. of Fuel Chem. Preprints 14, No. 5, 94, Sept. 1970.

6. Finch, R. A. and R. E. Taylor. Rev. Sci. Instr., 40, 1195 (1969).

7. Cezairliyan, A., M. S. Morse, H. A. Berman and C. W. Beckett. J. Res. Nat. Bur. Stds.-A. Phys. and Chem., 74A, No. 1, 65 (1970).

8. Cezairliyan, A., J. Res. Nat. Bur. Stds. - C. Eng. and Instr., 75C, No. 1, 7, (1971).

9. Parks, B. C. and H. J. O'Donnell. BuMines Bulletin 550, 1956, p. 25.

10. Van Krevelen, D. W., "Coal", Elsevier Publ. Co., Amsterdam, 1961, p. 266.

11. Kimber, G. M. and M. D. Gray. Combustion and Flame, 11, 360 (1967).

12. Field, M. A., D. W. Gill, B. B. Morgan and P. G. W. Hawksley. BCURA Mon. Bull., 31, 193 (1967).

13. Karn, F. S., R. A. Friedel and A. G. Sharkey, Jr. Fuel 48, No. 3, 297 (1969).

14. Fu, Y. C. and B. D. Blaustein. I and EC Process Design and Development, 8, 257 (1969).

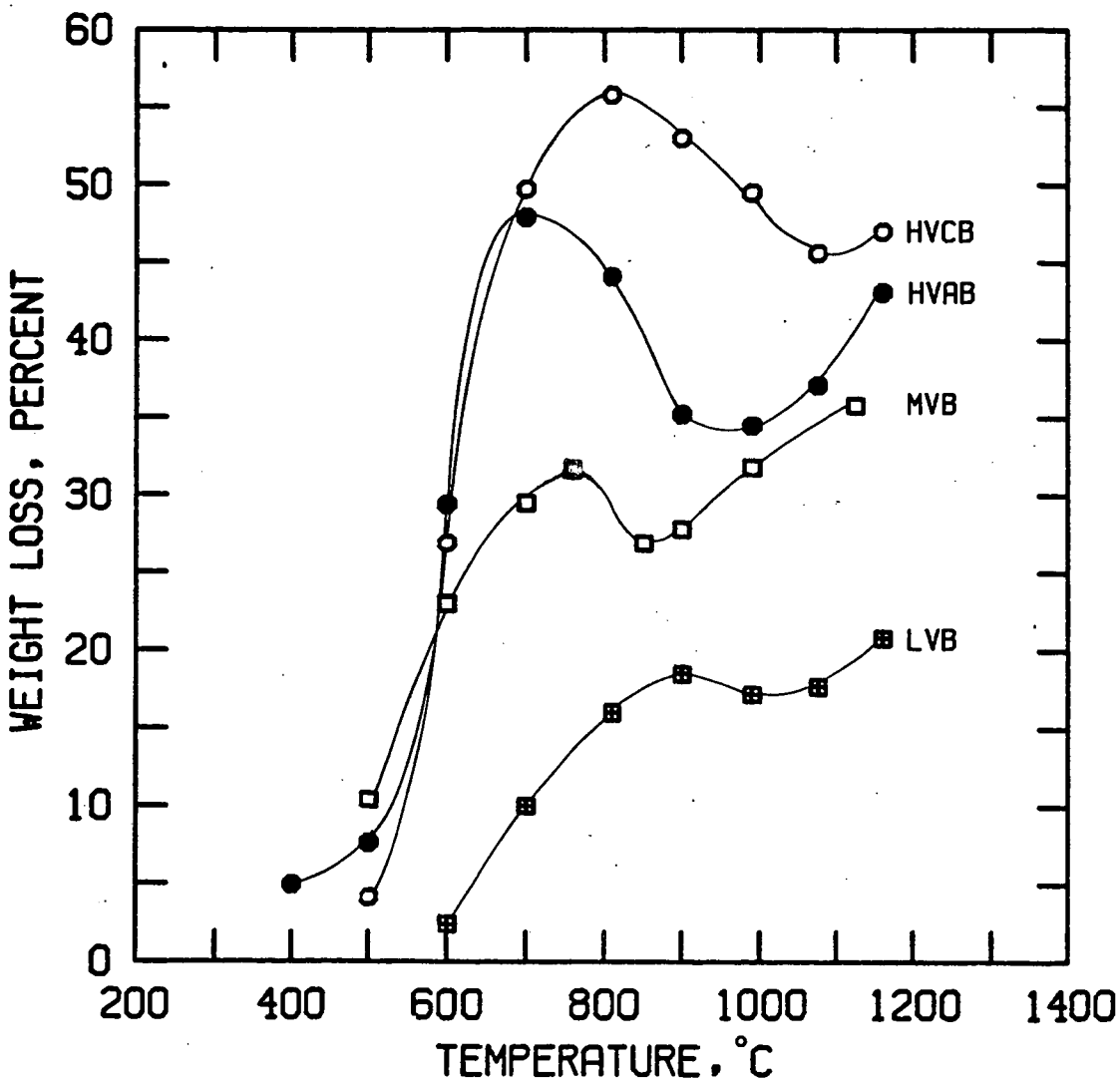

Figure 1.--Devolatilization of bituminous coals by rapid heating.

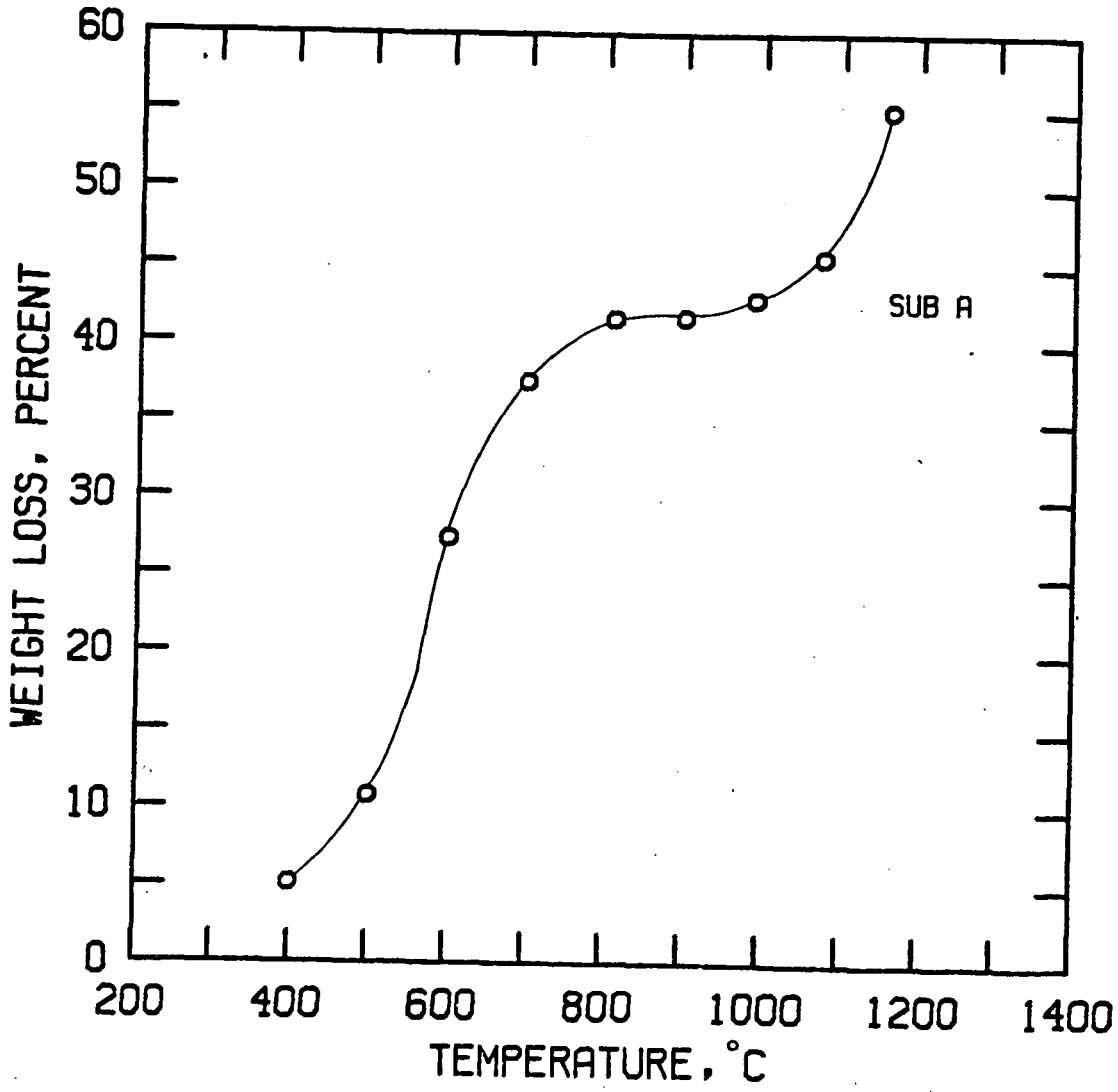

Figure 2.--Devolatilization of a subbituminous coal by rapid heating.

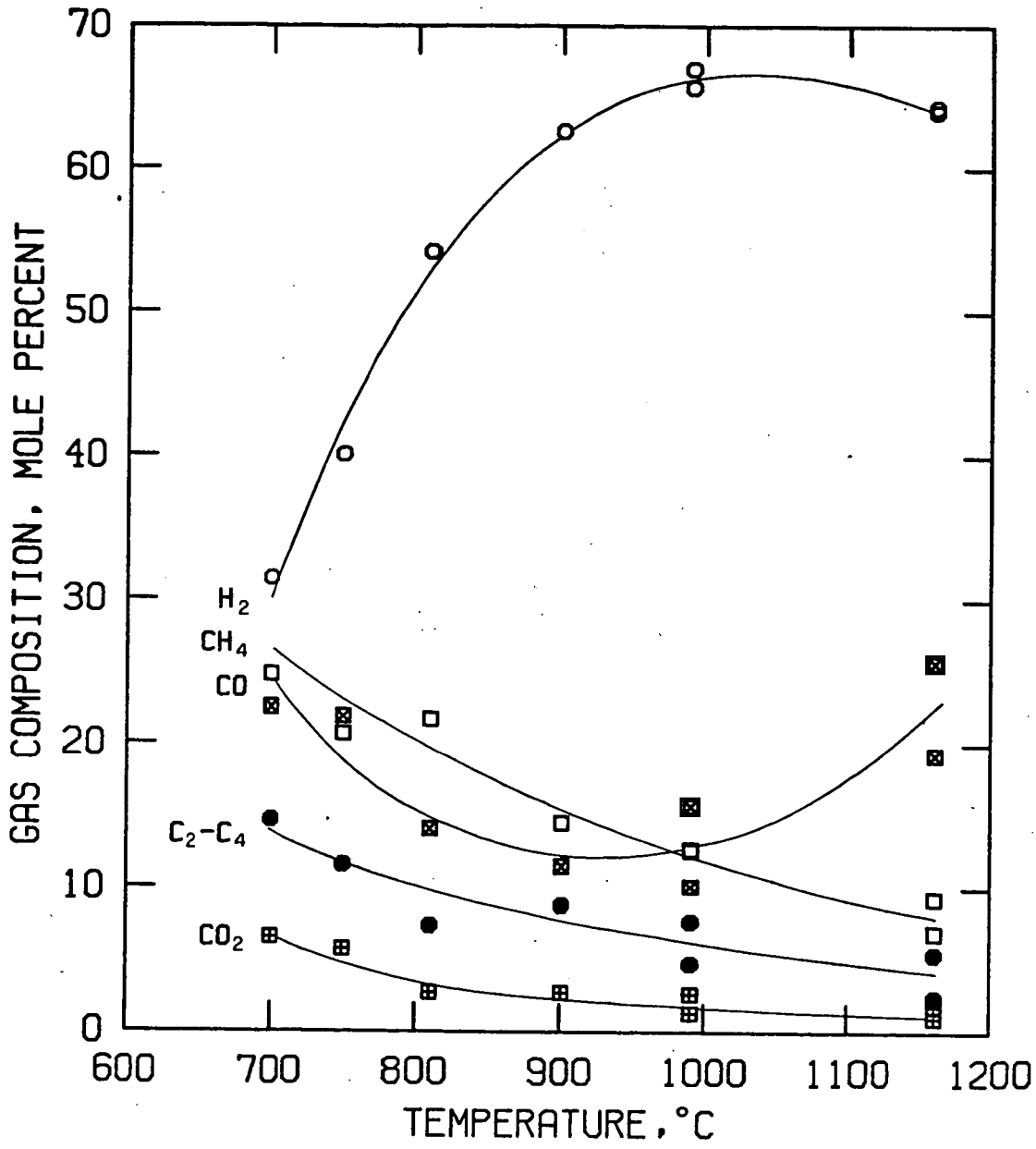

Figure 3.--Composition of gas from devolatilization of Pittsburgh hvAb coal.

COMP 2

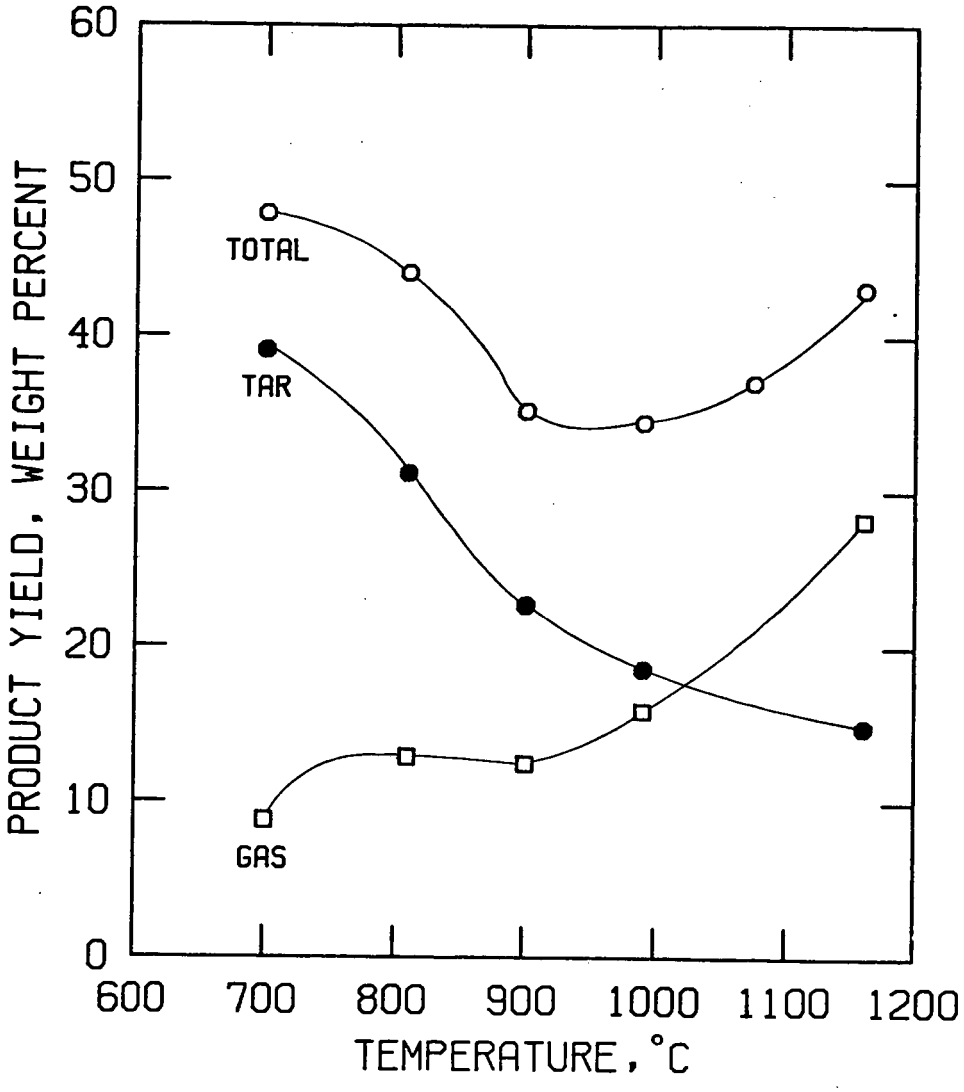

Figure 4.--Yields of tar and gas from devolatilization of Pittsburgh hvAb coal.

YIELD 4

PRODUCTION OF LOW BTU GAS INVOLVING COAL PYROLYSIS AND GASIFICATION

C. Y. Wen, R. C. Bailie, C. Y. Lin and W. S. O'Brien

Chemical Engineering Department
West Virginia University
Morgantown, West Virginia 26506

INTRODUCTION

Coal burning is a "dirty" process, with the major pollution culprits now considered as being solid flyash particulates and sulfur dioxide. More than likely, nitrogen oxides and other undesirables will come under attack after the SO_2 and flyash problems have been satisfactorally controlled. (Jimeson, 1972) Because coal is currently the most plentiful source of energy, the combined efforts of industries and governmental agencies are urgently needed to develop economical, efficient and acceptable methods to convert coal into clean electrical power.

In this paper, we are presenting a scheme to pyrolize caking coal in a fluidized bed, some experimental data, a pyrolysis-gasification reaction model and a conceptual flowscheme for a process to convert coal into electricity via the production of low-Btu gas. Although the experimental data presented here are not comprehensive, we hope to explore some of the alternatives involved in such a manner as to recognize the most efficient ways to maximize the coal-utilization efficiency.

EXPERIMENTAL

Equipment

An experimental 15-inch diameter fluidized bed was used at West Virginia University for the study of the pyrolysis of coal and other carbonaceous compounds. The schematic of the pilot-plant fluidized bed reactor and its auxiliary equipment is shown in Figure 1.

There are three sections to the fluidized bed reactor. The hot bottom is a mixing and gas combustion chamber where the fluidizing gases are preheated by burning natural gas (over 90% methane) inside the L-shaped chamber. The fluidizing gases are composed of specific ratios of the combustion products of the natural gas and additional air.

Between the gas combustion chamber bottom and the reactor bed section is the high-temperature grid plate. This gas distribution plate is 1/4 inch thick, 18 inches in diameter and made of Type 310 stainless steel. There are 584 holes in a square pattern located on 1/4 inch centers. Each hole is 0.0960 inches in diameter.

In the middle of the reactor is the fluidized bed. This reactor section has a 28-inch outside diameter and a 15-inch inside diameter. The insulation lining is 4 1/2 inches of Type 1620-K fire brick (Babcock and Wilcox Company, Augusta, Georgia) and 2 inches of "Plicast Tuff-Mix" castable refractory (Plibrico Company, Chicago, Illinois). The height of this section is eight feet. Above the fluidized bed section, the reactor diameter expands to a 35-inch outside diameter and a 22-inch inside diameter. This particle disengaging chamber is four feet high and is lined in the same manner as in the fluidized bed section.

After leaving the reactor, the effluent gases are cooled and then cleaned by passage through either a canister-type nylon-bag filter or a dry-gas cyclone (10 inches diameter and 22 inches in length). Before being finally exhausted to the building exterior, the effluent gases are scrubbed in a series of two wet scrubbers, the first being a tray-type and the second scrubber being packed with one-inch "Intalox Saddles" (U. S. Stoneware, Akron, Ohio).

The solids are fed into the fluidized bed by means of a screw conveyor having a specially designed feeder valve. The feed location is five inches above the gas distribution plate through a 6-inch flanged port in the wall of the reactor. The 2 1/2 inch screw is constructed of carbon steel with a Type 310 stainless steel coating on the wearing surfaces. The construction details of this feeder and the auxiliary solid feed hopper system have been described by Burton and Bailie (1973). The feeding unit has performed successfully in feeding 15 to 60 pounds of solids per hour smoothly into the fluidized bed.

The gases leaving the fluid-bed reactor are sampled every five minutes and analyzed by a Bendix "Chroma-Matic" Model 618 Process Gas Chromatograph (Process Instruments Division, The Bendix Corporation, Ronceverte, West Virginia). This unit quantitatively analyzes the gas for H_2, CO_2, CO, CH_4 and O_2/Argon. The O_2/Argon value is the additive sum of the oxygen and the argon compositions, since the gas chromatograph peaks of both components are identical when using a molecular sieve column. Periodically, grab-samples of the effluent gases were withdrawn and analyzed on a Beckman GC-2A Gas Chromatograph and a Fisher Scientific Company Gas Chromatograph for the gas components listed above, plus acetylene, ethylene, ethane and nitrogen.

Operating Procedure

The reactor is filled with 0.025 inch diameter sand to a collapsed bed height of 30 inches. The gas velocity through the bed is maintained at a level where a good fluidization of the sand is assured, and then the bed is heated up to the pre-selected temperature (1840°F) by the combustion of methane in the bottom section of the reactor. The operating conditions in the reactor are summarized in Table 1.

TABLE 1

OPERATING CONDITIONS FOR
FLUIDIZED BED PYROLYSIS REACTOR

OPERATING TEMPERATURE	1400 - 1900°F
OPERATING PRESSURE	0 - 10 psig
COLLAPSED BED HEIGHT	2.5 feet
EXPANDED BED HEIGHT	3.5 - 4 feet
AVERAGE PARTICLE SIZE OF SAND	0.025 inches
DENSITY OF SOLID SAND PARTICLE	100 pounds/cubic feet
SUPERFICIAL FLUIDIZING GAS VELOCITY	1.5 feet/second

After the bed reaches the desired temperature, the rate of air to the methane burner and the rate of inert gas flow are adjusted to give the oxygen level and gas flow rate specified in the experimental plan. The reactor system is then allowed to come to steady-state conditions as judged by a leveling of the effluent gas composition as read on the continuously operating process gas chromatograph and by constant bed temperatures.

The test begins by slowly introducing the solid feed into the bed via the screw feeder. The bed temperature immediately drops because of the sensible heat required to heat the solid to the reaction temperature plus the heat of pyrolysis. The solid feed rate is carefully adjusted so that the bed temperature does not drop below the desired 1400-1500°F range. The reaction system is then allowed to come to a new steady-state condition with a constant solids feed rate, and the feed rate of the solids is then determined by weight difference.

Experimental Data

The results of the coal and sawdust pyrolysis experiments are reported here. The composition of these two solid feed materials are listed in Table 2. Four tests were made with sawdust and one test using coal. In addition, several types of carbonaceous solids were pyrolyzed in the fluidized bed, including municipal solid waste, chicken and cow manure, rubber, plastic, and sewage sludge.

TABLE 2

COMPOSITION OF SOLID FEED MATERIAL

	SAWDUST	BITUMINOUS COAL
MOISTURE (Weight %, Wet Basis)	2.62	3.42
ULTIMATE ANALYSIS (Weight %, Dry Basis)		
CARBON	47.20	73.3
HYDROGEN	6.49	5.34
OXYGEN	45.34	10.23
SULFUR	-	2.80
NITROGEN	-	0.70
ASH	0.97	7.57
HEATING VALUE (Btu/Dry Pound)	8114	13,097
PARTICLE SIZE (Harmonic Mean Diameter) in microns	603	504

As described previously in this paper, in the course of the reaction test there were two periods of steady-state reactor operation, the first period just before the solid is introduced into the fluid bed, and the second period happening during the constant-rate solids feeding. In the case of all five tests, the reactor operation just prior to feeding the solids were identical, as listed in Table 3.

TABLE 3

OPERATING CONDITION VALUES
DURING PYROLYSIS EXPERIMENTS

INLET FLOW RATE OF AIR: 35.26 SCFM
INLET FLOW RATE OF NATURAL GAS: 3.40 SCFM
REACTOR TEMPERATURE PRIOR TO FEEDING SOLIDS: 1840°F
DRY COMPOSITION OF GAS EXITING REACTOR BEFORE SOLIDS FEED IS STARTED

H_2 - 0.1123%	CO_2 - 10.1674%
O_2/Argon - 1.1808%	CH_4 - 0.0726%

remainder is assumed to be N_2

STEADY-STATE CONDITIONS DURING SOLIDS PYROLYSIS

	COAL TEST	SAWDUST TESTS			
		A	B	C	D
Operating Time Under Steady-State Conditions (Minutes)	155	86	75	70	577
Reactor Temperature, °F	1430	1430	1460	1450	1500
Solids Feed Rate (Dry Pounds/Minute)	0.336	0.368	0.122	0.682	0.342

After the solids were fed into the reactor and after the system again reached steady-state conditions, the effluent gas was analyzed, with the resulting effluent gas composition values for each of the five experiments given in Table 4.

TABLE 4

PERCENT COMPOSITION OF EFFLUENT GAS (DRY)
DURING PYROLYSIS EXPERIMENTS

	COAL TEST A	SAWDUST TESTS B	C	D
MEASURED BY PROCESS GAS CHROMATOGRAPH				
H_2	4.954	4.577	2.498	6.030	5.208
CO_2	11.288	12.180	12.108	12.237	11.468
O_2/Argon	0.885	0.810	1.070	0.825	0.934
CH_4	1.790	2.235	0.318	3.305	1.850
CO	2.244	7.543	2.206	11.498	7.565
MEASURED BY RESEARCH GAS CHROMATOGRAPH				
C_2H_2	0.215	0.532	0.068	0.960	0.557
C_2H_4	NM	NM	NM	0.073	0.047
C_2H_6	0.113	0.113	0.035	0.159	0.055
N_2	73.451	73.451	80.783	66.745	73.527

NM - Not Measured

The composition values of CO_2, O_2/Argon, CO, CH_4 and H_2 were averaged from the analysis readings of the process gas chromatograph, and the composition values of C_2H_2, C_2H_4, C_2H_6 and N_2 were averaged from the analyses by the research gas chromatographs of several grab samples taken during the duration of the test.

Using these experimentally measured gas analysis values, a mass balance was computed about the reactor system using the nitrogen flow rate as the calculation base. The mass balances were quite good considering the 2-5% accuracy of the flow-measuring meters and analytical instruments. The gas produced from the coal or sawdust pyrolysis is considered to be the net gas flow rate value, after subtracting the volumetric flowrate of the effluent gases prior to feeding the solids from the flowrates of the gases leaving the reactor during the solids pyrolysis reaction. These computed "Pyrolysis Gas Production Values" for the five experimental runs are listed in Table 5.

TABLE 5

COMPUTED PYROLYSIS GAS
COMPOSITIONS AND PRODUCTION RATES

PYROLYSIS GAS COMPOSITION (Volume % dry)	COAL TEST	SAWDUST TESTS A	B	C	D
H_2	46.876	25.645	37.493	23.592	30.022
CO_2	11.685	14.965	24.256	14.075	11.105
CH_4	16.630	12.427	3.724	11.880	10.483
CO	21.722	43.264	33.824	45.714	44.513
C_2H_2	2.081	3.050	1.043	3.817	3.277
C_2H_4	NM	NM	NM	0.290	0.277
C_2H_6	1.007	0.648	0.537	0.632	0.324
PRODUCTION RATE (SCF/Pound Dry feed)	10.92	18.25	18.20	15.95	18.62
GAS HEATING VALUE (Btu/SCF)	435	398	286	412	399

NM - Not Measured

The results of these experiments indicate that coal can be pyrolyzed to yield 10.92 SCF of a 435 Btu/SCF gas per pound of dry feed. Similarly, one pound of dry sawdust can be pyrolyzed into 18.29 SCF of a 398 Btu/SCF pyrolysis gas.

ASPECTS OF A PYROLYSIS REACTION MODEL

Generalized Criteria for a Coal Pyrolysis Model

When a coal particle is pyrolyzed, the following products are generally found: gases such as CO, H_2, CH_4, C_2H_2, C_2H_6, CO_2, etc., condensible liquid hydrocarbons such as benzene, toluene, etc., aqueous compounds and solid char. When designing a coal conversion plant, one may design the reactor system to maximize the production of the gaseous hydrocarbon, the liquid hydrocarbon, or the char products. The slot-type coke oven is deliberately designed to maximize the char production by allowing the volatile gases to evolve slowly from the solid phase without exterior gas purging, thereby prolonging the gas-solid contact time.

Upon heating coal becomes softened and forms a metaplastic with simultaneous devolatilizations of vapor pushing surface bitumen from interior of particle. If heating rate is rapid, this phenomena is so

violent that the particle literally bursts and develops a solid with a large surface area solid mass. If the heating rate is slow, the products during pyrolysis tend to repolymerize into large, more thermally stable molecules of solid matter that are retained in the interstices of the residual char particle. At high temperatures, the products of pyrolysis are lower in molecular weight than those produced at lower temperatures.

The maximization of the condensible hydrocarbon production is reached when the evolved volatile product is quenched or cooled rapidly after leaving the solid phase, allowing a minimum of time for the larger molecules to thermally decompose into the lower molecular weight gases. In converse, the synthesis gas production is maximized if the volatile hydrocarbon products are held at a high temperature for a prolonged period of time. This exposure to high temperatures will crack the tars and other condensible molecules to lower chain aliphatics - CH_4, C_2H_6, C_3H_8, etc. The pyrolysis reaction mechanism has been discussed by a number of investigators. (Burton and Bailie (1972), Peters and Berthing, (1964), Kertamus and Hill (1964), Jones (1964), Kirov and Stephens (1967), and Squires (1972). Squires cites experimental data reported by Schroeder (1962) in which coal, catalyzed with 1% molybdenum and in a hydrogen atmosphere at 800°C yielded a 42.2% liquid hydrocarbon fraction after a 5 second gas residence time, a 23% liquid fraction yield after a gas residence time of 10 seconds, and, after a 25 second residence time of the gas, the liquid fraction yield was only 9.9%.

Although the liquid fraction was not collected in the experiments while feeding coal or sawdust, a liquid fraction and a char fraction was collected while pyrolyzing a municipal solid waste mixture. The liquid fraction was analyzed as representing 7.0% and the char fraction was 13.5% (moisture and ash-free weight basis) of the inlet solid feed. This contrasts with the data reported by Sanner, et al. (1970), who destructively distilled a municipal refuse in a retort, constructed to simulate a coke oven process. They found that at 900°C, the liquid fraction from the refuse was about 47% and the char fraction was close to 9%. The equipment used by Sanner, et al., allowed the effluent gases to be cooled immediately after leaving the retort, while the exiting gases were held for more than 8-10 seconds at close to the reaction temperature after leaving the pyrolysis zone of the fluid bed reactor, thus accounting for the condensible hydrocarbon fraction from the fluid bed being a 40% smaller value.

In Figure 2, the final conversion of coal attainable as a function of overall heating rate is shown. This figure indicates that rapid heating of the coal avoids the polymerization reaction which can turn the coal to stable char before volatile matter is evolved. Since the objective is to "cream off" the coal to obtain as high heating value gas as possible, a temperature of approximately 1400-1500°F was selected for experimentation.

Mathematical Model for Coal Pyrolysis Reaction

A mathematical model is formulated here based on an assumption that the weight loss during pyrolysis reaction is closely related to heating rate of the coal particle, while the products distribution is primarily determined by the vapor residence time.

A heat balance on a pyrolyzing coal particle may be written as:

$$k_s\left(\frac{\partial^2 T}{\partial r^2} + \frac{2}{r}\frac{\partial T}{\partial r}\right) - \frac{3}{R}(\text{rate})(\Delta H) = \rho_s C_{p_s}\frac{\partial T}{\partial t} \qquad (1)$$

$$\text{where rate} = \frac{\rho_s R}{3}\frac{dX}{dt} = k(f - X)$$

The rate of pyrolysis is assumed to be proportional to the amount of unconverted portion of coal which will eventually be distilled off at the given condition. Thus, f, the final conversion attainable is a constant which depends on reactor temperature and type of coal employed, as shown in Figure 3. Equation (1) can be solved numerically based on the following boundary conditions:

$$\left.\begin{aligned} &r = R,\ (\text{rate})(\Delta H) + \frac{\rho_s C_{p_s} R}{3}\cdot\frac{dT_s}{dt} = h(T_b - T_s) \\ &r = 0,\ \frac{\partial T}{\partial r} = 0 \\ &t = 0,\ T = T_o \text{ and } X = 0 \end{aligned}\right\} \qquad (2)$$

The heat transfer coefficient for the particle includes convective, conductive and radiative heat transfer. The heat of reaction for pyrolysis is normally rather small, roughly 300 Btu/pound coal. Thus, if the term associated with heat of pyrolysis is neglected, the solid temperature can be approximately related to time as:

$$1/2 \cdot \ln\frac{(T_b+T)(T_b-T_o)}{(T_b-T)(T_b+T_o)} + \tan^{-1}\frac{T_b(T-T_o)}{T_b^2+TT_o} = \frac{3h}{\rho_s C_{p_s} R}\,t \qquad (3)$$

When coal particles are blown into a hot fluidized bed, the heat transfer coefficient is so large (approximately 25 Btu/hr ft^2°F) that the particle reaches bed temperature within a few seconds as shown in Figure 4.

The calculated temperature and time relation for fluidized bed pyrolysis at the bed temperature of 1450° ∿ 1500°F is shown for bituminous coal of present study and Elkol coal reported by Jones, et al. (1964). The calculated conversion using a kinetic rate constant, $k = k_o \exp(-E/RT)$, where $k_o = 1.224 \times 10^3$ lb/(ft^2 hr) and E = 2100 Btu/lb-mole (4.6 Kcal/mole), is presented in Figure 5.

CONCEPTUAL FLOWSCHEMES OF LOW-BTU GAS FROM COAL AND SUBSEQUENT ELECTRICITY CONVERSION PROCESSES

A number of conceptual designs have already been proposed to convert a low-Btu gas and then coal into electrical power efficiently and cleanly. A modification of the Bituminous Coal Research's high-Btu "BI-GAS" Process two-stage gasifier has been proposed to utilize air instead of pure oxygen and to operate the gasifier at 300 psig. BCR concluded that an in-plant coal gasification process may compare favorably with other environmental control concepts (such as tail-end SO_2 removal), if the total coal-to-electricity process were to be re-designed into an optimal system, (Bituminous Coal Research (1971)).

In this section we intend to describe a conceptual process alternative based on the experimental data presented in the previous section, and to use this flowscheme to show that there will be a distinct advantage in considering a two-step coal gasification subsystem. In the first step, the coal is pyrolyzed to release the larger molecule hydrocarbons, such as methane, ethane, propane, etc., which Arthur Squires calls the "cream" of the decomposition products of the coal "molecule" (Squires (1972)). The second-step gasifier vessel reacts the residue pyrolysis char with steam and air to form the gas containing H_2, CO, CO_2 etc., that is needed to fluidize the pyrolyzer.

The two processes compared here are illustrated in Figures 6 and 7. In Figure 6, the "one-step" Coal Gasifier is illustrated, in which the raw coal is fed directly into the high-temperature (1900°F) synthesis gas generator operating at 150 psig. There, the coal is directly gasified with air and steam to produce a stream of H_2, CO, H_2O, CO_2, CH_4, H_2S and N_2. This product gas is cleaned of the H_2S and other impurities and is then burned in a combustion chamber. The effluent gases from the combustion chamber are then sent through a combined gas turbine - steam turbine cycle. The coal would have the same composition as was used in the present pyrolysis experiments (Table 2). In this model, the gasifier system was assumed to operate adiabatically, the gases - H_2, CO, CO_2, H_2O - are assumed to emerge from the reactor in the same composition ratio as the equilibrium composition of the water-gas-shift reaction, and the carbon-steam reaction products are at a 20% approach to thermodynamic equilibrium.

The "Two-Step Coal Pyrolysis-Gasifier" is illustrated in Figure 7. The raw coal is fed to the fluidized bed where the pyrolysis of the coal takes place at 1400°F. It is conservatively assumed that there are no chemical reactions between the fluidizing gases and the volatilized coal-pyrolysis product gases. It is also assumed that the product gases evolved from the coal pyrolysis reaction are produced at the same rate and in the same composition as was produced in the experimental bed described in the previous section. The char separated from the effluent gas is then reacted with air and steam to produce the fluidizing gases for

coal-pyrolyzer. A small amount of raw coal must be added to the char feed to the gasifier in order to maintain the 1900°F gasifier temperature and to produce enough gas to fluidize the incoming coal in the pyrolyzer. The gas produced in this two-stage gasification system is then purified to remove the sulfur and other undesriable compounds, and is then burned in the combustion chamber with the combustion gases processed to generate electricity in the same gas- and steam-turbine system as described previously.

In Table 6 effluent gas compositions from pyrolyzer and gasifier are listed respectively.

TABLE 6
COMPOSITIONS OF EFFLUENT GASES FROM PYROLYZER AND GASIFIER

	CO_2	CO	H_2	H_2O	CH_4	C_2H_2	C_2H_6	H_2S	N_2
GASIFIER	1.00	34.77	9.34	0.51	0.20	-	-	0.82	53.36
PYROLYZER	3.19	31.54	16.95	1.78	3.59	0.43	0.21	0.64	41.68

As can be seen in Figure 8, the "Two-Stage Pyrolyzer-Gasifier" System generates electricity with a 2% or better thermal efficiency than does the "Single-Step Coal Gasifier System". The thermal efficiency is defined as the heat equivalent of the product electricity generated divided by the heat of combustion of the inlet coal feed.

The electricity generating ability of the present day gas turbines are limited by the temperature of the inlet gases, the maximum allowable operating limit of around 2000°F governed by the thermal tolerance or the turbine construction metal. Figure 8 indicates the effect that a 200°F higher inlet gas temperature will make on the overall process efficiency.

A very important system design consideration is the degree of carbon utilization in the synthesis-gas generator. An increase of 5% carbon utilization in the gasifier implies an increase of approximately 2% overall plant thermal efficiency.

CONCLUSION

Experimental data of coal pyrolysis in a sand fluidized bed indicates that it is possible to extract considerable amounts of hydrocarbons from the caking coal by a rapid heating and subsequent cracking in the vapor

phase. This is done by blowing pulverized coal into a fluidized bed of hot sand and elutriating the char along with gaseous product from the fluidized bed. The extremely good heat transfer of the fluidized bed provides the rapid heating required for this process. In this manner, the valuable hydrogen in coal is extracted either as free hydrogen or as hydrocarbons in the gas phase product. A conceptual scheme is presented which utilizes the product char to generate synthesis gas by gasification with air and steam for use in the pyrolyzer. The thermal efficiency calculated based on the two stage process with the combined gas and steam turbine cycle shows that this scheme is a promising way to produce clean power from coal.

ACKNOWLEDGEMENTS

This work was partly supported by the Office of Coal Research, U. S. Department of the Interior, and partly by the Solid Waste Office of Research and Monitoring, U. S. Environmental Protection Agency.

NOTATION

C_{ps}	:	Heat capacity of solid	(Btu/lb)
E	:	Activation energy	(Btu/mole)
f	:	Final conversion attainable	-
h	:	Heat transfer coefficient, include convection and radiation	(Btu/ft^2-hr-°R)
k(T)	:	Rate constant	(lb/ft^2-hr)
k_o	:	Frequency factor	(lb/ft^2-hr)
k_s	:	Thermal conductivity of particle	(Btu/ft-hr-°R)
R	:	Radius of particle	(ft)
$\tilde{R}$	:	Gas constant	(Btu/mole-°R)
rate	:	Reaction rate	(lb/ft^2-hr)
r	:	Radial distance in particle	(cm)
T	:	Solid temperature at r = r	(°R)
T_o	:	Room temperature	(°R)
T_b	:	Bed Temperature	(°R)
T_s	:	Surface temperature of Solid particle	(°R)
t	:	Solid residence time	(hr)
X	:	Solid conversion, dry-ash-free basis	-
ρ_s	:	Solid density	(lb/ft^3)

REFERENCES

Bituminous Coal Research, Inc. (1971), "Economics of Generating Clean Fuel Gas from Coal Using an Air-Blown Two-Stage Gasifier", R & D Report No. 20, Final Report - Supplement No. 1, U. S. Office of Coal Research.

Burton, R. S., and R. C. Bailie (1973), "Fluid Bed Pyrolysis of Solid Waste Materials", submitted for publication in Combustion.

F. M. C. Corporation (1967), "Char-Oil-Energy-Development Project COED: January - October 1966", R & D Report No. 11, U. S. Office of Coal Research, February.

Frantz, J. F. (1961), "Fluid-To-Particle Heat Transfer in Fluidized Beds", Chemical Engineering Progress, 57, No. 7 (July), pp. 35-42.

Jimeson, R. M. (1972), "The Demand for Sulfur Control Methods in Electric Power Generation", presented at the 164th National Meeting, American Chemical Society, New York; Preprints of Division of Fuel Chemistry, Vol. 17, No. 1, pp. 88-101.

Jones, J. F., M. R. Schmid and R. T. Eddinger (1964), "Fluidized Bed Pyrolysis of Coal", Chemical Engineering Progress, 60, No. 6 (June), pp. 69-73.

Kertamus, N., and G. R. Hill (1964), "Pyrolysis Kinetics of a Western High Volatile Coal", presented at the 148th National Meeting, American Chemical Society, Chicago, September: Preprints of Division of Fuel Chemistry, Vol. 8, No. 3, pp. 89-96.

Kirov, N. Y.,and J. N. Stephens (1967), Physical Aspects of Coal Carbonization, University of New South Wales, Sidney, Australia.

Mills, G. A. (1971), "Gas From Coal-Fuel of the Future", Environmental Science and Technology, 5, No. 12 (December), pp. 88-101.

Peters, W., and H. Bertling (1964), "Kinetics of the Rapid Degasification of Coals", presented at the 148th American Chemical Society Meeting, Chicago, September: Preprints of Division of Fuel Chemistry, Vol. 8, No. 3, pp. 77-88.

Sanner, W. S., C. Ortuglio, J. G. Walters and D. E. Wolfson (1970), "Conversion of Municipal and Industrial Refuse into Useful Materials by Pyrolysis", Report of Investigations No. 7428, U. S. Bureau of Mines.

Schroeder, W. C. (1962), "Hydrogenation of Coal", U. S. Patent No. 3,030,297.

Squires, A. M. (1972), "The Coalplex: Gas, Gasoline, and Clean Electricity From Coal", presented at the 65th Annual Meeting, AIChE, New York, November 26-30.

Theobald, P. K., S. P. Schweinfurth and D. C. Duncan (1972), "Energy Resources of the United States", Circular No. 650, U. S. Geological Survey.

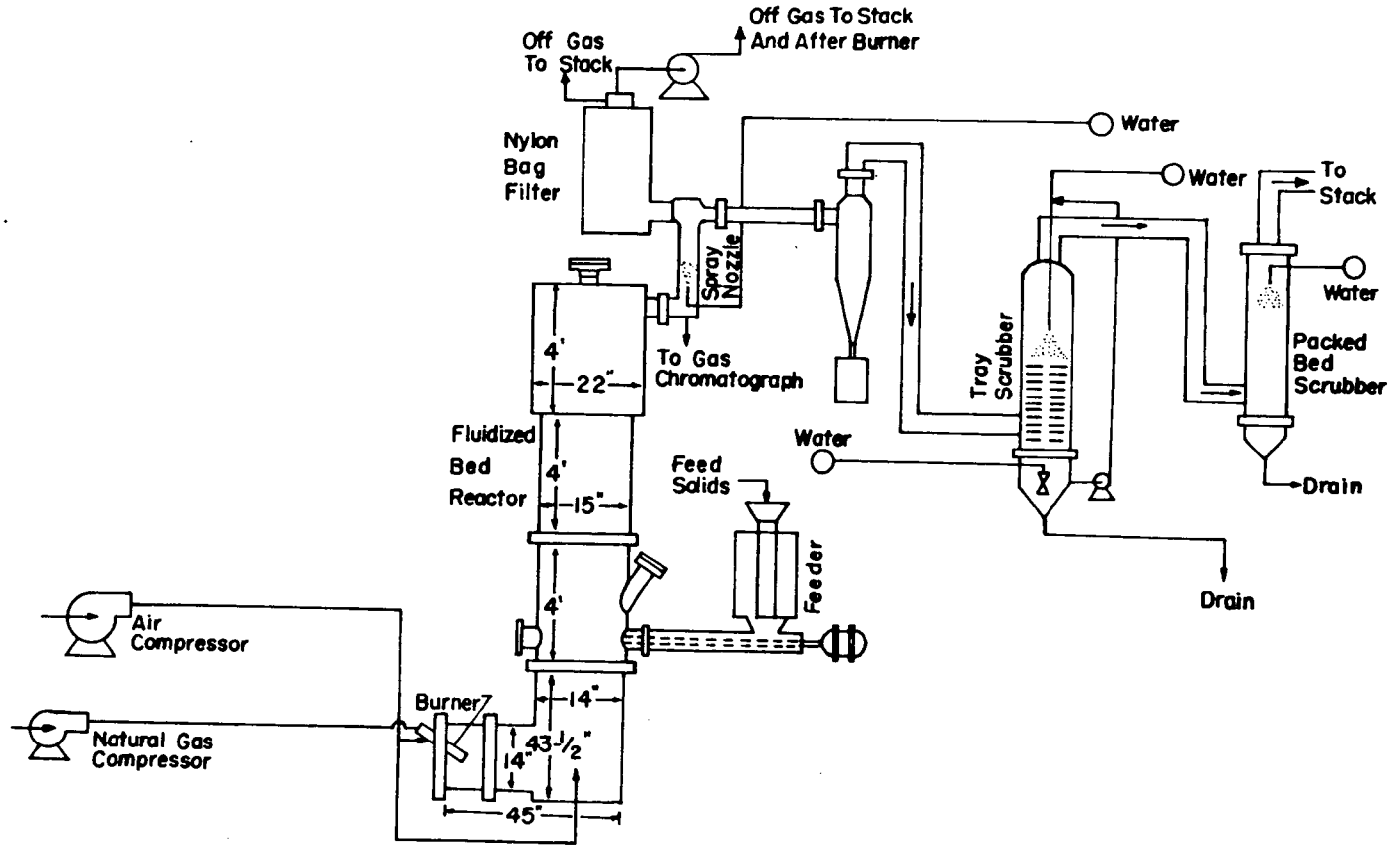

FIGURE 1 FLUIDIZED BED PYROLYSIS REACTOR SYSTEM

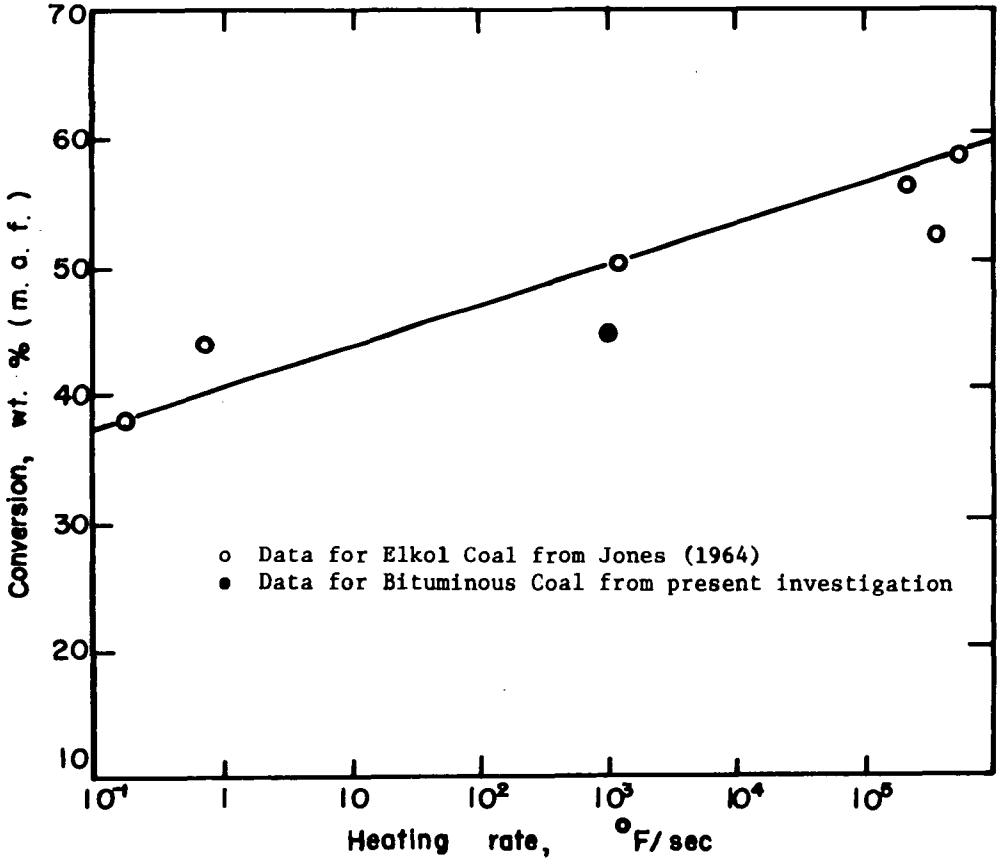

FIGURE 2

EFFECT OF OVERALL HEATING RATE ON DEVOLATILIZATION OF COAL

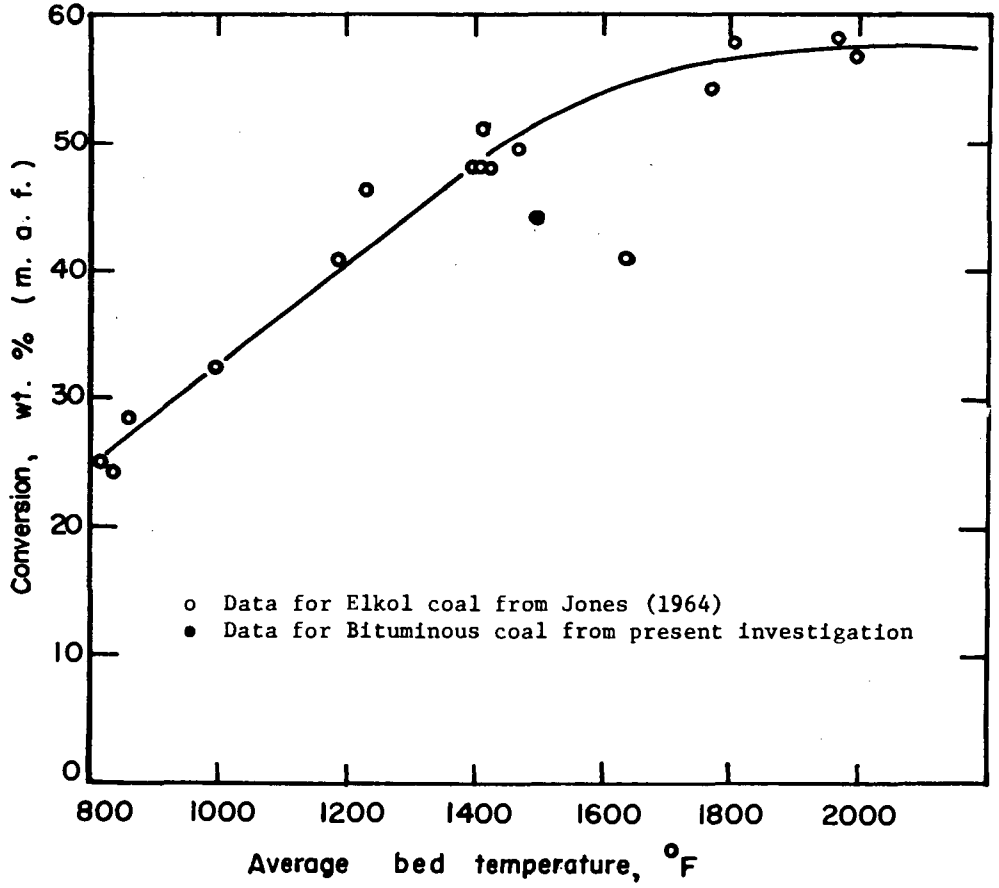

FIGURE 3

EFFECT OF TEMPERATURE ON THE FINAL CONVERSION OF COAL ATTAINABLE IN A FLUIDIZED BED REACTION

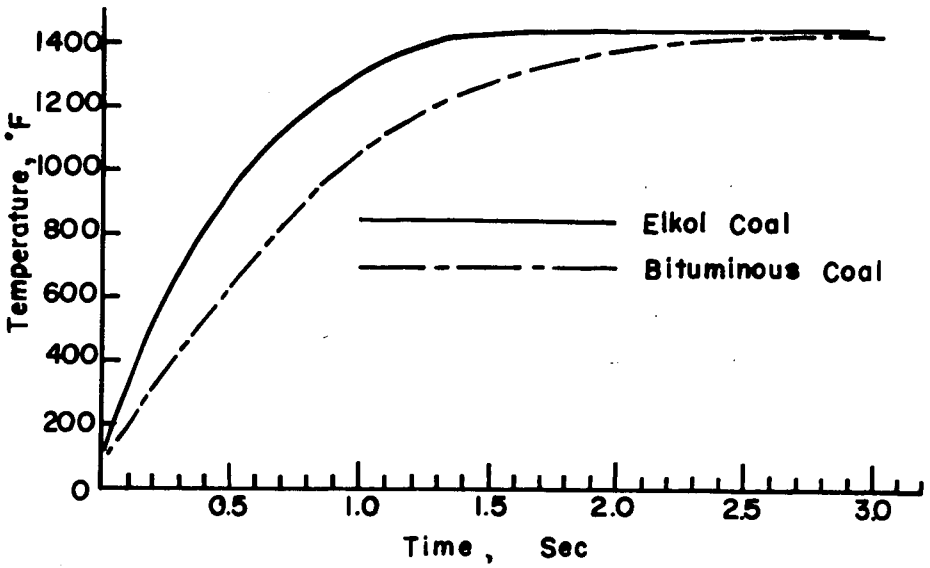

FIGURE 4

CALCULATED PARTICLE TEMPERATURE AS A FUNCTION OF TIME FOR PYROLYSIS REACTION IN FLUIDIZED BED SYSTEMS

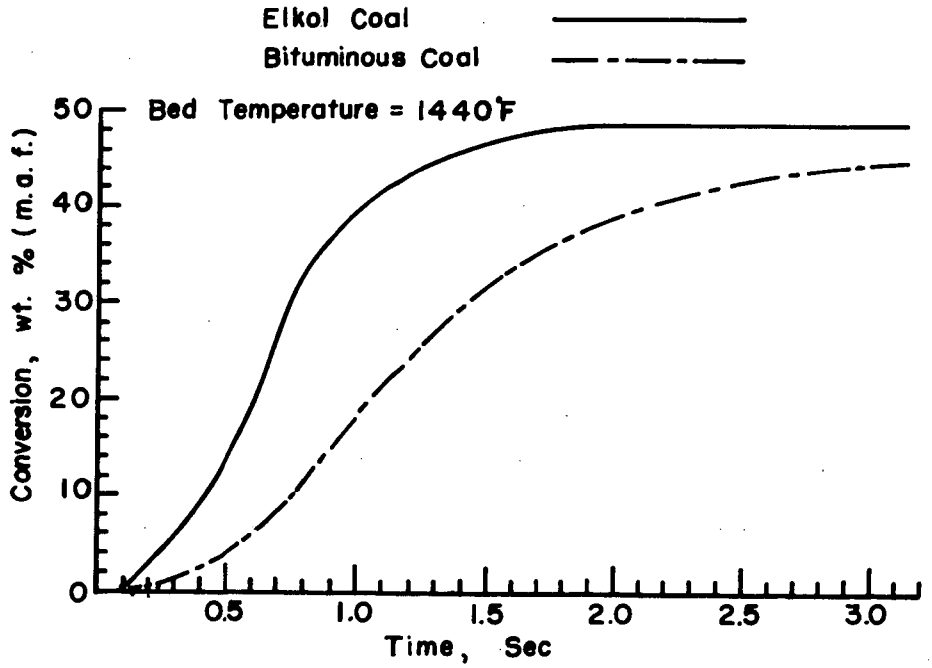

FIGURE 5

CALCULATED PARTICLE VOLATILE MATTER CONVERSION AS A FUNCTION OF TIME FOR PYROLYSIS REACTION IN FLUIDIZED BED SYSTEMS

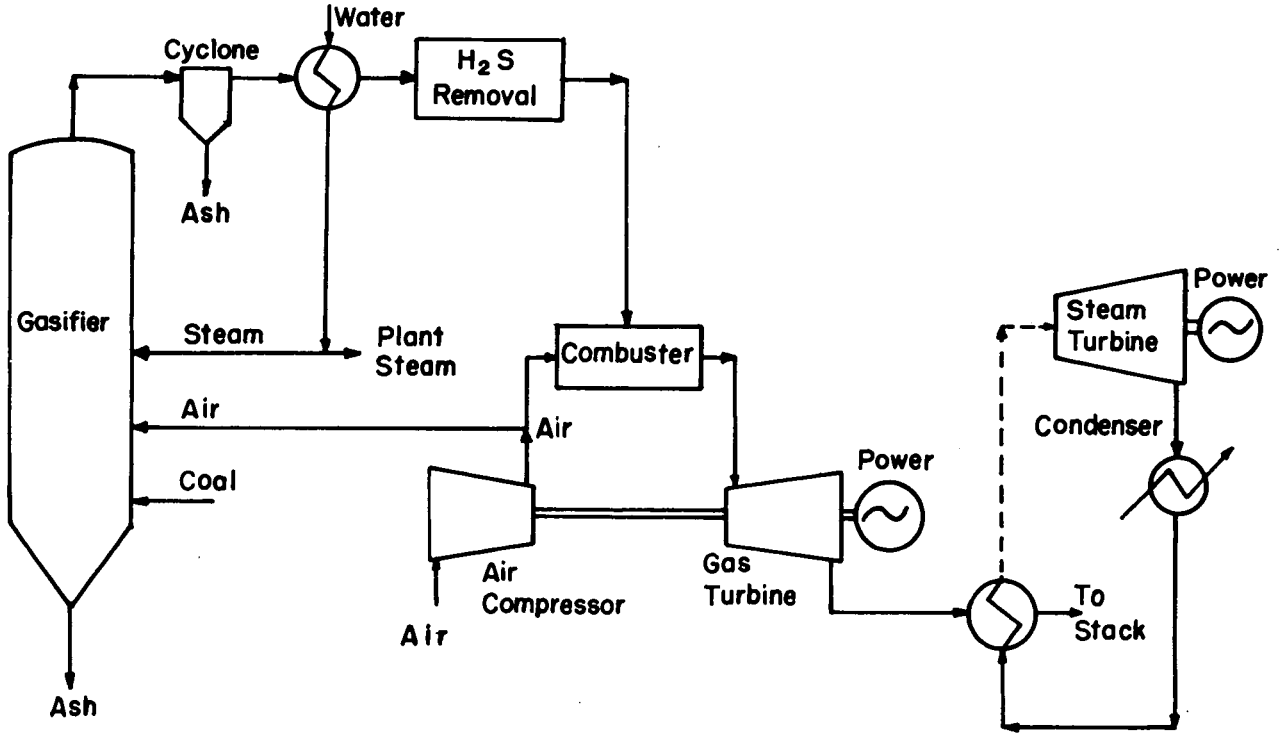

Figure 6 Power Generation Via Coal Gasification Combined Cycle
(One-Stage Coal Gasification System)

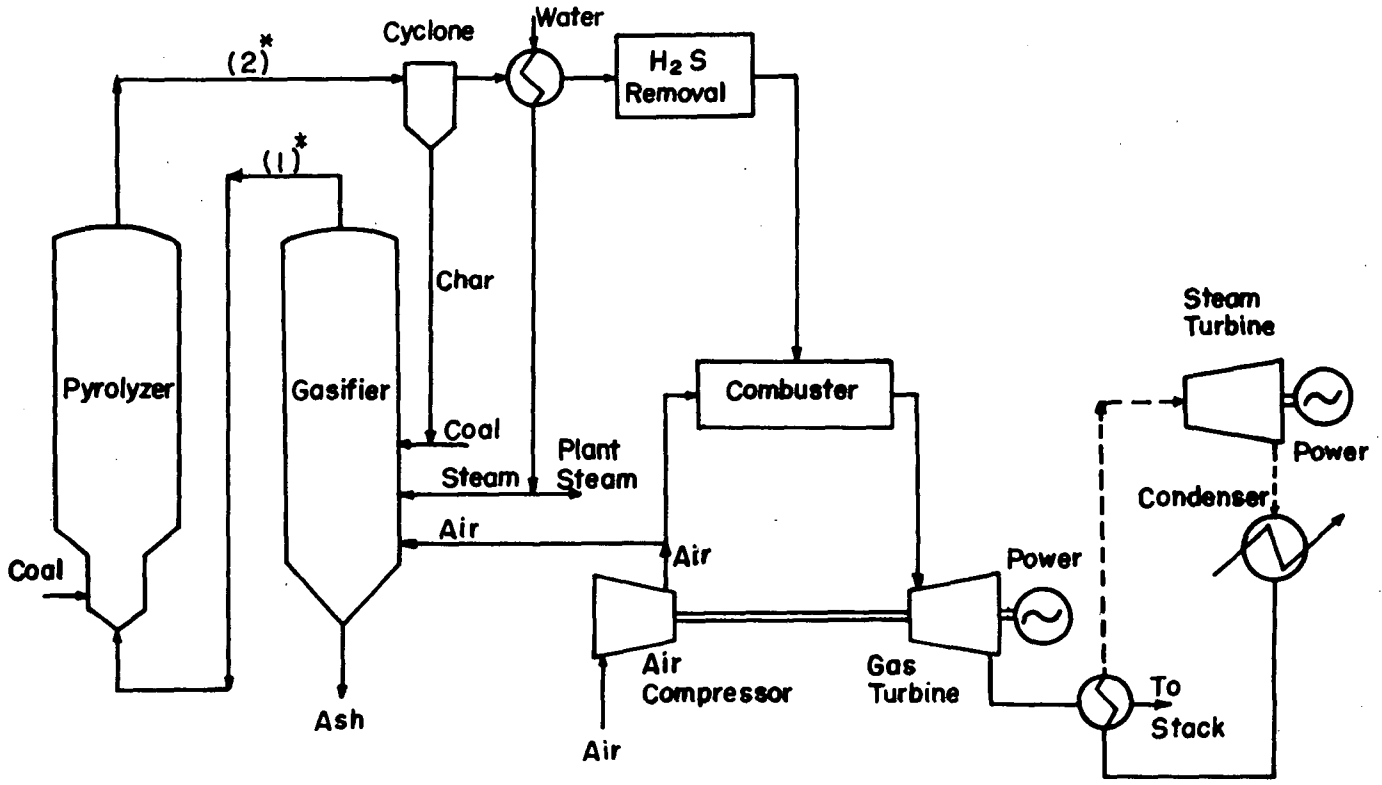

Figure 7 Power Generation Via Coal Gasification Combined Cycle

(Two-Stage Coal Pyrolysis Gasification System)

* Gas Compositions Are Given In Table 6 In The Text

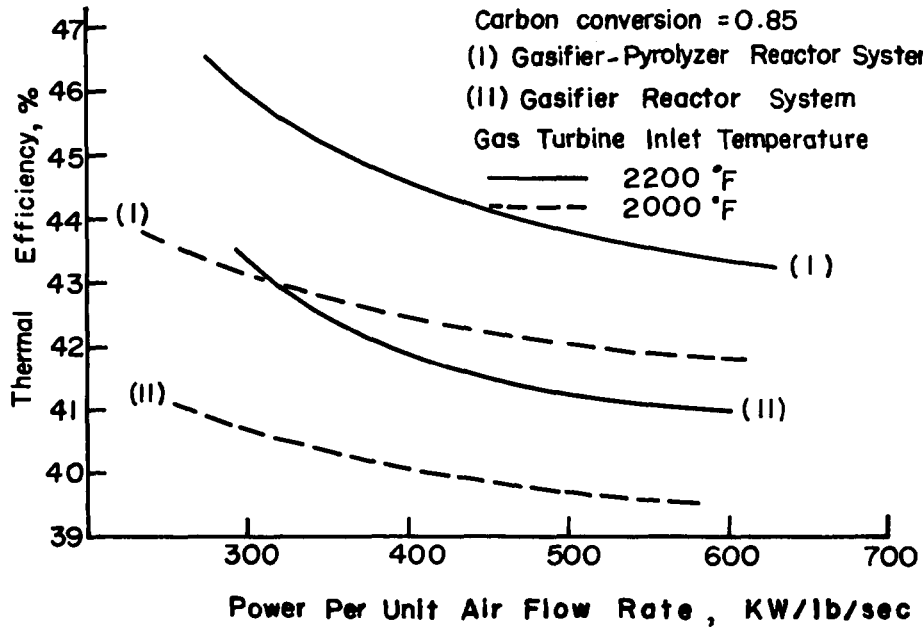

Figure 8 Thermal Efficiencies Of Two Processes Converting Coal To Electricity

DEUTERIUM AND CARBON-13 TAGGING STUDIES OF THE PLASMA PYROLYSIS OF COAL

V.J. Krukonis and R.E. Gannon

AVCO Corporation S/D
Lowell Industrial Park
Lowell, Massachusetts 01851

M. Modell

Massachusetts Institute of Technology
Department of Chemical Engineering
Cambridge, Massachusetts

INTRODUCTION

High temperature arc or plasma pyrolysis of coal produces acetylene as the principal hydrocarbon product[1-6]. Furthermore, yields of acetylene in a hydrogen atmosphere are enhanced a factor of three over those achieved in an argon atmosphere. Consistent with the experimental results, thermodynamic data show that acetylene is the only stable hydrocarbon molecule above 1500°C, and below about 1200°C its thermodynamic stability decreases rapidly[7,8,9]; experimental evidence also supports that high temperature acetylene-containing hydrocarbon streams must be quenched rapidly in order to prevent decomposition to carbon black[10].

During the duration of a program to convert coal to acetylene carried out at Avco/Systems Divisions Laboratories, a number of high temperature arc reaction concepts were tested. The initial conversion scheme utilized coal as the consumable anode of a DC arc, and the process schematic is shown in Figure 1. The consumable anode pyrolysis of coal has been described in detail in Reference 5, but here, briefly, crushed coal, typically 10-20 mesh, is fed into an electrical discharge sustained between a graphite cathode and the coal at a feed rate consistent with the surface pyrolysis rate. The rapid heating occurring at the surface pyrolyzes the coal, and the hydrocarbon products formed are quenched downstream of the arc zone by injecting a gas in order to preserve the acetylene produced in the discharge region. The solid residue, consisting of char and any unreacted coal, spills over the sides of the anode feed tube.

A schematic diagram of the experimental reactor showing the coal feed tube, gas quenching ports, and the product sampling positions is given in Figure 2. The gas sampling tubes were located at sequential positions downstream of the arc zone in order to determine if any acetylene decomposition were occurring in the gas stream. Simultaneous sampling at all three positions shown in Figure 2 produced identical results (although probing of the high temperature arc zone with a small diameter, water-cooled tube produced higher acetylene concentrations indicating that some decomposition was occurring even before the gas reached the first sampling position; the yield and decomposition data that are reported subsequently were obtained from downstream sampling positions and, thus, are not confused with ultra-high quench rate ambiguities).

Hydrocarbon product analyses were carried out on an F&M 700 chromatograph using a Porapak Q column and a flame ionization detector. (Other gases such as CO, H_2S, COS, CS_2, etc., were determined on a F&M 720 thermal conductivity chromatographic unit data using argon and hydrogen as quench gases are given in Figure 3, and the data show that at all power levels studied the yield of acetylene is 2-3 times greater with hydrogen as the quench medium.

Pyrolysis of coal with consequent formation of acetylene in an inert plasma environment is evidence that the carbon and hydrogen present in the coal are reacting, i.e.,

$$C \text{ (in coal)} + H \text{ (in coal)} \longrightarrow C_2H_2 \qquad (1)$$

although Equation (1) is obviously an oversimplification of acetylene formation, and no mechanism is implied.

Several explanations for the higher yields found with hydrogen can be proposed, viz.,

1. hydrogen generates additional acetylene from the carbon in coal via solid carbon-gaseous hydrogen reaction, a yield contribution which is absent in an inert atmosphere, i.e.,

$$C \text{ (in coal)} + H_2 \longrightarrow C_2H_2 \qquad (2)$$

2. hydrogen is a more effective coolant or preserver of acetylene than is argon because of mass transfer or thermal conductivity considerations,

or

3. hydrogen acts as some chemical reactant in the quenching step, preventing the decomposition of acetylene to carbon black.

The most obvious explanation for the improved acetylene yields found with a hydrogen quench is Postulate 1, viz., additional reactions occurring between carbon in the coal and the gaseous hydrogen environment, and this reaction contribution was subsequently tested by reacting char and hydrogen. Hydrogen-free char (collected from previous arc-coal tests) was reacted in the arc environment; however, acetylene yields were only minimal[5], far below the levels required to explain the factor of three difference between the argon and hydrogen results shown in Figure 3.

Other experiments in the consumable anode, arc reactor showed that if no quench were used, acetylene yields were very small with substantial carbon black formation on the reactor walls, indication that decomposition of acetylene in the product stream was occurring, again in agreement with the thermodynamic data and other experimental evidence.

The coal pyrolysis scheme underwent a number of modifications in both reactor design and reaction philosophy during the course of the program. It was found, for example, that one of the most serious causes of acetylene decomposition (in either the argon or hydrogen case) was the contact between the incandescent surface char layer and the acetylene which was generated below the surface. Examination of large char particles showed that carbon black was present in the pores of the structure[6]. Feeding hydrogen up through the coal resulted in increased yields, up to about 18% (based on total coal), but, finally, certain materials erosion problems shifted emphasis from the consumable anode concept to a plasma reactor shown in Figure 4. The reactor description and operation have been covered fully in Reference 10, but here, again briefly, powdered coal, typically -100 mesh, is carried downward via hydrogen through a magnetically rotated arc region, at a velocity of a several hundred ft/sec. A few inches downstream the hydrocarbon stream is quenched (and several alternatives employing coal, or a hydrocarbon, or solely hydrogen were tested). Acetylene yields and electrical energy consumptions in this reactor approached economically viable levels; in the rotating arc reactor hydrogen still produced substantially higher acetylene yields than did an argon quench.

In order to separate the acetylene forming step from the acetylene preserving step in this coal pyrolysis scheme, and also in order to determine quantitatively the role of hydrogen in the process, tests were carried out in which acetylene was injected into a carbon-free plasma stream, experiments designed to simulate only the "quenching-preserving" step. In the quenching studies, as in the coal tests, the decomposition of acetylene in an argon plasma was again found to be much greater than in hydrogen. Figure 5 gives the results of acetylene decomposition experiments, which have been previously reported[10], and shows that about 60% of the initial acetylene decomposes with an argon quench while with a hydrogen quench only about 10-12% of the acetylene decomposes.

As a result of the large differences in results with hydrogen and argon, other quench gases, viz., helium, nitrogen, and deuterium, were subsequently tested in an attempt to separate chemical effects from physical ones. For example, if gas diffusivity and thermal conductivity are important parameters in preserving acetylene as an intact species, acetylene decomposition in hydrogen, helium, and deuterium would be essentially the same because all three gases possess essentially identical mass and heat transport properties. If on the other hand, the heat capacity of the quench medium, i.e., its energy absorption and dissociation capability, were the important consideration, hydrogen, deuterium, and nitrogen would produce identical quenching results (ignoring for now nitrogen's somewhat higher stability relative to hydrogen). Finally, if chemical reactions between C_2H_2 and H_2 were in operation during the quenching step, H_2 and D_2 results would be identical. In addition to gas chromatography high resolution mass spectroscopy was carried out with the deuterium samples. The deuterium results, which have been reported previously[11], showed that substantial H-D exchange was occurring in the acetylene molecule.

Finally as a means of determining reactions in operation during the acetylene quenching step, "heavy" acetylene, $C_2{}^{13}H_2$, and "normal" acetylene, $C_2{}^{12}H_2$ were admixed and injected into the plasma quenching simulator so that carbon-carbon triple bond interaction at high temperature could be studied.

RESULTS AND DISCUSSION

A series of experiments to separate the complex reactions of acetylene generation and acetylene preservation occurring during the arc pyrolysis of coal was carried out as an integral part of the coal pyrolysis studies in the rotating arc reactor. In order to study the quenching reaction, acetylene was injected into a high temperature plasma stream, free of coal and char particles. A plasma generator attached to a 2" copper, water-cooled tube as shown in Figure 6 was used for the quenching studies. Acetylene was injected into the plasma stream about 1/2" from the nozzle, and a gas sampling tube was located about 12" downstream of the plasma generator; again as in the previous reactors, the gas sampling probe was purposely located far downstream of the plasma and injection position in order to allow all decomposition reactions to occur, eliminating the probing ambiguities described earlier. The acetylene concentration in the plasma was about 7%, closely approximating the concentration obtained in the rotating arc reactor. The entire plasma system was connected to a very large capacity rotary vacuum pump so that tests at various total reaction pressures could be carried out.

Tests were made, then, to determine the effect of operating pressure on decomposition and to determine the effects of using different gas quenches on preserving acetylene. Both sets of results are given in Figure 7. Most extensive testing was carried out with hydrogen, and it is seen that decomposition is a function of total pressure, but reaches only about 30% at 1 atm. Figure 7 also shows that decomposition of acetylene in both hydrogen and deuterium is identical at the two pressures studied, and, furthermore, shows that the decomposition is low relative to the other gases used, helium, argon, and nitrogen. The data in Figure 7 bring out then that hydrogen (and chemically-similar deuterium) has some other effect in preserving acetylene, effects not explainable by merely the physical properties of thermal conductivity, diffusivity, or heat capacity.

There was no way to determine chromatographically if the acetylene molecules sampled in the hydrogen quenched stream were the identical molecules injected into the plasma, and hence mass-spectrometric analysis of the deuterium gas samples was carried in order to determine if the composition consisted of C_2H_2 or of some deuterated species (and although it would have been possible, no effort was given to chromatographic separation of deuterated acetylenes). The analyses of the deuterium samples showed that H-D interaction to form C_2HD and C_2D_2 was occurring during the plasma quenching step. Table I gives the measured composition of acetylene in the product gas for the deuterium plasma-deuterium quench set of tests.

TABLE I

ISOTOPIC ACETYLENE COMPOSITION

Species	Composition (% of Undecomposed C_2H_2)
C_2H_2	1.1%
C_2HD	15.1%
C_2D_2	83.5%

As Table I shows, 99% of the C_2H_2 molecules have exchanged with D_2 to form C_2HD and C_2D_2.

A number of workers in very high temperature acetylene formation-decomposition studies have invoked radical recombinations to explain the fact that acetylene compositions "greater than equilibrium" were achieved in their studies. Plooster and Reed[12] postulated that high temperature equilibrium favors two carbon species, C_2H_2 and C_2H, and that during the quenching sequence two mechanisms contributed to the acetylene measured in the product, viz.,

$$C_2H_2 \text{ (present at high temperature)} \xrightarrow{\text{quench}} C_2H_2 \qquad (3)$$

$$C_2H + H \xrightarrow{\text{quench}} C_2H_2 \qquad (4)$$

Their model was based upon estimates of the thermodynamic properties, and their experimental results agreed well with the model of a C_2H radical. Other workers after Plooster and Reed, viz., Baddour and Iwasyk[13] and Baddour and Blanchet[14] also invoked the C_2H mechanism to explain their results of reacting hydrogen with carbon in a consumable anode arc reactor.

An equilibrium diagram for the carbon-hydrogen system is given in Figure 8 and shows that C_2H_2 and C_2H are, in fact, the most prevalent carbon species at high temperature*. Although calculated from free energy considerations to be present in relatively high concentrations, the C_2H radical, on the other hand, has not yet been experimentally verified to be present in any quantity. A quenching mechanism which both rapidly cools C_2H_2 and requires a recombination of a non-interconvertible C_2H radical with H does not explain the presence of large amounts of C_2D_2 in the product stream, i.e., if C_2H maintains its identity at high temperature, only C_2HD (along with the preserved" C_2H_2) could be formed during the quenching step; however, the data in Table I show that 83% of the C_2H_2 has exchanged to C_2D_2, and a random recombination of radical and atomic species was found to correlate the results.

Conservation of energy considerations, however, preclude the dissociation of all the species into atoms and/or radicals. For example, most of the tests in the plasma reactor were carried out at input power levels of about 15 kw; with a H_2 (or D_2) flow of 4.95 SCFM used in the tests, the average gas enthalpy was only about 40 kcal/gmol, much, much less than the 100 kcal/gmol required to dissociate even hydrogen alone (not including the dissociation of acetylene to C_2 and H). In spite of the impossibility of dissociating all the molecules to C_2, H, and D species, however, there is presented in Table II the predicted statistical concentrations of H- and D-exchanged acetylenic molecules, based upon the recombination of such species, and it is seen that the agreement is very good.

TABLE II

ISOTOPIC COMPOSITION OF ACETYLENE

Species	Measured Composition	Predicted Composition (Based Upon Combination of C_2, H, &D
C_2H_2	1.1	0.5
C_2HD	15.1	13.2
C_2D_2	83.5	86.0

*Figure 8 was calculated for a C/H ratio of 1/4, i.e., for methane, using JANAF data[9].

As a final study of the decomposition-recombination reactions of acetylene which could aid in the elucidation of the acetylene preservation mechanism in hydrogen, mixtures of carbon isotope acetylenes, $C_2^{12}H_2$ and $C_2^{13}H_2$, were injected into a hydrogen plasma stream, and analysis of the gas product again was determined by high-resolution mass spectroscopy. If the carbon-carbon triple bond maintained its integrity, only C^{12} and C^{13} acetylene should be present in the product stream; if, on the other hand, the triple bond were entering into the decomposition-preservation reactions, an interaction to form $C^{13}C^{12}H_2$ would be measured in the product.

For the C^{12}-C^{13} experiments the plasma reactor was also operated at about 0.5 atm with approximately a 50/50 mixture of the isotope acetylenes injected into the plasma stream. Gas chromatographic and high resolution, mass spectroscopy analyses were carried out on the samples. Gas chromatograph showed again that only about 10% of the original acetylene disappeared to carbon black (and the decomposition result is shown as a solid dot in Figure 7). Mass spectrograms of both the initial and final product acetylene streams are given in Figure 9. Figure 9 shows that some $C^{12}C^{13}H_2$ was present in the starting material (because the heavy acetylene could be obtained only as 90% C^{13} acetylene). A mass spectrogram of the final composition, obtained with the plasma generator operating at 15 kw, a power level identical to that of the deuterium tests, is also compared to the initial spectrogram in the figure, and a large increase in the $C^{12}C^{13}H_2$ peak is evident.

Acetylene compositions are given in Table III.

TABLE III

ISOTOPIC COMPOSITION OF ACETYLENE

	Composition %	
Species	Initial Mixture (Power Off)	Final Mixture (Quenched)
$C^{12}{}_2H_2$	47.6	30.6
$C^{12}C^{13}H_2$	11.9	48.5
$C^{13}{}_2H_2$	40.5	20.9

If 100% of C^{12} and C^{13} reacted, the calculated $C^{12}C^{13}H_2$ concentration would be 49.6% as shown in Table IV; the measured concentration of 48.5% indicates, therefore, that a 97% exchange occurred based upon the statistical model; again, however, energy considerations (with the plasma stream possessing only a maximum of 40 kcal/gm) preclude such a simple model.

TABLE IV

ISOTOPIC ACETYLENE COMPOSITION

Species	Measured (%)	Calculated (%)
$C^{12}{}_2H_2$	30.6	29.2
$C^{12}C^{13}H_2$	48.5	49.6
$C^{13}{}_2H_2$	20.9	21.2

A mechanism based upon sequential collisions will be presented.

ACKNOWLEDGMENTS

This work was supported by the Office of Coal Research, U.S. Department of the Interior, under Contract No. 14-01-000-493.

The technical contributions of Albert Bothe, Robert McDonough and Richard Reudiger in planning and performing the described experiments are acknowledged and appreciated. The mass spectrographic analyses were performed at the Massachusetts Institute of Technology using their high resolution mass spectrograph. The guidance and assistance of Professor Klaus Bieman and Dr. Guy Arsenault in analyzing the data were most valuable. Finally, sincere appreciation to Pat Sedota, who typed several rough drafts, at the last possible minute, because of the procrastination of one of the authors, finished the final copy so that it could be included in the agenda.

REFERENCES

1. Littlewood, K., McGrath, I.A., Paper C9, 5th International Conference on Coal Science, Cheltenham, (1963).

2. Rau, E., Seglin, L., Fuel 43, (2), 147-45, (1964).

3. Bond, R.L., Ladner, W.R., McConnel, G.I.T., Coal Sciences, Advances in Chemistry, Ser. 55, 650-65, (1966).

4. Kawa, W., Graves, R.D., Hiteshue, R.W., U.S. Bureau of Mines, Report of Investigation 6829, (1966).

5. Kawana, Y., Makino, M., Kimura Tatsuo, Kogyo Kagaku Zasshi, 69, (6), 1144-50, (6).

6. Krukonis, V.J., Schoenberg, T., Paper 5-132, 7th International Conference on Coal Science, Prague, (1968).

7. Wagman, D.D., Kilpatrick, J.E., Pitzer, K.S., Rossini, F.D., J. Res. Nat. Stand., 35, 467, (1945).

REFERENCES (Con't)

8. Howard, Wood, Kaltenbacher, Chem. Eng. Prog., 57, (11), 50, (1961).

9. JANAF Thermochemical Data Compiled and Calculated by the Dow Chemical Company, Thermal Laboratory, Midland, Michigan.

10. Krukonis, V.J., Gannon, R.E., Schoenberg, T., 19th Canadian Engineering Conference, Edmonton, Alberta, (1969).

11. Gannon, R.E., and V.J. Krukonis, ACS, Chicago, September 13-18, 1970.

12. Plooster, M.N., and Reed, T.B., J. Chem. Phys., 1959, 31, p. 66.

13. Baddour, R.F., and Iwasyk, J.M., I. and E.C. Process Design and Development, Vol. 1, No. 3, July 1962, p. 169.

14. Baddour, R.F., and Blanchet, J.L., I. & C. Proc. Design Devel., Vol. 3, p. 258, 1964.

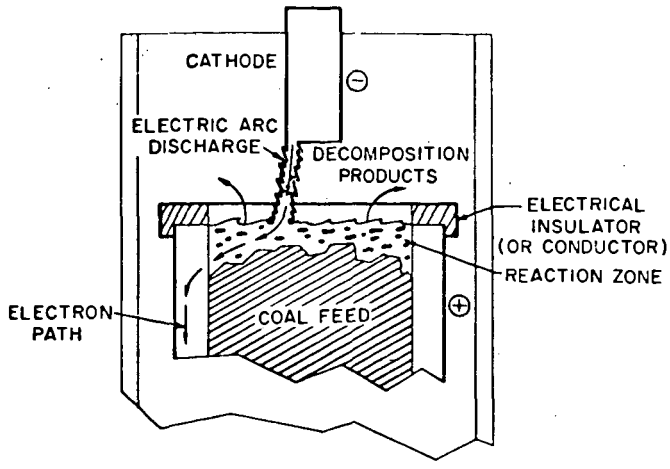

Figure 1 SCHEMATIC OF COAL CONVERSION ARC PROCESS

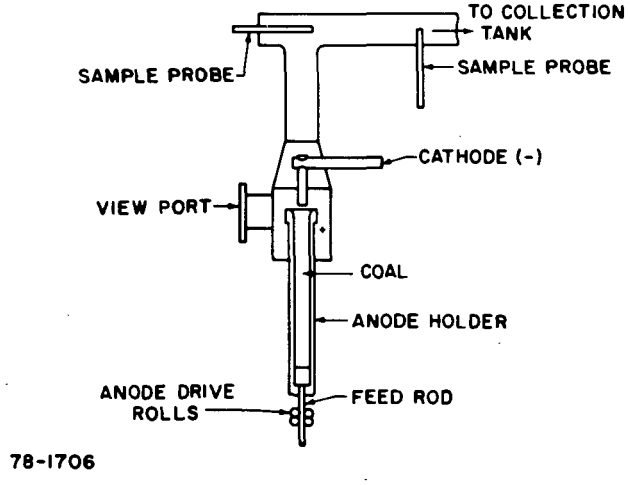

Figure 2 ARC COAL REACTOR

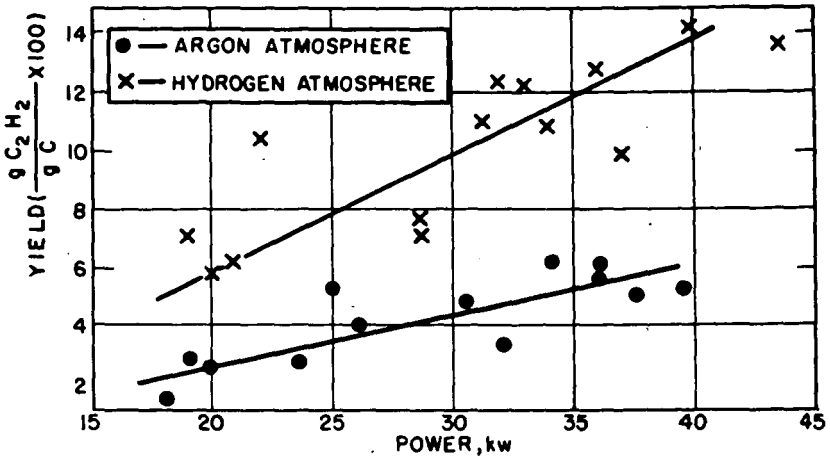

Figure 3 EFFECT OF ATMOSPHERE ON ACETYLENE YIELD

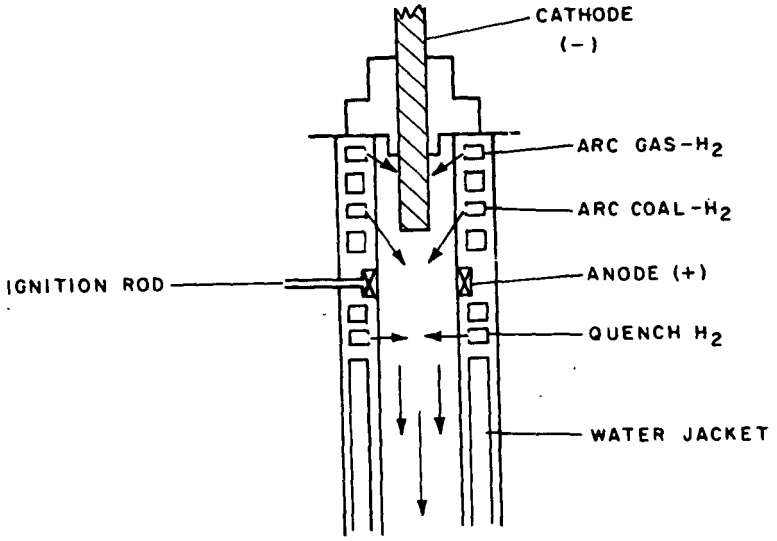

Figure 4 ROTATING ARC-REACTOR

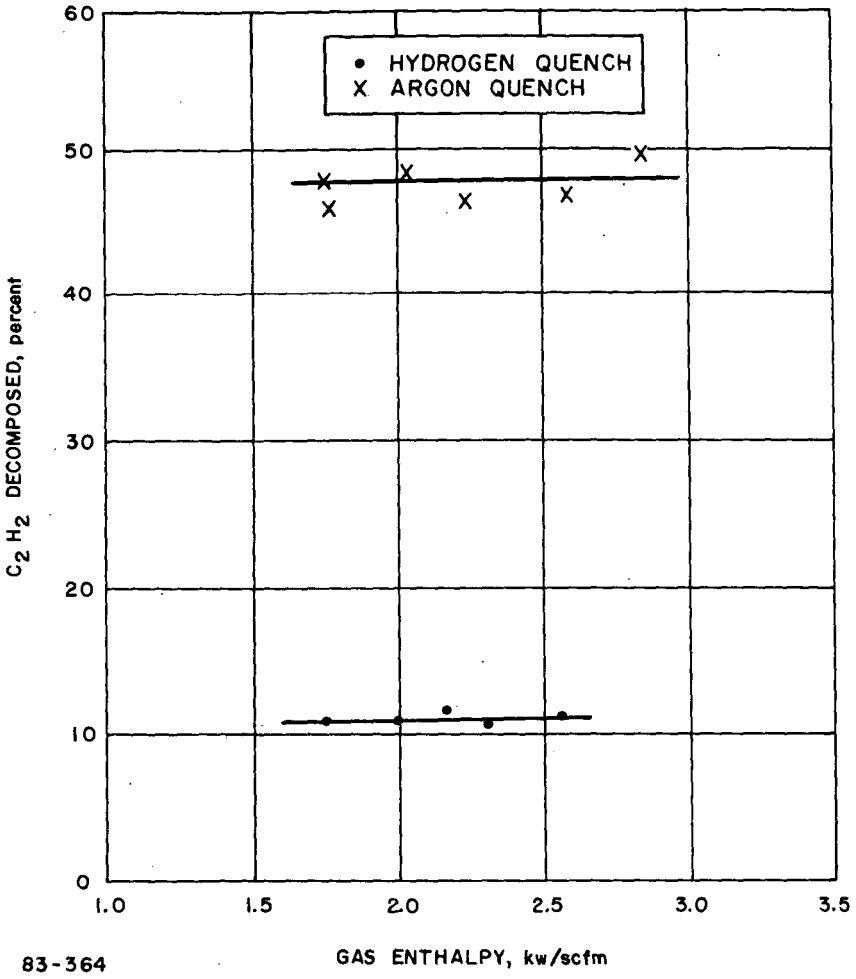

Figure 5 DECOMPOSITION OF ACETYLENE IN QUENCH SIMULATOR

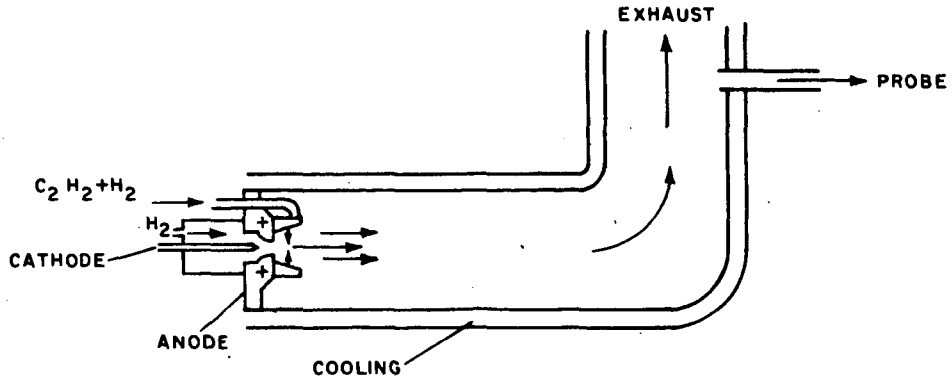

Figure 6 QUENCH SIMULATOR

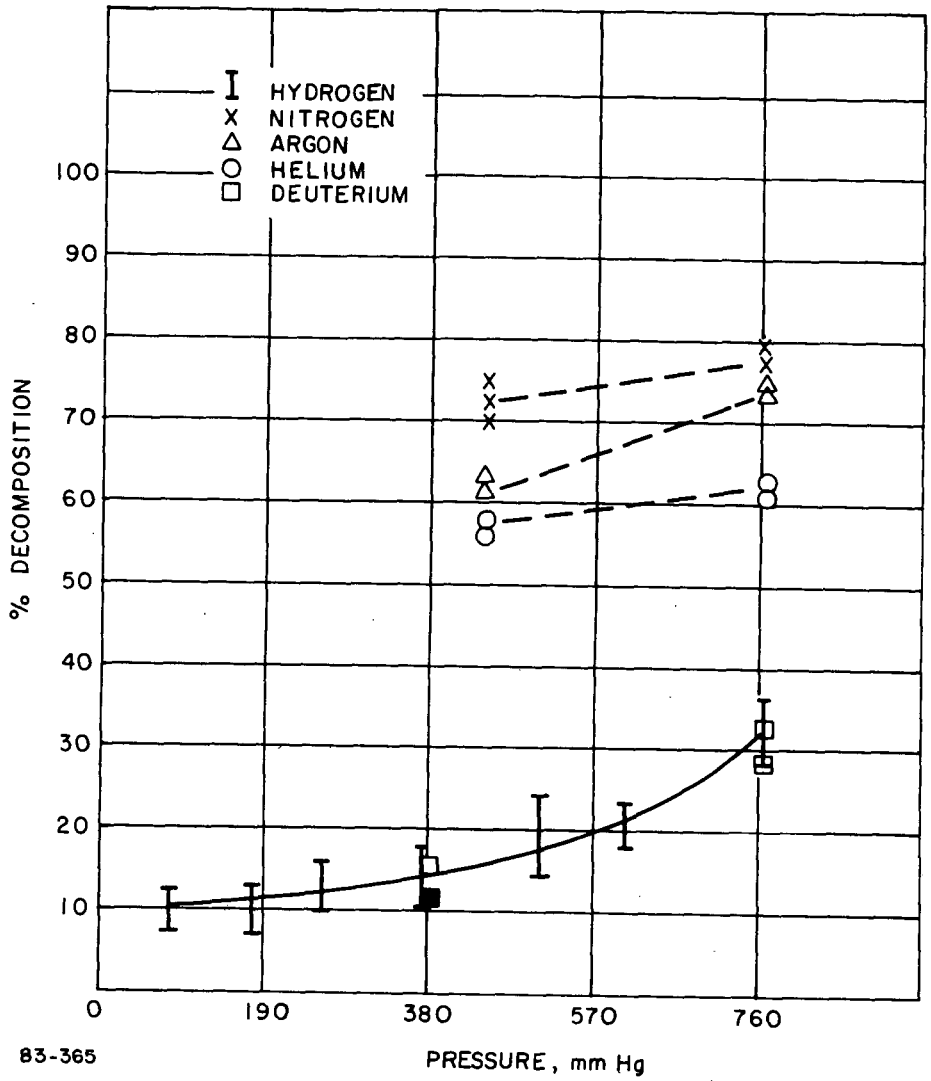

Figure 7 DECOMPOSITION OF ACETYLENE IN VARIOUS GASES

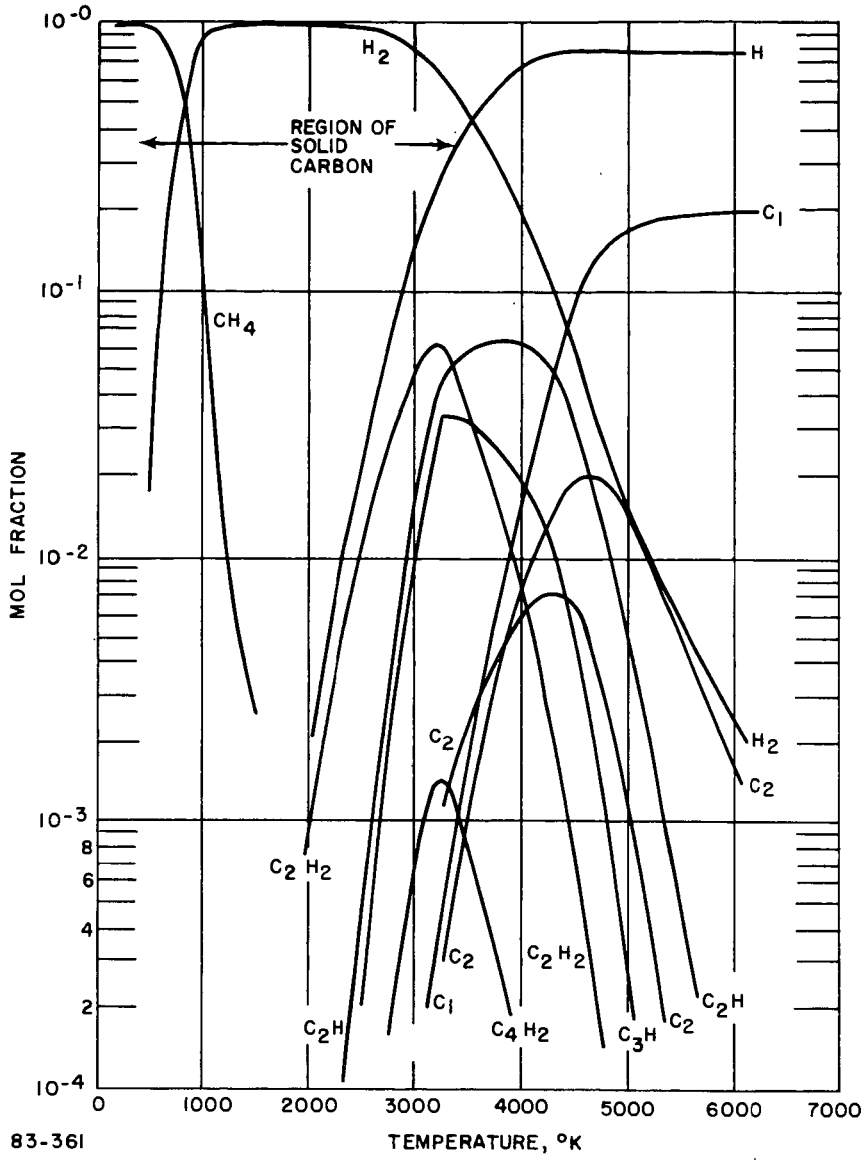

Figure 8 EQUILIBRIUM DIAGRAM FOR CARBON-HYDROGEN SYSTEM AT ONE ATMOSPHERE (C/H = 1/4)

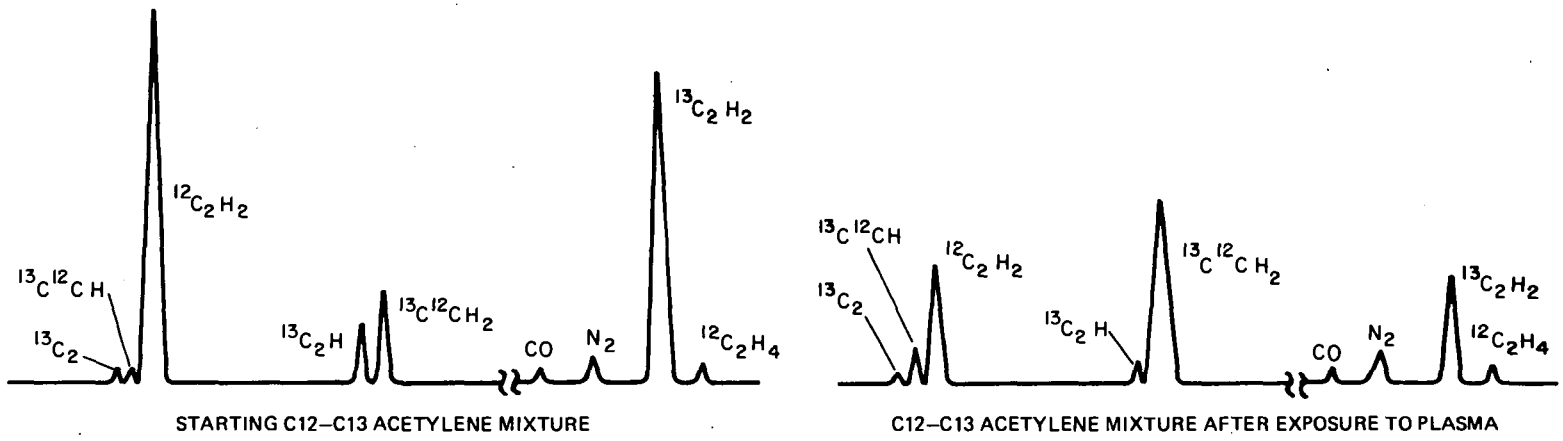

STARTING C12–C13 ACETYLENE MIXTURE

C12–C13 ACETYLENE MIXTURE AFTER EXPOSURE TO PLASMA

83-362

Figure 9 MASS SPECTRA OF ACETYLENE MIXTURE

SYNTHESIS OF HYDROCARBONS BY THE HIGH INTENSITY ARC

Charles Sheer and Samuel Korman

Columbia University, Chemical
Engineering Research Laboratories
New York, New York 10027

This report summarizes some of the results of an investigation into the use of a novel type of arc applied to hydrocarbon synthesis. The principal reacting system was carbon and hydrogen. Later substitutions for the hydrogen were employed in a limited way. These included, in turn, a 50-50 volume percent mixture of CO and H_2, steam, and a solid petroleum residue essentially $(CH_2)_x$.

The type of arc is one which was developed in our laboratory and whose properties for applications of the type reported here we have studied intensively for several years. It is a type of high intensity arc discharge characterized by a number of unique features, of which an important one is the fact that a relatively high rate of continuous through-put of feed material can be achieved. The feed is a fluid, is raised to high temperatures, and itself comprises the plasma environment of the discharge, particularly the electric conduction column maintained between the electrodes. As result it will be appreciated that the composition of the plasma is derived from that of the feed; however, the atomic, molecular, or free radical species comprising the plasma may differ significantly from the molecular composition of the feed.

Distinctive features of the High Intensity Arc

Conventional arcs, consisting of a gaseous electrically

conducting column joining two electrodes, a positive anode and a negative cathode, are used as a source of heat, as for example in electric smelting processes. The mechanism by which heat is usefully transferred to feed materials occurs by radiation and conduction from the hot column. The column is the zone of primary energy dissipation in which the input electrical energy is converted into radiant energy and sensible heat, both of which flow out in all directions through the intervening layer of atmosphere. The maximum temperature which may thereby be achieved and maintained in the surrounding charge is limited by practical considerations to about 2500°C.

In such arcs little if any of the material to be treated enters the energy dissipating region within the arc conduction column itself. The opportunity for successfully accomplishing this became available with the discovery in 1910 by Beck[1] of the type of discharge now known as the "high intensity arc". The use of this type of arc to treat materials to temperatures higher than 2500°C in a continuous and practical manner is one of the central themes of this paper. [2-6]

In the high intensity arc, significant amounts of feed material can penetrate and pass through the conduction column, and are thereby heated with high energy transfer efficiency to very high temperatures; i.e., up to 10,000°K or more. In the early forms of the high intensity arc this was accomplished by incorporating the feed into the anode and allowing the anode to vaporize continuously into the arc. This is suitable however only for the treatment of normally solid feed materials.

Recently a means was developed in this Laboratory whereby the injection of large quantities of gases into the arc column can be made to operate in a practical manner, even for reactive gases. In this modification, the gas is injected from the cathode end rather than through the anode of the discharge, by means of a specially designed annular nozzle surrounding the cathode. This device has been termed the "fluid convection cathode".

Basis of the Fluid Convection Cathode

Referring to Figure 1, the arc column at the cathode is characterized by a converging shape to a small tip at the cathode surface. This convergence, representing an inhomogeneous electric current flux, therefore defines a zone of inhomogeneity in the accompanying magnetic field. This in turn has the effect of producing a fluid mechanical thrust away from the cathode in the direction of the anode, thus giving rise to a pressure gradient away from the cathode tip. To stabilize this gradient, ambient gas is aspirated into the arc column in the region of inhomogeneity. This region represents the only portion of the arc other than the anode crater through which appreciable quantities of gas may be injected without disturbing the stability and maintenance of the arc discharge.

The FCC was developed during an investigation[7] of the influence of gas convection into the base of the arc column near the cathode of a high intensity arc. The technique consists essentially in surrounding the conical tip of the cathode with an annular nozzle which terminates upstream of the tip and which directs the gas in a converging high speed layer into the

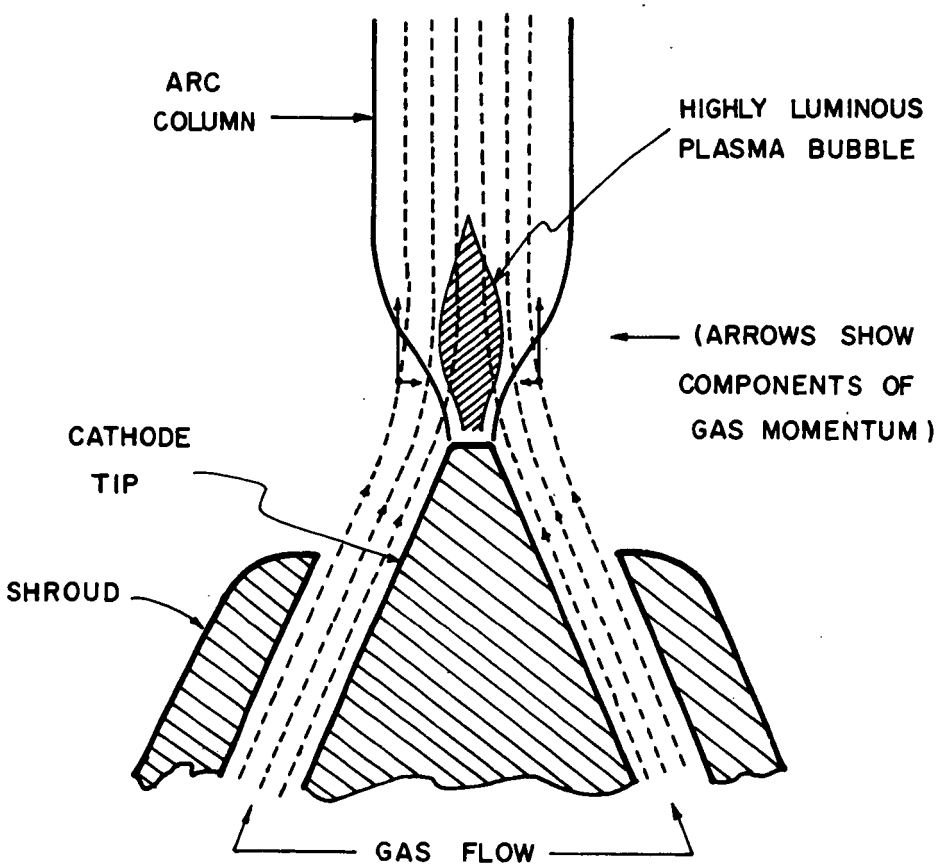

Fig. 1 Sketch of FCC showing compressive effect of gas flow on base of arc column.

column of the arc very close to the point where it originates on the cathode. It was found that if this were done in a manner which causes the gas to impinge on the arc column in the region just in front of the cathode where the column is converging from the broader discharge column, then the gas will preferentially enter the column and can be injected at 10 to 20 times the aspiration rate, whereas, if an attempt were made in the classical manner, to force the gas into the arc column proper in order to energize the gas, such impingement is fruitless and tends to unstabilize and blow out the arc.

Again, with conventional confined arcs, where stability is sought by enclosing the arc discharge within a water-cooled chamber, and forcing the gas into the chamber with the intention of imparting arc energy to it, both theoretical and experimental results have proven that over 70% of the injected gas never enters the column[9], and does not obtain any significant amount of activation energy from the arc.

Experimental Method

Figure 2 is a diagram of the D.C. high intensity arc apparatus, showing an FCC cathode through which the hydrogen gas is injected into the conduction column and a 1" diameter cylindrical carbon anode. The anode has a 1/4" diameter hole along its longitudinal axis. The anode is connected at its back end by 3/16" I.D. metal tubing to a 1-1/6" diameter Type 304 stainless steel tube surrounded by an electrically heated laboratory tube furnace. Leaving the furnace is a water-cooled heat exchanger following a tee-connection valved to permit the gas stream to go in either of two directions: (1) to a flowmeter

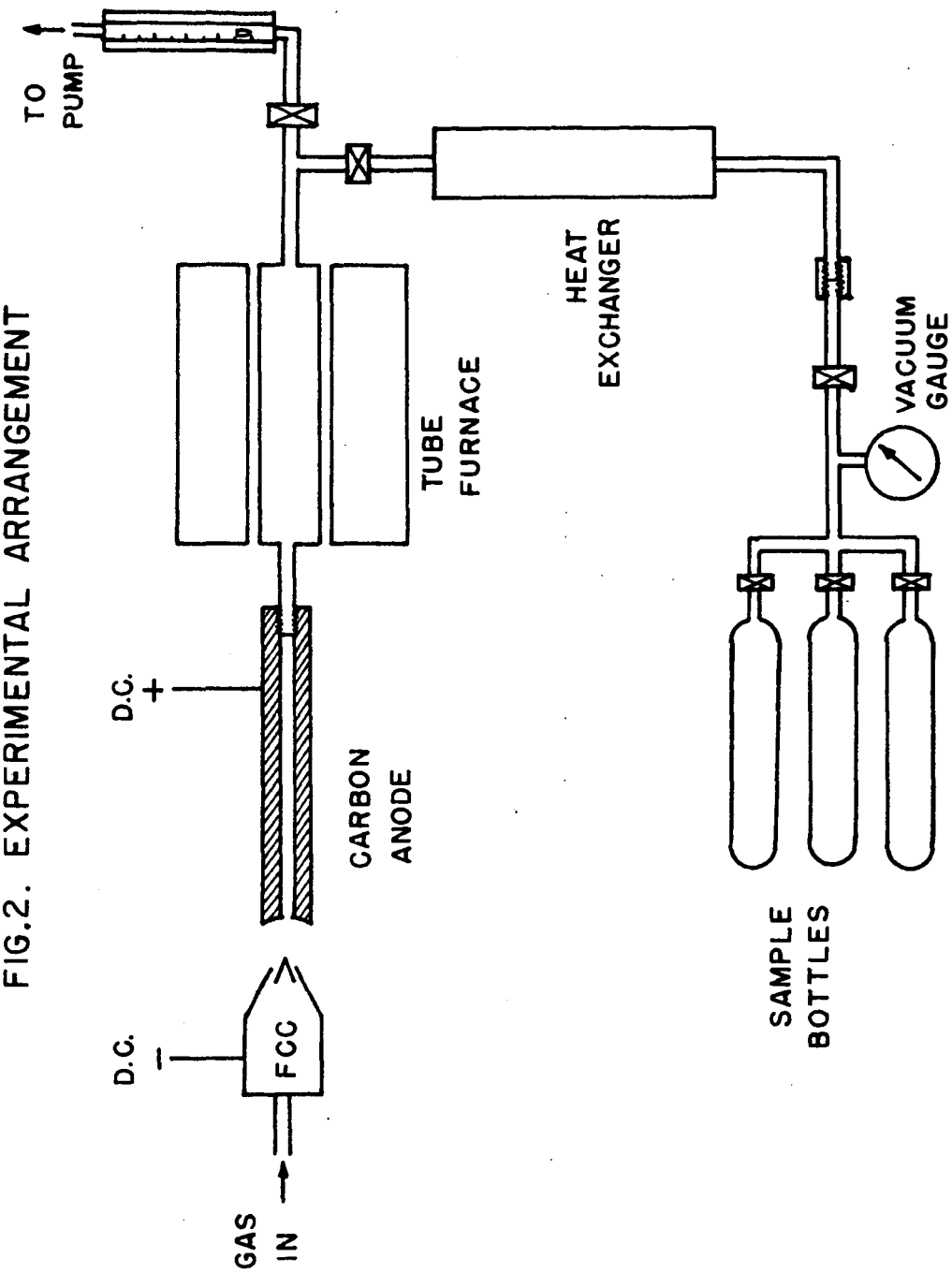

FIG.2. EXPERIMENTAL ARRANGEMENT

and laboratory pump, or (2) to a manifold of a large-dialled mechanical vacuum gauge and several valved 500 cc gas sampling bottles. These are evacuated prior to use. The carbon anode can thus serve as a combination source of solid carbon, and of carbon vapor issuing from the anodic arc terminus into the plasma column, as well as an arc crater gas sampling probe.

Depending upon the pumping flow rate or timed pressure rise in the sampling branch, it is thus possible to draw an arc flame effluent gas stream from the reaction zone through the tube furnace to vary the residence time at any temperature up to about 1000°C, and thence through the heat exchanger and into the sample bottles in sequence.

In operation with diametrically opposed electrodes the FCC arc column bears directly on the carbon anode, which is completely covered by the arc crater at a current of 150 amperes or more. The pump valve is opened sufficiently to meter the plasma down through the anode hole, to purge and equilibrate the effluent hot zone in the tube furnace, and then to meter samples into the gas sampling bottles in sequence at timed rates, measuring the rise period of the vacuum gauge pressure.

Analysis of the samples was carried out by gas chromatography, using helium carrier gas and an air-hydrogen flame in a model 609 F and M Scientific Corporation flame ionization chromatograph with a Poropak Q column. A test gas mixture containing the aliphatic compounds CH_4, C_2H_2, C_2H_4, C_2H_6, C_3H_6, and C_4H_8 was used to calibrate the analytical procedure.

Results

Since the early objectives of the program were primarily

exploratory, the results reported here are essentially qualitative, although within a given test series weight can be given to concentration ratios of components of a test sample mixture for purpose of comparison.

Series I. Hydrogen Flow Rate Through the FCC

This was effected by operating the arc at standard conditions of 150 amperes, maintaining the effluent hot zone at 800°C, sampling at about 30 - 60 seconds per sample, and varying the hydrogen flow rate into the FCC. Comparison of hydrocarbon composition is shown in Table 1, in terms of the relative distribution of the volume concentration of the products found. The distribution was obtained by calculating the percentage contribution which each chromatograph amplitude recording made to the sum of all, in arbitrary scale divisions. There appears to be a significant dependence of effluent hydrocarbon composition upon the amount of hydrogen fed into the FCC.

Series II. Time Factor

In this series, standard conditions of 150 amperes and 8.5 mols per minute of hydrogen were used, with varying sampling rates through the 800°C effluent hot zone. Results are tabulated in Table 2. No other hydrocarbons were observed. These data suggest that methane and acetylene are produced and disappear at different rates.

Series III. Hot Zone Temperature

In this series, standard conditions included 150 amperes, 8.5 mols H_2 per minute through the FCC, sampling rate through the effluent hot zone at 2 1/2 minutes, with variation of the hot zone temperature. Results are shown in Table 3. It is

TABLE I. RELATIVE DISTRIBUTION IN EFFLUENT vs. H_2 FLOW THROUGH FCC

H_2 (MOLES/MIN.)	CH_4	C_2H_2	C_3H_6
3.4	0	100	0
6	4.4	66.2	29.4
8.5	45.6	45.6	8.8
14.1	85	15	0

TABLE 2. RELATIVE DISTRIBUTION vs. SAMPLING FLOW TIME THROUGH HOT ZONE

TIME	CH_4	C_2H_2
10 SECS	44	56
12	75.5	24.5
20	91.5	8.5
30	95.5	4.5
1-1/4 MIN.	93	7
2-1/2	100	0
4	0	0
12	0	0

TABLE 3. RELATIVE DISTRIBUTION vs. HOT ZONE TEMPERATURE

TEMP. °C	CH_4	C_2H_2	C_3H_6
800	100	0	0
500	35	65	0.
400	40	60	0
200	2	87.5	10.5
25	0.5	99.5	0

evident that the hot zone temperature has a significant effect on the hydrocarbon composition of the effluent.

Series IV. Hot Zone Surface Area

Noting the result of increased time of flow in the sampling rate shown above in Series II, and assuming that 8.5 mols H_2 per minute through the FCC creates a steady state for carbon + hydrogen in the plasma at the arc crater, the sampling source, then the time of exposure to the hot zone wall of Type 304 stainless steel was observed. This was accomplished at 150 amperes, 8.5 mols H_2 per minute, and 800°C hot zone temperature, in two diameters of hot zone tubes, 1-1/6" and 9/16", -- a cross-sectional area ratio of 4:1. To equate the sample residence times, the sample flow periods were adjusted to this ratio. Results are shown in Table 4. No acetylene was found in the 9/16" diameter samples, while the small amounts in the 1-1/6" samples were consistent with the distribution for 20 and 30 seconds checked with similar times observed in the earlier Series II above.

Series V. Further Effect of Hot Zone Area

The result of Series IV was followed by further observations comparing hydrocarbon yields and ratios in two cases and at two temperatures, as follows:

A. 1-1/16" diameter at 800° and at 500°C

B. 1-1/16" diameter, into which tube a section of stainless steel wool was added, also at 800° and 500°C.

These conditions were compared, since any effect due to exposure to large surface of stainless steel would not require comparably rapid sampling flow. In other words, the effect of increased

TABLE 4. HYDROCARBON RATIO vs. HOT ZONE SURFACE

DIAMETERS	SAMPLING RATE (SEC)	CH_4 RATIO
9/16 : 1-1/16	80 : 20	1 : 11
	120 : 30	1 : 8

surface area alone could be observed. The hydrocarbon distribution at each temperature with and without added stainless steel wool is shown in Table 5. Table 5 indicates that the preponderance of methane and absence of acetylene is not affected at 800°C. To interpret the apparent shift, however, at 500°C, it is necessary to compare the relative concentrations of all samples. This is shown, in terms of their ratios, in Table 6. It will be noted that the effect of stainless steel hot zone is relatively constant and appreciable for the times and temperatures of exposure. At 800°C, no acetylene is present, as expected, for reasons of temperature, as shown in Table 3 above, while at 500°C, the time-related suppression of acetylene previously observed in Table 2 above is also seen to be more strongly enhanced by the increased stainless steel surface area. We interpret this to mean that acetylene disappears much more rapidly than methane under these conditions, and that the disappearance is related to the surface area of the stainless steel hot zone.

Series VI. Effect of Hot Zone Surface Composition

Noting that the time-related suppression of methane and acetylene appeared to suggest a hot zone surface effect when stainless steel was used, this material was replaced by several others, using tubes of 1-1/16" diameter. Arc crater gas samples taken under otherwise identical conditions (viz., 150 amperes, 8.5 mols H_2 per minute, hot zone temperature 800°C, parallel sampling flow rates) produced hydrocarbon compositions as shown in Figures 3 through 6.

In the case of fused silica, it is seen in Figure 3 that

TABLE 5. HYDROCARBON DISTRIBUTION vs. SURFACE AREA

SAMPLING TIME (SECS)	800°C				500°C			
	WITHOUT ST.ST. WOOL		WITH ST. ST. WOOL		WITHOUT ST.ST. WOOL		WITH ST. ST. WOOL	
	CH_4	C_2H_2	CH_4	C_2H_2	CH_4	C_2H_2	CH_4	C_2H_2
30	94	6	100	0	18	82	84	16
150	100	0	100	0	35	65	100	0

TABLE 6. RATIO OF HYDROCARBON CONCENTRATIONS IN SAMPLES

SAMPLING TIME (SECS)	800 °C RATIO +/-		500 °C RATIO +/-	
	CH_4	C_2H_2	CH_4	C_2H_2
30	1/1.3	0/0	1/1.7	1/27
150	1/4	0/0	1/ 4.8	1/200

NOTE: + = WITH STAINLESS STEEL WOOL

— = WITHOUT STAINLESS STEEL WOOL

FIG. 3. SILICA

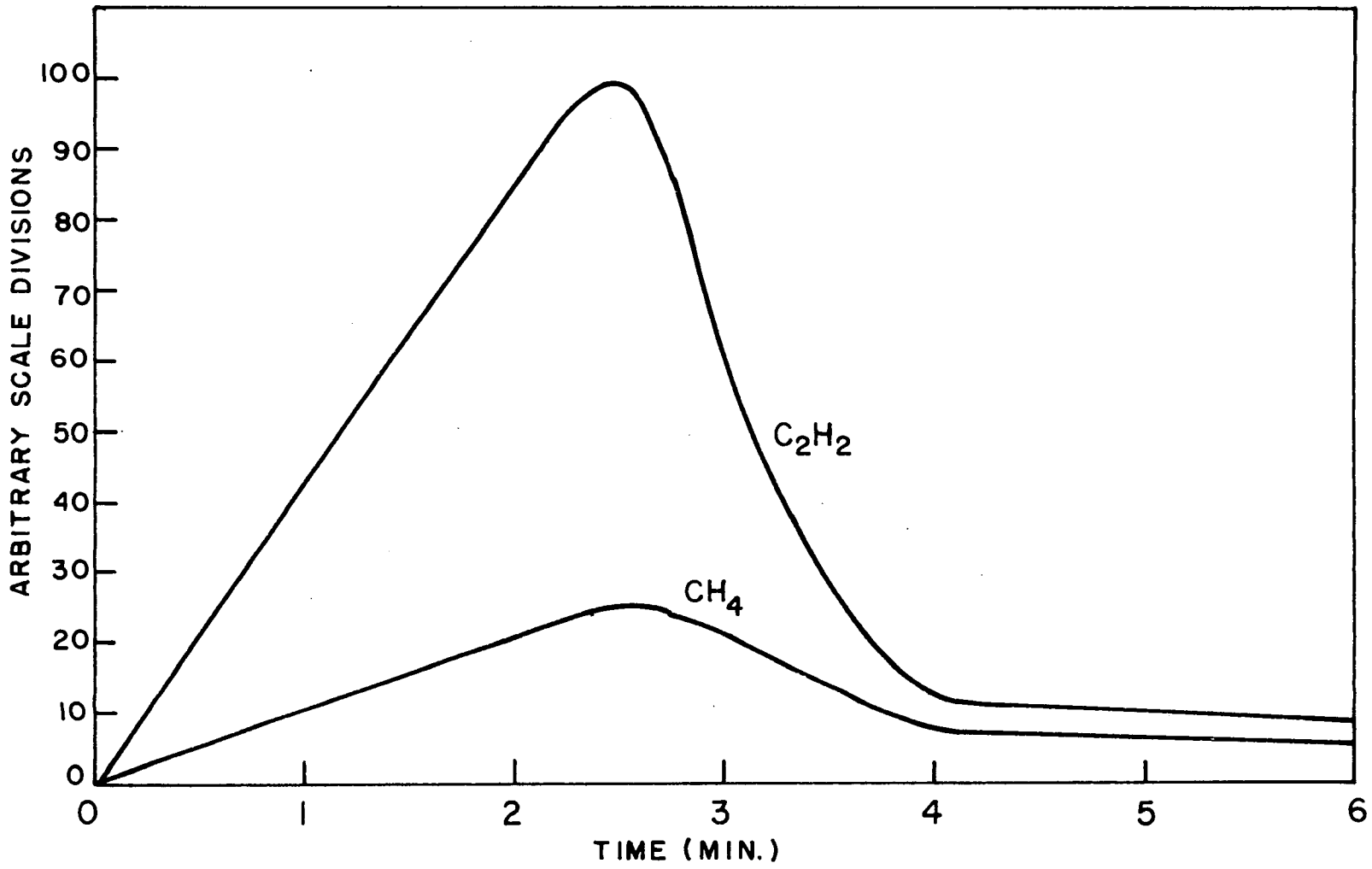
ARBITRARY SCALE DIVISIONS
100
90
80
70
60
50
40
30
20
10
0
0
1
2
3
4
5
6
TIME (MIN.)
C_2H_2
CH_4

FIG. 4. IRON

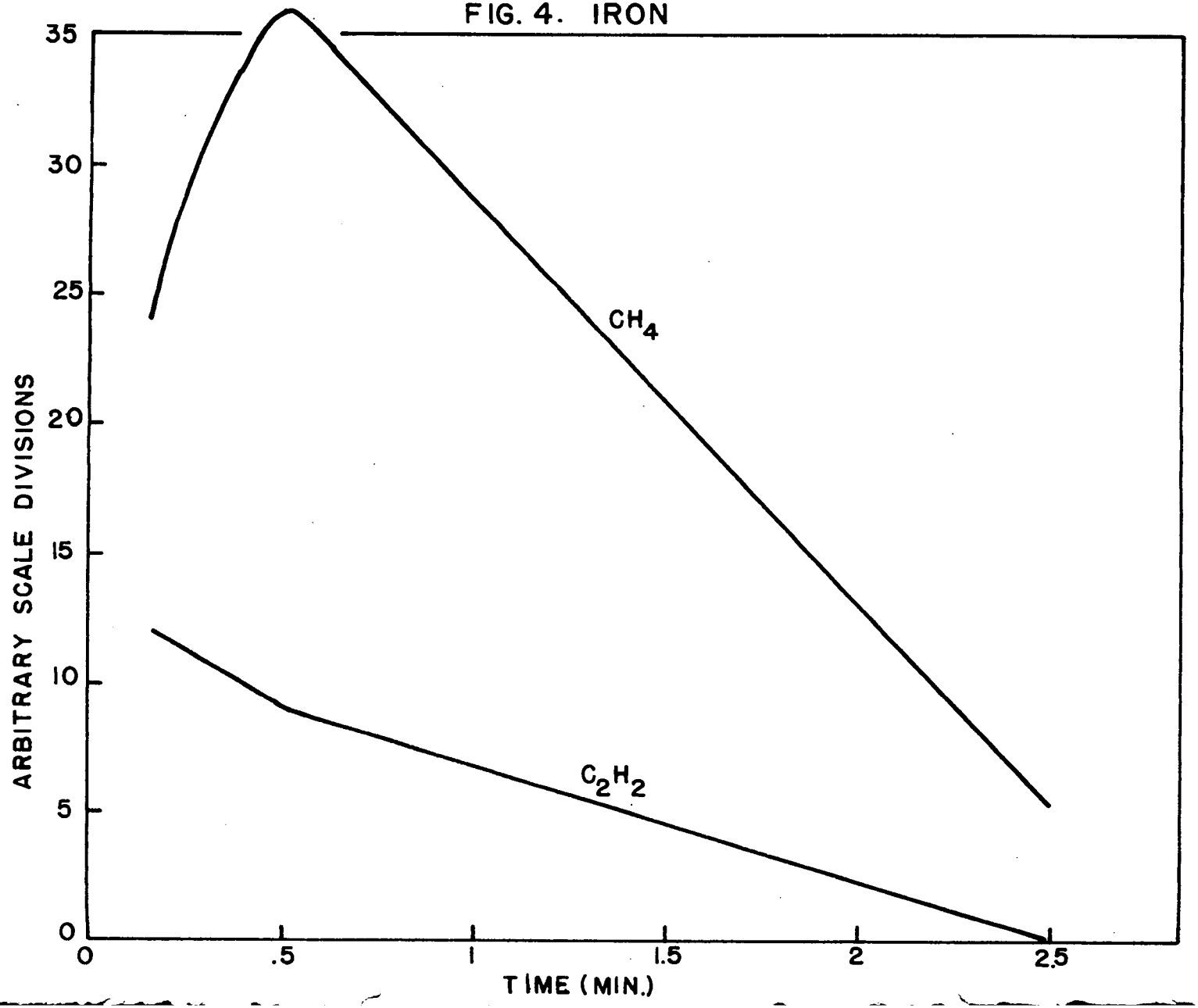
35
30
25
20
15
10
5
0
ARBITRARY SCALE DIVISIONS
CH_4
C_2H_2
0
.5
1
1.5
2
2.5
TIME (MIN.)

FIG. 5. STAINLESS STEEL TYPE 304(8%Ni,74%Fe)

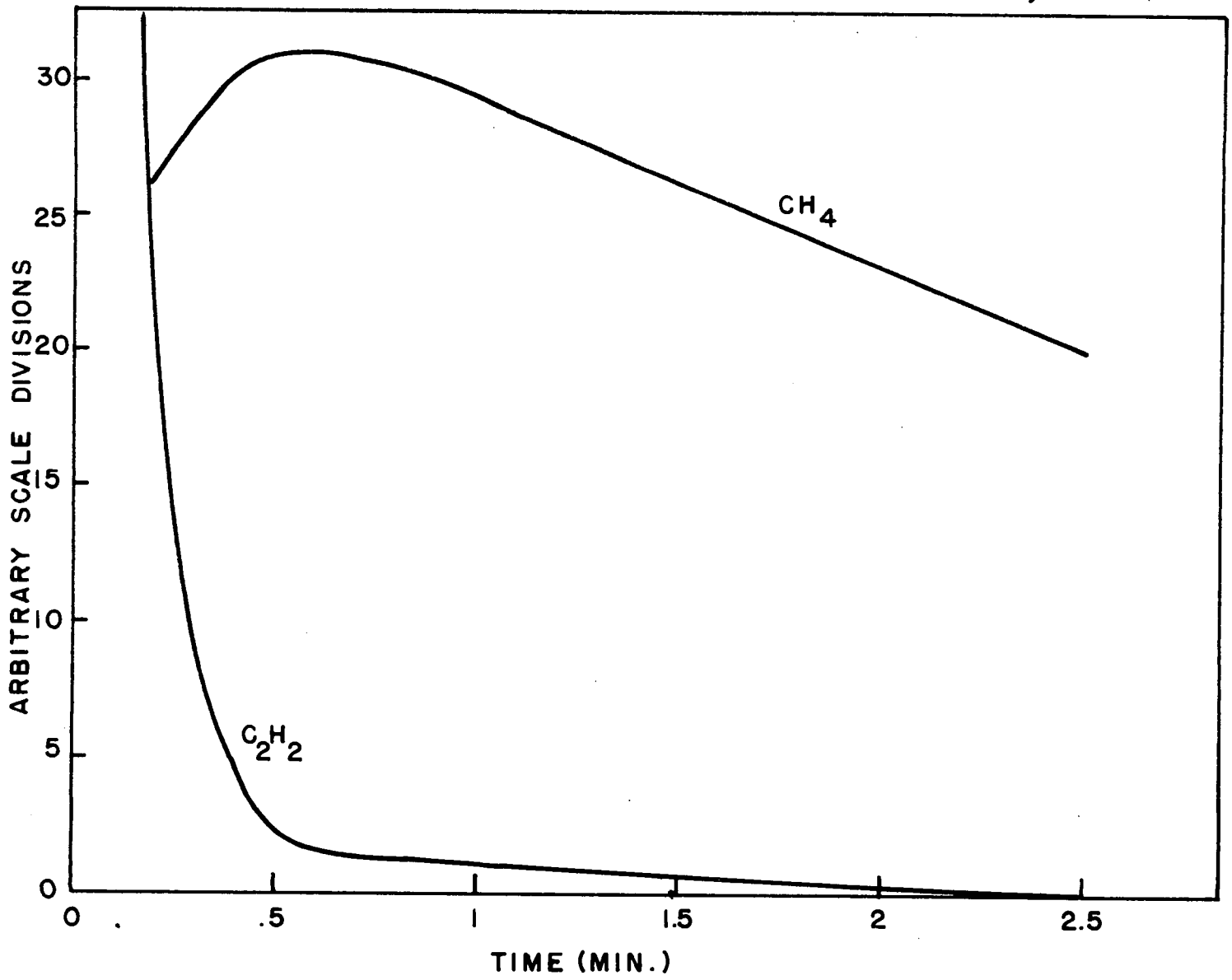

FIG. 6. INCOLOY 800(32 % Ni, 46 % Fe) ; Ni-200(99.5 % Ni)

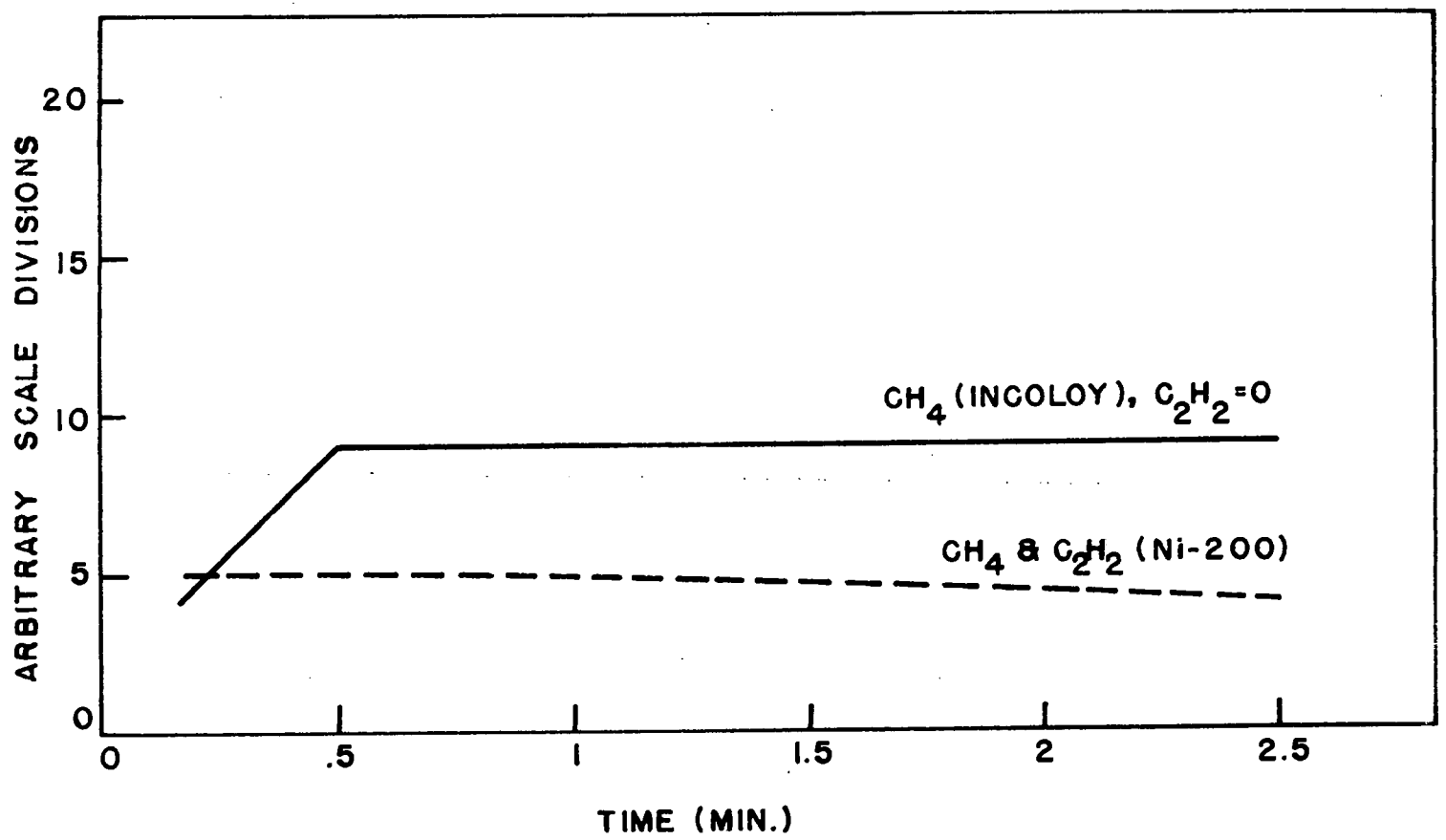

the time of exposure in the 800°C hot zone has roughly parallel effects upon the presence and disappearance of both methane and acetylene.

This is in contrast with iron (Figure 4) and Type 304 stainless steel (Figure 5), where acetylene disappears rapidly while methane persists.

Increasing the nickel content by the use of Incoloy 800 (32% Ni, 46% Fe) and Nickel-200 (99.5% Ni) appears to produce further suppression of both acetylene and methane, -- an effect which does not appear to be especially time-sensitive.

Some Results with Other FCC Gas Feeds

Preliminary tests were carried out in which substitution was made for hydrogen as the FCC-injected gas. The first substitute was a H_2 - CO 50-50 volume percent mixture. The usual standard test conditions were employed, except that the gas volume flow rate was set to a value which included a relatively small amount of hydrogen (0.6 mol per minute). The results shown in Table 7 compares the (interpolated) analog distribution resulting from the same amount of pure hydrogen alone with the distribution using the mixture with CO. The absolute amount of acetylene in the CO - H_2 mixture tests also increased with time whereas the acetylene in the low rate pure hydrogen analog diminishes rapidly and no hydrocarbon was found after 10 seconds.

The next FCC gas used was steam, with corresponding results shown in Table 8. In comparing absolute concentrations by measuring chromatograph deflection amplitudes, the total product yield of hydrocarbon was found to have increased with increasing

TABLE 7. HYDROCARBON DISTRIBUTION: $(CO+H_2)$ vs. H_2

SAMPLE TIME	$(CO+H_2)$	H_2
	$CH_4 : C_2H_2 : C_3H_6$	
10 SECS	30 : 60 : 10	100 % C_2H_2
30	40 : 60	0
2-1/2 MIN	16 : 81 : 3	0

TABLE 8. HYDROCARBON DISTRIBUTION RATIO FOR FCC-STEAM+CARBON ANODE

STEAM GMS/MIN	CONTAINED H (GM/MIN)	SAMPLE TIME	DISTRIBUTION RATIO CH_4 : C_2H_2
2	.22	30 SEC	5 : 4
2	.22	90	3 : 5
4	.44	10	8 : 1
4	.44	30	CH_4 ONLY
6.3	.7	10	4 : 1

flow rate of steam. As with the water gas tests, short time intervals with steam produced appreciable methane under conditions which would have yielded only a small amount of acetylene or no hydrocarbons, if the same amount of contained hydrogen were fed as pure H_2 in equivalent rates to the FCC arc.

Solid Carbonaceous Feed

Finally, preliminary tests were carried out in which a powdered solid was entrained in argon and injected into the FCC arc. The solid was a petroleum refinery "bottom" having a softening point of 327°F and an approximate composition of $(CH_2)_x$. The argon was chosen as a neutral carrier to avoid ambiguity concerning the source of hydrogen in the product. For simplicity, no effluent hot zone was used, and so the sample gas was considered as being quenched to room temperature. As expected, in every instance the hydrocarbon product was preponderantly acetylene, although there were traces of methane also.

Discussion

Based upon the results of the tests described above, it is suggested that two distinct sets of processes are operative. One involves the phenomena within the arc and the other relates to the conditions to which arc-generated gases are exposed in the effluent stream.

Exploratory as this investigation is to this point, it affords no evidence which discloses the undoubtedly complex mechanisms underlying the observed effects. However it seems reasonable to assume that a time-related catalytic effect exists which is related to the composition and temperature of the hot

zone surface to which the arc sample effluent was exposed. The rapid transition in hydrocarbon composition from acetylene to methane in the presence of iron or stainless steel is one indication. Thermal effects and increased residence time in the presence of hydrogen were shown to lead to progressive diminution and disappearance of hydrocarbons, suggesting another slower process which may be pyrolytic or possibly inhibitory.

It is submitted, also, that effects which occur within the hot zone are not necessarily independent of the arc reactions. The composition of the effluent which leaves the arc crater and enters the hot zone has an important effect upon the ultimate product composition. For example, the contrast, under otherwise identical test conditions, which is evident as substitution was made for pure hydrogen as the FCC gas feed produced a noteworthy change. With a mixture of CO and H_2, or H combined with O as steam, hydrocarbons were produced with appreciable or major fractions of methane, where pure hydrogen yielded only small amounts of acetylene or no hydrocarbons at all. One may infer that the presence of CO or O within the plasma possibly alters the course of the reaction, and hence the effluent composition.

From our basic studies of FCC gas injection[8] into the arc conduction column, together with concurrent temperature measurements, it is fairly certain that upwards of 80% of the injected gas penetrates the column and uniformly reaches temperatures in the range of 10,000° - 20,000°K. Our current investigations of this arc, using hydrogen as FCC gas feed and a carbon anode, indicates clearly that the hydrogen in the arc conduction

column approaching the anode is monatomic. We are presently studying the plasma composition in front of the anode crater, where this monatomic hydrogen is mixing with or impinging upon carbon at its sublimation temperature. The objective of identifying the plasma species in this zone, with hydrogen and ultimately with H_2 + CO or with steam, offers the possibility of determining how the ultimate quenched effluent composition, as well as the function of the secondary species, such as CO or O, in altering the process, may be predicted.

Additionally the exposure of a carbonaceous solid into this plasma, producing acetylene in accordance with expectation, indicates in a preliminary way the probability of employing these arcs effectively for gasification involving coal or other carbonaceous feeds.

Summary

A novel type of arc discharge, the FCC high intensity arc, employing a carbon anode and a cathode designed to afford effective enhanced introduction of hydrogen-bearing gas feeds into the arc conduction column, was employed to study the synthesis of hydrocarbons. In the temperature range of this arc, -- that is, 10,000° - 20,000°K -- in the cathode conduction column, the hydrogen is monatomic and impinges on the carbon anode at its sublimation temperature (about 4000°K) in the arc crater.

Gas samples, drawn from this region during standard arc operation, were found by gas chromatography to contain hydrocarbons. The composition of these depended upon the flow rate of hydrogen fed into the arc column, the temperature and resi-

dence time of the arc effluent in a downstream hot zone, and the wall composition of the hot zone. Hydrogen, though always in excess of stoichiometry, caused a transition in the hydrocarbon product ranging from 100% acetylene, at low flow rate (3.4 mols H_2/min) to mixtures of methane and acetylene with occasional presence of propylene, becoming predominantly methane at high flow rates (14.1 mols H_2/min) for intermediate residence times (about 30 seconds) at 800°C in a Type 304 stainless steel hot zone. Shorter residence times (about 10 seconds) with adequate hydrogen (8.5 mols/min) at 800°C in stainless steel hot zone produced hydrocarbon mixtures which were predominantly acetylene. The effect of residence time thus also showed a transition in hydrocarbon composition from 100% acetylene at 10 seconds to 100% methane in from 30 seconds to 2-1/2 minutes.

Under the same test conditions, a similar transition was observed when the hot zone wall was iron instead of Type 304 stainless steel. When the wall was Incoloy 800 (32% Ni, 46% Fe) and Nickel-200 (99.5% Ni) both hydrocarbons were substantially suppressed regardless of residence time. With a fused silica wall, mixtures of acetylene and methane appeared in all time intervals.

In the transitional cases, acetylene diminished from the product time samples, dropping rapidly from 10 seconds and disappearing in 2-1/2 minutes, while methane rose to a maximum in 30 seconds and slowly diminished. No hydrocarbons were found after 4 minutes. With silica, both acetylene and methane

rose and diminished in parallel manner to constant low levels after 2-1/2 minutes, persisting after 6 minutes.

The effect of temperature in the hot zone was studied with the stainless steel wall at a residence time of 2-1/2 minutes. At 800°C, the only hydrocarbon produced was methane. At 25°C the product contained acetylene with a trace of methane. Intermediate temperatures produced mixtures of the two in transitional proportions.

Substitution of 50-50 volume percent mixture of CO and H_2 for pure H_2 for FCC-injection produced hydrocarbons which were mixtures of methane and acetylene (with a small amount of propylene in one 10-second sample), whereas the same fractional volume flow rate of contained hydrogen, if fed as pure hydrogen alone, would have produced only a small amount of acetylene or no hydrocarbons at all.

When steam was substituted for hydrogen into the FCC arc the principal hydrocarbon component was methane, increasing in proportion to acetylene with increasing steam flow, whereas, again, the equivalent H, if fed as pure hydrogen, would have shown a small amount of acetylene or no hydrocarbons.

A solid pulverized petroleum residue corresponding to $(CH_2)_x$, fed entrained in argon into the FCC, produced acetylene predictably under conditions corresponding to the analogous H_2 feed.

Two processes are believed to participate in determining the hydrocarbon composition of the effluent product. One process is thought of as interaction of the feed materials within

the arc column at the anode crater, transformed into high temperature plasma species. The resultant composition is believed to influence the course of the second process which is a time- and temperature-related catalysis occurring in a downstream hot zone, leading to the final effluent composition. Upon further exposure to the hot zone, the over-all quantity of hydrocarbons in the effluent diminishes. This is believed to be related principally to the temperature of the hot zone, as evidenced by the collateral diminution of acetylene and methane at 800°C in a fused silica hot zone. Differential transition from acetylene to methane occurred in the cases of iron and Type 304 stainless steel, and a time-independent constant suppression of both methane and acetylene was obtained when the hot zone wall at 800°C was either Incoloy 800 (32% Ni, 46% Fe) or Nickel-200 (99.5% Ni).

Preliminary tests with pulverized solid $(CH_2)_x$ entrained in argon and fed into the FCC arc, as well as the alteration in favor of methane in the steam cases, lend support to the belief that these results with the FCC high intensity arc may lead to practical applications in the gasification of coal and other carbonaceous feeds.

Acknowledgement

The authors are endebted to the Consolidated Natural Gas Service Company and to the Plasma Research Fund for support of this investigation, and to Dr. Robert C. Weast for his interest and encouragement. Basic investigation of the fluid convection cathode was carried out under the sponsorship of the Aero-mechanics Division, Air Force Office of Scientific Research, Contract No. F44620-69-C-0104.

References

1. Beck, H., Elektrotech. Zeit. 42, 1921, p. 993.

2. An informative discussion of the regions of the low intensity arc is given in The Electric Arc, by J. M. Somerville, John Wiley and Sons, N. Y., 1959, p. 5 et seq.

3. For further details on energy dissipation see "Arc Jets in Science and Technology", by Charles Sheer, Chap. 7 in Vistas in Science, ed. by D. L. Arm, Univ. of New Mexico Press, 1968 p. 140 et seq.

4. Finkelnburg, W., Der Hochstromkohlebogen, Springer, Heidelberg, 1948.

5. Sheer, C. and Korman, S., "The High Intensity Arc in Process Chemistry", in Arcs in Inert Atmosphere and Vacuum, ed. by W. E. Kuhn, John Wiley and Sons, N. Y. 1956, p. 175 et seq.

6. Sheer, C., Korman, S., Stojanoff, C. G., and Tschang, P.S., Final Scientific Report, AFOSR 70-0195, Mechanics Division, Air Force Office of Scientific Research, p. 33 et seq.

7. To be published. Investigation supported by Aeromechanics Division, Air Force Office of Scientific Research.

8. To be published. Investigation supported by Aeromechanics Division, Air Force Office of Scientific Research.

9. Emmons, H. W., "Recent Developments in Plasma Heat Transfer", in "Modern Developments in Heat Transfer, Warren Ibele, ed., Academic Press, New York, 1963, p. 465 et seq.

THE REACTION OF ATOMIC HYDROGEN WITH CARBON

Alan Snelson
IIT Research Institute
Chicago, Illinois 60616

ABSTRACT

A thermally produced beam of atomic hydrogen was reacted on a carbon target at temperatures between 30-950°C. The reaction products were isolated on a liquid helium cold finger and subsequently analyzed by gas chromatography. Over the temperature range examined the major reaction products were: $CH_4 \approx 91\%$, $C_2H_6 \approx 8.4\%$, $C_3H_8 \approx 0.6\%$. C_2H_4, C_3H_6 and C_4 hydrocarbons were minor constituents, if formed at all. Hydrocarbon formation increased with temperature, no maximum in the yield occurring at about 770°K as reported in previous studies. The methane yield-temperature dependence showed three distinct phases and activation energies were obtained. At 30° and 950°C, about 1% and 3% respectively, of the available H atoms reacted with carbon to form hydrocarbons.

INTRODUCTION

The discovery that H atoms react with carbon was made by Avramenko (1) in 1946. To date the results of ten other studies have been reported (2)-(11). In all but one investigation, H atoms were produced by electric discharge techniques; the one exception (7) using thermal methods. Chemical analyses of the reaction products were attempted with varying degrees of sophistication in all except one study (5). Agreement between the different investigations as to the hydrocarbons formed in the H atom-carbon reaction is not good, some or all the following have been reported: CH_4, C_2H_2, C_2H_4, C_2H_6, C_3H_8 and various butanes and butenes. Several authors believe that methane is the primary reaction product, with higher hydrocarbons resulting from hydrogen abstraction reactions and free radical recombination processes. There is some indication that the formation of acetylene and ethylene may be associated with ionic species formed in the electric discharge used to produce the atomic hydrogen. In some of the experimental studies the products reported as being formed in the H atom-carbon reaction could also have arisen by H atom attack on organic materials, vacuum grease and O-rings, which were part of the system. Most investigations of the H atom-carbon reaction were made at ambient temperatures, but in two cases (8,9) where an extensive temperature range was investigated, a maximum in

the hydrocarbon yield was reported at 770 $\pm$ 50°K. In two kinetic studies (6,9) on the reaction, data were obtained for the rate of carbon removal as a function of temperature and H atom concentration, but no effort was made to correlate these data with the hydrocarbon production.

In this investigation, the H atom-carbon reaction has been re-examined in an effort to determine; 1) the nature of the hydrocarbon products, 2) the yields of hydrocarbon products as a function of temperature and, 3) the efficiency of conversion of atomic hydrogen to hydrocarbons.

EXPERIMENTAL

In designing the experimental arrangement for studying the H atom-carbon reaction, an effort was made to avoid some of the features which may have vitiated the results obtained in previous studies. E.g. Possible pyrolysis of the reaction products, reaction between H atoms and O-rings or vacuum grease, and reaction between hydrogen ions and carbon. To attain these goals, a low pressure atomic hydrogen beam carbon reactor was constructed utilizing a liquid helium cold finger to remove reaction products. This is shown schematically in Figure 1. All materials used in the construction of the reactor were either metal, (copper, brass, Kovar and stainless steel) or glass. Demountable joints were soft soldered using an inorganic flux and all surfaces were acid cleaned prior to assembly. A mechanical vacuum pump

and oil diffusion pump were used to evacuate the system, and pressures in the 10^{-6} mm range were routinely achieved.

Hydrogen atoms were formed by thermal low pressure (10^{-7}-10^{-5}) atm. dissociation of molecular hydrogen in a tungsten effusion tube. The effusion tube, 0.067" O.D. and 0.030" I.D. was heated over 2" of its length to a temperature of 2600 $\pm$ 50°K by electrical induction. The temperature was measured with a Leads Northrop optical pyrometer with emissivity corrections being made. To increase the probability of equilibrium being attained within the tungsten effusion tube for the chemical reaction $H_2 \xrightarrow[\text{Temp.}]{\text{High}} 2H$, three tungsten wires about 1" long and 0.010" diameter were inserted into the bore of the tube to help increase residence times. Matheson Research Grade hydrogen was used in the study and was stored in a glass vacuum line prior to use. The flow rate of hydrogen to the effusion tube was controlled by varying the gas pressure across a fixed leak. Hydrogen flow rates to the effusion tube varied from 0.5 to 9 x 10^{-5} moles hour^{-1}. In most experiments a rate of 2 x 10^{-5} moles hour^{-1} was used. The amounts of gas being fed to the reactor were determined from P.V.T. data using standard vacuum line techniques. These hydrogen flow rates correspond to pressures of the order 5 x 10^{-7} to 2 x 10^{-5} atm at the lowest and highest flow rates, respectively. At the most commonly used hydrogen feed rate (2 x 10^{-5} moles hour^{-1}) the pressure in the effusion tube was approximately 4 x 10^{-6} atm. Using data

given in the JANAF Tables, (12) it may be shown that at this pressure the resulting effusate is essentially pure atomic hydrogen. At the highest experimentally used effusion tube pressure (2×10^{-5} atm.) the effusate was $\gtrsim$98% atomic hydrogen.

The carbon used in the H atom-carbon reaction was obtained from the Ultra Carbon Corp., Michigan. It had a certified purity of 99.9995% and a density of 1.72 g. $cm.^{-3}$ and was in the form of a solid cylinder, 1" long x 1" diameter. In the reactor, the carbon was mounted in a steel holder on the same axis as the tungsten effusion tube and 2-5/8" from it, presenting the H atoms with a flat target surface of 1" diameter. The carbon target, was heated by four Waltow cartridge heaters of 100 watts each, and the temperature controlled by varying the applied voltage across the heaters. A chromel-alumel thermocouple, inserted into the carbon target with the temperature sensing junction about 1/16" from the reaction face, was used to measure the target temperature. The thermocouple output was measured against that of an ice junction using a Leeds Northrop potentiometer. Target temperatures were constant to $\pm$ 2°C in experiments which usually lasted one hour. A maximum target temperature of about 1000°C was possible and prior to use in the H atom-carbon reaction, the carbon was outgassed at 950°C for three days under vacuum.

The glass liquid helium cold finger used to freeze out reaction products was about 2" diameter and had a capacity of

1 liter. To minimize heat leakage it was surrounded by a liquid nitrogen heat shield. All surfaces in the Dewar system were silvered. After an experiment the cryogenic fluids were removed from the cold finger and the system warmed to room temperature. The reaction products were then removed by a Toepler pump and their total volume measured. During this process the temperature of the carbon target was maintained at 200 $\pm$ 20°C to help minimize adsorption of gas. Provision was made in the collection section of the vacuum line to raise the pressure of the collected sample to slightly above ambient. This was done to help improve the reliability of the gas sampling for chromatographic analysis.

Gas samples from the H atom-carbon reaction were analyzed on a Varian-Aerograph gas chromatograph, Model 1800. A 6 ft. long, 1/4" diameter stainless steel column packed with 216 grams of a 'Poropak' Q stationary phase was used for separating the various hydrocarbons. The column was used isothermally (60°C) for the analysis of CH_4, C_2H_4 and C_2H_6. For higher hydrocarbons the column temperature was programmed at 10°C min^{-1} for six minutes and the column then kept isothermal at 120°C. With this chromatograph, the detection of 10^{-11} moles of a simple hydrocarbon was attainable. Prior to every analysis, the calibration of the chromatograph was checked against injections of known volumes of methane and ethylene. In a typical experiment, 0.15 cc of the collected gas from the atomic hydrogen-carbon reactor was injected

into the chromatograph resulting in hydrocarbon yields of the following magnitude; CH_4 = 4-18 x 10^{-8} moles, C_2H_4 = 1-2 x 10^{-9} moles, C_2H_6 = 3-7 x 10^{-9} moles, C_3H_6 = 0.5 - 2 x 10^{-10} moles, and C_3H_8 = 2-5 x 10^{-10} moles. The over-all accuracy of the measured hydrocarbon yields is believed to be about $\pm$ 7%.

RESULTS AND DISCUSSION

Operating Characteristics of the Reactor, Without the Carbon Target

The reactor, without the carbon target in place, was exposed to H atom attack using a hydrogen flow rate to the reactor of $\approx$2 x 10^{-5} moles hour^{-1}. The resulting product gases were analyzed chromatographically. The following species were found; CH_4, C_2H_4, C_2H_6, C_3H_6, C_3H_8 and traces of butanes and butenes. These findings were surprising since great efforts were made to remove organic materials from all reactor surfaces prior to assembly. The reactor was disassembled and all surfaces inspected and recleaned. On reassembly and subjection to H atom attack, hydrocarbons were again produced. The effect of exposing the reactor to H atom attack over prolonged periods of time was therefore studied. Samples of the reaction products were analyzed periodically.

Data obtained from these experiments are given in Table I. To permit comparison between different experiments, reaction product yields are all quoted in terms of moles of

hydrocarbon formed per mole of molecular hydrogen fed to the reactor at the stated molecular hydrogen feed rate to the reactor. Quantitative yields for the C_4 hydrocarbons are not given in Table I since their amounts were too small for meaningful analysis. In Figure 2 the methane yield as a function of time is presented from the data given in Table I with a hydrogen feed rate to the reactor of 2×10^{-5} moles $hour^{-1}$. It is at once apparent that the yield of methane decreases quite markedly with the number of hours of H atom attack,(conditioning) and after some 60-80 hours appears to reach a constant minimum. The production of C_2H_4, C_2H_6, C_3H_6 and C_3H_8 all showed the same type of behavior as methane with respect to yields as a function of H atom conditioning time. After some 60-80 hours a stable minimum was attained for all species. The reactor was disassembled, inspected, and surfaces cleaned, and re-assembled. The hydrocarbon yield as a function of H atom conditioning time was re-investigated. The same type of behavior resulted as in the prior experiments, a moderate initial hydrocarbon yield,decreasing with time after some 60-80 hours to the same value as obtained previously. Conditioning was continued for a total of 150 hours without any further change in the hydrocarbon yield occurring. In Table II the stable hydrocarbon yields obtained after prolonged H atom conditioning of the reactor are given.

From these data it is necessary to conclude that despite all efforts to maintain reactor cleanliness, the system was contaminated with carbon or organic material. The initial relatively large production of hydrocarbons obtained directly after assembling the reactor could have resulted from hydrogen atom attack on freshly adsorbed carbon species, CO, CO_2 and possibly some hydrocarbons, on the inside of the reactor after exposure to the laboratory atmosphere. The apparently smaller constant yield of hydrocarbons obtained after prolonged hydrogen atom attack suggests the presence of a fairly large though not particularly accessible supply of organic material. There are two possible sources: 1) carbon in the steel used in fabricating some parts of the reactor, and 2) organic material trapped during the formation of the silver reflective coating on the liquid helium Dewar. (The latter coatings are prepared by the reduction of ammonical silver solutions with sugar). In view of the large silvered surface area of the liquid helium dewar $\approx$5000 cm^2, a small amount of trapped organic material in the silver coating could well be the major source of organic contamination in the reactor.

After establishing that a small constant yield of hydrocarbons could be obtained from the reactor on hydrogen atom attack, a few experiments were tried in which the hydrogen feed rate to the reactor was varied from 0.25-9.75 x 10^{-5} moles $hour^{-1}$ and the reaction products analyzed. These data are recorded in Table I. In Figure 3, the methane yield as a

function of the hydrogen feed rate is presented based on data given in Table I. Similar curves also resulted for the other hydrocarbons and for this reason they are not presented individually. From these data it appears that hydrocarbon yields vary by a factor of about eight with respect to hydrogen feed rate, increasing at the lower feed rates and decreasing at the higher feed rates. As noted in the experimental section, over this range of feed rates the hydrogen species leaving the effusing tube are essentially pure atomic hydrogen, with at most a 1 to 2% variation occurring between the lowest and highest flows. Such small changes in the H atom concentration cannot explain the observed variation in hydrocarbon yield as a function of feed rate. At lower hydrogen feed rates, H atom recombination reactions will occur at a lower rate than at higher hydrogen feed rates. It is possible that the decreased H atom recombination rates at the lower feed rates, and hence longer H atom life time increases the probability for H atom surface reactions producing hydrocarbons. A more detailed study of the effect was not undertaken.

A few experiments were tried to determine if significant cracking of hydrocarbons occurred in the reactor on the hot effusion tube. To this end small quantities of methane were introduced into the reactor and allowed to impinge on the carbon target before being frozen out on the liquid helium cold finger. The products were subsequently analyzed.

Within the sensitivity of the chromatographic detection, no noticable cracking of the methane occurred.

The above experiments served to characterized the operation of the H atom reactor. The apparent inability to remove all traces of organic material from reactor surfaces exposed to H atoms was not expected. It is interesting to note that in all previous experimental studies on the H atom-carbon reaction in which hydrocarbon reaction products were analyzed, no reports were made of tests to determine possible hydrocarbon yields in the absence of the carbon target. Sufficient experimental details were given in some of these studies to indicate that H atom attack on O-rings and vacuum greases in the reactor system probably occurred.

H-Atom-Carbon Reaction

The carbon target was placed in the reactor which was then conditioned to H atom attack for some 100 hours. Experiments were then conducted to determine the hydrocarbon yield from the H atom-carbon reaction as a function of temperature, over the range 30°-950°C. Hydrogen flow rates of 2×10^{-5} moles hour^{-1} were used in all experiments. The following hydrocarbons were detected, CH_4, C_2H_4, C_2H_6, and C_3H_8, with possibly minute traces of some C_4 species. The amounts of the latter were similar to those detected in the background yield without the carbon target present and reliable quantitative measurements were not possible. Qualitatively, C_4 hydrocarbon yields were estimated at $<10^{-3}$

of the methane. For the C_1, C_2 and C_3 hydrocarbons, yields for the hydrogen atom reaction with the carbon target were calculated by subtracting the background yield from the total in the sample. This method of calculating the hydrocarbon yield assumes that the background level of hydrocarbons is not affected by the presence of the competing process at the carbon target. This subject will be discussed later.

The data obtained from 25 experiments are shown in Table III. The hydrocarbon yields are presented in terms of moles of hydrocarbon formed per mole of molecular hydrogen fed into the reactor at the stated temperature. In Figures 4, 5 and 6 the data are shown graphically for methane, ethane and propane. The scatter of the individual points on the methane curve shown in Figure 4 may be considered as acceptable in terms of the expected experimental errors, but the scatter of the points on the ethane and propane curves is considerably larger. The reason for the increased scatter in these data points is not certain. It was observed that yields of ethane and propane obtained in a low temperature experiment performed directly after a high temperature experiment appeared to be significantly higher than the yield obtained when performing two low temperature experiments consecutively. This behavior suggests some type of hysteresis effect is occurring which results in these hydrocarbons being more slowly released during sample collection, than the methane. It is probable that these two hydrocarbons are more strongly adsorbed by

the surfaces in the reactor than the methane, and this might account for the rather poor precision of the data. Unfortunately it was not possible to examine this problem in more detail.

The data presented in Table III for yields of ethylene and propene in the H atom-carbon reaction shows in many cases negative values. This situation arises from the mode of calculations of the yield which was explained earlier. The negative values indicate that smaller quantities of ethylene and propylene are being formed in the presence of the carbon target than in its absence, suggesting that the interaction of the H atoms with the carbon target reduces the background yield of these hydrocarbons. From the data presented in Table III for C_2H_4 and C_3H_6, it appears that their respective yields are not noticably temperature dependent. Assuming this to be true, the average yield of C_2H_4 = $-(0.009 \pm 0.039) \times 10^{-3}$, and of C_3H_6 = $-(0.0014 \pm 0.0035) \times 10^{-3}$ moles per mole of H_2 fed to the reactor over the temperature range investigated. The error limits associated with these values are quite large, consequently it cannot be unequivocally stated that no ethylene or propene is formed during the H atom-carbon reaction. However the data do suggest values close to, if not zero, for yields of these two unsaturated hydrocarbons. To add further credence to this conclusion, at the end of the series of experiments the carbon target was removed from the reactor and the background yield of hydrocarbons again determined.

After some 80 hours of conditioning the yields of hydrocarbons were all found to agree, within the experimental error, with the values obtained previously.

Finally in Figure 7 an Arrhenius plot of the H atom-carbon reaction data is presented, based on the methane yields given in Table III. Three distinct reaction regions are indicated. A least squares fit on the data resulted in activation energies for the production of methane of, 4.5 $\pm$ 1.2 kcal $mole^{-1}$, 0.15 $\pm$ 0.05 kcal $mole^{-1}$ and 0.94 $\pm$ 0.20 kcal $mole^{-1}$ in the high, medium and low temperature regions respectively. The precision limits are the standard deviations calculated from the experimental data. No attempt was made to fit the data obtained from the ethane and propane yields to an Arrhenius type curve due their poor precision.

Hydrocarbon Product Distribution

The present investigation has established that the reaction of hydrogen atoms, at an initial temperature of about 2600°K, with a carbon surface at approximately 30°C produces the following saturated hydrocarbons, $CH_4 \approx 91$ mole % $C_2H_6 \approx 8.6$ mole % and $C_3H_8 \approx 0.4$ mole %. These ratios do not appear to vary significantly over the temperature range studied. There is a possibility that very minor amounts of C_2H_4, C_3H_6 and C_4 species may also be formed. In earlier studies on the atomic hydrogen-carbon reaction, Wood and Wise(9) (1969) reported hydrocarbon yields of $CH_4 \approx 91\%$ with C_2 through $C_8 \approx 9\%$; Harris and Tickner (2) (1947) have reported $CH_4 \approx 91\%$ and

C_2 through C_5≈9%. In both these studies low pressure electric discharges were used to produce hydrogen atoms. In the former study, sufficient experimental details were given to indicate that ionic species from the electric discharge probably did not take part in the reaction. The possibility that some H atom attack on O-rings in the system occurred cannot be ruled out. The reported presence, though presumably small, of hydrocarbons in the C_4 through C_8 range suggests, based on the results obtained in this study, that H atom attack on some material other than the carbon target occurred. Lack of experimental details does not allow an assessment of the validity of the results obtained in the Harris and Tickner study to be made. In the study by Gill, Toomey and Moser (7) (1967) low pressure thermally produced hydrogen atoms reacting with various carbons were reported to produce methane yields from 89.4 to 49.8%, with higher hydrocarbins, C_2-C_4 making up the balance. In this study hydrogen atom attack on organic material within the reaction vessel undoubtedly occurred, and these results must therefore be discounted. It is not possible to compare the values obtained for the relative yields of the individual higher hydrocarbons determined in this study, with those of earlier investigations, since either no specific data were given, or in those cases where they were (9), the experimental procedures were obviously unreliable.

It has been suggested that CH_4 is the primary product in the H atom-carbon reaction and that higher hydrocarbons are the result of secondary processes. The latter could be surface or gas phase interactions between H atoms and CH_4 or between radical species, CH_3, CH_2 or CH. In the present investigation, significant quantities of both C_2H_6 and C_3H_8 were formed in addition to CH_4, and although the experimental conditions probably eliminated secondary gas phase reactions, secondary surface processes could certainly have occurred. The possible primary or secondary nature of C_2H_6 and C_3H_8 in the H atom-carbon reaction cannot be determined from data obtained in this study. Had the precision of the yield data for both C_2H_6 and C_3H_8 been comparable to that for CH_4, and reaction studies made with different H atom flux rates, more definite conclusions with respect to this question might have been obtained. Further clarification of this point could probably also have been derived from electron spin resonance and matrix isolation investigations.

The finding that methane comprises 91% of the total hydrocarbon yield in the H atom-carbon reaction in this study and those of Wise (9) and Harris (2) is interesting in that different reaction conditions were used. In this study the initial hydrogen atom temperature before interacting with the carbon target was 2600°K, whereas in the earlier studies hydrogen atom temperatures in the range 300° - 373°K were used. Despite these differences the relative yield of

of methane with respect to the other hydrocarbons remained unchanged, implying that the factors responsible for the observed product distribution are independent of the H atom temperature. Surface controlled phenomena appear to be dominant. The effective hydrogen atom pressure at the carbon target in this study was at least a factor of 10^3 lower than that used by Wise (9) and Harris (2). If gas phase reactions were important in determining the product distribution a noticeable variation between the different investigations might be expected. That this was not the case again suggests that the carbon surface reactions largely control the product distribution.

H Atom-Carbon Reaction as a Function of Temperature

The investigation of the hydrogen atom-carbon reaction as a function of temperature was followed by measuring hydrocarbon yields over the temperature range 300-1220°K. The best data were obtained for methane and showed that the reaction rate increased continuously with temperature over the entire range. Similar trends were found for ethane and propane. In two earlier studies a maximum in the reaction rate at about 720°K (9) and 820°K (8) was reported. The former study was based on the carbon removal rate after H atom attack, while in the latter, the methane yield was used as the rate indicator. These results are in obvious disagreement with those obtained in this study. The maximum was justified in terms of the thermodynamic instability of

methane at about 850°K (8,9) at which temperature its free energy of formation changes from negative to positive. These arguements must be regarded as specious since the thermodynamic instability predicted for methane at 850°K requires H_2 and CH_4 to be at unit fugacity and for carbon to be in its standard state, with a state of thermodynamic equilibrium existing between the three species. Obviously in the H atom-carbon reaction, these criteria for the application of thermodynamic reasoning do not apply, and in fact, the conditions are deliberately chosen so that the results are kinetically controlled. If thermodynamic reasoning in any form could be applied to the reaction, and have any meaning, the system $4H + C = CH_4$ should have been considered. It is easily determined that for this process the reaction at 850°K has a free energy changes of about -160 kcal. Simply, a maximum in the H atom-carbon reaction rate cannot be justified on a thermodynamic basis. It is probable that in the earlier studies pyrolysis of the hydrocarbon reaction products on the high temperature carbon target was responsible for the observed maximum product yield temperature. In the experimental design used in the present study pyrolysis of this type was kept to a minimum by virtue of the high pumping rate of the liquid helium cold finger.

From the Arrhenius plot of the experimental data for methane shown in Figure 7, three fairly well defined different reaction regimes were found; 300 to 500°K, $E = 0.94 \pm 0.20$

kcal mole^{-1}, 500 to 1,000°K, $E_a = 0.15 \pm 0.05$ kcal mole^{-1} and 1,000 to 1,200°K, $E_a = 4.50 \pm 1.20$ kcal mole^{-1}. It should be noted that the data shown in Figure 7 must be considered as a pseudo-Arrhenius plot since the temperatures of the H atoms and the carbon target were considerably different from each other, whereas the simple reaction rate theory assumes equal temperatures for all reactants. Justification for the occurrence of three different reaction rate regions might be possible if data were available on the adsorption characteristics of H atoms on a carbon surface; unfortunately this is not the case. Data on the adsorption characteristics of molecular hydrogen on carbon (13,14) are known. Below 100°K hydrogen is physically adsorbed; between 100 and 550°K, it is only very weakly adsorbed; between 550 and 950°K, slow changes in the adsorption characteristics occur and above 950°K strong adsorption occurs with the equilibrium being rapidly attained. A heat of adsorption of $\approx$50 kcal mole^{-1} was obtained indicating strong chemisorption in this latter region. It is interesting to note that the three different temperature regions for the adsorption of molecular hydrogen on carbon roughly parallel the three different reaction rate temperature regimes for the atomic hydrogen-carbon reaction. It appears highly probable that above 1,000°K the rapid chemisorption of molecular hydrogen and possibly atomic H could be responsible for the increased reaction rate observed in this region.

Although activation energies for the H atom-carbon reaction have been reported (6,9), the values were based on the rate of carbon removal, not on the yield of methane as in this study. Since ethane and propane are produced in significant quantities in addition to the methane, the two sets of activation energies are not strictly comparable. However, in this study the yield of both ethane and propane followed similar trends with temperature as that of methane, and it is possible that the activation energies based on methane yields and carbon removal rates are not too different. Wise (6) has reported activation energies based on carbon removal rates of 9.2 and 7.1 kcal $mole^{-1}$, in the temperature range 365 to 500°K, and 5.15 kcal $mole^{-1}$ in the 450-715°K region. These values are all considerably larger than those obtained in this study. Hydrogen atom temperatures below 370°K were used in the carbon removal rate method of determining activation energies, (6,9) whilst in this study hydrogen atom temperatures of 2600°K were used. The latter have a thermal energy (translational) $\approx$5 kcal $mole^{-1}$ whereas the former have about 0.7 kcals $mole^{-1}$. If the hydrogen atom translational energy is important energetically in the H atom-carbon reaction, then the activation energies obtained in this study should be increased by about 4 kcal $mole^{-1}$ to be comparable with those of the earlier studies. This improves somewhat the agreement between the two different sets of experimental activation energies.

Hydrogen Atom-Hydrocarbon Conversion Efficiency

The data obtained in the present study allow some limits to be placed on the efficiency with which hydrocarbons are produced in the H atom-carbon reaction. In the following calculations it is assumed that all hydrogen fed to the reactor leaves the effusion tube entirely as atoms. From data in Table III, calculations shows that 1 mole of hydrogen atoms formed in the reactor result in the production of about 1.25×10^{-3} moles of CH_4, 1.2×10^{-4} moles of C_2H_6 and 7.5×10^{-6} moles of C_3H_8 at 30°C. If it is assumed that all hydrogen atoms effusing into the reactor can potentially react with the carbon target to produce hydrocarbons then 0.6%, 0.07% and 0.06% of the atoms are utilized to form respectively CH_4, C_2H_6 and C_3H_8. These figures imply that one out of every 140 hydrogen atoms entering the system is involved in the formation of hydrocarbons.

Of course, not all of the hydrogen atoms formed in the reactor have an opportunity to interact with the carbon target. Using molecular beam properties and the geometry of the reactor system, (15,16,17 & 18) it may be shown that between 60-70% of all atoms leaving the effusion tube will interact directly with the carbon target. It is possible that some H atoms interact with the carbon target after undergoing reactor wall collisions. The number of such secondary target collisions is likely to be small since the

target surface area $\ll$ than the total internal surface area of the reactor. Assuming that only those H atoms interacting with the target directly after leaving the effusion tube are likely to produce hydrocarbons, the fraction of atomic hydrogen collision leading to CH_4, C_2H_6, and C_3H_8 is calculated at approximately 1.0%, 0.1% and 0.1% respectively. These numbers imply that about one out of eighty three H atoms colliding with the target produces hydrocarbons. At about 950°C, the hydrocarbon yield values are increased by about a factor of three and hence the collision efficiency of H atoms to produce hydrocarbons becomes about one out of twenty eight H atoms.

It is not possible to compare directly the H atom-hydrocarbon conversion efficiencies obtained in this study with those of other workers, since the data are either not reported, or the experimental conditions are not analogous to those used in the present study. In two studies (9,11),where the latter condition holds, H atom conversion efficiencies were reported of between one and two orders of magnitude lower than obtained in this investigation. It appears probable that the higher hydrogen pressures used in the earlier studies, resulted in experimental conditions in which H atom recombination rates were substantially greater than in the present study with the corresponding dimunition in hydrocarbon forming processes.

CONCLUSIONS

1. The reaction of atomic hydrogen with carbon at 30°C results in the production of $CH_4 \approx 91\%$, $C_2H_6 \approx 8.4\%$, and $C_3H_8 \approx 0.6\%$. The formation of C_2H_4, C_3H_6 and C_4 species in the reaction is zero or close to zero.

2. About 1.2% of the atomic hydrogen interacting with the carbon target is converted to hydrocarbons at 30°C. At 950°C this fraction increases to about 3.6%.

3. Over the temperature range 30-950°C the hydrocarbon product distribution remains essentially unchanged

4. Previous reports of a maximum in the hydrocarbon yield at 720-820°K were not substantiated. The previously reported maximum is believed to be a function of the experimental arrangements.

5. The H atom-carbon reaction rate to produce methane has three distinct phases. Activation energies were determined: 300 to 500°K, $E_a = 0.94 \pm 0.20$ kcal mole^{-1}; 500 to 1000°K, $E_a = 0.15 \pm 0.05$ kcal mole^{-1}; and 1000 to 1200°K, $E_a = 4.5 \pm 1.2$ kcal mole^{-1}.

Acknowledgement

The author gratefully thanks the Cleveland Consolidated Natural Gas Service Company Inc. for supporting this research and Dr. Lester G. Massey for his keen interest in the work.

REFERENCES

1. L. J. Aramenko, J. Phys. Chem. USSR 20, 1299 (1946).
2. G. M. Harris and A. W. Tickner, Nature 160, 871 (1947).
3. J. D. Blackwood and F. K. McTaggart, Australian J. Chem. 12, 533 (1959).
4. M. M. Shahin, Nature, 195, 992, 1965.
5. F. J. Vastola, P. L. Walker and J. P. Wightman, Carbon 1, 11 (1963).
6. A. B. King and H. Wise, J. Phys. Chem., 67, 1169 (1963).
7. P. S. Gill, R. E. Toomey and H. C. Moser, Carbon, 5, 43 (1967).
8. M. Coulon and I. Bonnetain, Compte Rend. Acad. Sci. Paris 269, 1469 (1969).
9. B. J. Wood and H. Wise, J. Phys. Chem., 73, 1348 (1969).
10. Y. Sanada and N. Berkowitz, Fuel 48, 375 (1969).
11. B. McCarroll and D. W. McKee, Carbon, 9, 301 (1971).
12. JANAF Thermochemical Tables, Thermal Research Laboratory, The Dow Chemical Co., Midland, Michigan.
13. M. R. Barrer and K. E. Rideal, Proc. Roy. Soc., A218, 311, (1953).
14. M. R. Barrer, J. Chem. Soc., 1256 (1936).
15. L. Davis, D. E. Nagle and J. R. Zacharias, Physical Review 76, 1068, 1949.
16. J. G. King and J. R. Zacharias, Advances in Electron Physics 8, 1, (1956).
17. M. V. Smoluchowski, Ann. d. Physik., 33, 1559 (1910).
18. M. Knudsen, Ann. d. Physik., 31, 633 (1910).

TABLE I

EXPERIMENTS TO DETERMINE BACKGROUND HYDROCARBON YIELD DUE TO HYDROGEN ATOM REACTION WITH RESIDUAL CARBON OR CARBON SPECIES IN REACTOR

Expt. No.	H_2 Feed Rate (Moles x 10^{-5}/hour)	Moles x 10^{-3} of Hydrocarbon Formed Per Hour Per Mole H_2 Reacted				
		CH_4	C_2H_4	C_2H_6	C_3H_6	C_3H_8
52	1.9430	9.4765	1.2666	0.7516	0.0983	0.1629
53	1.9350	3.0493	0.3192	0.1939	0.0147	0.0276
54	1.8917	1.6025	0.0890	0.1266	0.0057	0.0240
55	2.1736	2.2031	0.1710	0.1711	0.0114	0.0303
56	1.9635	1.7013	0.1188	0.1406	0.0076	0.0267
57	1.9293	1.8502	0.1024	0.1196	0.0091	0.0233
58	2.0461	1.2485	0.1344	0.1217	0.0055	0.0192
59	2.0885	1.2118	0.1719	0.1142	0.0056	0.0206
60	1.9907	1.6453	0.0809	0.1457	0.0092	0.0258
61*	0.5061	4.0439	0.6047	0.4110	0.0170	0.0810
62	2.1318	2.0290	0.0813	0.1960	0.0057	0.0337
63*	0.7561	2.5788	0.2263	0.3853	0.0090	0.0677
64*	9.7126	0.3339	0.0127	0.0315	0.0005	0.0052
65*	4.0310	0.5501	0.0401	0.0310	0.0045	0.0052
66*	6.5012	0.7081	0.0220	0.0750	0.0005	0.0049

* These data points were used in establishing the curve shown in Figure 3.

TABLE II

HYDROCARBON YIELD AFTER CONDITIONING THE REACTOR FOR A PROLONGED PERIOD OF TIME (>80 HOURS) AT A HYDROGEN FEED RATE OF 2×10^{-5} MOLES/HR^{-1}

Hydrocarbon	Moles of Hydrocarbon per Mole of H_2 Fed to the Reactor
CH_4	$(1.69 \pm 0.21) \times 10^{-3}$ [a]
C_2H_4	$(1.18 \pm 0.27) \times 10^{-4}$
C_2H_6	$(1.42 \pm 0.20) \times 10^{-4}$
C_3H_6	$(7.5 \pm 1.6) \times 10^{-6}$
C_3H_8	$(2.55 \pm 0.34) \times 10^{-5}$

(a) Reported error limits are the standard deviations of the observed experimental values.

TABLE III

DATA FOR HYDROCARBON YIELDS IN THE TEMPERATURE RANGE 301 TO 1222°K WITH A HYDROGEN FEED RATE OF 2×10^{-5} MOLES $HOUR^{-1}$

Expt. No.	Target Temp. T°K	$I/T°K \times 10^{-3}$	CH_4 Yield* $\times 10^{-3}$	C_2H_4 Yield $\times 10^{-3}$	C_2H_6 Yield $\times 10^{-3}$	C_3H_6 Yield	C_3H_8 Yield	Log_{10} CH_4 Yield
1	1137	0.880	5.950	0.0053	0.595	0.0036	0.0482	0.775
2	983	1.017	4.706	0.0081	0.331	0.0108	0.0252	0.673
3	804	1.244	4.354	0.0046	0.294	-0.0025	0.0275	0.639
4	626	1.597	4.265	0.0483	0.298	-0.0030	0.0276	0.630
5	428	2.336	3.876	-0.0021	0.221	-0.0036	0.0206	0.588
6	1108	0.903	6.460	0.0374	0.648	-0.0003	0.0400	0.810
7	508	1.969	4.000	-0.0068	0.275	-0.0029	0.0225	0.602
8	1206	0.829	7.109	0.0501	0.725	0.0012	0.0548	0.852
9	1075	0.930	5.265	-0.0086	0.400	-0.0029	0.0246	0.721
10	333	3.003	2.838	-0.0540	0.264	0.0037	0.0148	0.453
11	1101	0.908	5.519	0.0262	0.580	-0.0037	0.0311	0.742
12	898	1.114	4.217	-0.0375	0.259	-0.0031	0.0173	0.625
13	301	3.322	2.723	0.0183	-	-	-	0.435
14	1144	0.874	6.188	0.0319	0.664	-	0.0296	0.792
15	370	2.703	3.293	-0.0604	0.215	0	0.0072	0.518
16	352	2.841	3.350	-0.0718	0.199	0	0.0071	0.525
17	305	3.279	2.580	-0.0040	0.201	-0.0019	0.0255	0.412
18	945	1.058	4.470	-0.0565	0.218	-0.0032	0.0093	0.650
19	482	2.075	4.171	-0.0129	0.216	-0.0045	0.0170	0.620
20	770	1.299	4.163	-0.0364	0.208	-0.0016	0.0093	0.619
21	675	1.482	4.130	0.0404	0.241	-0.0022	0.0158	0.616
22	306	3.268	2.399	-0.0318	0.240	-0.0042	0.0239	0.380
23	386	2.590	3.758	-0.0743	0.264	-0.0039	0.0122	0.575
24	1222	0.818	6.814	0.0207	0.536	-0.0023	0.0466	0.833
25	616	1.623	3.932	-0.0648	0.274	-0.0051	0.0100	0.595

* Yields are presented in terms of moles of hydrocarbon formed, per mole of H_2 fed to the reactor.

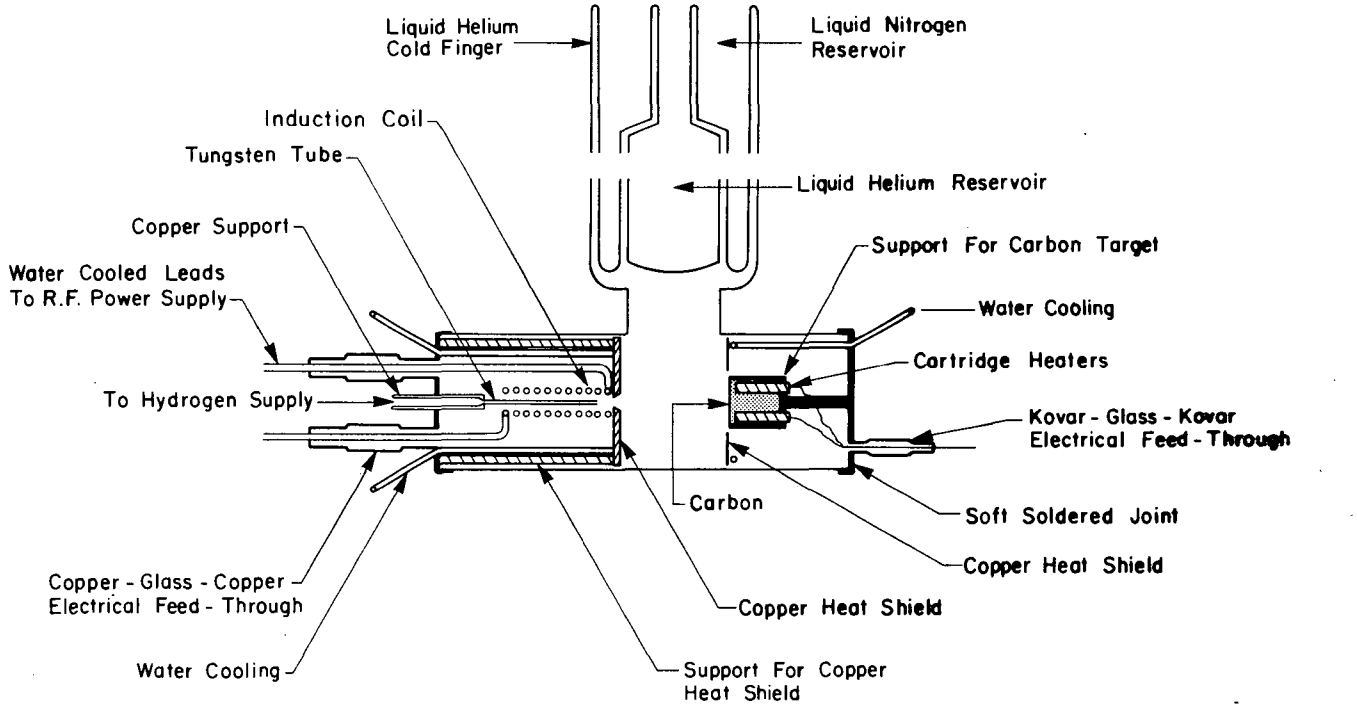

Fig. 1 SCHEMATIC ARRANGEMENT OF ATOMIC HYDROGEN/CARBON REACTION CELL

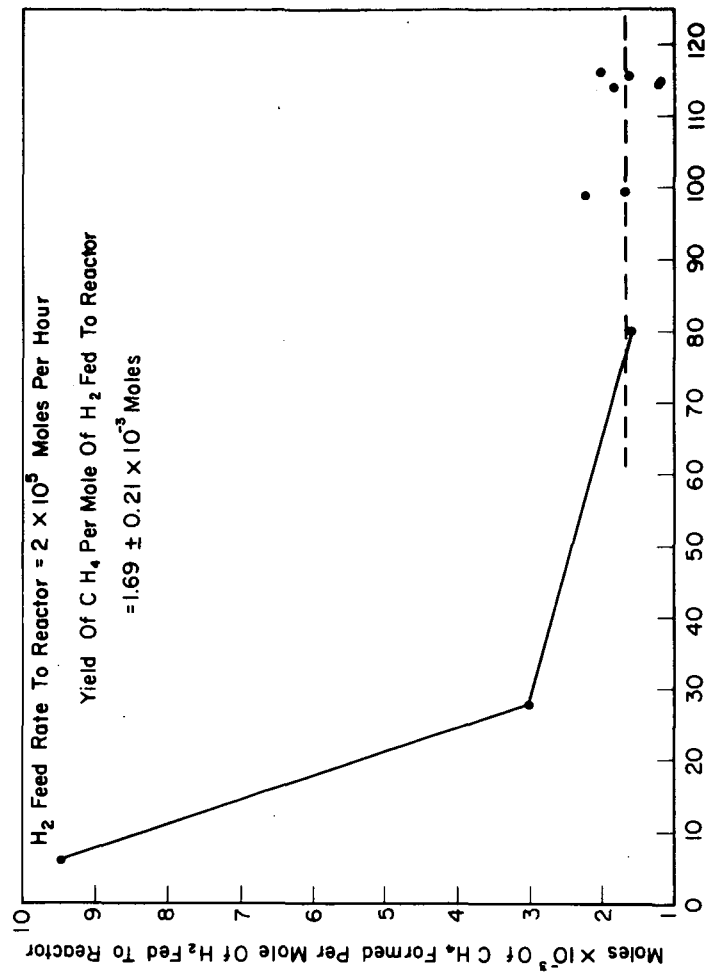

Fig. 2 YIELD OF CH_4 IN REACTOR WITHOUT CARBON TARGET AS A FUNCTION OF H ATOM CONDITIONING TIME

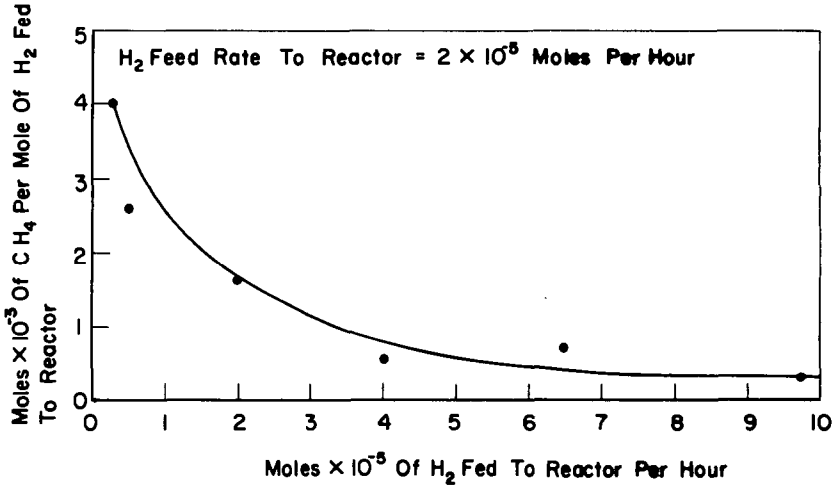

Fig. 3 CH_4 YIELD AS A FUNCTION OF H_2 FEED RATE

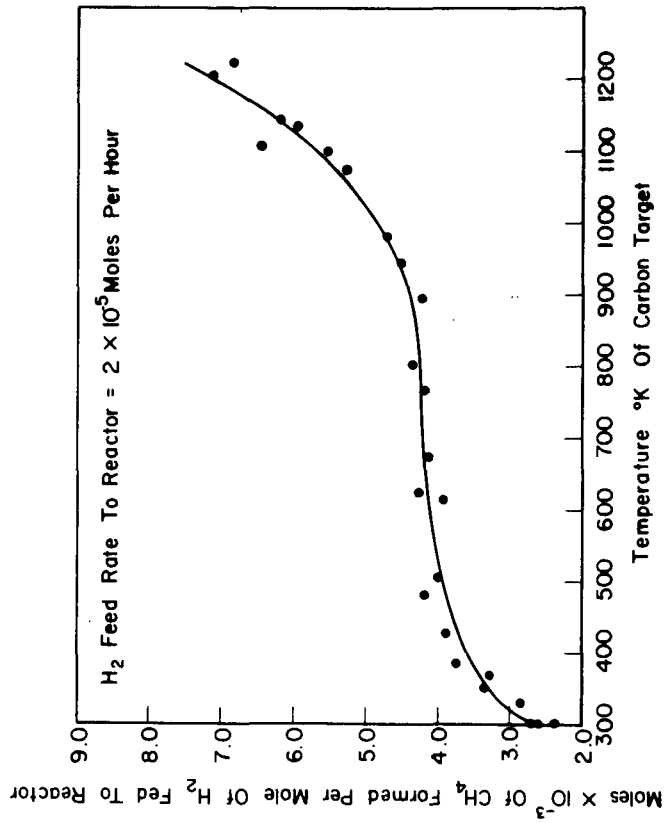

Fig. 4 METHANE PRODUCTION AS A FUNCTION OF TEMPERATURE

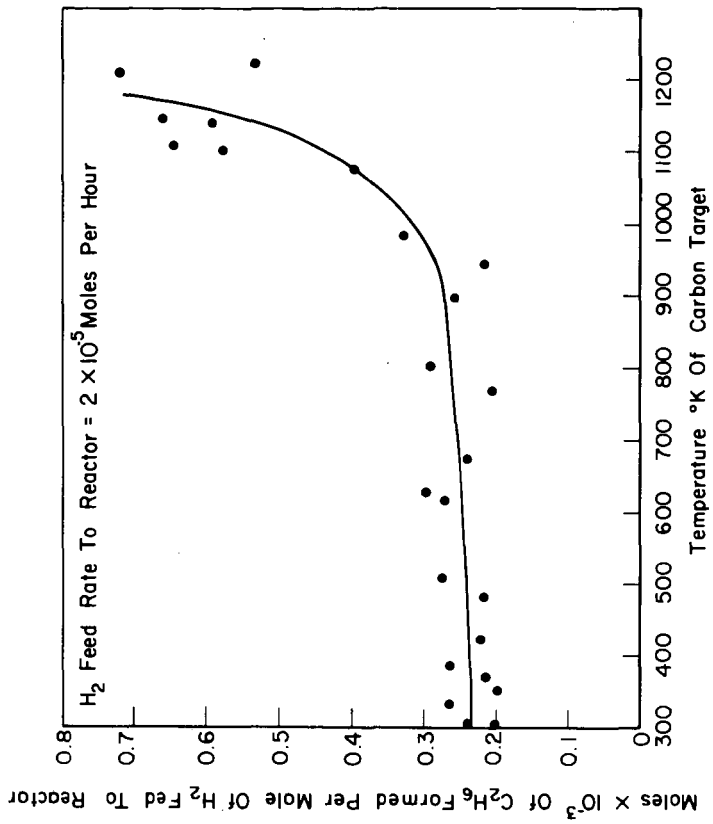

Fig. 5 ETHANE PRODUCTION AS A FUNCTION OF TEMPERATURE

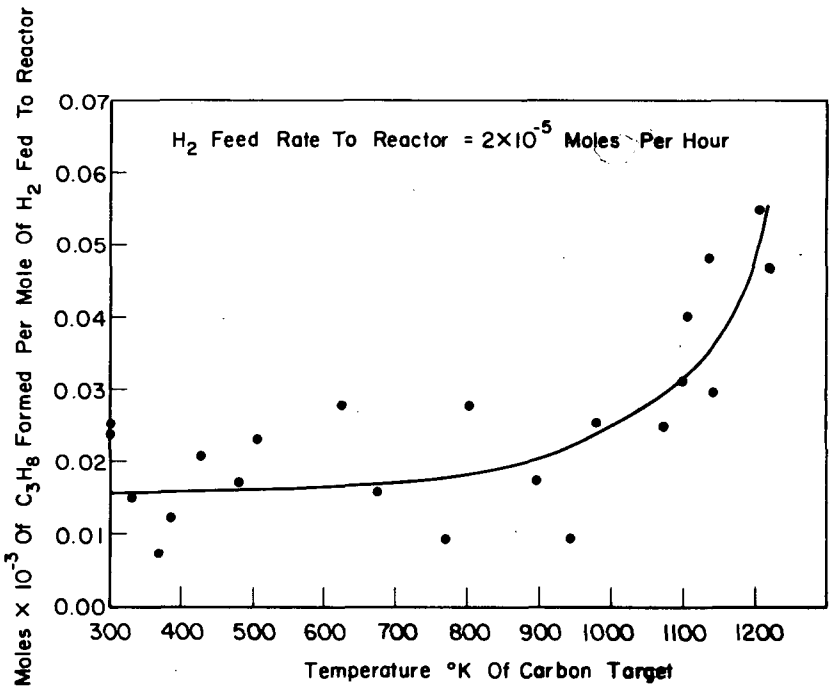

Fig. 6 PROPANE PRODUCTION AS A FUNCTION OF TEMPERATURE

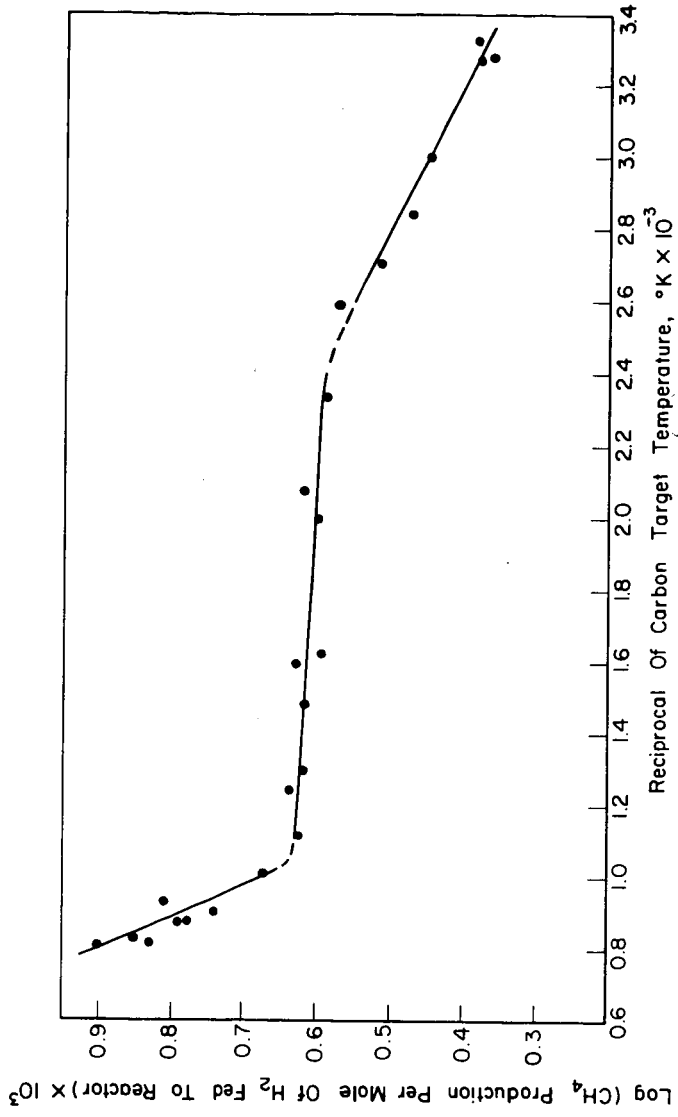

Fig. 7 ARRHENIUS PLOT FOR METHANE PRODUCTION

PROBLEMS IN PULVERIZED COAL AND CHAR COMBUSTION

By

David Gray, Research Associate
John G. Cogoli, Graduate Research Assistant
Robert H. Essenhigh, Professor of Fuel Science

Combustion Laboratory
The Pennsylvania State University
University Park, Pennsylvania 16802

Abstract

Interest in char combustion derives from the need to utilize the char produced during some gasification processes. Successful use of char in combustion may depend on use with supplementary fuel. The critical factor determining this appears to be the char "reactivity" which may be variations in intrinsic reactivity depending on differences in thermal history, or it may be dependent on differences in internal surface. In preparation for an experimental program to determine the relative significance of these alternatives (or others), what are considered relevant contributions is the existing experimental literature have been re-evaluated. Although overall surface reaction rates have been evaluated for many coal chars there appears to have been a fundamental omission in the kinetic analysis, and an attempt to remedy this has been made. The picture now developed is that of char particles that may burn either in Zone I or Zone II depending on the particle permeability. Zone III combustion is not encountered with particles below about 100 microns. In Zone I and II combustion, however, the intrinsic reaction is evidently a zero order, high activation energy process (E about 45 kcal) at temperatures in the region of 1000°K, changing to a first order, low activation energy process (E about 7 kcal) at temperatures approaching 2000°K, with both processes significant in the transition range between the two limits. This new evaluation modifies the conventional views of reaction order and activation energies.

Introduction

The dwindling supplies of natural gas and the predicted shortage of oil have initiated considerable research concerned with the conversion of coal to easily utilizable synthetic gas and oil. These conversion processes inevitably yield a high proportion of relatively unreactive char as a by-product. In order to render the overall process economically viable, the char must be recoverable as an energy source. This necessity to return to coal has reopened the whole field of study on

p.f. combustion to reanalysis in order to gain deeper understanding of several phases of the general process still not totally understood.

This paper will provide a critical evaluation of the state of the knowledge on the subject of p.f. combustion, reviewing all the possible mechanistic processes involved and distinguishing between those that are generally accepted by the majority of workers in the field and those that are still questionable, either because of inadequate experimental evidence or because of arguable theoretical interpretation.

A theory cannot be acceptable until it is formulated in such a manner that certain definitive experiments are able to substantiate it or disprove it. Mere data gathering is not sufficient; the data must be used to the fullest extent to positively identify the proposed mechanisms. Can certain elusive questions concerning the mechanisms of p.f. combustion be answered by reanalysis of existing data? An attempt to answer this has been made by a reanalysis of rate data for the combustion of a size graded char (1). Nevertheless, the total process is still not fully comprehended. Differences in opinion on many of the issues involved are converging to agreement, but outstanding questions still need answers backed up with the necessary experimental data and theory. Even with the much less complicated reaction of the purest carbon with oxygen, which has been investigated for many years, there are still many unknowns. The coal system is much more complex, involving in many cases simultaneous mechanisms and great advances in comprehending the process have already been made. Hopefully, by isolating the unknown from the known, and by carefully designing experiments to test disputable points, an even finer comprehension of the processes involved in the combustion of p.f. will be obtained.

From a macroscopic viewpoint, the combustion of p.f. particles can be broken down into two main processes: (i) pyrolysis of volatiles and their subsequent combustion, and (ii) heterogeneous combustion of the solid residue. These two processes will be dealt with separately in spite of the frequent overlap of the volatile and heterogeneous regimes.

The following topics and the degree to which they are currently understood will be discussed:

(1) Effect of temperature, time history, rate of heating and environment on the evolution of volatile matter.

(2) The temporal sequence of devolatilization and heterogeneous combustion.

(3) Reaction order in oxidant and activation energies in heterogeneous combustion.

(4) The relative importance of chemisorption and desorption control.

(5) Particle size dependence of combustion characteristics.

(6) Change in total available surface area during combustion: pore size distribution and modification.

(7) Relative importance of mass transfer and chemical control.

(8) Discrepancies between the interpretation of available kinetic data on the combustion of char particles.

(9) Effect of internal diffusion through the porous structure of particles.

(10) Real and apparent orders and activation energies in the combustion process.

Pyrolysis

Introduction

When coal is pyrolyzed the central mechanism can only be the detachment or chemical formation of components of a volatile nature that are then able to escape from the solid involatile matrix under varying circumstances. It should theoretically be possible to isolate four regimes for pyrolysis of coal particles. If the volatile components are able to escape from the matrix as rapidly as they are formed, the overall rate of the pyrolysis will be controlled by the chemical reaction for the volatile formation. When diffusional escape of volatiles takes a finite time which is long compared with the reaction time, the diffusion process will determine the pyrolysis rate. For larger particle sizes or higher heating rates, so that a temperature gradient is generated within the particle, the condition for a pyrolysis wave can be obtained. Here pyrolysis will occur in a zone with unreacted material on the one side and devolatilized char on the other. The pyrolysis rate is then determined by the rate of heat input into the interior of the particle and not by the reaction rate or the diffusional escape. At even higher heating rates, heat reaches the pyrolysis sites faster than it can be utilized and the temperature rises rapidly and the pyrolysis becomes reactivity controlled once more. In the limit the particle could theoretically reach such a temperature that particle burn out could be complete before any significant pyrolysis had time to occur. Such a situation is believed to occur in the explosion flame system.

In the past it has been generally assumed that in pulverized coal flames particle pyrolysis proceeds heterogeneous carbon burn out and that ignition occurs in the volatiles, however there is some evidence (2) to modify this simple concept and their conclusion is that there is parallel pyrolysis and heterogeneous combustion in the flame and that the ignition itself was heterogeneous in origin.

It has been customary to classify coal by means of the proximate analysis test wherein the coal is devolatilized in a crucible under specified conditions of sample size, temperature, and duration of decomposition. Coal has long been considered to be made up of fixed amounts of volatile matter and involatile "fixed carbon" (3), (4), and the proximate test categorizes the coals in terms of percentages of fixed carbon, volatile matter and ash on a dry basis. This test procedure is an example of a medium rate of carbonization. In the pulverized coal flame heating rates may be as high as 10^4 or 10^5 °C/sec., so information obtained about pyrolysis from the proximate analysis test may or may not be relevant to the situation in the p.c. flame. Attempts to approach these high heating rates in the study of pyrolysis and hence more nearly to approximate the conditions in the p.c. flame have been made by several workers.

Loison and Chauvin (5) devolatilized 50-80 micron coal particles on a wire gauze electrically heated to 1000°C (heating rate ≈ 1500 °C/sec.) and found that the yeild of volatiles produced was often greater than the yield of volatiles obtained by the proximate test. They also noted changes in the composition of the volatile products, obtaining a higher ratio of tars to gas at the higher heating rates.

Badzioch and Hawksley (6) designed an apparatus not only to approximate the heating rates in a p.c. system but also to approximate the environment of pyrolysis in those systems. They used an essentially isothermal flow reactor and devolatilized the coal particles (size graded) in nitrogen which acted as dilluent and inert atmosphere. They thereby eliminated the complications of combustion of volatiles and heterogeneous reaction and concentrated only on the pyrolysis process itself. Their results will be discussed in more detail later but the essential results were in agreement with Loison and Chauvin, that the weight loss produced was in all cases greater than the difference in the proximate volatile yield of parent coal and partially pyrolized char.

Kimber and Gray (7) using essentially the same apparatus as Badzioch and Hawksley also found the weight losses during pyrolysis to be considerably greater than the proximate analysis results. They pyrolized to much higher temperatures (≈1900 °C) and were able to obtain their weight losses by direct measurement, whereas Badzioch and Hawksley used ash as a tracer.

Howard and Essenhigh (2), using a plane flame furnace have studied the devolatilization process in conjunction with the heterogeneous combustion of carbon and the combustion of the volatiles. On the basis of their results, they have formulated an overall picture of the combined process and its temporal sequence, this will be discussed later.

It is thus apparent that the amount of volatiles produced from a coal is not a constant quantity but depends to a greater or lesser extent on the following factors:

1) rate of heating
2) final decomposition temperature obtained
3) duration of the decomposition at that temperature
4) the environment under which the coal is devolatilized

Points of General Agreement

It is now generally agreed that pyrolysis is an activated process and the amount of volatiles produced and their composition will depend on the conditions. Different results are expected between the relatively slow decomposition of particles in a closely packed

bed and rapid decomposition of particles in a dilute suspension, like a dust cloud. In the first case pyrolysis products have time to interact with each other and with other partially pyrolyzed coal particles in their passage through the bed, while in the second case the volatiles are rapidly diluted in a gaseous environment which effectively prevents mutual and particle interactions.

Badzioch and Hawksley (6), postulate that the yield of volatiles depends upon the rate of heating, the final temperature and the duration of heating at that temperature, and on the dilution effect. They devolatilized the coal at short heating times at essentially isothermal conditions so they could not therefore substantiate the first of their postulates. However, they found that the weight loss between the original coal and the char produced was always greater than the change in the proximate volatile matter of coal and char. This change in volatile matter ΔV was measured as a percentage of the original dry ash free coal.

$$\Delta V = VM_o - R$$

where VM_o was the proximate volatile matter of original dry ash free coal and R was the proximate volatile matter of the char produced expressed as a percentage of the weight of the original dry ash free coal.

The weight loss was ΔW where

$$\Delta W = 100 - Y$$

and Y was the yield of char expressed as a percentage of original dry ash free coal. The experimental conditions did not allow them to directly weigh the char produced so they assumed that no ash would be lost during the decomposition process and thus could be used as a tracer. They showed the correlation between ΔW and ΔV to be linear but the regression line did not pass through the origin. This apparent anomaly is discussed later. The constant of proportionality was termed Q so that

$$\Delta W = Q \Delta V$$

Kimber and Gray (7), also found Q factors for the coals studied to be greater than one. They found that the devolatilization at higher heating rates appeared to be a two stage process; that the amount of weight loss increases with increasing heating rate although they admitted that at short heating times the effects of rate of heating and final temperature could not be isolated; that the amount of weight loss increased with increased temperature. The important conclusion of Q factors being greater than one is that during pyrolysis either some of the so called fixed carbon is lost as volatile matter and thus the quantity of fixed carbon

determined by proximate analysis decreases, or that the proximate test fails to show all of the possible volatile matter and that some portion of it is somehow captured or otherwise altered by the coal during the carbonization.

Points of Disagreement

Although it is accepted that ΔW is not equal to ΔV, the reasons for this inequality are not fully agreed upon.

The phenomena can be caused by one or a combination of the following:

1) rate of attainment of final pyrolysis temperature
2) value of final temperature and duration of the process
3) devolatilization environment

Badzioch and Hawksley (6), claim that the mechanism and the amount of decomposition depends on the rate of heating. However, in the analysis of their data they subtract out the correction for the heating stage of the particles arguing that since the rate of decomposition is sensitive to temperature the amount of decomposition that occurs during the heating stage is negligible, so actually they observe weight losses for isothermal conditions. Howard and Essenhigh (2), claim that the amount of volatiles produced depends on the final temperature, the duration of the process and the particle size, i.e., when a particle is large enough to sustain a temperature gradient within it. They do not specify the possible effects of the environment of pyrolysis, yet they do warn that considerable discretion must accompany the use of experimental results obtained under conditions differing markedly from those of the application. Preliminary results obtained in this laboratory on the effects of markedly different rates of heating on the amount of volatile matter produced are discussed later.

Badzioch and Hawksley (6), infer from their experimental data that the variation of volatile matter with time for isothermal conditions may be exponential and they expressed the fractional volatile change in the form:

$$\Delta V/VM_o = (1 - C)[1 - \exp(-k\tau)]$$

For decomposition temperature >900°C the proximate volatile matter of the char had almost reached a constant value in the 100 millisecond pyrolysis time considered (8). Kimber and Gray found that for decomposition temperatures above 1000°C the weight loss was even higher and at 1900°C the residual proximate volatile matter in the char approached zero.

The environment of pyrolysis effect has been discussed earlier and it is agreed that the physical conditions under which the decomposition occurs does indeed affect the volatile yield. However, the relative importance of this effect over and above the other factors has never been satisfactorily demonstrated. Recent results obtained in this laboratory shed more light on the quantitative significance of the effect and are discussed below.

Attempted Clarification of Disputed Issues

Badzioch and Hawksley (6), found that the regression line on their plot of ΔW against ΔV did not pass through the origin and dismissed this as an artifact they thought was caused by a loss of ash; however, another explanation could explain the effect. The slope of this plot $\Delta W/\Delta V$ was termed Q and represented a correction factor proposed to account for the fact that actual weight loss incurred during pyrolysis under certain conditions for a coal could be different from that measured by the change in volatiles in the proximate analysis procedure. Dryden (9), has discussed the possibility that volatiles could be entrapped or cracked within the interstices and pores of the coal particles and this could be responsible for a lower yield of volatiles than would have been obtained with finer particles or with a thinner bed or maybe with ambient sweep gas to remove the volatile components rapidly from the vicinity of the pyrolyzing particles. The extreme example of this latter case is, of course, the pyrolysis environment produced in the Badzioch and Hawksley experiments.

The reason for the Q factor being greater than unity would seem therefore to be either the elimination of these entrapments, cracking and back or side reactions or the actual loss of the so called fixed carbon because of conditions not realized in the proximate test. Of course, both effects may be present to varying degrees of significance.

Let us assume there to be a capture factor for the parent coal α such that

$$VM_o = VM_{act}(1 - \alpha)$$

where VM_o is the proximate volatile matter of the original coal and VM_{act} is the "real" volatile matter of the original coal and α is the fraction of the volatile matter that is captured or otherwise lost during the proximate analysis procedure.

Then the weight loss is

$$\Delta W = \frac{VM_o}{1 - \alpha} - \frac{R}{1 - \beta}$$

where R is (as defined by Badzioch and Hawksley) the proximate volatile matter of the char and β is the capture factor for the char, which because of partial devolatilization and physical changes in nature is assumed to be different from that of the parent coal.

$$\Delta V = VM_o - R \qquad \text{by definition}$$

$$\text{thus} \qquad \Delta W = \frac{\Delta V + R}{1 - \alpha} - \frac{R}{1 - \beta}$$

$$\text{and} \qquad \Delta W = \frac{\Delta V}{1 - \alpha} + R \left[\frac{1}{1 - \alpha} - \frac{1}{1 - \beta}\right]$$

But R is not a constant so we substitute $(VM_o - \Delta V)$ for R in the above; thus

$$\Delta W = \frac{\Delta V}{1 - \beta} + VM_o \left[\frac{\alpha - \beta}{(1 - \alpha)(1 - \beta)}\right]$$

$$\text{thus} \qquad \Delta W = Q\Delta V - Q(\beta - \alpha)VM_o/(1 - \alpha)$$

$$\text{where} \qquad Q = \frac{d(\Delta W)}{d(\Delta V)} = \frac{1}{1 - \beta}$$

This represents the equation of a straight line with slope $1/(1 - \beta)$ and intercept $Q(\beta - \alpha)\ VM_o/(1 - \alpha)$.

When $\Delta W = 0$, $\Delta V = VM_o\ (\beta - \alpha)/(1 - \alpha)$

and if $\beta > \alpha$, then $\Delta V > 0$

When $\Delta V = 0$, $\Delta W = QVM_o(\alpha - \beta)/(1 - \alpha)$

and if $\beta > \alpha$, then $\Delta W < 0$

Although this adequately explains the intercept obtained on the ΔW against ΔV plot, it was necessary to determine the expected magnitude of a capture factor effect in the proximate analysis test, so a series of experiments were performed in this laboratory, whereby the percentage weight loss obtained in the test was plotted as a function of the depth of coal (proportional to weight) in the crucible. The experiments were carried out to the exact specifications of the ASTM test procedure apart from the variation in the quantities of coal used. The results obtained are shown graphically in Figure I. It can be seen that there is a significant effect that can be attributed to a capture factor, yet the effect is not of sufficient

magnitude by itself to explain a Q factor as high as 1.5 or 1.8. The effect shown is of the order of 10 percent. For a Q factor of 1.5 the effect would have to be on the order of 30 percent. Thus although volatile capture does apparently occur in the proximate test, the effect is not large enough to cause the difference between ΔW and ΔV produced in the Badzioch and Hawksley, and Kimber and Gray experiments. The only other explanation is that some of the "fixed carbon" is actually lost during the devolatilization produced under the conditions of their experiments. This almost certainly means that a similar process is occurring in p.c. systems.

In Figure I the squares represent pyrolysis at 1200°C and there is no difference in percentage weight loss than at 950°C. The lower points show devolatilization under conditions of very slow rates of heating, approximately 20-30°C/minute. There is a significant lowering of percentage weight loss under these conditions which suggests that the rate of heating does have an effect upon the quantity of volatiles produced.

As an extension to the two component hypothesis of coal, it appears as if there is a transitional component between the fixed carbon and the volatile component parts which may become volatile or involatile depending on the conditions of decomposition. If the pyrolysis is rapid the thermal energy flux is high enough to promote a substantial portion of the transitional component to the vapor phase. With slow decomposition, preferential polymerization occurs with the evolution of a smaller proportion of volatile matter, the remainder adding to the fixed carbon. This three component hypothesis of coal seems to be well supported from the experimental evidence quoted in this paper.

Remaining Questions

A knowledge of the processes occurring during pyrolysis of coal is required for understanding the combustion of coal particles in p.c. flames, and the way in which the pyrolysis results are used in calculations of p.c. systems will depend on just when and in what order pyrolysis and heterogeneous combustion occur. Essenhigh and Howard (2), suggest that the heterogeneous combustion and pyrolysis occur simultaneously in the plane flame system, but the complexities of studying both combustion and decomposition together make such conclusions extremely difficult to establish.

Although it is accepted that pyrolysis is an activated process, values for activation energies are varied. Juntgen's studies (10), showed that the activation energies for the processes could be divided into two ranges; either 15 or 30 kcal/mole which he identified as activated diffusion and chemical decomposition respectively. He used an average or global activation energy concept in his

analysis of the pyrolysis of coal (11). Badzioch and Hawksley obtained an activation energy of approximately 18 kcal/mole for all the coals that they studied, while the activation energy quoted by Van Krevelen (12), for coal carbonization is about 56 kcal/mole.

The modes of devolatilization and their dependence on particle size are now beginning to be understood, and it should now be possible to assign limits to the various pyrolysis regimes already mentioned. Two models for pyrolysis are proposed by Essenhigh and Howard (2), the first assumes devolatilization occurs uniformly throughout the particle, so the rate of reaction at any time is proportional to the mass (or volume) of unreacted material remaining in the particle, i.e., pyrolysis is a volumetric reaction. Since the total mass of material is independent of the size of particles containing it, the model indicates that pyrolysis should be independent of particle size. The second model assumes pyrolysis to occur in a thin zone surrounding a core of undecomposed material, here the mass of volatile matter present in the zone is proportional to the surface area of the particle, thus the pyrolysis should show a particle size dependence. For the p.c. system they eliminated the latter model on grounds that: 1) the observed time required for pyrolysis was much greater than that predicted from the model for both physical and chemical control, 2) that evidence from Ishihama (13) indicated that there is no size dependence below 60 microns diameter, and 3) an estimation of the temperature distribution inside the particle in a flame indicated that the pyrolysis could not be a surface reaction due to a temperature gradient inside the particle for diameters less than about 50 microns. Thus for particles smaller than approximately 50 microns, the rate of pyrolysis should become independent of particle size and be first order in unreacted volatile material.

Heterogeneous Combustion

Generally Accepted Mechanisms*

In the reaction of a gaseous component with a solid surface it is generally agreed that the process can be divided into three basic steps:

i) Transfer of the gaseous reactant to the solid surface

ii) Chemical reaction of gas with the surface

iii) Diffusion of the products of the reaction away from the surface

Considering now the carbon oxygen system we can say that the rate of weight loss of carbon per unit external surface area R_t is given by the so called "resistance equation":

$$1/R_t = 1/R_{mt} + 1/R_{chem}$$

Here R_{mt} represents the rate at which oxygen molecules are transported across the boundary diffusion layer to the surface where they immediately react to form products and R_{chem} represents the case when there is no resistance to transport of oxygen molecules to the surface but that the reaction takes a finite time. Thus R_{mt} and R_{chem} are the limiting values for mass transfer and chemical reaction.

If the rate is controlled exclusively by the mass transfer process, this implies that the concentration of the oxidant at the surface is effectively zero so the particles if spherical can be treated as impervious spheres, no matter what their internal structure is, which shrink from the outside surface inwards as the reaction proceeds at constant density, thus:

$$\frac{-dm}{dt} = -4\pi r^2 \sigma_A \frac{dr}{dt} = 4\pi r^2 R_t$$

$$\text{and} \quad \tau = -\frac{\sigma_A}{R_t} \int_{r_o}^{o} dr \qquad (1)$$

where σ_A is the density and τ is the burning time when $r = 0$.

If there is turbulent mixing throughout the system of oxidant gas and carbon or coal particles and thus relative motion between gas and particles, the boundary layer thickness can be reduced and mass transfer across it is enhanced. It can be shown that for a relative velocity of u, the rate of mass transfer is given by:

*The authors of this paper are indebted to the excellent review article of Mulcahy and Smith (14) for the formulation of this section.

$$R_{mt}(u>0) = R_{mt}(u=0)\,[1 + a\,(N_{Re})^{b}(N_{Sc})^{c}] \qquad (2)$$

where N_{Re} is the gas-particle Reynolds number, N_{Sc} is the Schmidt number and a, b, and c are constants. By taking values for the constants a, b, and c and evaluating the ratio $R_{mt}(u>0)/R_{mt}(u=0)$ for various particle sizes at different values of the acceleration, the conclusion arrived at (14) is that in the p.f. size range very little increase in mass transfer results even with an acceleration of 1000 g. It is then reasonable to assume that p.f. particles are effectively stationary relative to their gaseous environment.

It is then permissible to use Nusselt's (15) treatment for the calculation of R_{mt} assuming Fick's Law of Diffusion. The result of this treatment is:

$$R_{mt} = 48\,(D_o(f_m/d)\rho_o)(T/_{To})^{0.75}/32 \qquad (3)$$

where f_m is the mass fraction of oxidant in the bulk phase, d is the particle diameter, ρ_o is the gas density and T is the reaction temperature, the subscript o refers to standard conditions. This shows that the rate is proportional to 1/d and has a small temperature coefficient. The derivation of the above assumes that one oxygen molecule liberates two carbon atoms as CO. If account is taken of Stefan flow (16),(17) the above expression is modifife to:

$$R_{mt} = -48\,[(D_o/d)\rho_o(T/T_o)^{0.75}\ln(1-\gamma f_m)/\gamma]/32 \qquad (4)$$

Since this equation shows that the rate of mass transfer is inversely proportional to the particle diameter, as d becomes small enough R_{mt} will become large so that below a certain particle size $R_{mt} >> R_{chem}$. When this condition is met the chemical reaction rate will become the rate controlling process. We can then elaborate upon point (ii) above and differentiate between the process of chemisorption and desorption, either one of which can be the rate controlling step.

Expressions for the maximum rates of chemisorption and desorption in gas/solid systems have been derived (18), (19) and are:

for chemisorption (adsorption)

$$R_{chem} = [2M_O P_{O_2}/(2\pi RTM_{O_2})^{1/2}]\exp(-E_{ads/RT}) \text{ gm/cm}^2 \text{ sec.} \qquad (5)$$

where E_{ads} is the activation energy for chemisorption. This rate is seen to be first order in oxygen concentration.

for desorption (from absolute rate theory (7))

$$R_{\text{chem des}} = C_s\, k\, \frac{k_B T}{h}\, \frac{f^+}{f_s}\, \exp\left(-E_{\text{des}}/RT\right) \quad \text{gm/cm}^2 \text{ sec.} \qquad (6)$$

$$\text{or } R_{\text{chem des}} = \left[(12RTC_s)/(N^2 h)\right] \exp\left(-E_{\text{des}}/RT\right) \quad \text{gm/cm}^2 \text{ sec.} \qquad (7)$$

where C_s = number of carbon atoms/cm^2 of graphite lattice

k = transmission coefficient

k_B = Boltzmann constant

f^+, f_s are partition functions

E_{des} is the activation energy for desorption

In this case, the rate is seen to be independent of oxygen concentration, i.e., zero order in oxygen.

The transition between a system whose rate is controlled by chemical reaction to one whose rate is controlled by mass transfer is often depicted on an idealized Arrhenius diagram as shown in Fig. II. For a fixed particle size as the temperature is increased the rate of the chemical reaction will increase much faster than the rate of mass transfer until above a critical temperature T_c the mass transfer limits the overall rate of the reaction. The temperature at which this transition occurs depends on particle size since R_{mt} is proportional to 1/d while R_{chem} is independent of the particle diameter. Mulcahy and Smith (14) attempted to estimate the value of T_c that would hold for a 40 micron particle if the chemical rate was calculated from equations 5 and 7 and the mass transfer rate was given by equation 4. However, the assumptions they had to make in order to evaluate these rates from the equations, especially for the desorption rate are probably unrealistic so that any conclusions obtained from this ideal analysis should be used cautiously. Nevertheless their conclusion is that if E_{ads}>5 kcal/mole, combustion at atmospheric pressure of virtually all particles in the p.f. range will be chemically controlled.

After Nusselt's work it was generally assumed that the rate of mass transfer to a particle could be automatically equated to the rate of combustion, but Hottel and Stewart (21) found evidence of chemical rate control in a reanalysis they performed on some existing data. Essenhigh (22) and Essenhigh and Beer (23) found strong evidence of chemical rate control from their experimental data and subsequent workers (24), (25) have supported these conclusions. Mulcahy and Smith (14) have plotted rate data derived from investigations on the combustion of anthracites, bituminous coals, soots, charcoals

and bulk graphites on an Arrhenius diagram. They have plotted on the same diagram the theoretical line for mass transfer to a 40 micron particle and although the plotted rates are considerably scattered, they are all less than the rate of this mass transfer to a 40 micron particle. Also the strong dependence of the rate on the fuel type is very indicative of chemical control. All this evidence tends to strongly imply that chemical control is operative in the combustion of p.f. sized particles at atmospheric pressure.

In the above discussion we have been implicitly considering the particles to be impervious and that they burn at constant density as progressively shrinking spheres. Although this is implied it in no way changes the qualitative conclusions that have been arrived at. However, in order to study practical systems of combusting particles, we must realize that this simple model is often incorrect. The variation in chemical reactivity of a particle can depend on the intrinsic chemical nature of the material or on the physical structure of the material. The most likely factor determining the reactivity is the total surface area available to the oxidant, this in turn depends on the roughness of the surface and the porosity of the particle, i.e., on the internal structure and extent of micro, transitional and macropores. When the particle is porous and oxidant can penetrate into the interior, the pore structure is modified during the reaction as the walls of the pores are themselves consumed during the combustion process. It might be expected that the rate of oxidation would increase from low to 50 percent burn off as the accessibility of surface increases, and then decrease as pores coalesce and reduce the total internal surface area. Microscopic and photographic examination of coals and chars during various conditions of heating and combustion have been undertaken (26)-(32) and in some cases combustion has been observed to occur in the pores. The only conclusion from this is that the effect of porosity with the possibility of internal burning must be considered in any discussion of combustion processes of p.f. particles.

The schematic Arrhenius plot of Fig. III shows the case for an impervious sphere as well as the case for a porous particle. This latter case shows three regimes which are now briefly discussed.

In zone I the oxidant concentration is the same throughout the particle and equal to that of the bulk phase. The reaction rate per unit total surface area is

$$R_{chem,\ tot} = A\, C^{n} \exp(-E/RT) \qquad (8)$$

where n and E are the true order and activation energy for the reaction.

In zone II the concentration of oxidant within the porous structure is not constant but varies from effectively zero at the center of the particle to the bulk phase value at the periphery. Thus the rate of reaction is in part determined by the internal diffusion of oxidant through the porous structure (33). The rate of reaction is then given by (14):

$$R_{chem} = 2N\pi r_p [(r_p D_p A C^{n+1} \exp(-E/RT)) (n+1)^{-1}]^{1/2} \quad (9)$$

The apparent order is then (n+1)/2 where n is the true order and the apparent activation energy becomes E/2 where E is the activation energy in zone I, since both expressions appear under the square root sign in the rate equation.

In zone III the increase in temperature has increased the reaction rate so that it has become too fast to control the overall rate and oxidant molecules react as soon as they arrive at the particle surface. The overall rate is then controlled by mass transfer. It is important to realize that there is no sharp cut off from one zone to another, but rather a continuous transition between the zones.

Another regime exists characterized by a solid whose reactivity is great enough to prevent oxidant penetration further than the mean free path λ, but not fast enough to cause mass transfer control. This regime is termed the "outer kinetic region" (17) and has zone I kinetic characteristics. However in this case there is an increased area for reaction because of the external roughness of the surface of the particle.

The regime in which the reaction is occurring can be determined by calculating the depth to which the oxidant can penetrate into the particle. If the depth of penetration is L, then from our definitions above we see that for rough sphere particles $L<\lambda$; for zone I $L>>r$ (the particle radius); and for zone II $\lambda<L\leq r$. Mulcahy and Smith (14) adopting the idealized pore model of Wheeler (34) used observed combustion rates to estimate values of L as a function of the particle porosity (θ) and the mean pore radius ($\bar{r}_p$) using the relation for zone II conditions:

$$L\ (C = 0) = D_p \Theta C_s / [(n+1)^{1/2} R_{chem}] \quad (10)$$

where C_s is the concentration at the surface.

They found that $L>\lambda$ for reasonable values of the porosity when $\bar{r}_p > 0.1$ microns for a reactive coal and $\bar{r}_p > .01$ for a less reactive coal. Values of $\bar{r}_p$ below .05 microns for reactive coal and 0.005 microns for less reactive coal gave rise to rough sphere conditions, i.e., $L<\lambda$. For $\bar{r}_p \geq 1$ micron all particles

in the p.f. range were found to be completely penetrated at the lower chosen value for R_{chem}. At the same pore size and highest R_{chem}, particles <20 microns were found to be completely penetrated (zone I kinetic region) and 100 micron particles were 40 percent penetrated. Thus the conclusions of this analysis were that if all the porosity was contained in micropores rough sphere kinetics would always apply, but if the particle were macroporous, then zone II conditions would be applicable.

Thus chars produced from anthracites and brown coals which are highly microporous would be expected to combust under rough sphere conditions. The conclusions just stated were arrived at by applying the simple cylindrical pore model developed orginally by Wheeler (34) to place reactions within porous catalysts on a theoretical basis. Evidence from microscopy hardly supports this simple model, many pyrolized particles have complete voided structures varying from "pop corn" type through lacy to hollow cenospheres (35). However the important points to emerge from this analysis are firstly that the value of the rate of chemical reaction at the start of the combustion process may not remain constant throughout the whole burn-out period even in isothermal conditions because of the evolution of the internal structure of the particle, and secondly that the temperature and oxidant concentration are not the only variables to consider when interpreting the kinetics of such reactions.

Disputed Issues

For a simple reaction the rate per unit surface area can be expressed as

$$R_{chem\ tot} = A\ C^{n} \exp(-E/RT) \qquad (11)$$

where n and E are the true order and activation energy of the reaction independent of temperature, and A has only a slight temperature dependence in comparison to the exponential term. The true parameters n and E in combustion systems have been extremely difficult to determine for several reasons. Among these reasons are:

(i) the difficulty in avoiding zone II and III conditions

(ii) the difficulty in controlling the particle temperature because of the high heat of reaction

(iii) the change in the available surface area during the course of the combustion process

Therefore there is still considerable uncertainty pertaining to values of E and n for impure carbons. This uncertainty even applies to the case of pure carbons where although many investigations to determine the values of these parameters have been undertaken,

there is still considerable inconsistancy and uncertainty in the experimental results. Walker (36) et al have reviewed the carbon oxygen system and point out that as θ' (the surface coverage) tends to unity, that the reaction order would be expected to be zero with respect to covering agent and when θ' tends to zero, a first order dependence is predicted. These authors correctly imply that an important factor affecting θ' is the pressure of oxidant but also the temperature of the particle surface is probably an equally important factor. This factor may explain why Gulbransen and Andrews (37) obtain a zero order dependence at relatively low pressures in a low temperature range of 400-500°C, and similarly Blyholder and Eyring (20) obtain a zero order dependence at 800°C at low pressures. Orders intermediate between zero and one have been found by several workers (38)-(42) using highly purified graphites.

Variations in activation energies between about 80 kcal/mole down to zero have been obtained under various conditions for the oxygen pure carbon system and for the impure carbon system, similar, but not so large, variations in activation energy have been found, with the value often being strongly temperature dependent.

Disagreement also exists in the p.f. system as to the value and temperature dependence of activation energies. Smith in two papers on the kinetics of combustion of size graded particles (43), (44) finds activation energies on the order of 17 kcal/mole and an order of unity in surface oxygen concentration. He represents R_{ac}, the rate per unit external surface area, by an Arrhenius expression of the form:

$$R_{ac} = A \exp(-E_a/RT_p) \quad gm/cm^2 \text{ sec atm } O_2 \qquad (12)$$

where T_p is the particle temperature calculated from a simple heat balance on the particle assuming CO to be the primary product (45).

Field (1), (46) in experiments on the rates of combustion of size graded fractions of char attempted to fit his data to an expression of the Arrhenius form, but found that the activation energy could not be taken as constant, but would need to vary as a function of temperature, decreasing from about 35 kcal/mole at 1300°K to about 10 kcal/mole at 1800°K. Smith in an attempt to account for the non-linearity of Field's Arrhenius plot suggested that Field's data is compatible with a transition between rate control in zone I to zone II, brought about possibly by the differences in pore structure of the chars used. However, if this were the explanation, the activation energy in Field's data should never fall below a value of E/2, where E is the value obtained in zone I, hence Field's activation energy should never be less than 17 kcal/mole, whereas in fact the activation energy falls to 10 kcal/mole and apparently is still falling with increasing temperature. The scatter in Smith's data makes it difficult to say whether E_a is constant or does in fact level off slightly in the higher temperature region as does Field's data.

Another possible explanation as to this change in activation energy with temperature is given in the next section (Attempted Clarification of Disputed Issues by a Reanalysis of Existing Data), where some of Field's original data is reanalyzed.

Attempted Clarification of Disputed Issues by a Reanalysis of Existing Data

Changes in the temperature dependence of a reaction that can be depicted on an Arrehnius diagram are consistent with change from chemical to mass transfer dominance as discussed earlier, or change from zone I to zone II kinetic dominance, also discussed above. However, the temperature variation of the activation energy and apparent (or real) order in oxygen can also be explained by a transition from desorption to chemisorption dominance in the reaction. Chemisorption is known to occur extensively on carbons at room temperature (47), so it is reasonable to expect the activation energy for chemisorption to be low, with the order in oxygen being unity. Activation energies for desorption are expected to be high (20) and an order in oxygen of zero. So we can expect at low temperatures, where the chemical rate is slow, the surface to be covered with oxidant so the reaction rate must be controlled by the desorption process. In this case, the order in oxygen should be zero for zone I conditions and 1/2 for zone II. The activation energy E_{des} is expected to be high, perhaps in the region of 40-80 kcal/mole. As the temperature increases, so does the reaction rate and the surface coverage tends to zero, so that the process now limiting the reaction rate is the chemisorption of oxidant onto the surface of the carbon. This would lead to an apparent and real order of unity and a low value for the activation energy (E_{ads}). To lend support to this hypothesis, the results of Field (1) have been reanalyzed in the discussion contained below.

Field (1) shows his results plotted on a linear plot of K_s (surface reaction rate coefficient gm/cm^2 sec atm) against surface temperature T_s °K. The exponentially rising curve shown also on the same graph represents the best fit to the data of past workers at atmospheric pressure and at temperatures above 1000 °K, as given in the review by Field, Gill, Morgan and Hawksley (49). The curve is given by:

$$K_s = A \exp(-E/RT_s)$$

where $A = 8710$ gm/cm^{2}sec atm

$E = 35{,}700$ cal/mole

$R = 1.986$ cal/mole °K (13)

This exponential curve is based on measurements from other workers below 1650°K, and it is evident from the graph that the new measurements of Field are consistent with the curve up to this temperature. However,

for temperatures above 1650°K, the values of Field's data fall considerably below the extrapolated exponential curve.

Field therefore represents his data by a linear relationship of the form:

$$K_s = -0.49 + 3.85 \times 10^{-4} T_s \qquad (14)$$

$$\text{or} \quad K_s = K_o + A T_s$$

In Field's second paper on combustion rates of p.c. (46), he represents his rate variance with temperature by the following expression for various coals:

$$K_s = K_{s,1600\ °K} + A (T_s - 1600) \qquad (15)$$

The simple model assumed for the interpretation of Field's data is that of the Langmuir Adsorption Isotherm (50). Although this model is necessarily subject to the underlying assumptions of this theory (47), the general conclusions derived from this treatment are applicable.

From Langmuir's treatment, we can say that the rate of reaction is given by:

$$\text{Rate} = \frac{K_1 K_2 p_s}{K_1 p_s + K_2} \qquad (16)$$

where K_1 and K_2 are the rates for chemisorption and desorption respectively, and p_s is the oxygen concentration at the surface. Expressing the rate in terms of Field's nomenclature (1) we have:

$$K_s p_s = \frac{K_1 K_2 p_s}{K_1 p_s + K_2}$$

$$\text{and} \quad 1/K_s p_s = 1/K_2 + 1/K_1 p_s$$

where $K_1 = k_1 \exp(-E_1/RT_s)$ and $K_2 = k_2 \exp(-E_2/RT_s)$. Here, k_1 and k_2 are the pre-exponential factors for chemisorption and desorption respectively, and E_1 and E_2 are the activation energies for chemisorption and desorption respectively. Rearranging the above expression leads to:

$$1/K_s = \frac{\exp\ (E_1/RT_s)}{k_1} + \frac{p_s\ \exp(E_2/RT_s)}{k_2} \qquad (16a)$$

$$1/K_s = (1/k_1)\ \exp\ (E_1/RT_s)\ \{1 + \frac{k_1 p_s}{k_2}\ \exp\ [(E_2 - E_1)/RT_s]\} \qquad (17)$$

$$\ln K_s = \ln k_1 - \frac{E_1 + RT_s\ \ln\ \{1 + b\ \exp\ [(E_2-E_1)/RT_s]\}}{RT_s}$$

This last expression gives an apparent activation energy E_a, where

$$E_a = E_1 + RT_s\ \ln\ [1 + b\ \exp(\Delta E/RT)] \qquad (18)$$

Here there are three variable parameters E_1, b and ΔE, where $\Delta E = E_2 - E_1$ and $b = k_1 p_s / k_2$.

Field's expression for his temperature dependent activation energy is:

$$E = RAT_s^{\,2}/K_s \qquad \text{(eq. 10 ref. (46))} \qquad (19)$$

Values of activation energy E were calculated from equation (19) at various temperatures T_s. A least squares fit of the activation energies calculated from equation (19) was performed using the functional form of equation (18). The fitting parameters that were varied to obtain the best least squares fit were E_1, b and ΔE. The results obtained from this analysis were:

$$E_1 \simeq 6{,}000 \text{ cal/mole}$$

$$E_2 \simeq 37{,}000 \text{ cal/mole}$$

$$b \simeq 0.000126$$

Using these values of the three fitting parameters, equation (18) matches equation (19) almost exactly.

Starting with equation (16a), we can rearrange it in the following forms:

$$1/K_s = (p_s/k_2)\exp(E_2/RT_s)\{1 + (k_2/k_1p_s)\exp[(E_1-E_2)/RT_s]\}$$

$$1/K_s = (p_s/k_2)\exp(E_2/RT_s)\{1 + (1/b)\exp(-\Delta E/RT_s)\} \quad (20)$$

$$\text{and } 1/K_s = (p_s/k_2)\exp(E_2/RT_s)[1 + X] \quad (21)$$

Equations (17) and (20) are equivalent forms of equation (16a). As the temperature T_s tends to zero, X tends to zero, and we see from equation (21) that K_s approaches $(k_2/p_s)\exp(-E_2/RT_s)$, or that K_sp_s approaches $k_2\exp(-E_2/RT_s)$. Thus we find that as T_s tends to zero, we tend towards a zero order rate expression whose limit is $k_2\exp(-E_2/RT_s)$ or K_2.

It is interesting to determine the value of X with increasing temperature, and hence the departure of the rate expression from the pure zero order dependence component K_2. Below 1400°K, $X<<1$ (in fact less than .01) and the low temperature limit is applicable. In the range of temperatures 1400°K to 2000°K, the value of X grows from 1.47×10^{-2} to 0.763 (see Table I). At approximately 1600°K, ten percent divergence from a pure K_2 dependence would be incurred, with ever increasing divergence occurring at higher temperatures as is shown in Fig. III.

Referring to Field's statement (1) that data from previous workers at lower temperatures (<1650°K) could be fitted with an Arrhenius rate expression with an activation energy of 35,700 cal/mole, it is not surprising to obtain this result in view of the above analysis. Recall that E_2, the low temperature limit activation energy for the desorption process, was calculated to be approximately 37,000 cal/mole, and that significant divergence from this simple Arrhenius expression occurs only above 1650°K. The oxygen dependence was also shown to be zero order for the temperature range in the analysis presented here.

The above explanation and analysis appear to fit the facts as far as order in oxygen and temperature dependence of activation energy are concerned, especially for the data of Field. More precise rate determinations are required, especially in the high temperature region, if more experimental substantiation of this theory is to be obtained.

More evidence to support this hypothesis comes also from the study of pure carbon systems. Rosner and Allendorf (48) found in

their study of the reaction of oxygen with pure graphite at high temperatures that the activation energy changed from 31 kcal/mole at 1300°K to 0 at 1600°K. At 1200°K the apparent order was 0.56, which implies that the real order is zero, if pore diffusion is present and the reaction is in the desorption controlled regime. At 1440°K the apparent order is unity and this is compatible with chemisorption control. So perhaps detailed mechanistic arguments were not that premature from their data.

Blyholder and Eyring (20) find a zero order reaction with an activation energy of 80 kcal/mole at 800°C for very thin coatings of graphite rubbed on ceramic rods. This was twice as large as the activation energy observed for samples 1 mm. thick where the rate is obviously pore diffusion controlled. The order in this case was found to be 1/2 in oxygen.

Departures of the activation energy at high temperatures towards the limiting value of chemisorption control may not occur to any substantial extent until very high combustion temperatures are reached, as was shown from the above analysis. Also, much of the existing data on burn out of small p.f. particles is expectedly quite scattered because of the difficulties involved in extracting reliable data from such systems, so direct substantiation of the proposed picture set out in this paper may be difficult. However, this has been an attempt to consolidate some results in the carbon oxygen system, especially as it is applicable to p.f. systems, and fit them into a workable, although simplistic model.

References

1. Field, M.A., Comb. and Flame, 13, 237 (1969)

2. Howard, J.B. and Essenhigh, R.H., Ind. and Eng. Chem. Process Des. and Dev., 6, 76 (1967).

3. Wheeler, R.V., Trans. of the Chem. Soc., 103, 1715 and 1754 (1913).

4. Essenhigh, R.H. and Howard, J.B., Am. Conference on Coal Science 1964, Paper 44, P.S.U., Ind. and Eng. Chem., 58 15 (1966).

5. Loison, R. and Chauvin, R., Chim. Ind., 91, 269 (1966).

6. Badzoich, S. and Hawksley, P.G.W., Ind. and Eng. Chem. Process Des. and Dev., 9, 521 (1970).

7. Kimber, G.M. and Gray, M.D., Comb. and Flame, 11, 360 (1967).

8. Field, M.A., Gill, D.W., Morgan, B.B., and Hawksley, P.G.W., "Combustion of Pulverized Coal" (BCURA, Leatherhead, 1967), Fig. 4.5, p. 166.

9. Dryden, LG.C., Fuel, 30, 93 (1967).

10. Juntgen, V.H., Seminar P.S.U., July, 1967.

11. Juntgen, V.H. and Van Heek, N.H., Fuel London, 47, 103 (1967).

12. Van Krevelen, D.W., Schuler, J., "Coal Science" (American Elsevier, New York, 1957), p. 295.

13. Ishihama, W., Eleventh Int. Conf. of Director of Safety in Mines Research, Warsaw, Poland (1961).

14. Mulcahy, M.F.R. and Smith, I.W., Rev. Pure and Appl. Chem., 19, 81 (1969).

15. Nusselt, W., Z. Ver. deut. Ing., 68, 124 (1926).

16. Rosner, D.E., Int. J. Heat and Mass Transfer, 9, 1233 (1966).

17. Frank-Kamenetskii, D.A., "Diffusion and Heat Exchange in Chemical Kinetics," 1947 (Trans. Thon, N., Princeton University Press, 1955).

18. Moelwyn-Hughes, E.A., "Physical Chemistry" (Pergamon Press, London, 1957) p. 45.

19. Glasstone, S., Laidler, K.J., and Eyring, H., "The Theory of Rate Processes" (McGraw-Hill, New York, 1961) p. 351.

20. Blyholder, G. and Eyring, H., J. Phys. Chem., 61, 682 (1957).

21. Hottel, H.C. and Stewart, I. McC., Ind. Eng. Chem., 32, 719 (1940).

22. Essenhigh, R.H., Sheffield Univ. Fuel Soc. Journal, 6, 15 (1955).

23. Beer, J.M. and Essenhigh, R.H., Nature, 187, 1106 (1960).

24. Howard, J.B., Ph.D. Thesis, P.S.U.

25. Beer, J.M. and Thring, M.W., Bulletin 75, M.I. Expt. Station, P.S.U., 25 (1961).

26. Shibaoka, M., Journal Inst. Fuel, 42, 59 (1969).

27. Gray, M.D., Kimber, G.M., and Granger, D.E., Fuel London, 46, 399 (1967).

28. Ramsden, A.R., Journal Inst. Fuel, 41 651 (1968).

29. Littlejohn, R.F., Journal Inst. Fuel, 40, 128 (1967).

30. Lightman, P. and Street, P.J., Fuel London, 47, 7 (1968).

31. Lightman, P. and Street, P.J., Fuel London.

32. Tucker, A.C.N., Fuel London, 48, 105 (1969).

33. Weisz, R.B. and Psalter, C.D., Advances in Catalysis, 6, 143 (1954).

35. Sinnatt, F.S., J. Soc. Chem. Ind. London, 47, 151 (1928).

36. Walker, P.L., Jr. and Rusinko, F., and Austin, L.G., Advances in Catalysis, 11, 133 (1959).

37. Gulbransen, E.A. and Andrews, K.E.,Ind. Eng. Chem., 64, 1036 (1952).

38, Bonnetain, L., and Hoynant, G., "Les Carbones," ed. Le Groupe Francais d'Etude des Carbones (Masson, Paris, 1965), 2, p. 277.

39. Duval, X., "Les Carbones," ed. Le Groupe francais d'Etude des Carbones (Masson, Paris, 1965), 2, p. 256.

40. Rebaudieres, P., and Guerin, H., Compt. rend., 260, 6864 (1965).

41. Amariglio, H., and Duval, X., J. Chimie phys., 64, 916 (1964).

42. Lewis, J.B., Connor, P., and Murdoch, R., Carbon, 2, 311 (1964).

43. Smith, I.W., Comb. and Flame, 17, 303 (1971).

44. Smith, I.W., Comb. and Flame, 17, 621 (1971).

45. Ayling, A.B. and Smith, I.W., Comb. and Flame, 18, 173 (1972).

46. Field, M.A., Comb. and Flame, 14, 237 (1970).

47. Hayward and Trapnell, "Chemisorption" (Butterworths, 1964).

48. Rosner, D.E. and Allendorf, H.D., Carbon, 3, 153 (1965).

49. Field, M.A., Gill,D.W., Morgan, B.B., and Hawksley, P.G.W., "Combustion of Pulverized Coal", (BCURA, Leatherhead, 1967), pp. 189-192, 329-365.

50. Langmuir, I., J. Amer. Chem. Soc., 40, 1361 (1918).

Table I

T °K	$\frac{\Delta E}{RT}$	exp (-ΔE/RT)	$(\frac{1}{b})$ exp (-ΔE/RT)
0	∞	0	0
1000	18.5	9.25×10^{-9}	7.35×10^{-5}
1200	15.4	2.05×10^{-7}	1.63×10^{-3}
1400	13.2	1.85×10^{-6}	1.47×10^{-2}
1600	11.6	9.17×10^{-6}	7.28×10^{-2}
1800	10.3	3.36×10^{-5}	0.267
2000	9.25	9.61×10^{-5}	0.763

Figure I

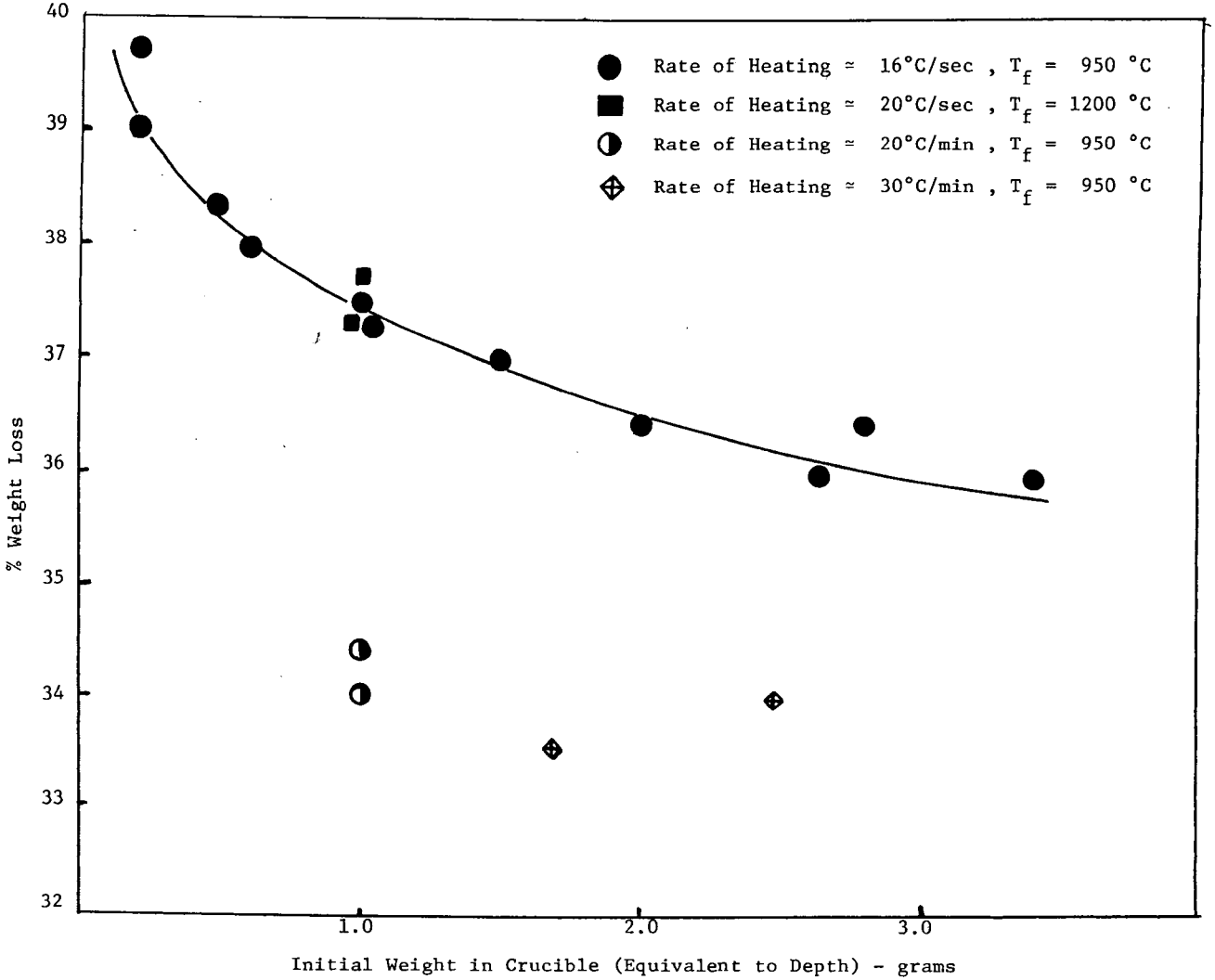
Rate of Heating ≃ 16°C/sec , T_f = 950 °C
Rate of Heating ≃ 20°C/sec , T_f = 1200 °C
Rate of Heating ≃ 20°C/min , T_f = 950 °C
Rate of Heating ≃ 30°C/min , T_f = 950 °C
% Weight Loss
40
39
38
37
36
35
34
33
32
1.0
2.0
3.0
Initial Weight in Crucible (Equivalent to Depth) - grams

Figure II

Arrhenius Diagram Showing Rate Controlling Regimes in Gas-Solid Reactions

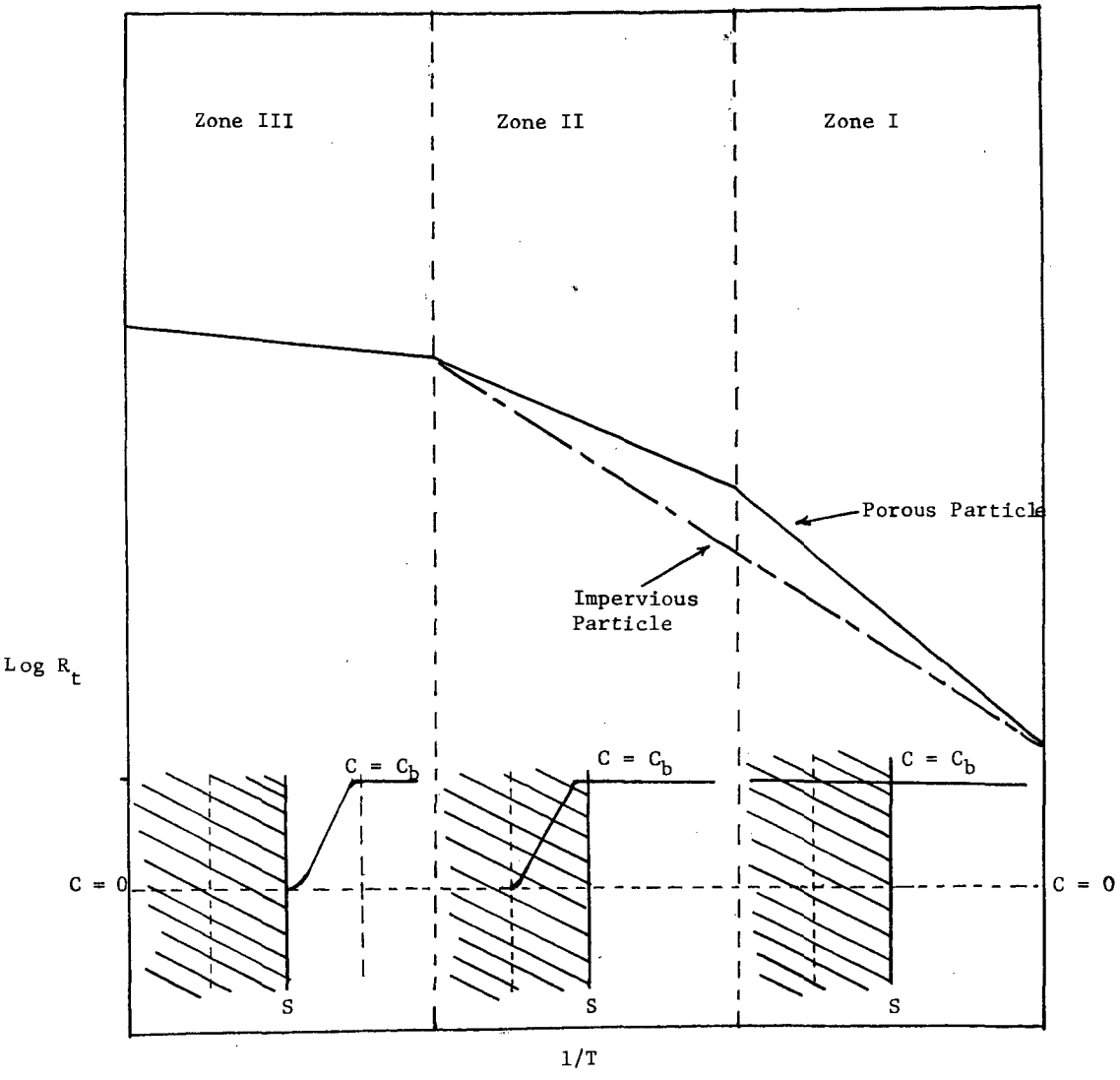

S = Particle Surface

C_b = Bulk Concentration

Figure III

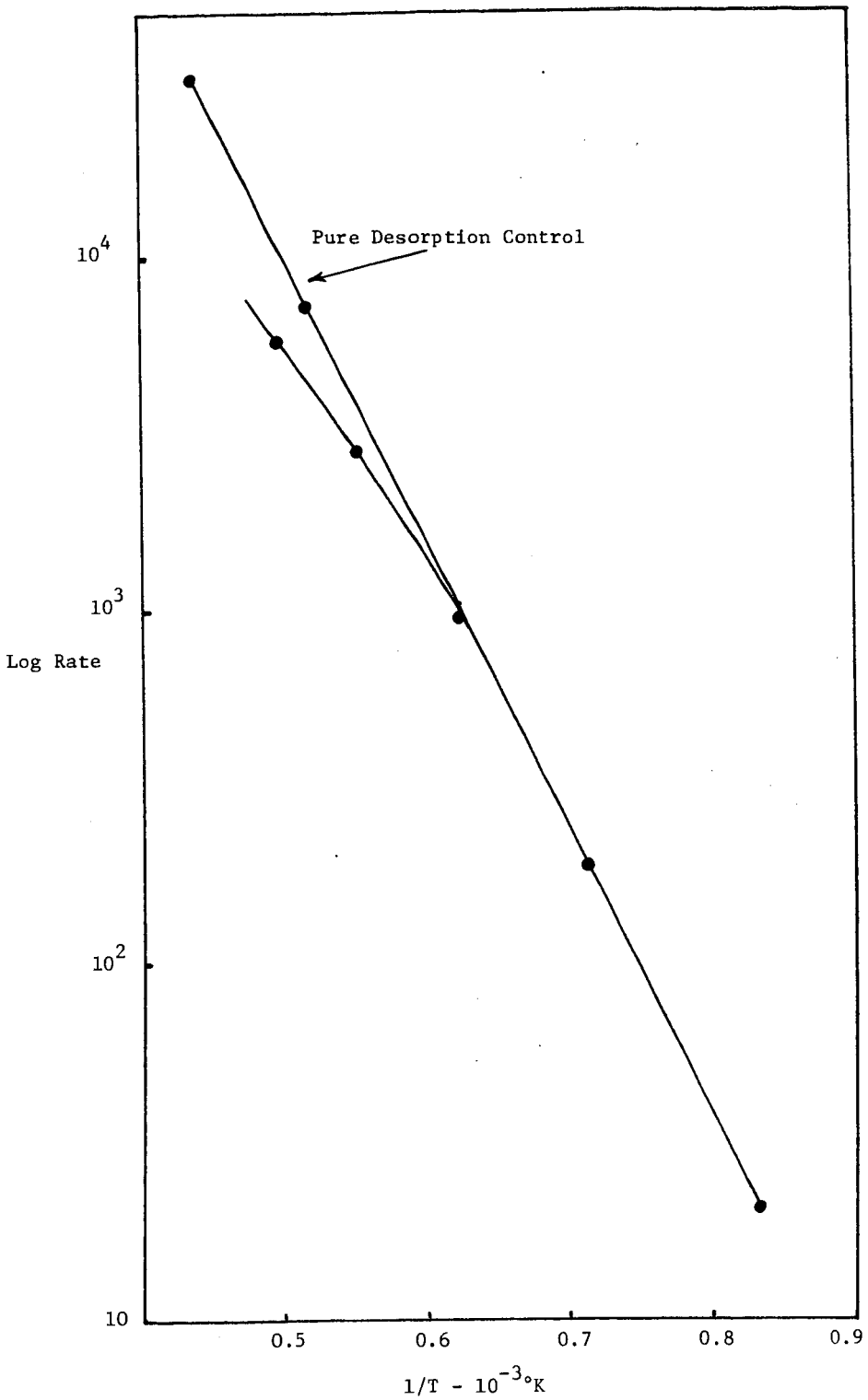
Pure Desorption Control
10^4
10^3
10^2
10
Log Rate
0.5
0.6
0.7
0.8
0.9
1/T - 10^{-3}°K

COAL GASIFICATION IN A LOW PRESSURE, LOW RESIDENCE TIME, ENTRAINED FLOW REACTOR

R. L. Coates, C. L. Chen, and B. J. Pope

Chemical Engineering Department
Brigham Young University
Provo, Utah 84601

INTRODUCTION

Prior studies in which finely-ground coal was heated very rapidly have shown that the fraction of the coal that can be volatilized increases with both the rate of heating and the final temperature to which the coal is heated. For example, Eddinger, et al [1], have presented data from an entrained flow reactor which show that volatile products amounting to 49.9 percent of the coal fed may be produced from a finely-ground coal having an ASTM volatility of only 35.5 percent, even though maximum reactor temperature was less than the 950°C reached in the standard volatility test. Kimber and Gray [2] reported coal pyrolysis data in an entrained flow reactor operated at temperatures up to 2200°K. They observed volatiles as much as 87% greater than that from the standard test and concluded both higher heating rates and higher final temperatures increase the amount of volatile products.

Another characteristic of high-rate, high-temperature pyrolysis of coal that is not found in normal carbonization is the production of significant quantities of acetylene and ethylene in the pyrolysis gas. These products are commonly observed during coal pyrolysis in a plasma or by flash heating.[3]

The present study was undertaken to investigate the potential for increased volatility and also the production of unsaturated hydrocarbons as a result of rapid pyrolysis using partial combustion as the source of pyrolysis energy. This paper represents a progress report on the experimental work accomplished to date.

EXPERIMENTAL PROCEDURES

An entrained flow reactor was designed in which the finely-ground coal could be rapidly mixed with oxidizing combustion gases. The combustion gases were produced from a pre-mixed flame of pure oxygen with hydrogen. The reactor volume was designed for short residence times, and the products were quenched by water spray immediately downstream of the reactor.

A diagram of the reactor is shown in Figure 1. The reaction tube was made of alumina. This tube was placed inside an annular electrical heating element for preheating and to reduce heat loss during the run. The reaction tube and heating elements were insulated with a fibrous alumina insulation and encased with a water-cooled section of 6-inch aluminum pipe. Reaction tubes 4 5/8 inches in length with inside diameters of 3/4, 1 1/2, and 2 inches were tested. The use of smaller diameter tubes permitted testing at reduced residence times. The water-cooled injector head was made of aluminum. The coal was injected through two copper injectors located 180° apart and at an angle of 30° with the centerline of the reaction tube. The impingement point for these injectors was a distance of 3 inches below the orifice through which premixed combustion gases were fed to the reactor. A platinum/13% platinum-rhodium thermocouple was inserted near the base of the reactor to record the reactor temperature.

The coal tested was a high volatile B Utah coal from the Orangeville, Carbon County, area. Typical proximate and ultimate analyses of coal from this area are listed in Table 1. The coal was dried, ball-milled, and screened to minus 200 mesh for these tests. The moisture as used in the tests was less than one percent.

The coal was entrained into a stream of carrier gas, either hydrogen or nitrogen, with an auger-driven feeder. A variable-speed auger drive was employed to obtain feed rates ranging from 0.5 to 5.0 pounds of coal per hour. Entraining gas flows of from 13 to 15 SCFH were used in the 1/4-inch diameter feed line.

The product gas was separated from the quench water, passed through a filter and then through a gas meter. Samples of filtered gas were withdrawn for analysis with a gas chromatograph. The char was filtered from the quench water, dried and analyzed for ash content to verify material balance calculations.

The operating parameters varied were the feed rates of the coal and combustion gases and the stoichiometry of the combustion gases. Run times following preheating of the reactor ranged from 2 to 22 minutes. The range of feed rate variables tested and the range of reactor operating conditions that resulted are listed in Table 2.

RESULTS

A total of thirty-two test runs were made with the 2-inch diameter reaction tube, twenty with hydrogen as the carrier gas and twelve with nitrogen. Twelve tests were made with the 1 1/4-inch diameter reaction tube, and seven tests were made with the 3/4-inch diameter tube. Typical data obtained from these tests are presented in Table 3.

Effect of Hydrogen Concentration. It was observed that conversions to the hydrocarbon gases were generally higher the greater the concentration of hydrogen in the reactor. Data illustrating this effect are presented in Figure 6. In this figure the conversions to methane, ethylene, and acetylene at temperatures ranging from 1200 to 1400°K are plotted versus the hydrogen partial pressure at the reactor outlet. The conversion to methane is shown to be the most sensitive to this operating variable.

Although the observed effect of hydrogen concentration on the methane yield is in the direction expected from the hydrogenation reaction, i.e., $C + 2H_2 = CH_4$, the equilibrium constant, K_p, for this reaction is much lower than the observed ratio of $P_{CH_4}/P^2_{H_2}$. The observed ratios are compared with the curve representing hydrogenation equilibrium in Figure 7. It seems clear from this comparison that the hydrocarbon gases are nonequilibrium species resulting from pyrolysis reactions.

Steam Carbon Reaction. The composition and volumes of the product gas indicated that a significant fraction of the steam produced by the combustion gases reacted with the coal to form hydrogen and carbon monoxide. The calculated steam decomposition is plotted versus the oxygen/coal ratio in Figure 8. This plot also shows the effect of the two carrier gases, hydrogen and nitrogen. The higher hydrogen concentrations resulting from the use of hydrogen carrier gas is shown to suppress the steam decomposition. The approach of the reaction $C + H_2O = CO + H_2$ toward equilibrium is indicated by the data presented in Figure 9. It is apparent from this comparison that the steam-carbon reaction is far from equilibrium for all of the run conditions that were tested.

Shift Reaction. The conversion of carbon to carbon dioxide was observed to be rather low relative to the conversion to carbon monoxide, as mentioned above. In all cases the equilibrium constant, K_p, for the shift reaction, $CO + H_2O = CO_2 + H_2$, was observed to exceed the observed ratio of $P_{CO_2} P_{H_2}/P_{CO} P_{H_2O}$. This is illustrated by the data shown in Figure 10. The observed ratios are seen to correspond to equilibrium K_p's at substantially higher temperatures than those measured at the reactor outlet.

Volume and Heating Value. The volume of dry gas produced, less the volume of coal carrier gas fed to the reactor, is shown in Figure 11 as a function of the oxygen/coal ratio. The volume produced is seen to increase uniformly with this ratio. The corresponding heating value of the dry, carrier-free gas is shown in Figure 12.

Combustion Equivalence Ratio. The effect of varying the equivalence ratio of combustion hydrogen to combustion oxygen was tested by operating the reactor with coal feed rate, oxygen to coal ratio, and carrier gas rate constant, and varying the combustion hydrogen feed rate. Combustion hydrogen was varied to give an equivalence ratio, i.e., the moles H_2 per mole O, from 0.4 to 1.1. As illustrated in Figure 13, the weight of carbon in hydrocarbon gases per 100 pounds of coal increased and the molar ratio of carbon dioxide to carbon monoxide decreased with the equivalence ratio.

Reactor Temperature. Analysis of the data showed that the primary variable governing the composition of the reactor products was the temperature. The temperature as indicated by the thermocouple measurements was observed to increase with the amount of combustion gas fed to the reactor per pound of coal. Although the reactor tube was electrically heated, the feed rates and heat transfer area were such that the heating elements exerted a rather small effect on the reaction temperature, serving primarily to reduce heat losses. Figure 2 presents the measured temperatures as a function of the ratio of combustion oxygen per pound of coal. The effects of reaction tube diameter and coal feed rate are also indicated on this figure.

Effect of Temperature. Figure 3 presents data showing the conversion of the carbon in the coal to the hydrocarbon gases methane, acetylene, and ethylene, and to carbon monoxide and carbon dioxide. The conversion data are plotted versus the measured temperature without regard for variations in the other operating variables. These conversions were computed from the measured volume and composition of the gas produced, after condensation of the water vapor, and the feed rate of the coal. It is of interest to note first that in contrast to gasification products of conventional low-pressure coal gasifiers, significant conversion to the three hydrocarbon gases, methane, acetylene, and ethylene, were observed. Secondly, the trend of conversion with reactor temperature is clearly evident. The methane conversion rises to a maximum and then decreases with increasing temperature, the conversion to acetylene increases with temperature, and the conversion to ethylene decreases with temperature.

The effect of replacing hydrogen as the coal carrier with nitrogen on the conversion to carbon oxides is also indicated on this figure. The conversion to carbon monoxide appears to be principally dependent on temperature; however, the carbon dioxide yield is significantly greater with the lower hydrogen concentrations resulting from the use of nitrogen carrier gas. It is of interest to note that the amount of carbon dioxide produced relative to the amount of carbon monoxide is low as compared to the products from conventional gasifiers.

Effect of Residence Time. The effect of average residence time in the reactor on the conversion to the three hydrocarbon gases is indicated by the data shown in Figures 4 and 5. Figure 4 shows conversion data from three different sizes of reactor tubes each operated at a coal feed rate of 1.2 pounds of coal per hour. These data show only a slight effect of reactor size on the product yields. In Figure 5 the conversions for reactor temperatures in the range 1200-1400°K are plotted versus the average residence time. Although the data are scattered, there is a trend to lower conversions with increasing residence time. This trend is most evident in the conversion to acetylene. The data corresponding to Figure 4 and 5 show that reactor residence times of less than fifty milliseconds are sufficient for gasification to occur in this temperature range and that these products tend to disappear as the residence time increases.

SUMMARY

The observations and conclusions drawn from the experimental runs may be summarized as follows:

1. Reactor temperature was found to be the most important parameter affecting the overall gasification of coal. The temperature was controlled principally by the combustion oxygen fed per pound of coal. As much as 57 percent of the mass of coal fed was gasified, and the space time conversion corresponding to this yield was 408 lb carbon gasified/ft^3 hr.

2. Significant yields of methane, ethylene and acetylene were produced. Up to 14 percent of the coal carbon was converted to these gases. The yield of ethylene was observed to decrease with increasing reactor temperature while the yield of acetylene increased. The conversion to methane was observed to pass through a maximum at a reactor temperature of about 1200°K. Maximum yields of methane, ethylene and acetylene were 6, 4, and 6 percent of the coal carbon respectively.

3. The yield of hydrocarbon gases was observed to increase with increasing hydrogen concentration and to decrease with increasing residence time. Residence times shorter than 50 milliseconds are indicated for optimum yield of hydrocarbon gases. Comparison of the methane yield data with hydrogenation equilibrium indicates that the hydrocarbons in the product result not from hydrogenation reactions but from non-equilibrium pyrolysis reactions.

4. Although significant steam decomposition was observed, conversion of carbon to carbon monoxide was substantially less than predicted for steam, carbon equilibrium. The conversion of carbon to carbon dioxide was observed to be much lower than predicted by the shift reaction equilibrium.

5. The yield of hydrocarbon gases and the yield of carbon dioxide relative to carbon monoxide depends strongly on the stoichiometry of the combustion gas. Combustion gases lean in hydrogen fuel cause the hydrocarbon gas yield to be reduced and the ratio of CO_2 to CO to be increased from the yields with stoichiometric combustion gases.

6. The volume of gas produced per pound of coal increases uniformly with the oxygen/coal ratio. At the ratio corresponding to maximum hydrocarbon gas yield the volume produced is 22 SCF per pound of coal.

7. The carrier-free heating value of the product gas decreases uniformly with increasing oxygen/coal ratio. At the ratio corresponding to maximum hydrocarbon gas yield, the heating value is in the range of 370-420 BTU/SCF.

ACKNOWLEDGEMENT

This work was carried out under contract to Bituminous Coal Research, Inc., with funds supplied by the U.S. Office of Coal Research.

REFERENCES

1. Eddinger, R. T., Friedman, L. D., and Rau, E., "Devolatilization of Coal in a Transport Reactor," Fuel 45, 245-252 (1966).

2. Kimber, G. M., and Gray, M. D., "Rapid Devolatilization of Small Coal Particles," Combustion and Flame 11, 360-362 (1967).

3. Bond, R. L., Ladner, W. R., and McConnell, G. I., "Reactions of Coal in a Plasma Jet," Fuel 45, 381-395 (1966).

TABLE 1.- Coal analysis - weight percent as received

PROXIMATE		ULTIMATE	
Moisture	5.65	Carbon	70.05
Ash	6.20	Hydrogen	5.76
Volatile Matter	34.35	Nitrogen	1.30
Fixed Carbon	53.80	Sulphur	0.64
	100.00	Oxygen	10.40
		Moisture	5.65
		Ash	6.20
			100.00

Coal size (-200 MESH)

TABLE 2.- Range of Feed Rate Variables

Coal Feed Rate, lbs/hr	0.7-4.1
Oxygen/Coal Ratio	0.3-1.6
Combustion Gas Equivalence Ratio	0.4-1.1
Coal Carrier Gas (13-15 SCFH)	Nitrogen or Hydrogen

Range of reactor operating conditions

Average Temperature	1200-2500°F
Average Residence Time	0.012-0.343 sec.
Space Time Conversion	13-408 lbs C gasified/ft^3-hr
Steam Partial Pressure (Reactor exit)	0.125-0.255 atm
Hydrogen Partial Pressure (Reactor exit)	0.194-0.553 atm

TABLE 3.- Typical data obtained from gasification tests

Run No.	5-8-4	5-8-2	5-8-1	6-9-4	7-31-1	8-23-2
Reactor Diameter, inches	2.000	2.000	2.000	2.000	1.250	0.750
Feed Rates, lbs/hr						
Coal	1.590	1.590	1.590	2.043	1.670	1.180
Hydrogen Carrier	0.082	0.082	0.082	--	0.082	0.082
Hydrogen Combustion	0.069	0.102	0.140	0.167	0.167	0.113
Oxygen	0.540	0.800	1.050	1.260	1.340	0.900
Nitrogen Carrier	--	--	--	1.020	--	--
Oxygen/Coal Ratio	0.339	0.503	0.660	0.616	0.802	0.762
Combustion Equivalence Ratio	1.022	1.025	1.066	1.060	0.997	1.008
Reactor Temperature, °F	1445	1750	1955	1966	2157	1913
Volume Gas Produced (Dry)						
Total, SCFH	30.9	37.6	45.9	56.5	60.3	39.7
Carrier Free Basis, SCF/lb Coal	10.2	14.4	19.6	21.2	27.3	21.1
Gas Analysis (Dry, Volume %)						
Hydrogen	74.12	69.88	69.75	26.38	64.23	67.14
Oxygen	0.20	0.42	0.15	8.30	1.65	1.39
Nitrogen	0.81	1.33	0.45	46.89	4.12	4.66
Methane	5.33	5.02	3.85	1.81	2.34	3.22
Carbon Monoxide	15.35	18.41	20.85	12.96	23.48	18.83
Ethane	0.14	0.04	0.01	0.00	0.00	0.01
Ethylene	1.62	1.26	0.64	0.12	0.19	0.52
Carbon Dioxide	1.55	2.06	2.51	2.68	2.39	2.57
Acetylene	0.88	1.58	1.79	0.86	1.60	1.66
Carrier Free Heating Value, BTU/CF	449.4	430.2	395.0	358.9	365.7	392.1
Steam Decomposed, Percent	18.28	28.79	38.81	48.67	46.86	36.84
Ash in Char, Weight percent	9.3	14.9	15.8	16.5	15.68	13.94

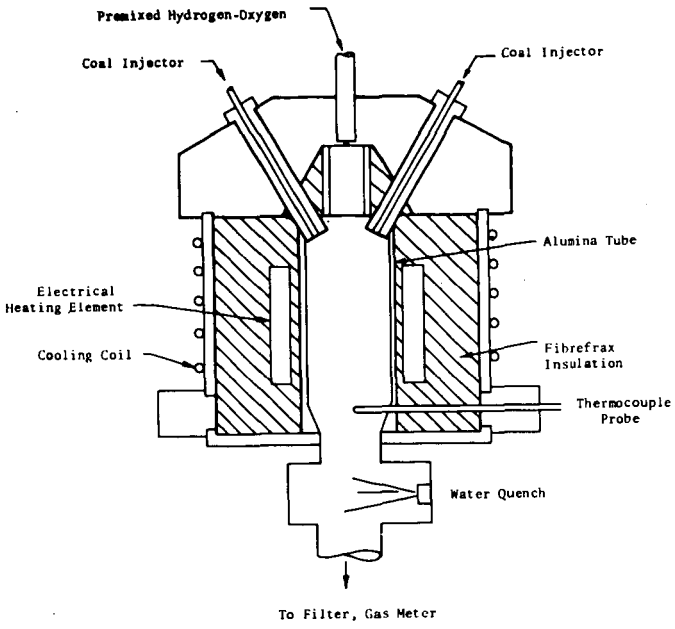

Figure 1. Schematic Diagram of Reactor.

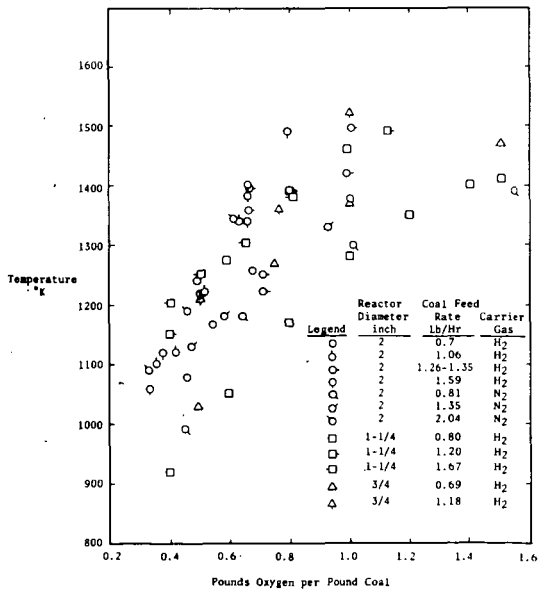

Figure 2. Measured reactor outlet temperature versus the oxygen fed per pound of coal.

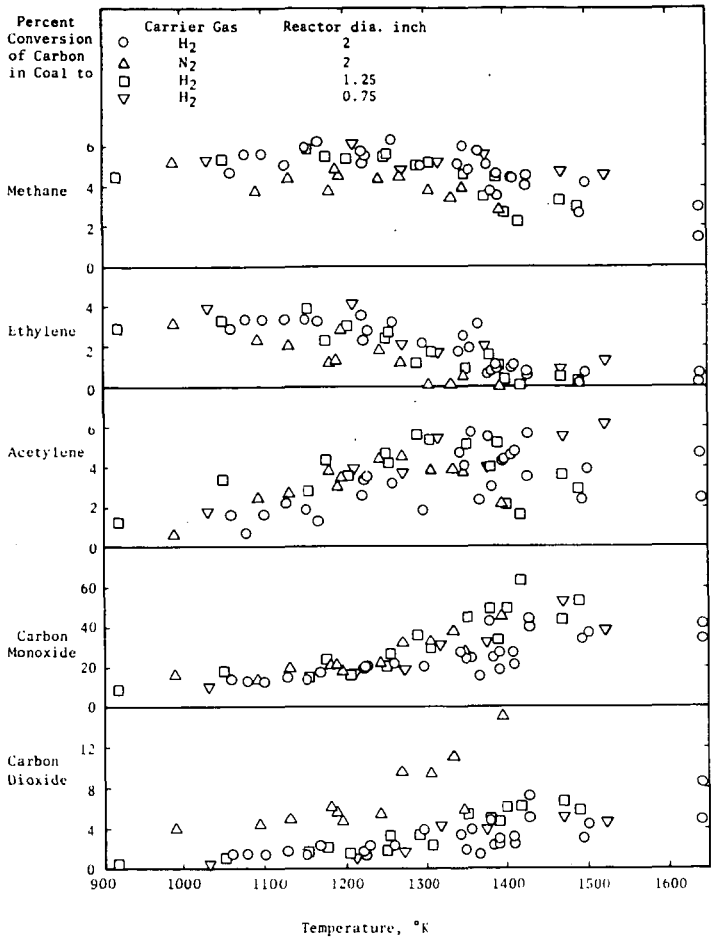

Figure 3. Conversion of Carbon in Coal to Hydrocarbon Gases, carbon monoxide and carbon dioxide versus reactor temperature.

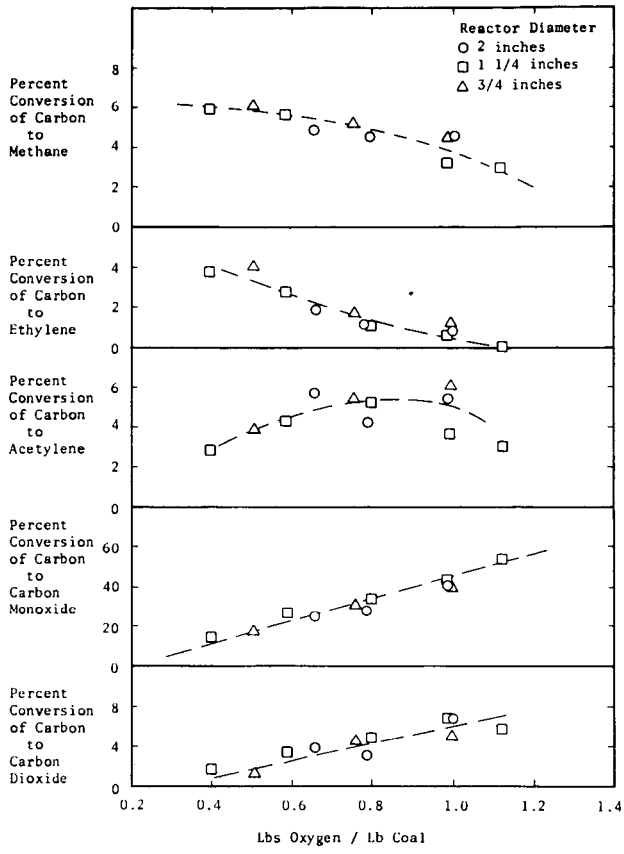

Figure 4. Conversion data showing small effect of varying the reactor size. Data shown are for a coal feed rate of 1.2 lbs/hr.

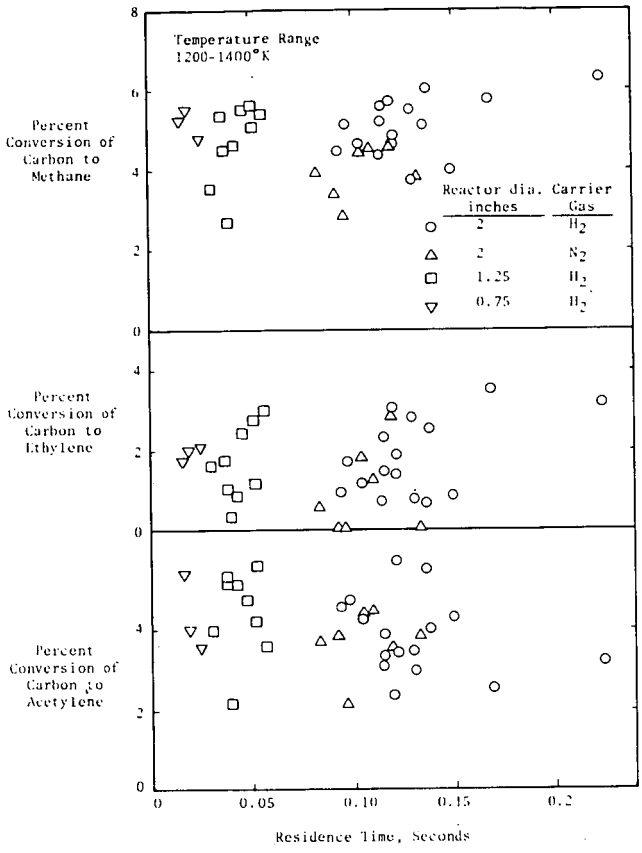

Figure 5. Conversion data showing small effect of average reactor residence time. All data shown are for a coal feed rate of 1.2 lb/hr.

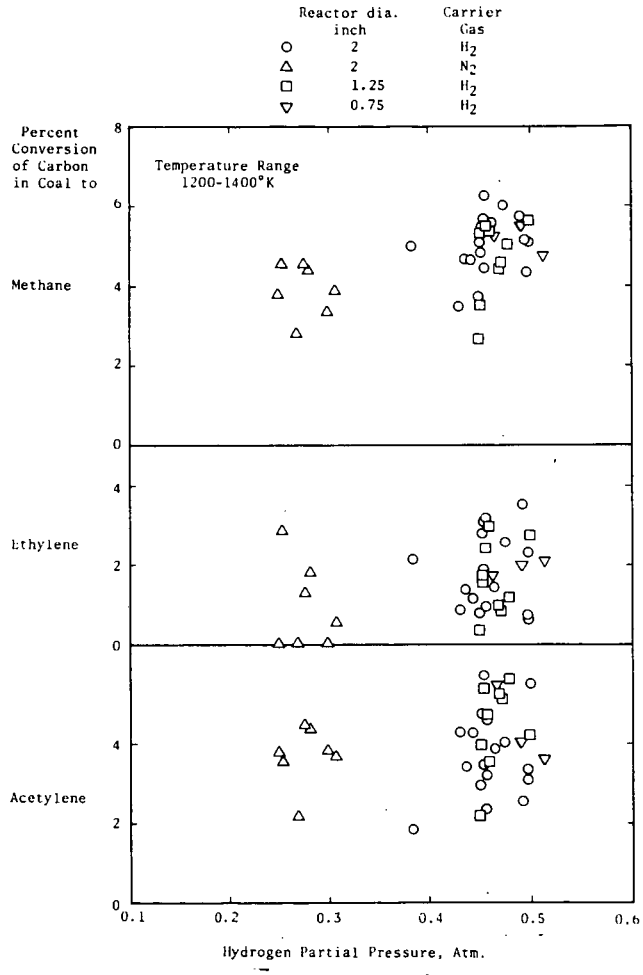

Figure 6. Data showing the effect of hydrogen partial pressure on hydrocarbon yields.

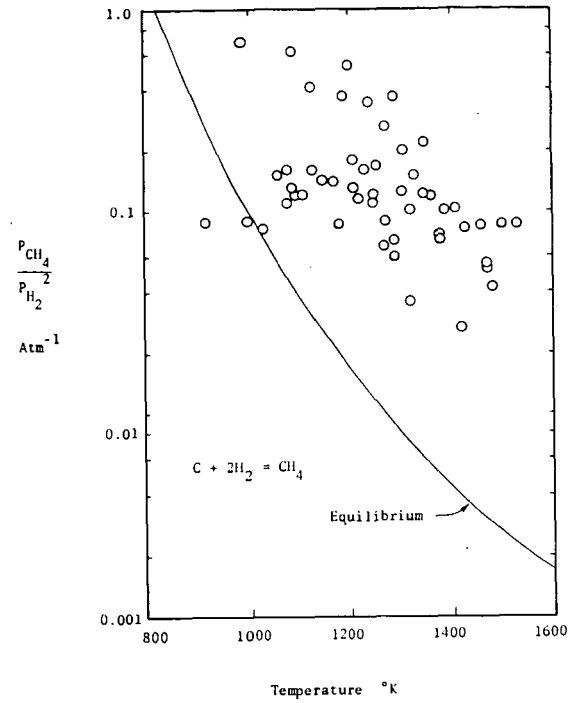

Figure 7. Comparison of equilibrium pressure ratios for the hydrogenation reaction with measured ratios.

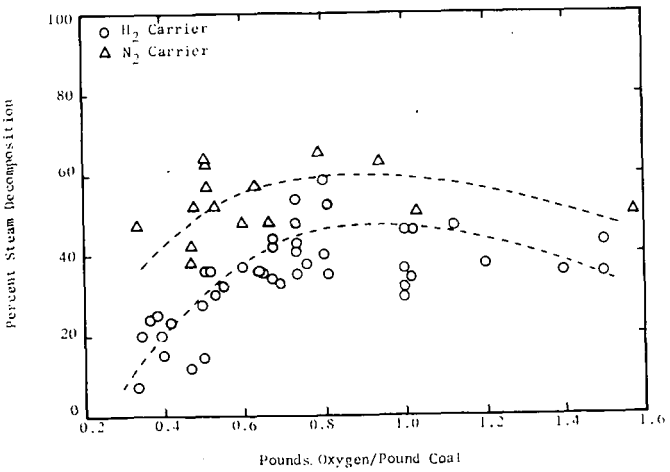

Figure 8. Calculated steam decomposition versus the oxygen fed per pound of coal.

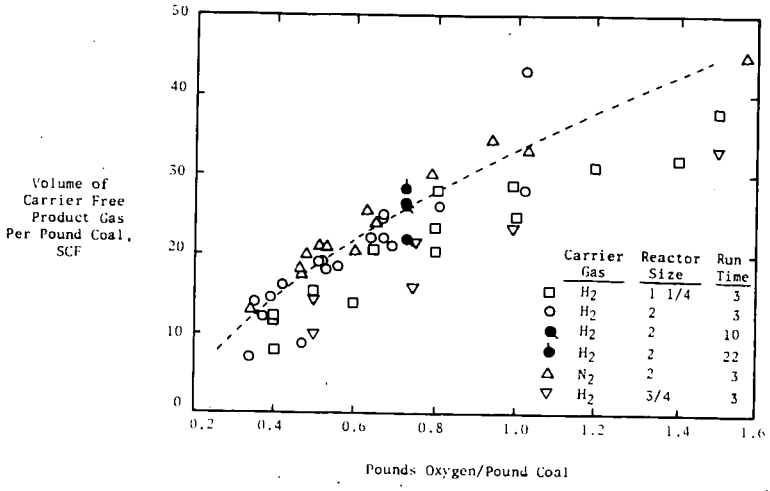

Figure 11. Net volume of product gas per pound of coal fed as a function of oxygen to coal ratio.

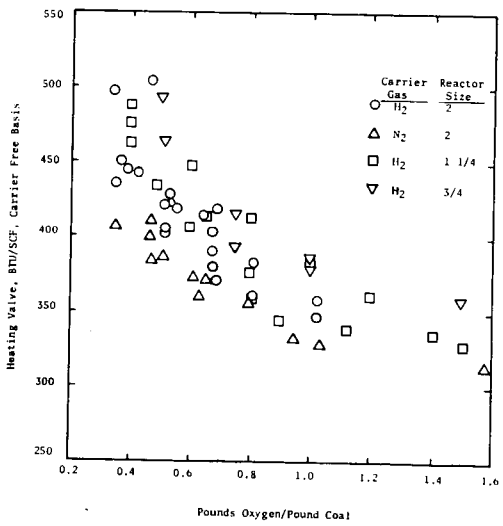

Figure 12. Data showing the variation of the heating value of the dry, carrier-free product gas with the oxygen-coal ratio.

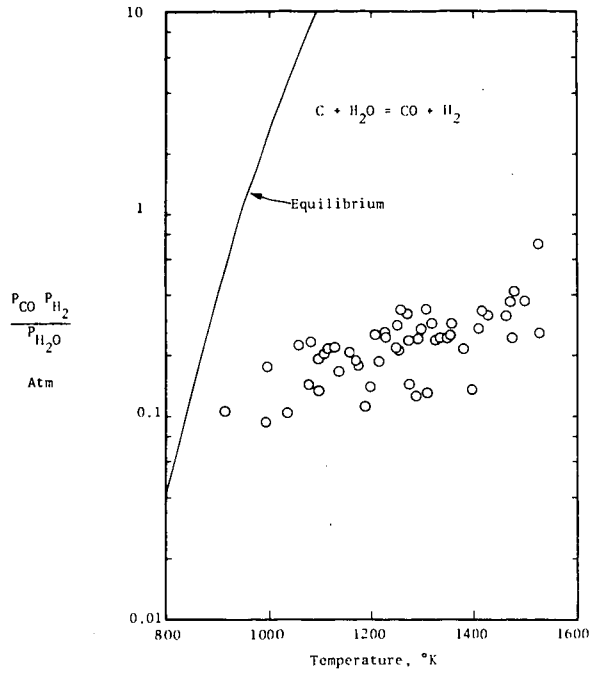

Figure 9. Comparison of equilibrium pressure ratios for the steam-carbon reaction with measured ratios.

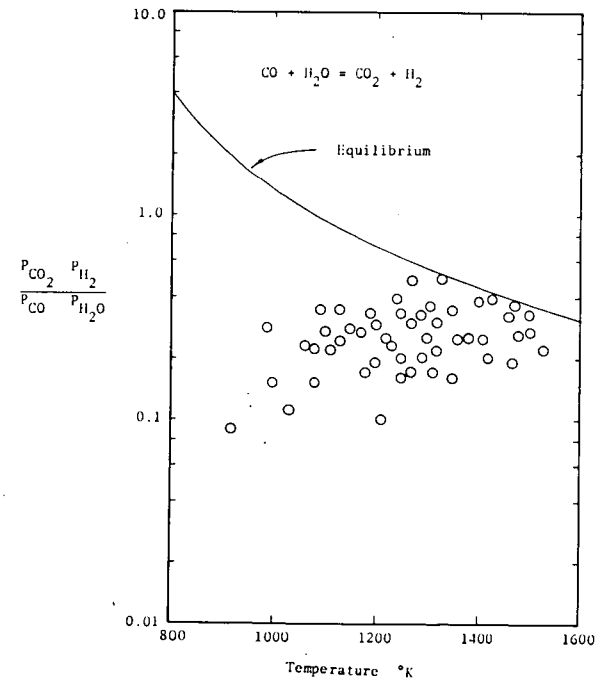

Figure 10. Comparison of equilibrium pressure ratios for the shift reaction with measured values.

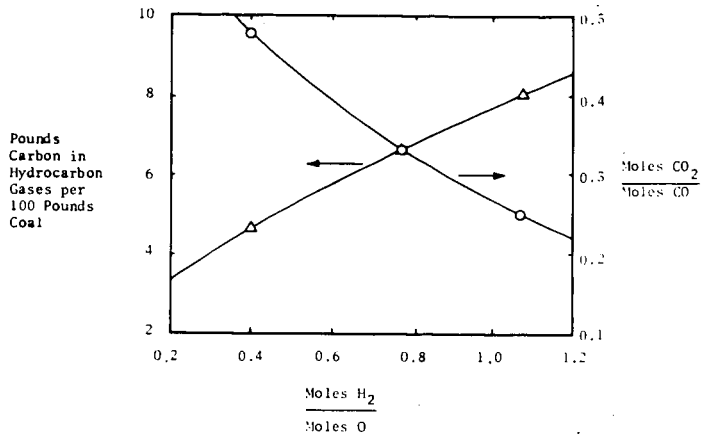

Figure 13. Data showing the effect of varying combustion gas equivalence rates. The coal feed rate was 2 lbs/hr and the O_2/coal ratio was 0.51.

PRESSURIZED HYDROGASIFICATION OF RAW COAL IN A DILUTE-PHASE REACTOR

Herman F. Feldmann, Joseph A. Mima and Paul M. Yavorsky

Pittsburgh Energy Research Center, U.S. Department of the Interior,
Bureau of Mines, 4800 Forbes Avenue, Pittsburgh, Pa. 15213

INTRODUCTION

The direct conversion of raw coal to methane can be achieved by reacting the coal with hydrogen. This approach to converting coal to methane is the basis of the U.S. Bureau of Mines Hydrane Process[1] and the high thermal efficiency resulting from this direct process approach offers substantial potential economic advantages over other routes to pipeline gas.[2] Converting coal directly to methane by reaction with hydrogen was first reported by Dent.[3] The thermodynamic advantages of producing methane directly, rather than by first converting the coal to synthesis gas which is then converted to methane after water-gas shift and methanation, were quickly recognized when investigators in the United States started exploratory work on converting coal to pipeline gas. For example, Channabasappa and Linden[4] concluded that hydrogenating coal to methane with hydrogen which is produced by steam-oxygen gasification of carbon is more thermally efficient than steam-oxygen gasification followed by methanation. However, at first the experimental difficulties in directly hydrogenating raw coal to methane proved to be extreme because of the severe agglomerating properties of most American coals in high-temperature, high-pressure hydrogen atmospheres. This agglomeration problem caused a shift away from attempting to directly hydrogasify raw coal. Instead, the coal was "pretreated" with air or oxygen to destroy its agglomerating properties. While the mild oxidation with air or oxygen was successful in preventing the coal from agglomerating, it adversely reduced its reactivity for methane formation. In fact, the reactivity of the pretreated coal is so reduced that it is impossible to produce a gas by direct hydrogenation of pretreated coal that has a sufficiently high concentration of methane to allow its introduction into a pipeline without costly physical separation of the hydrogen-methane mixture. Thus, while the thermodynamic and chemical advantages of direct hydrogasification of raw coal were clear, the practical difficulties encountered in developing reactor systems to utilize raw coal required that the coal be pretreated before being contacted with hydrogen, but this reduced the process efficiency. Results of directly hydrogasifying pretreated coals in continuous reactors were reported by Institute of gas Technology investigators.[5,6,7]

The problem of processing agglomerating raw coal was solved at the Bureau of Mines when a technique was developed for directly hydrogenating raw coal in a free-fall dilute-phase (FDP) reactor described by Hiteshue.[8] Some results of FDP reactor experiments using raw coal[9,10] have already been presented. However, the results in references 9 and 10 were obtained for rather high pressures of 1,500 and 3,000 psig. Even though operation with raw bituminous coal at 3,000 psig does allow the direct production of raw product gases containing over 80 percent methane and having carbon monoxide contents down to 0.1 vol pct, design considerations indicate pressures around 1,000 psig are more economically attractive. This paper therefore summarizes our FDP reactor data at pressures in the neighborhood of 1,000 psig. These data are useful for the design of the FDP section of the Hydrane process or other processes using similar conditions.

EXPERIMENTAL

Equipment and Procedure

Details of the experimental reactor system and method of operation are given in reference 10. Briefly, the FDP reactor is simply a 3-inch id heated tube contained in a 10-inch pressure vessel. The coal is injected into the top of the 3-inch reactor through a water-cooled nozzle. The coal falls freely through the reactor tube concurrent with the reacting gas which is also injected in at the top of the reactor. Because of rapid heating and a dilute solids phase, agglomeration was avoided; particles were plastic and sticky for only a short time during which particle-particle collisions are few. The heated length of the reactor for all except two of the experiments presented here is 5 ft. The residence time of the coal in the reacting zone is simply the reactor length divided by the average terminal velocity of the coal particles. The char produced in the FDP reactor is collected in a cooled hopper and analyzed after a run. Gas flow rates and compositions are measured over the steady state portion of the run. Ordinarily the capacity of the pressurized char collector allowed a run duration of approximately one hour with approximately fifty minutes of steady state operations during which data could be collected.

Tabular Results

Results of our most recent FDP reactor operations are summarized in table 1 and the analyses of the feed coals used are listed in table 2. The main objectives of these experiments were to: (1) establish the feasibility of directly producing a high-Btu gas by hydrogasifying raw coal in a continuous reactor at economically attractive pressures, (2) measure the yields and distribution of coal hydrogasification reaction products, and (3) provide data for scaling-up the FDP reactor.

Production of High-Btu Gas

The feasibility of producing a gas having a heating value of 900 or more Btu/scf (after cleanup methanation) was established by several experiments. These experiments were designed to simulate the operation of an integrated Hydrane reactor which consists of two stages.[1] In such an integrated reactor, the hydrogen is first fed to a fluid bed where it reacts with char produced by the FDP reactor. The product gas from this fluid bed is the feed gas to the top of the FDP reactor and it consists of about 50 vol pct methane with the remainder hydrogen plus a small amount of carbon monoxide. Thus, the composition of the feed gas to the experimental isolated FDP reactor was adjusted to simulate the fluid-bed product gas from an integrated operation.

Table 3 compares carbon conversion, gas composition, and gas yields for specific experiments with the results used to guide an economic evaluation of the Hydrane process.[2] These results show that the goal of producing a high-Btu gas can be achieved at pressures of 1,000 psig and higher. For all three coals evaluated, Pittsburgh Seam hvab coal, Illinois No. 6 hvcb coal, and lignite, it was shown that the gas produced after methanation to reduce CO to an acceptable level was substitutable for natural gas. Of course, with lignite, the higher oxygen content results in higher yields of CO and this gas will therefore require more methanation than the product gas from the Illinois or Pittsburgh Seam bituminous coals. However, even with lignite the fraction of the total methane that is produced directly rather than by methanation is greater than can be achieved by other process routes using bituminous coal. In an actual plant where hydrogen is produced from the residual char, the catalytic water-gas shift reaction ($CO + H_2O \rightarrow H_2 + CO$) would not be carried to completion. Instead, as the base case analysis of the feed gas to the dilute phase indicates, some CO would be

left in the hydrogen resulting in a somewhat higher CO concentration in the raw product gas from the FDP reactor. This additional CO would result in increased hydrogen consumption during methanation and thereby lower the hydrogen content and increase the heating value of the final product gas. The heating value of the final product gas was therefore calculated based on a constant 4 vol pct CO in the raw dry product gas from the FDP reactor.

Examination of these FDP results indicate the controllable parameters that determine whether the raw product gas will, after methanation of the 4 vol pct CO, have a heating value of at least 900 Btu/scf are the following:

a. Percent methane in the feed gas to the FDP reactor
b. Gas-to-coal feed ratio
c. Reactor pressure
d. Coal residence time (reactor length)

Fortunately, the combination of above variables required to produce 900+ Btu gas are easily achievable in practical reactor systems. For example, the reactor can operate at gas transmission line pressures, both the gas/coal feed ratio and the methane concentration in the feed gas allow operation at carbon conversion levels resulting in balanced plant operation,* and a sufficient coal residence time was achieved in an FDP reactor only 5 ft long. Increases in the percent methane in the feed gas to the FDP reactor, at constant CO concentration, will further increase the heating value of the final product gas.

In our experiments, the reactor pressure shell was pressurized with the feed gas. Because this gas was in direct contact with the reactor electrical heating elements, carbon deposition from methane cracking and subsequent shorting of the electrical elements became a problem when the methane concentration in the feed gas was higher than 50 vol pct. This artificial limitation would not exist in a commercial reactor system where no electric heating elements would be used. Methane concentrations above 50 vol pct would be generated by the fluidized-bed stage of the Hydrane reactor system and therefore allow higher methane concentrations into the FDP reactor. As examples, Pyrcioch and Linden[5] in studying the fluid-bed hydrogasification of a char produced by low temperature pretreatment achieved methane concentration over 50 vol pct, and Lewis and co-workers[9] reported methane concentrations over 60 vol pct from direct moving-bed hydrogasification of chars produced by hydrogasification in an FDP reactor. Thus, the results presented here must be regarded as conservative and higher methane concentration product gases could be produced in commercial FDP reactors where the methane concentration in the intermediate feed gas to the FDP reactor is not limited by artificial constraints.

Product Yields and Distribution

The major products from the dilute-phase hydrogasification of raw coal are gas and char plus smaller amounts of organic liquid products and water. The liquid yield measurement is rather inaccurate because of the relatively small amount of liquids formed and the difficulty of their quantitative recovery. For all the experiments reported in table 1, measured yields of organic liquids varied from less than .01 to .06 lb/lb coal. Attempts to correlate the organic liquid yields with reactor parameters thought to have the greatest effect on these yields, such as reactor wall temperature, hydrogen partial pressure, and gas phase residence time, have been unsucessful. Since, in a base-load pipeline gas plant the organic liquid production will be substantial even at the lowest yields measured, additional work is now going on to characterize these organic liquids.

*Balanced operation means the overall plant produces no surplus char. To achieve balanced operation, the fraction of carbon in the coal converted to methane is regulated so that the remaining carbon is just sufficient to produce process hydrogen and plant power.

Water is produced by both the simple vaporization of moisture in the coal and by the reaction of hydrogen with oxygen in the coal. Recoveries of water both from condensers and as moisture on the char ranged from .01 to .08 lb/lb of coal fed. However, as table 1 indicates, the water recoveries did not exhibit the same degree of fluctuation as did the organic liquid recoveries and most of the measured yields were between .05 and .06 lb/lb coal fed. The water recoveries measured for the Illinois #6 hvcb coal and the single run made with lignite were higher because of the higher oxygen contents of these feeds. For the Illinois coal, water yields varied from about .05 to .09 lb/lb coal. These water yield data indicate that much of the oxygen is either present as bound water or combines with hydrogen to form water during hydrogasification.

Char Yields and Desulfurization

In the overall Hydrane process, the char from the FDP reactor will be further converted in a fluid-bed reactor which is in series with the FDP reactor. The yield of char from the FDP reactor depends on the carbon conversion level as shown in figure 1.

Sulfur is eliminated from the char during hydrogasification as H_2S and the degree of elimination is related to the carbon conversion as shown in figure 2. The scatter may be due to either the influence of parameters other than carbon conversion and/or to inaccuracies in the sulfur determinations. The important point to be demonstrated is that the coal sulfur is extremely reactive under hydrogasification conditions as evidenced by the fact that the coal residence time in the FDP reactor is on the order of one to two seconds. In fact, figure 2 indicates the sulfur in the coal to be more reactive than the carbon in the coal. The Pittsburgh Seam hvab coal contains approximately equal amounts of pyritic and organic sulfur. However, as yet no tests have been made on the char to indicate whether either type is selectively removed during free-fall hydrogasification. Since, in the integrated Hydrane process the char spends additional residence time in a fluid bed at higher hydrogen partial pressures than exist in the FDP reactor, additional char desulfurization will occur in the fluid bed. In preliminary experiments with an integrated FDP fluid-bed reactor system, the sulfur removal from the Pittsburgh Seam coal has been on the order of 85 percent. These results are encouraging because they indicate that char from the Hydrane reactor may be an acceptable fuel to provide the plant's energy and steam requirements without complicated sulfur removal systems and without exceeding air quality restrictions on atmospheric release of sulfur compounds.

Scale-Up of the FDP Reactor

The FDP reactor has two important functions. It must convert the coal to a nonagglomerating char for the subsequent fluid bed and it must convert enough carbon to methane so that the FDP product gas is, after acid gas removal and light methanation, an acceptable pipeline gas.

In the 3-inch id FDP reactor used in our experiments, the coal particles are heated to reaction temperature in the reactor by mixing with the preheated feed gas and by heat transfer from the hot walls of the FDP reactor. However, heat transfer analysis of larger reactors[11] indicates that as one increases the reactor diameter, the amount of heat transfer from hot reactor walls to the particles inside becomes negligible. Therefore, in larger diameter reactors, the coal particles can be raised to reaction temperature only by mixing with the hot methane-hydrogen mixture shunted from the fluid bed. Calculations indicate that the mixing temperature of the hot gas and coal at the top of a large FDP reactor will be on the order of 480° to 540° C. It is therefore important to evaluate the FDP hydrogasification behavior at these

relatively low temperatures. This is difficult to do in the present 3-inch id FDP reactor because the coal quickly heats to the reactor wall temperature and, if the wall temperature is below 725° to 800° C, the coal adheres to the reactor walls and eventually plugs the reactor. In spite of this drawback, experiments were conducted at reduced reactor wall temperatures of 485°, 530°, and 580° C. In these experiments, coal hitting the reactor walls stuck to them and eventually plugged the reactor. However, the coal that did not contact the walls, passed through the reactor and was collected and its conversion and caking properties determined. Results of these lower reactor wall temperature experiments are shown in figures 3 and 4 where the effect of temperature on both the volatile matter and the carbon conversion of the FDP reactor char are shown at the reduced wall temperatures. Figure 3 shows an interior thermocouple temperature at the reactor bottom and figure 4 shows the average reactor wall temperature because the actual particle temperature is not known. The true average particle temperature is probably between the interior thermocouple temperature and the reactor wall temperature. Also shown in figures 3 and 4 is the temperature boundary above which the char is not agglomerating when tested in a fluid bed with hydrogen at 1,000 psig and 900° C. Chars produced at reactor wall temperatures below the boundary temperatures agglomerated when tested at the above conditions. Thus, if one conservatively assumes that the particle temperature is close to the wall temperature, it appears that simply mixing the hot methane-hydrogen mixture produced in the fluid-bed reactor with the coal at the top of the FDP reactor will produce an acceptable nonagglomerating char if the char temperature reaches 580° C even if for residence times of only a second or two.

Previous reaction rate analyses of FDP reactor data[10] at higher hydrogen partial pressures (1,500 to 3,000 psig) and at reactor wall temperatures of 725° and 900° C indicated that the conversion of carbon in raw coal occurs in three stages with each stage having greatly different reactivities toward hydrogen. At the short (one to two seconds) particle residence times in the FDP reactor at 3,000 psig and with wall temperatures of 900° C, all of the first stage (the most reactive) carbon behaved as if it were converted "instantaneously". However, the conversion of the second stage carbon varied with reactor conditions and this variation of rate with reactor conditions was correlated by this simple rate equation:

$$(1) \qquad U_T \frac{dx}{dL} = k p_{H_2} (1-x)$$

where U_T is the average terminal velocity of the particles, k is the rate constant, p_{H_2} the partial pressure of hydrogen; L the location in the reactor (the distance from the coal inlet), and x the carbon conversion level. The fraction of carbon that behaved as though it were instantaneously converted was denoted by E and was determined by finding the value that allowed the best fit of experimental data with the integrated form of equation (1):

$$(2) \qquad \int_E^x \frac{dx}{p_{H_2}(1-x)} = \frac{k}{U_T} L$$

At conditions where the conversion of second stage carbon, x-E, was small, errors or variations in either x or E caused large fluctuations in the value of k, making a kinetic analysis of the data difficult. This occurs where the total carbon conversion is mostly due to the "instantaneous" carbon reaction because conditions are not severe enough to react a substantial fraction of the second stage carbon. As an example of

"severe conditions", operation at 3,000 psig, 900° C wall temperatures and with pure hydrogen feed gas allowed total carbon conversions, x, ranging from 0.40 to 0.50 in the FDP reactor. At these conditions the value of E is approximately 0.14 and the spread between x and E is sufficiently large to allow a reasonable determination of k. For the experiments reported in reference 10, E varied from about 0.15 to 0.20.

At the conditions reported in this paper where the total pressure is closer to 1,000 psig, and the feed gas to the FDP reactor is an approximately equimolar mixture of hydrogen and methane, the total carbon conversions are closer to the fraction of carbon that instantaneously reacts and kinetic interpretation is even more difficult. Therefore, the kinetic analysis is not yet complete. However, for the purposes of FDP reactor simulation, a mathematical model was used that assumed all the carbon reacts at a rate dictated by the equation,

$$(3) \quad \frac{dx}{dL} = \frac{k}{U_T} p_{H_2} (1-x)$$

This equation is felt to be conservative because it does not allow for the fraction of carbon that may react at a considerably faster rate than the final amount of carbon conversion which was used to evaluate the rate constant k. The temperature dependency of k used for our initial reactor simulation studies[11] has been reported.[1] While the more detailed kinetic analysis may result in a modified rate equation, the results of our simulation study[11] indicate that radiant heat transfer plays a dominant role in small FDP reactors such as the one used in this study. Due to the diminishing effect of radiant heat transfer from the reactor walls as the diameter of the reactor increases, temperature profiles in commercial reactors will be considerably different than those existing in our present 3-inch id FDP reactor thus indicating the necessity of using larger diameter pilot plants to obtain reliable scale-up data.

CONCLUSIONS

The feasibility of producing on the order of 95 percent of the total methane production by the direct reaction of raw caking coals with hydrogen in an FDP plus fluid-bed reactor system has been established. The experimental results show that the product gas is of pipeline quality after minor methanation of the small amount of carbon monoxide (only 4 percent) without any need for hydrogen separation.

Further, the experiments indicate the above desirable results can be achieved without encountering agglomeration problems even when unpretreated highly caking coals are used.

REFERENCES

1. Feldmann, H. F., C. Y. Wen, W. H. Simons, and P. M. Yavorsky. Supplemental Pipeline Gas From Coal by the Hydrane Process. Presented at the 71st National AIChE Meeting, Dallas, Texas, Feb. 20-23, 1972.

2. Wen, C. Y., C. T. Li, S. H. Tscheng, and W. S. O'Brien. Comparison of Alternate Coal Gasification Processes for Pipeline Gas Production. Presented at the 65th Annual AIChE Meeting, New York, N.Y., Nov. 26-30, 1972.

3. Dent, F. J., W. H. Blackburn, and H. C. Millet. Inst. Gas Engrs. Commun. No. 190 (1938), 69 pp. Trans. Inst. Gas Engrs., 88, 150-217 (1938-39).

4. Channabasappa, K. C. and H. R. Linden. Ind. Eng. Chem., 48, 900-905 (1956).

5. Pyrcioch, E. J. and H. R. Linden. Ind. Eng. Chem., v. 52, No. 7, July 1960, pp. 590-594.

6. Lee, B. S., E. J. Pyrcioch, and F. C. Schora, Jr. Fuel Gasification, Advances in Chem. Series 69, ACS, Wash., D.C., 1967, pp. 104-127.

7. Wen, C. Y. and J. Huebler. Ind. Eng. Chem. Process Design and Development, v. 4, No. 2, 1965, pp. 142-147 and pp.

8. Hiteshue, R. W. Proceedings of the Synthetic Pipeline Gas Symposium, Pittsburgh, Pa., Nov. 15, 1966, pp. 13-23.

9. Lewis, P. S., S. Friedman, and R. W. Hiteshue. Fuel Gasification, Advances in Chem. Series, 69, ACS, Wash., D.C., 1967, pp. 50-63.

10. Feldmann, H. F., W. H. Simons, J. A. Mima, and R. W. Hiteshue. ACS Div. of Fuel Chem. Preprints, v. 14, No. 4, Part II, Sept. 1970, pp. 1-13.

11. Feldmann, H. F., W. H. Simons, C. Y. Wen, and P. M. Yavorsky. Simulation of a Reactor System for the Conversion of Coal to Methane by the Hydrane Process. Fourth International Congress of Chemical Engineering, Chemical Equipment Design and Automation, Marianske Lazne, Czechoslovakia, Sept. 11-15, 1972.

TABLE 1.- Operating data for FDP hydrogasification of raw coal
Feed coal is 50 x 100 mesh except where noted.

Test No., IHR-	146	147	149	151	153	154
Temperature, ° C	900	900	900	900	900	900
Pressure, psig	1000	1000	1200	1100	1100	2000
Coal	hvab	hvab	hvab	hvab	hvab	hvab
Coal rate, lb/hr	12.17	12.44	12.38	11.88	10.92	12.51
Feed gas rate, scfh	153.5	155.2	161.0	158.6	150.6	164.5
Vol %, Hydrogen	50.5	56.0	53.0	48.0	99.2	52.5
do. Methane	41.9	42.3	44.5	49.2	0.2	46.4
do. Nitrogen	6.3	1.8	2.5	2.6	0.6	1.0
Total scf/lb	12.61	11.99	13.00	13.35	13.82	13.15
Hydrogen, scfh	77.5	86.9	85.3	76.1	149.4	86.3
Hydrogen, scf/lb	6.37	6.72	6.89	6.41	13.71	6.90
Product gas, scfh	169.6	171.8	175.5	167.1	143.8	175.0
Vol %, Hydrogen	22.7	25.5	23.6	22.1	49.0	19.8
do. Methane	66.4	67.8	69.7	71.7	46.5	75.9
do. Ethane	0.3	0.4	0.3	0.1	0.3	0.1
do. Carbon monoxide	2.7	3.2	3.0	2.5	3.4	2.2
do. Carbon dioxide	1.0	1.1	0.8	0.5	0.2	0.4
do. Nitrogen	6.4	1.7	2.3	2.7	0.5	1.5
Product yield, Methane	3.97	3.93	4.09	3.52	6.10	4.52
Scf/lb, Ethane	0.04	0.05	0.04	0.01	0.04	0.01
do. CO	0.38	0.43	0.43	0.35	0.45	0.31
do. CO_2	0.00	0.15	0.11	0.04	0.03	0.06
Feed H_2 reacted, scf/lb	3.21	3.33	3.55	2.46	7.23	4.13
Char residue, lb/lb	0.697	0.702	0.698	0.698	0.663	0.694
Condensed liquid, lb/lb						
Water	0.051	0.037	0.033	0.029	0.032	0.038
Oil	0.013	0.009	0.014	0.008	0.005	0.008
Residue moisture, lb/lb	0.009	0.012	0.011	0.008	0.003	0.018
Conversion, maf coal	32.5	32.5	33.1	32.8	36.5	33.0
(Wt pct), Carbon	25.6	25.0	25.5	25.3	28.5	25.1
do. Hydrogen	64.2	66.6	66.4	65.2	70.0	66.6
do. Sulfur	48.8	44.3	43.9	46.5	55.9	46.8
do. Nitrogen	25.1	24.6	27.2	30.6	38.0	26.4
Recovery, overall	96.3	96.0	96.3	93.2	95.7	96.2
(Wt pct) Carbon	94.6	96.3	96.1	94.4	99.0	97.2
do. Hydrogen	98.9	95.2	97.1	92.4	94.5	97.3
do. Ash	100.2	100.2	104.0	99.4	103.4	92.4

(Continued on next page)

TABLE 1.- (Continued)

Test No., IHR-	156	157	158	160	165	176*
Temperature, ° C	850	850	900	900	850	850
Pressure, psig	1000	2000	2000	1500	1500	1000
Coal	hvab					hvab
Coal rate, lb/hr	12.84	13.00	12.61	12.29	12.94	12.47
Feed gas rate, scfh	157.8	161.7	160.9	161.3	158.8	156.2
Vol %, Hydrogen	49.0	49.9	51.8	53.8	51.3	48.0
do. Methane	49.4	48.4	46.6	43.4	47.0	49.4
do. Nitrogen	1.6	1.7	1.6	2.6	1.7	2.2
Total scf/lb	12.29	12.44	12.76	13.12	12.27	12.53
Hydrogen, scfh	77.3	80.7	82.9	86.8	81.5	75.0
Hydrogen, scf/lb	6.02	6.21	6.61	7.06	6.30	6.24
Product gas, scfh	171.8	180.8	177.0	166.4	173.8	173.1
Vol %, Hydrogen	22.4	18.1	18.0	19.7	21.7	22.8
do. Methane	71.4	79.0	78.7	75.2	73.4	71.6
do. Ethane	0.5	0.1	0.1	0.3	0.1	0.2
do. Carbon monoxide.	3.2	0.5	1.1	1.4	2.1	2.5
do. Carbon dioxide..	0.7	0.4	0.4	0.8	0.6	0.7
do. Nitrogen	1.4	1.7	1.6	2.4	2.0	1.9
Product yield, Methane	3.48	4.97	5.10	4.49	4.13	3.70
Scf/lb, Ethane	0.06	0.01	0.01	0.04	0.01	0.03
do. CO	0.43	0.07	0.15	0.19	0.28	0.35
do. CO_2	0.09	0.06	0.06	0.08	0.08	0.10
Feed H_2 reacted, scf/lb	3.02	3.69	4.08	4.39	3.38	2.85
Char residue, lb/lb	0.700	0.658	0.703	0.697	0.696	0.706
Condensed liquid, lb/lb						
Water	0.036	0.042	0.050	0.049	0.058	0.048
Oil	0.018	0.015	0.004	0.005	0.012	0.022
Residue moisture, lb/lb	0.015	0.023	0.014	0.019	0.017	0.008
Conversion, maf coal	32.8	37.3	32.2	33.7	33.1	32.2
(Wt pct), Carbon	25.0	30.0	25.0	24.2	23.3	24.0
do. Hydrogen	62.4	65.9	68.0	66.0	62.4	63.5
do. Sulfur	30.0	40.2	45.4	49.2	46.4	45.9
do. Nitrogen	21.3	34.2	29.7	30.6	25.8	24.7
Recovery, overall	95.1	94.1	98.1	95.8	96.8	96.9
(Wt pct), Carbon	95.1	94.1	97.9	96.7	97.6	98.5
do. Hydrogen	95.4	102.0	100.6	96.9	100.9	98.5
do. Ash	106.8	102.2	104.3	101.8	96.9	98.0

*Feed coal particle size range is 100 x 200 mesh.

(Continued on next page)

TABLE 1.- (Continued)

Test No., IHR-	166	167	172	173	174	177
Temperature, ° C	850	800	850	900*	850*	850
Pressure, psig	1200	1000	2000	1000	1000	1000
Coal	hvab					hvab
Coal rate, lb/hr	12.68	13.21	12.40	12.61	12.86	11.70
Feed gas rate, scfh	156.3	153.1	163.4	149.1	156.8	155.3
Vol %, Hydrogen	49.2	48.4	50.6	52.7	49.6	99.3
do. Methane	48.7	48.2	46.4	45.2	47.0	0.4
do. Nitrogen	2.1	3.3	3.0	2.1	3.3	0.3
Total scf/lb	12.33	11.60	13.18	11.82	12.19	13.18
Hydrogen, scfh	76.9	74.1	82.7	78.6	77.8	154.2
Hydrogen, scf/lb	6.07	5.62	6.11	6.23	6.05	13.11
Product gas, scfh	168.7	170.3	171.9	163.0	174.1	150.9
Vol %, Hydrogen	22.7	27.3	20.4	25.0	27.9	52.9
do. Methane	72.2	67.0	75.8	70.4	66.4	43.6
do. Ethane	0.1	1.0	0.1	0.2	0.8	0.2
do. Carbon monoxide.	2.3	1.2	0.7	1.6	1.4	2.1
do. Carbon dioxide .	0.5	0.2	0.2	0.4	0.6	0.3
do. Nitrogen	2.3	3.1	2.6	2.1	2.6	0.5
Product yield, Methane	3.60	3.05	4.39	3.76	3.26	5.57
Scf/lb, Ethane	0.01	0.13	0.01	0.03	0.11	0.03
do. CO	0.31	0.15	0.10	0.21	0.19	0.27
do. CO_2	0.07	0.03	0.03	0.05	0.08	0.04
Feed H_2 reacted, scf/lb	3.04	2.10	3.84	3.00	2.27	7.21
Char residue, lb/lb	0.691	0.709	0.674	0.721	0.692	0.646
Condensed liquid, lb/lb						
Water	0.049	0.041	0.053	0.037	0.041	0.042
Oil	0.018	0.029	0.012	0.029	0.030	0.018
Residue moisture, lb/lb	0.019	0.014	0.015	0.018	0.019	0.014
Conversion, maf coal	34.8	30.5	35.0	31.4	33.7	38.2
(Wt pct), Carbon	25.6	25.0	28.0	21.4	23.4	30.8
do. Hydrogen	63.5	59.1	64.3	62.4	59.1	67.1
do. Sulfur	42.8	52.7	44.9	61.8	42.1	45.9
do. Nitrogen	21.7	20.3	32.6	23.7	21.5	27.8
Recovery, overall	94.5	94.1	93.6	96.0	95.0	93.8
(Wt pct), Carbon	92.9	94.0	93.4	99.1	96.9	95.5
do. Hydrogen	97.3	98.9	99.3	98.5	100.8	97.2
do. Ash	110.1	100.7	104.1	99.4	98.0	99.2

* Reactor length - 3 ft.

(Continued on next page)

TABLE 1. (Continued)

Test No., IHR-	178	180	181*	182	183*	186
Temperature, °C	800	900	900	900	850	900
Pressure, psig	1000	1000	1000	1000	1000	500
Coal	hvab					hvab
Coal rate, lb/hr	11.70	12.53	12.72	24.10	3.94	6.73
Feed gas rate, scfh	161.1	441.2	168.0	323.1	151.4	70.0
Vol %, Hydrogen	98.9	99.3	99.2	52.6	51.6	99.0
do. Methane	0.4	0.5	0.5	45.7	46.5	0.4
do. Nitrogen	0.4	0.2	0.3	1.7	1.9	0.6
Total scf/lb	13.77	35.21	13.20	13.41	38.43	10.40
Hydrogen, scfh	159.0	438.1	166.7	170.0	78.1	69.3
Hydrogen, scf/lb	13.59	34.96	13.11	7.05	19.83	10.30
Product gas, scfh	147.5	412.6	155.1	335.0	152.1	76.8
Vol %, Hydrogen	73.0	76.3	44.2	28.5	39.8	50.9
do. Methane	23.9	21.9	50.2	66.9	57.3	44.1
do. Ethane	0.7	trace	0.0	0.2	trace	0.0
do. Carbon monoxide.	1.5	1.4	4.7	2.1	1.0	4.2
do. Carbon dioxide .	0.2	0.0	0.2	0.3	0.1	0.0
do. Nitrogen	0.4	0.2	0.4	1.7	1.7	0.5
Product yield, Methane	2.96	7.04	6.06	3.17	4.25	5.12
Scf/lb, Ethane	0.09	trace	0.00	0.03	0.0	0.0
do. CO	0.19	0.46	0.57	0.29	0.38	0.47
do. CO_2	0.00	0.00	0.04	0.04	0.04	0.0
Feed H_2 reacted, scf/lb	4.38	9.84	7.71	3.09	4.46	4.59
Char residue, lb/lb	0.705	0.648	0.630	0.708	0.602	0.618
Condensed liquid, lb/lb						
Water	0.039	0.028	0.042	0.038	0.004	0.036
Oil	0.029	0.010	0.007	0.019	0.054	0.017
Residue moisture, lb/lb	0.011	0.013	0.015	0.014	0.010	0.006
Conversion, maf coal	34.7	37.7	40.5	32.8	43.0	40.5
(Wt pct), Carbon	28.1	31.6	33.2	26.0	36.2	33.4
do. Hydrogen	61.0	71.3	71.8	61.5	71.2	74.4
do. Sulfur	48.4	52.5	56.7	49.1	61.6	64.0
do. Nitrogen	21.9	38.1	41.6	25.3	43.7	46.0
Recovery, overall	81.8	96.6	95.9	92.6	91.9	90.6
(Wt pct), Carbon	88.8	98.6	95.2	92.5	90.2	91.0
do. Hydrogen	86.3	99.6	92.9	94.3	97.2	95.5
do. Ash	112.6	97.7	99.4	107.7	101.8	99.6

*Feed coal particle size range is 100 x 200 mesh.

(Continued on next page)

TABLE 1.- (Continued)

Test No., IHR-	189	190	184
Temperature, ° C	850	850	850
Pressure, psig	1000	1000	1000
Coal	hvab	hvab	lignite
Coal rate, lb/hr	12.94	13.01	13.23
Feed gas rate, scfh	166.9	165.1	162.6
Vol %, Hydrogen	52.4	49.4	50.1
do. Methane	44.0	46.0	47.8
do. Nitrogen	3.4	4.3	1.8
Total scf/lb	12.90	12.69	12.29
Hydrogen, scfh	87.5	81.6	81.5
Hydrogen, scf/lb	6.76	6.27	6.16
Product gas, scfh	191.4	184.2	204.1
Vol %, Hydrogen	25.1	23.3	27.9
do. Methane	68.0	69.2	57.5
do. Ethane	0.2	0.2	0.1
do. Carbon monoxide	2.7	2.6	6.3
do. Carbon dioxide	0.8	0.6	5.9
do. Nitrogen	3.0	3.9	2.1
Product yield, Methane	4.38	3.98	3.25
Scf/lb, Ethane	0.03	0.03	0.02
do. CO	0.37	0.34	1.03
do. CO_2	0.12	0.07	0.99
Feed H_2 reacted, scf/lb	3.05	2.99	2.01
Char residue, lb/lb	0.714	0.714	0.494
Condensed liquid, lb/lb			
Water	0.008	0.033	0.102
Oil	0.020	0.017	0.018
Residue moisture, lb/lb	0.009	0.018	0.020
Conversion, maf coal	33.1	30.6	50.7
(Wt pct), Carbon	23.9	22.0	32.1
do. Hydrogen	66.4	60.9	77.4
do. Sulfur	47.5	38.6	51.0
do. Nitrogen	30.1	19.0	51.0
Recovery, overall	95.7	96.7	93.5
(Wt pct), Carbon	98.8	96.9	97.6
do. Hydrogen	98.7	106.9	97.0
do. Ash	109.1	89.6	101.8

(Continued on next page)

TABLE 1.- (Continued)

Test No., IHR-	161	162	163	164	191	192
Temperature, ° C	900	900	900	900	725	650
Pressure, psig	1000	1500	2000	1200	1000	1000
Coal	Ill.#6	Ill.#6	Ill.#6	Ill.#6	Ill.#6	Ill.#6
Coal rate, lb/hr	10.53	12.31	12.77	11.78	12.19	12.04
Feed gas rate, scfh	157.2	156.2	158.8	165.1	169.8	188.9
Vol %, Hydrogen	54.5	48.8	52.0	50.1	56.5	60.1
do. Methane	44.5	49.3	46.1	47.7	42.8	39.4
do. Nitrogen	1.0	1.8	1.9	2.2	0.7	0.5
Total scf/lb	14.93	12.69	12.94	14.02	13.93	15.69
Hydrogen, scfh	85.6	76.2	82.6	82.7	96.0	113.5
Hydrogen, scf/lb	8.14	6.19	6.73	7.02	7.87	9.43
Product gas, scfh	182.3	185.3	190.1	199.4	190.4	202.0
Vol %, Hydrogen	27.9	20.4	20.0	21.9	43.0	52.2
do. Methane	68.6	75.0	73.8	72.8	52.0	45.3
do. Ethane	trace	trace	0.2	trace	2.3	0.9
do. Carbon monoxide.	1.4	1.9	2.2	2.4	1.6	0.9
do. Carbon dioxide.	0.6	0.8	1.3	0.7	0.6	0.2
do. Nitrogen	1.4	1.7	2.3	1.9	0.4	0.4
Product yield, Methane	5.28	5.03	5.47	5.64	2.16	1.42
Scf/lb, Ethane	trace	trace	0.03	trace	0.36	0.15
do. CO	0.24	0.29	0.34	0.41	0.25	0.15
do. CO_2	0.10	0.11	0.20	0.12	0.09	0.03
Feed H_2 reacted, scf/lb	3.31	3.12	3.63	3.31	1.15	0.67
Char residue, lb/lb	0.622	0.658	0.663	0.653	0.702	0.782
Condensed liquid, lb/lb						
Water	0.079	0.068	0.048	0.063	0.043	0.038
Oil	0.032	0.011	0.006	0.010	0.062	0.035
Residue moisture, lb/lb	0.012	0.013	0.013	0.014	0.010	0.009
Conversion, maf coal	38.0	37.6	36.6	35.5	31.4	24.3
(Wt pct), Carbon	29.8	27.8	26.3	27.8	25.1	19.1
do. Hydrogen	70.1	70.3	72.0	70.6	55.5	47.0
do. Sulfur	43.8	50.9	63.8	51.2	51.8	42.1
do. Nitrogen	26.2	30.5	37.9	34.1	17.4	13.7
Recovery, overall	94.6	97.2	99.0	98.7	95.8	94.5
(Wt pct), Carbon	96.5	96.1	100.0	99.5	97.1	95.1
do. Hydrogen	104.7	106.0	105.4	106.7	100.6	97.3
do. Ash	102.4	100.0	100.6	102.1	101.6	105.7

TABLE 2.- Typical analyses of coals used in this study

	Pittsburgh Seam hvab coal	Illinois #6 hvcb coal	N. Dakota lignite
Proximate Analysis			
Moisture	1.2	1.4	7.8
Volatile matter	36.4	36.8	39.7
Fixed carbon	56.7	55.9	46.9
Ash	5.7	5.9	5.6
Ultimate Analysis (Dry Basis)			
C	79.09	75.45	64.64
H	5.22	5.12	4.48
N	1.60	1.72	0.76
S	1.10	1.32	0.76
O (by difference)	7.22	10.41	23.29
Ash	5.77	5.98	6.07
	100.00	100.00	100.00

Hvab coal from U.S. BuMines experimental mine, Bruceton, Pa.
Hvcb coal from Orient #3 mine, Freeman Coal Co., Waltonville, Ill.
Lignite from Baukol-Noonan mine, Burke Co., N. Dakota.

TABLE 3.- Production of pipeline quality gas in FDP reactor

Test No., IHR-	Base	156	176	151	166
Pressure, psig	1000	1000	1000	1100	1200
Coal	hvab	hvab	hvab	hvab	hvab
Feed gas/coal ratio, scf/lb	11.1	12.3	12.5	11.9	12.3
Feed gas composition, vol pct					
Hydrogen	46.1	49.0	48.0	48.0	49.2
Methane	47.5	49.4	49.4	49.2	48.7
Nitrogen	0.0	1.6	2.2	2.6	2.1
Carbon monoxide	4.0	0.0	0.0	0.0	0.0
Carbon dioxide	1.7	0.0	0.0	0.2	0.0
Carbon conversion, wt pct	20.0	25.0	24.0	25.3	
Product gas (water-free)/coal ratio, scf/lb	14.8	13.4	13.9	14.1	13.3
Product gas composition, water-free					
Hydrogen	21.4	22.4	22.8	22.1	22.7
Methane	68.8	71.4	71.6	71.7	72.2
Ethane	0.0	0.5	0.2	0.1	0.1
Carbon monoxide	4.2	3.2	2.5	2.5	2.3
Carbon dioxide	1.3	0.7	0.7	0.5	0.5
Nitrogen	1.0	1.4	1.9	2.7	2.3
Hydrogen sulfide		0.4	0.2	0.4	0.2
Methane/hydrogen in product	3.21	3.19	3.14	3.24	3.18
Heating value, as-received, Btu/scf	779	817	812	802	815
Heating value w/4% CO Methanation, Btu/scf	927	918	908	903	914
Pct methane equivalent (CH_4+C_2H_6) made directly	94.2	94.7	94.7	94.7	94.8

(Continued on next page)

(TABLE 3.- Continued)

Test No., IHR-	160	165	154	157	158	172
Pressure, psig	1500	1500	2000	2000	2000	2000
Coal	hvab	hvab	hvab	hvab	hvab	hvab
Feed gas/coal ratio, scf/lb	13.1	12.3	12.5	12.4	12.8	13.2
Feed gas composition						
Hydrogen	53.8	51.3	52.5	49.9	51.8	50.6
Methane	43.4	47.0	46.4	48.4	46.6	46.4
Nitrogen	2.6	1.7	1.0	1.7	1.6	3.0
Carbon monoxide	0.0	0.0	0.0	0.0	0.0	0.0
Carbon dioxide	0.2	0.0	0.0	0.0	0.0	0.0
Carbon conversion, wt pct	24.2	23.3	25.1	30.0	25.0	28.0
Product gas (water-free)/ coal ratio, scf/lb	13.5	13.4	14.0	13.9	14.0	13.9
Product gas comp., water-free						
Hydrogen	19.7	21.7	19.8	18.1	18.0	20.4
Methane	75.2	73.4	75.9	79.0	78.7	75.8
Ethane	0.3	0.1	0.1	0.1	0.1	0.1
Carbon monoxide	1.4	2.1	2.2	0.5	1.1	0.7
Carbon dioxide	0.8	0.6	0.4	0.4	0.4	0.2
Nitrogen	2.4	2.0	1.5	1.7	1.6	2.6
Hydrogen sulfide	0.1	0.2	0.1	0.2	0.2	0.2
Methane/hydrogen in product.	3.82	3.38	3.83	4.36	4.37	3.72
Heating value, as-received, Btu/scf	835	823	842	863	862	839
Heating value with 4% CO methanation, Btu/scf	928	916	936	948	949	920
Pct methane equivalent ($CH_4+C_2H_6$) made directly	95.0	94.8	95.0	95.2	95.2	95.0

(Continued on next page)

(TABLE 3.- Continued)

Test No., IHR-	164	162	163	184
Pressure, psig	1200	1500	2000	1000
Coal	hvcb	hvcb	hvcb	lignite
Feed gas/coal ratio, scf/lb	14.0	12.7	12.9	12.3
Feed gas composition				
Hydrogen	50.1	48.8	52.0	50.1
Methane	47.7	49.3	46.1	47.8
Nitrogen	2.2	1.8	1.9	1.8
Carbon monoxide	0.0	0.0	0.0	0.2
Carbon conversion, wt pct	27.8	27.8	26.3	32.1
Product gas (water-free)/coal ratio, scf/lb	16.9	15.0	15.5	10.6
Product gas composition, water-free				
Hydrogen	21.9	20.4	20.0	27.9
Methane	72.8	75.0	73.8	57.5
Ethane	trace	trace	0.2	0.1
Carbon monoxide	2.4	1.9	2.2	6.3
Carbon dioxide	0.7	0.8	1.3	5.9
Nitrogen	1.9	1.7	2.3	2.1
Hydrogen sulfide	0.3	0.2	0.2	0.1
Methane/hydrogen in product	3.32	3.68	3.69	2.06
Heating value, as-received, Btu/scf.	818	833	824	695
Heating value with 4% CO methanation, Btu/scf	914	928	925	902
Pct methane equivalent (CH_4+C_2H_6) made directly	94.8	94.9	94.9	90.1

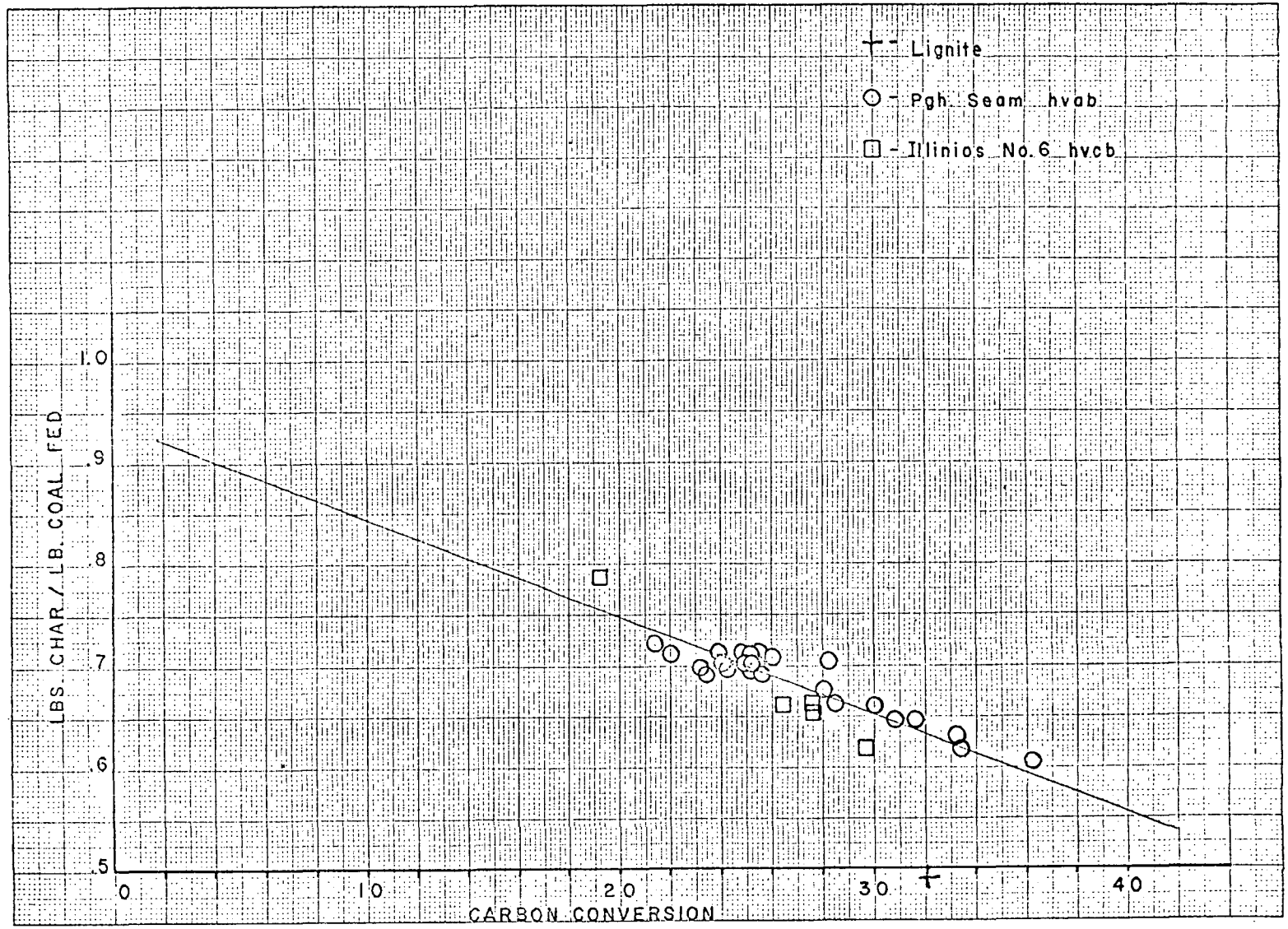

Fig. 1 DEPENDENCE OF FDP REACTOR CHAR YIELD ON CARBON CONVERSION

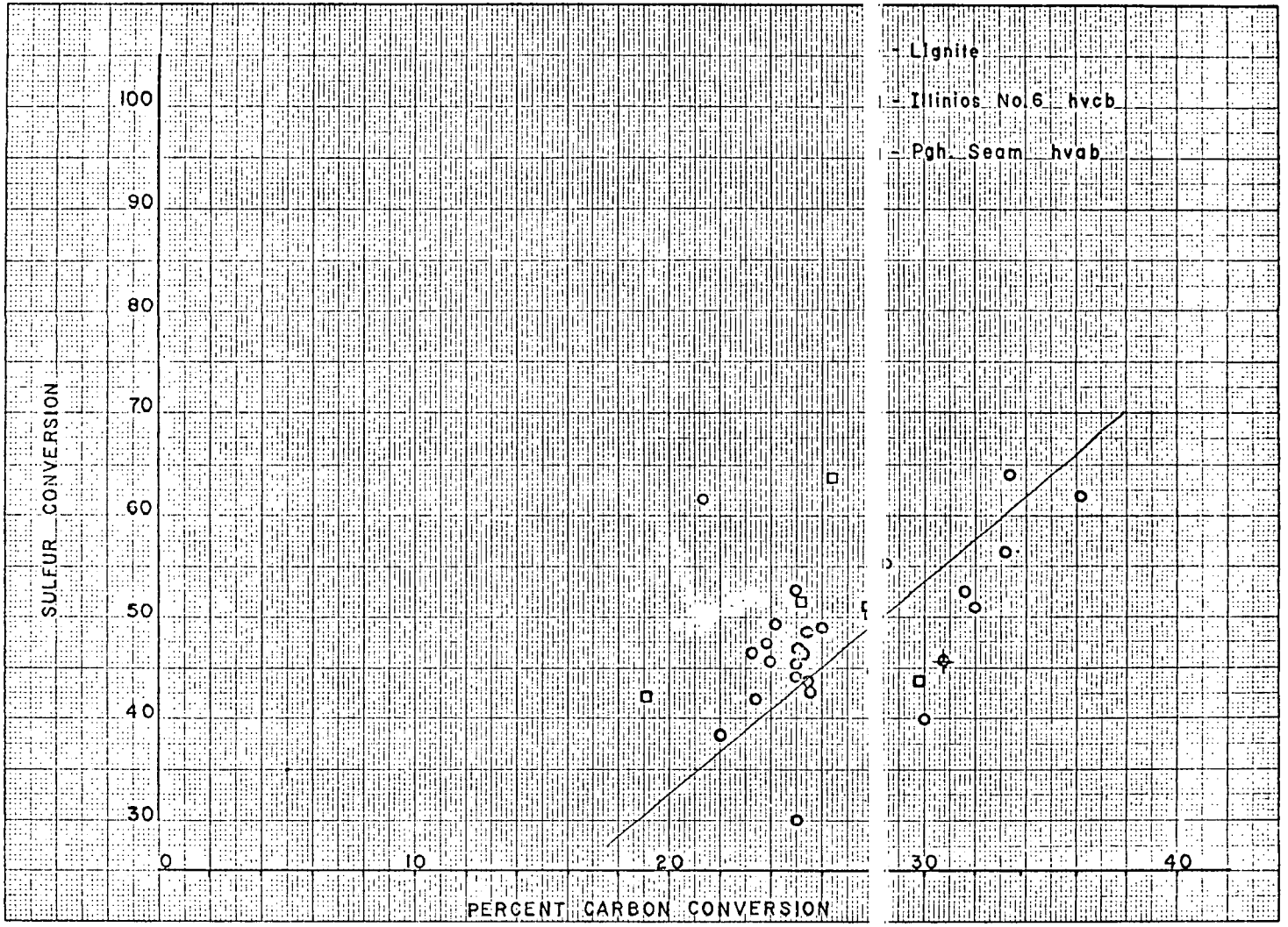

Fig. 2 SULFUR ELIMINATION IN FDP REACTOR

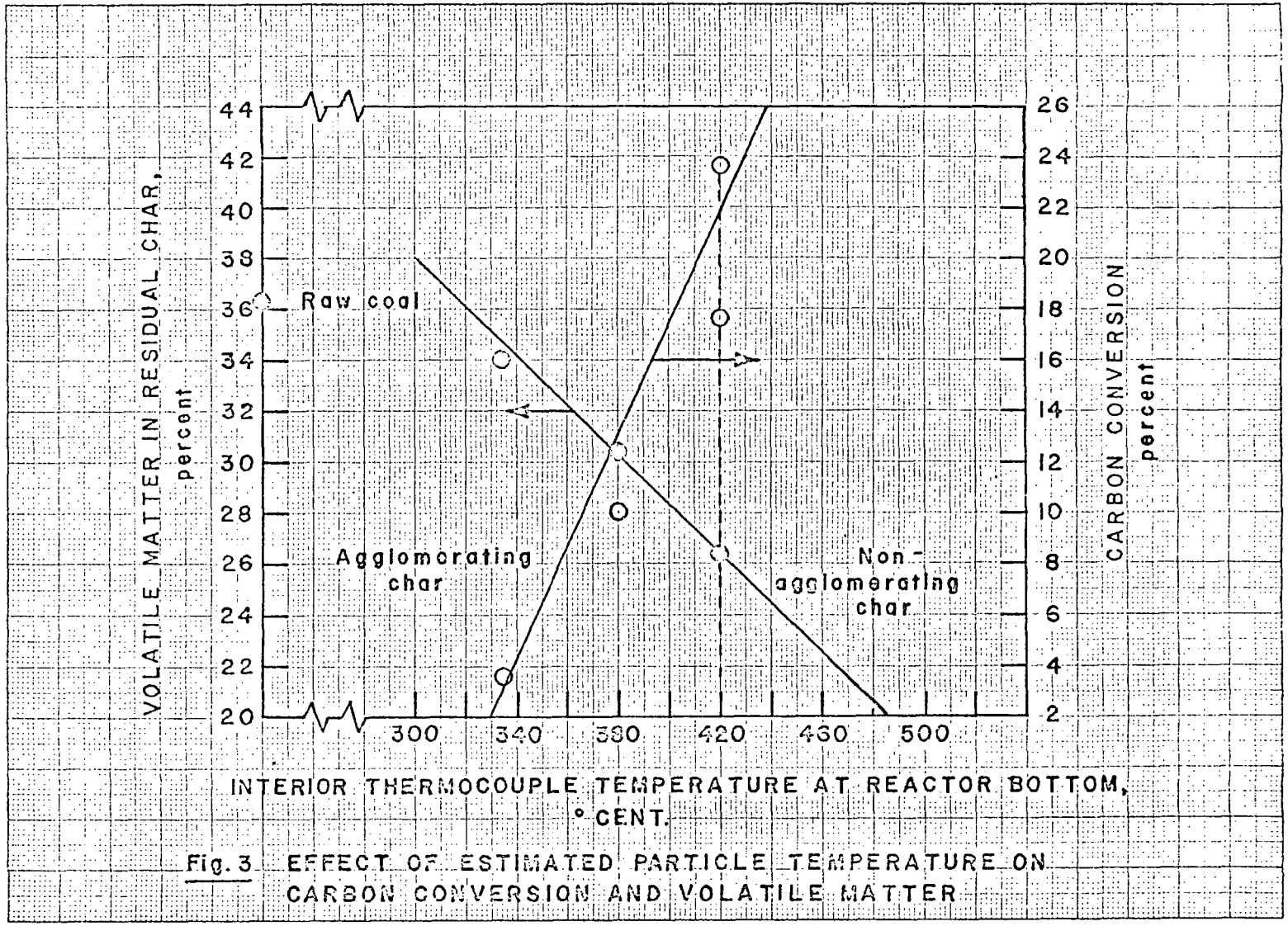

Fig. 3 EFFECT OF ESTIMATED PARTICLE TEMPERATURE ON CARBON CONVERSION AND VOLATILE MATTER

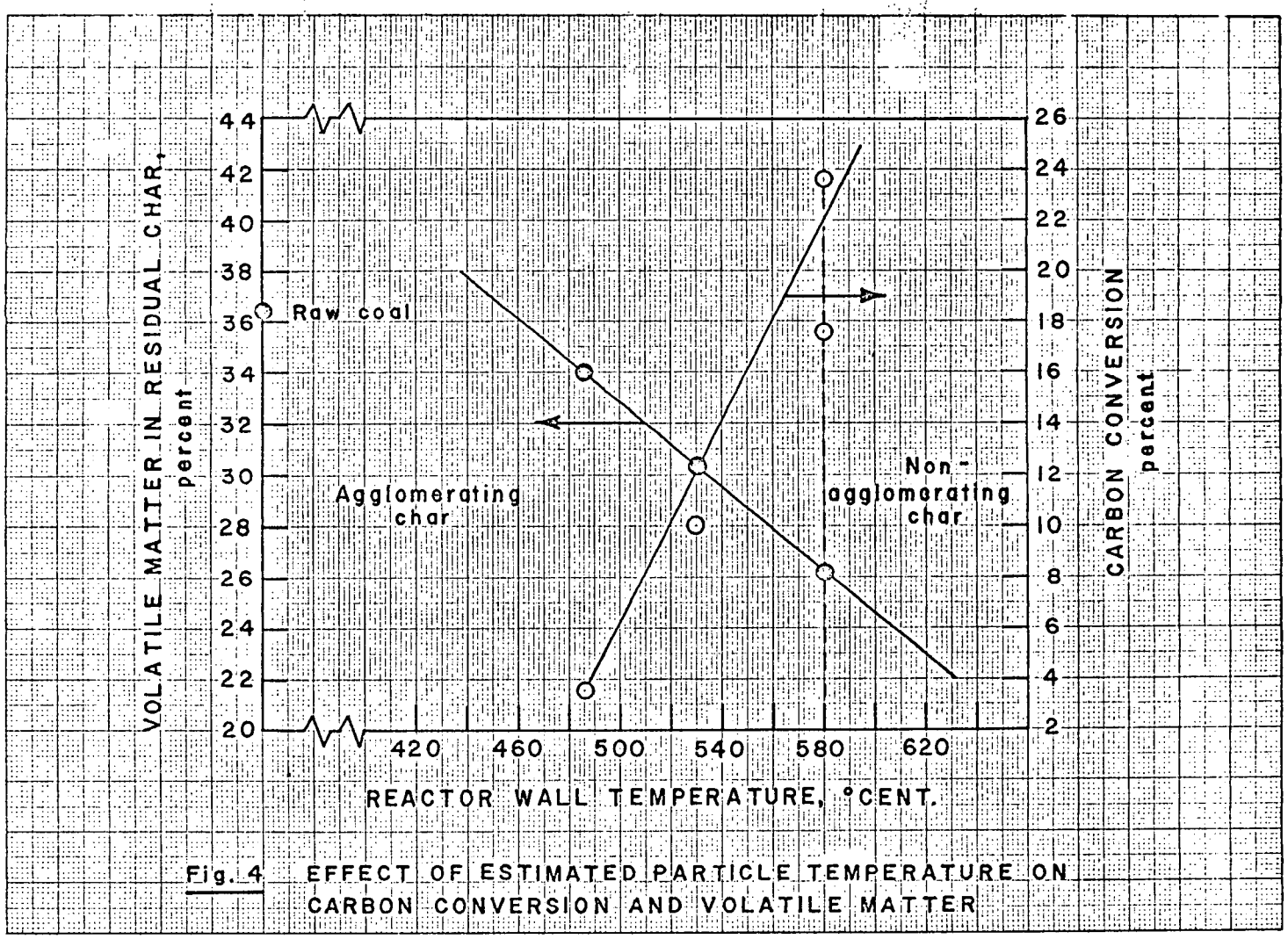

Fig. 4 EFFECT OF ESTIMATED PARTICLE TEMPERATURE ON CARBON CONVERSION AND VOLATILE MATTER

CHEMISTRY AND PHYSICS OF ENTRAINED COAL GASIFICATION

R. L. Zahradnik
National Science Foundation
Washington, D. C.

R. J. Grace
Bituminous Coal Research, Inc.
Monroeville, Pennsylvania

INTRODUCTION

The BI-GAS process [2,3]* for the production of synthetic natural gas is being developed by Bituminous Coal Research, Inc. under the joint sponsorship of The Office of Coal Research and The American Gas Association. The key features of the process are illustrated in Figure 1. Fresh coal is introduced into the upper section (Stage 2) of a two-stage gasifier at system pressures of 70 to 100 atm. Here, it contacts a rising stream of hot synthesis gas produced in the lower section (Stage 1) of the gasifier and is partially converted into methane and more synthesis gas. The residual char is swept out of the gasifier together with the gas; the char is separated from the gas stream and returned to the bottom section of the gasifier. Here, the char is completely gasified under slagging conditions by reaction with oxygen and steam, producing both the synthesis gas required in the upper section of the gasifier and the heat needed to complete the endothermic reactions.

To meet pipeline specifications, the product gas requires further processing. It is cleaned and subjected to partial water gas shift to adjust its H_2/CO ratio; it is scrubbed to remove acid gases (CO_2, H_2S); and finally it is subjected to catalytic methanation to raise the heating value to pipeline quality.

The basic component of the process is the entrained two-stage gasifier. The major emphasis of the BCR program to date has been to develop data sufficient to optimize the operation of Stage 2 of the gasifier. Initial experiments were carried out with coal slurries in rocking autoclaves at pressures of 3000 to 4000 psig and temperatures 1380 F to 1400 F.[1] These experiments showed that large amounts of methane could indeed by produced from the contact of coal with superheated steam. However, the tests were of necessity batch in nature and involved relatively slow heating rates and long residence times. Consequently, the results could not be applied directly to an integrated entrained gasifier, and data from experiments under more realistic conditions were sought.

The next step in the BCR program consisted of tests that were continuous in nature and involved a short coal-steam-synthesis gas contact time

---

* Numbers refer to references cited.

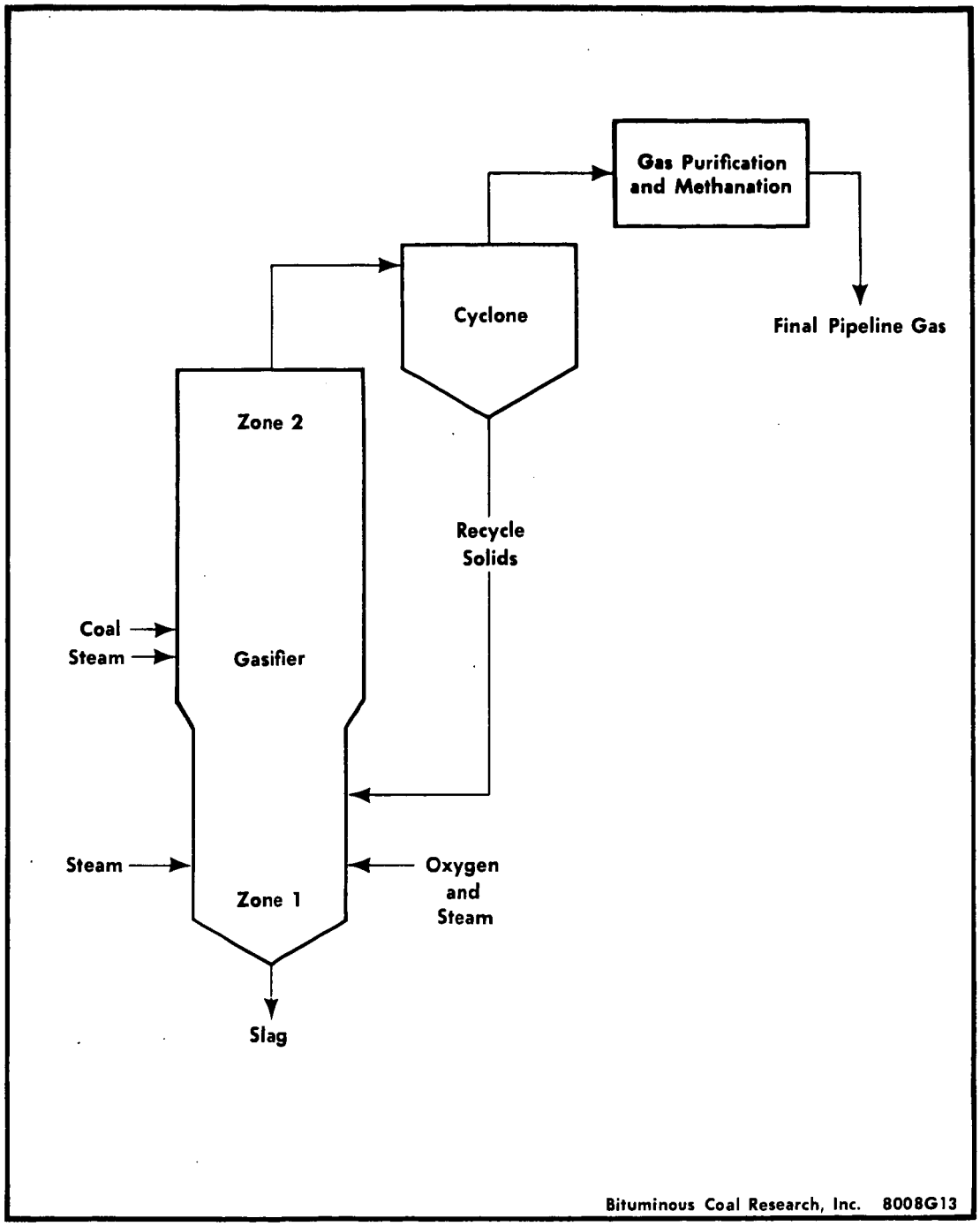

Figure 1. Simplified Flow Diagram for Two-stage Super-pressure Gasifier

with rapid heating. Over 100 experiments were conducted under conditions simulating those of Stage 2 using a 5 lb/hr continuous flow reactor (CFR). Lignite, a Wyoming subbituminous coal, and Pittsburgh seam high volatile bituminous coal were tested. These experiments showed conclusively that appreciable amounts of methane could be produced during short contact times of 2 to 20 seconds between steam, synthesis gas, and fresh coal at about 1000 psi and 1750 F.[5]

The experiments carried out in the 5 lb/hr unit involved the simultaneous heating of the simulated Stage 1 gas, the superheated steam, and the fresh coal. Because of the limitations of the equipment, the reaction conditions did not exactly duplicate those conditions expected in the integrated gasifier. Nevertheless, the results warranted the construction of a process and equipment development unit in which fresh coal and steam could be contacted with hot Stage 1 gas under conditions that more closely duplicate those in Stage 2. The design features of this PEDU have been given elsewhere[2,6,7,9]. Nearly sixty individual experiments were conducted, using the same series of coals as were used in the CFR. The range of operating conditions for these tests is reported in Table 1; the range of results is given in Table 2.

Initial results from the PEDU using lignite were reported in earlier publications[2,8]. The purpose of this paper is to present data for the gasification of Pittsburgh seam coal in the PEDU and to discuss these data on the basis of the chemistry and physics of entrained gasification.

GASIFICATION CHEMISTRY

The physical and chemical processes which take place between the hot synthesis gas from Stage 1 and the fresh coal and steam in Stage 2 are complex and any attempt to model them must be regarded as approximate. Nonetheless, it is possible to develop reasonable correlations in terms of certain basic gasifier variables suggested by the gasification chemistry.

As a result of the very rapid heating of the coal, a significant devolatilization takes place in a matter of milliseconds.[4] This devolatilization step produces a variety of gases including hydrogen and methane.

The remainder of the gasification process may be characterized by the carbon-hydrogen reaction

$$C + 2H_2 \rightarrow CH_4 \qquad (1)$$

and by the carbon-steam reaction

$$C + H_2O \rightarrow CO + H_2 \qquad (2)$$

The overall methanation process has been described by Moseley and Paterson[10,11,12] as consisting of three steps. The first step is the rapid devolatilization of coal which produces, in addition to volatile products, an active carbon species. This active carbon reacts, in the second step, either with hydrogen to form more methane or with itself in a cross-linking

TABLE 1. RANGE OF OPERATING CONDITIONS FOR 100 LB/HR PEDU TESTS

Coal Feed Rates	43 lb/hr to 108 lb/hr
System Pressure	220 psig to 1,420 psig (15 atm to 96.5 atm)
Outlet Temperature	1,375 F to 2,160 F (746 C to 1,180 C)
Hydrogen Partial Pressure	56 psig to 308 psig (3.8 atm to 21 atm)
Total Steam/Coal Ratios	0.90/1 to 2.78/1
Total Carbon Gasified	32 percent to 68 percent
Total Btu in Gas/Btu in Coal	38 percent to 85 percent
Residence Times	3 sec to 22 sec

TABLE 2. RANGE OF RESULTS FOR 100 LB/HR PEDU TESTS

Coal Tested	Coal Feed Rate (lb/hr)	Methane Yield, Percent	Total Carbon Gasified, Percent	Preformed Methane, Percent
Design Basis	100	15.0	33	62
Lignite	62-108	12-20	32-68	30-79
Elkol	43-104	18-23	39-64	47-86
Pittsburgh	50-77	16-26	33-57	61-84
Lower Kittanning	64-66	14-17	34-38	59-68

polymerization to form an inactive char. The third step involves the slow reaction of hydrogen with the inactive char.

In Stage 2 of the BCR two-stage process, this third step is relatively unimportant. Zahradnik and Glenn[15] have shown that the direct methanation of coal in Stage 2 can be described adequately as a two-step process which is independent of residence time when residence time is greater than a few seconds. On this basis, it is possible to relate the yield of methane, MY, expressed as the fraction of the carbon in coal appearing as methane, to hydrogen partial pressure in the following way.

$$MY = \frac{a + b\ (P_{H_2})}{1 + b\ (P_{H_2})} \tag{3}$$

where a and b are kinetic parameters.

Zahradnik and Glenn[15] were able to correlate the CFR data, the data of Moseley and Paterson, and data obtained by the U.S. Bureau of Mines with this expression. Data obtained in the 100 lb/hr PEDU for lignite were also shown to be correlated by Equation (3)[8], demonstrating its validity for larger sized equipment.

For data correlation purposes, Equation (3) can be written as:

$$\left(\frac{MY-a}{1-MY}\right) \frac{1}{(P_{H_2})} = b \tag{4}$$

On the basis of earlier tests, the value of a is taken to be 0.08 and is assumed to depend on temperature in an Arrhenius manner. Thus, a plot of the natural logarithm of the left-hand side of the above equation, as a function of reciprocal temperature, should yield a straight line. Figure 2 is such a plot for Pittsburgh seam coal, under comparable physical and geometrical configurations, and for residence times between 14 and 17 seconds. The correlation is quite good.

A complete tabulation of the data on which Figure 2 is based is given in Reference 2. The experimental and analytical techniques used to obtain these data were reported in a previous publication by Grace, Glenn, and Zahradnik[8].

Not all the data points from the PEDU experiments with Pittsburgh seam coal fell on the correlating line of Figure 2, however. A more detailed explanation of their behavior is in order.

METHANE DECOMPOSITION

Experiments in the externally heated 5 lb/hr CFR showed that methane, once formed, did not decompose under the Stage 2 simulation achieved with this unit. However, because of the higher mixing temperatures attained in the PEDU, such decomposition is possible. In order to test whether methane does decompose, tests were conducted whereby a stream of methane was injected

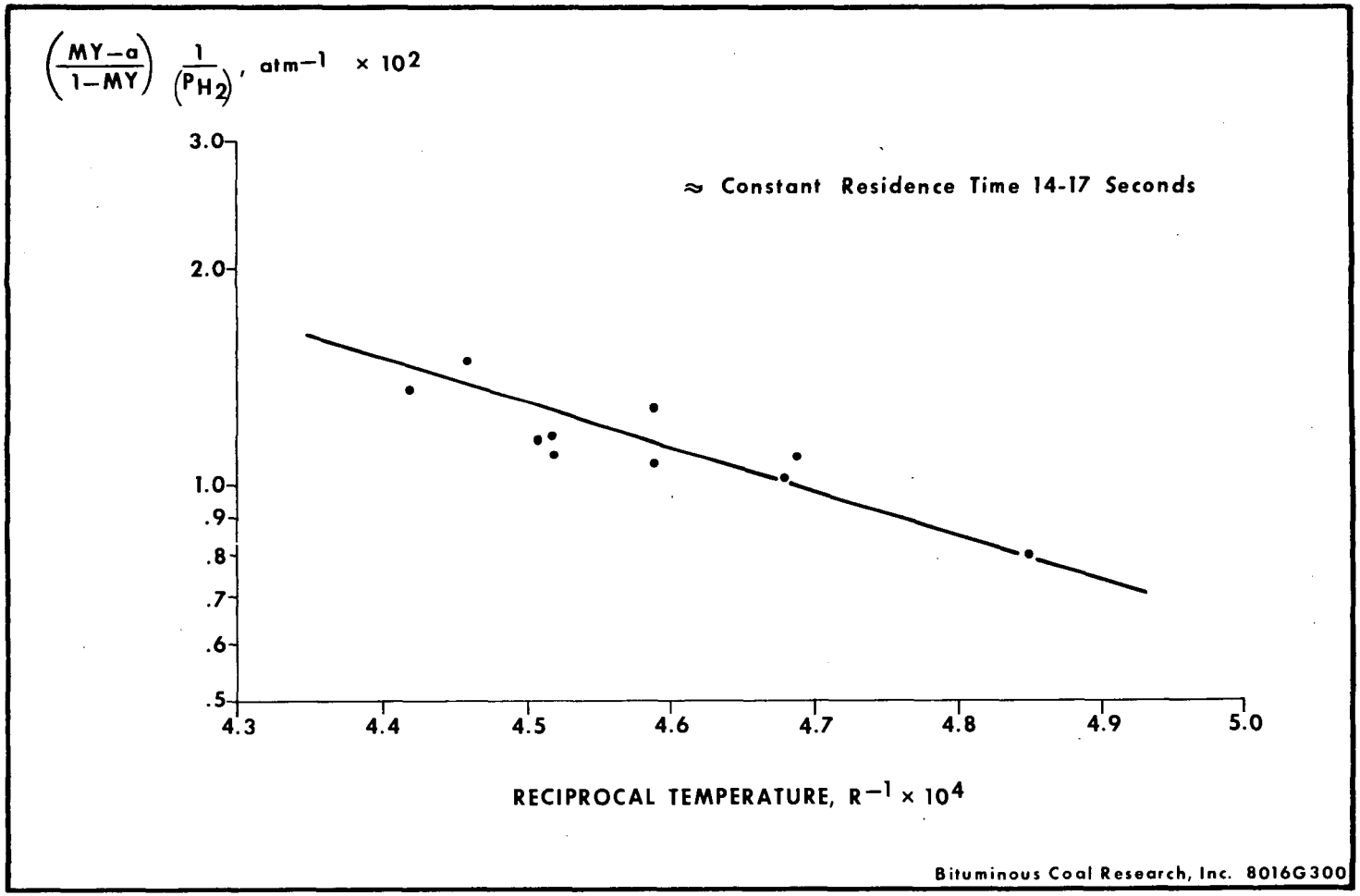

Figure 2. Methane Yield per Atmosphere of Hydrogen Partial Pressure as a Function of Reciprocal Outlet Temperature at Constant Residence Time for Pittsburgh Seam Coal

into the simulated Stage 1 gas. It was noted that the methane experienced partial decomposition.

The exact nature of the destruction of methane is not clear. However, it is most likely that the steam in the Stage 1 gas promotes the reforming reaction:

$$CH_4 + H_2O \rightarrow CO + 3H_2$$

Analysis of the material balance data from the methane decomposition tests suggests that the latter reaction is occurring. One of the tests was carried out at 200 psig in order to permit observation of the mixing temperature by an ultra-violet pyrometer. The results can be explained by assuming that methane decomposes at a rate proportional to its concentration, i.e.:

$$\frac{d\,[CH_4]}{dt} = k\,[CH_4]$$

Although it is likely that the reaction rate is influenced by steam, hydrogen, and carbon monoxide partial pressures, these did not vary significantly during the tests, and their effect cannot be determined at this time.

Integration of the rate expression gives:

$$\ln\,[1 - f] = -k\tau \qquad (5)$$

where, τ = residence time
f = fraction of methane decomposed
k = reaction rate constant

The residence time of the individual tests was constant. Since the reaction rate constant is temperature-dependent, an Arrhenius plot of ln (ln [1 - f]) versus the reciprocal of the observed mixing zone temperature should yield a straight line. That this is indeed the case is shown in Figure 3. The temperature effect on the rate of methane decomposition is quite pronounced, corresponding to an activation energy of 30 Kcal/g mole.

The fact that methane injected into the PEDU decomposes to a certain extent suggests that methane formed directly from coal could also decompose. Thus, the methane yield predicted by Equation (3) would have to be modified as in Equation (5). This gives the following equation for methane yield:

$$MY = \left(\frac{a + b\,(P_{H_2})}{1 + b\,(P_{H_2})}\right) e^{-k\tau} \qquad (6)$$

Note that this equation indicates that methane yield is dependent upon residence time, but in an unusual and unexpected way.

Because both parameters b and k depend on temperature, it is difficult to express the relationship of Equation (6) in a form convenient for graphical display. However, certain first order simplifications and approximations can be made.

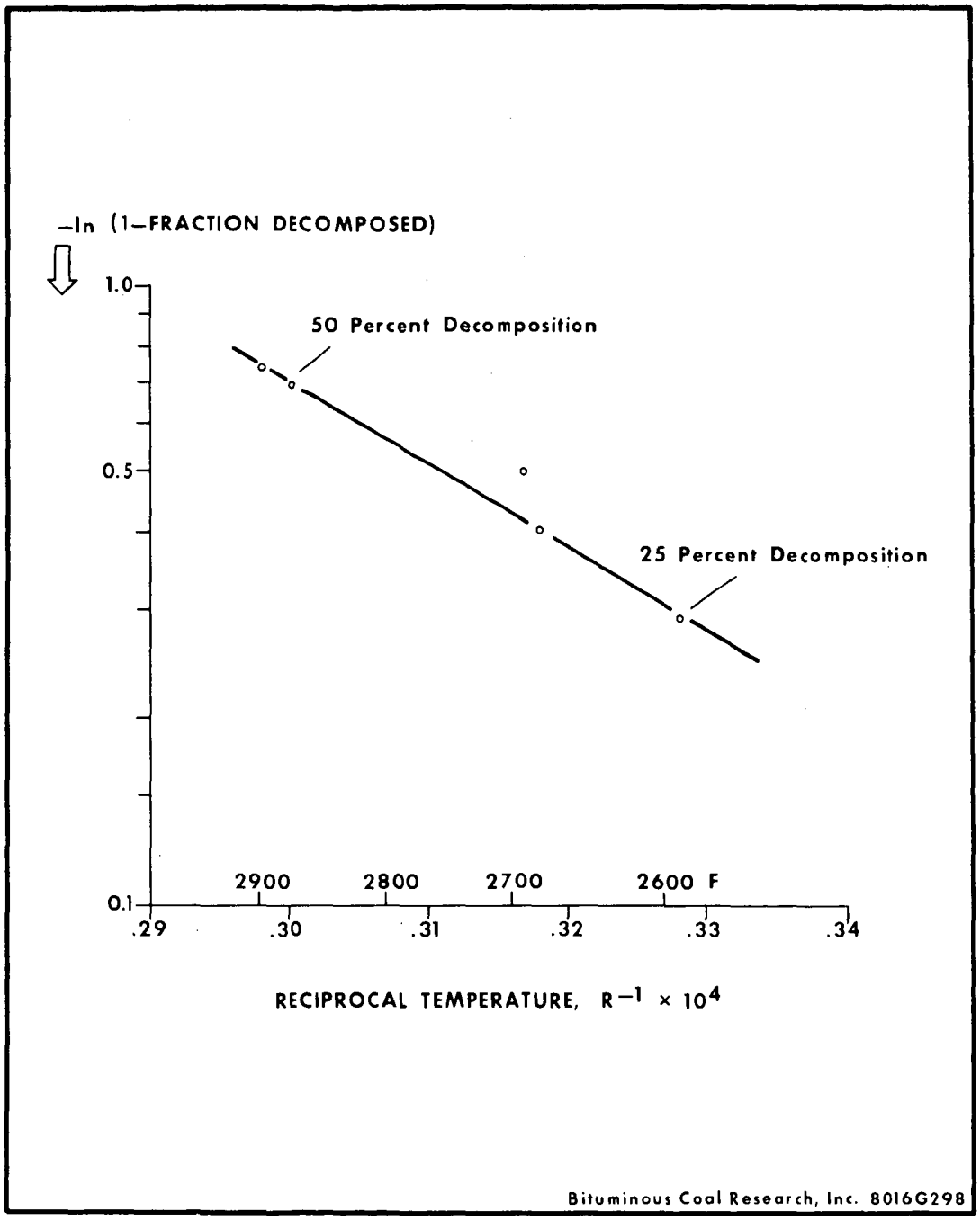

Figure 3. Methane Decomposition in the PEDU

Thus, if we make the following approximation

$$e^{-k\tau} \cong 1 - k\tau,$$

Equation (6) can be written in the following form:

$$\left(\frac{MY - a}{1 - MY}\right)\left(\frac{1}{(P_{H_2})}\right) = b - \frac{k\tau[a + b\ (P_{H_2})]}{(P_{H_2})\ (1 - MY)} \tag{7}$$

Furthermore, if we note that the group $\left(\frac{a + b\ (P_{H_2})}{(P_{H_2})}\right)$ is relatively insensitive to the partial pressure of hydrogen in the range of experiments conducted, then Equation (7) becomes

$$\left(\frac{MY - a}{1 - MY}\right)\left(\frac{1}{(P_{H_2})}\right) = b - k_1\left(\frac{\tau}{1 - MY}\right) \tag{8}$$

Thus, a plot of

$$\left(\frac{MY-a}{1-MY}\right)\left(\frac{1}{(P_{H_2})}\right) \text{ versus } \frac{\tau}{1-MY}$$

should give a straight line, provided temperature is constant. Figure 4 is such a plot for those Pittsburgh seam coal tests whose exit temperature was in the range 1720 to 1800 F. The trend is unmistakable. Although Equation (8) is the result of a number of assumptions and mathematical simplifications, it does provide a format for displaying and correlating the PEDU methane yield data. In addition these data do suggest that methane formed in the direct methanation process is destroyed in its passage through the remainder of the PEDU. The percent decomposition indicated by Equation (8) ranges from 10 percent at the low residence time tests to 25 percent at the high residence time tests.

If the correlating line in Figure 4 is extrapolated to zero residence time, a value is obtained for the b parameter in the methane yield equation:

$$b = 0.0165$$

An extension to higher temperatures of the Arrhenius plot for b obtained by Zahradnik and Glenn shows this value to correspond to a temperature of 2240 F[15]. This is probably a reasonable estimate of the mean reaction temperature of the methanation process taking place in the PEDU, when the exit temperature is between 1720 and 1800 F.

At a temperature of 2240 F, the methane decomposition correlation (Figure 3) gives a value for $k\tau$ of 0.085. The residence time in the methane decomposition tests was 7.5 seconds, so that a k value can be calculated.

$$k = \frac{0.085}{7.5}\ \text{sec}^{-1} = 0.0113\ \text{sec}^{-1}$$

A k value can also be obtained from the gasification tests, since from

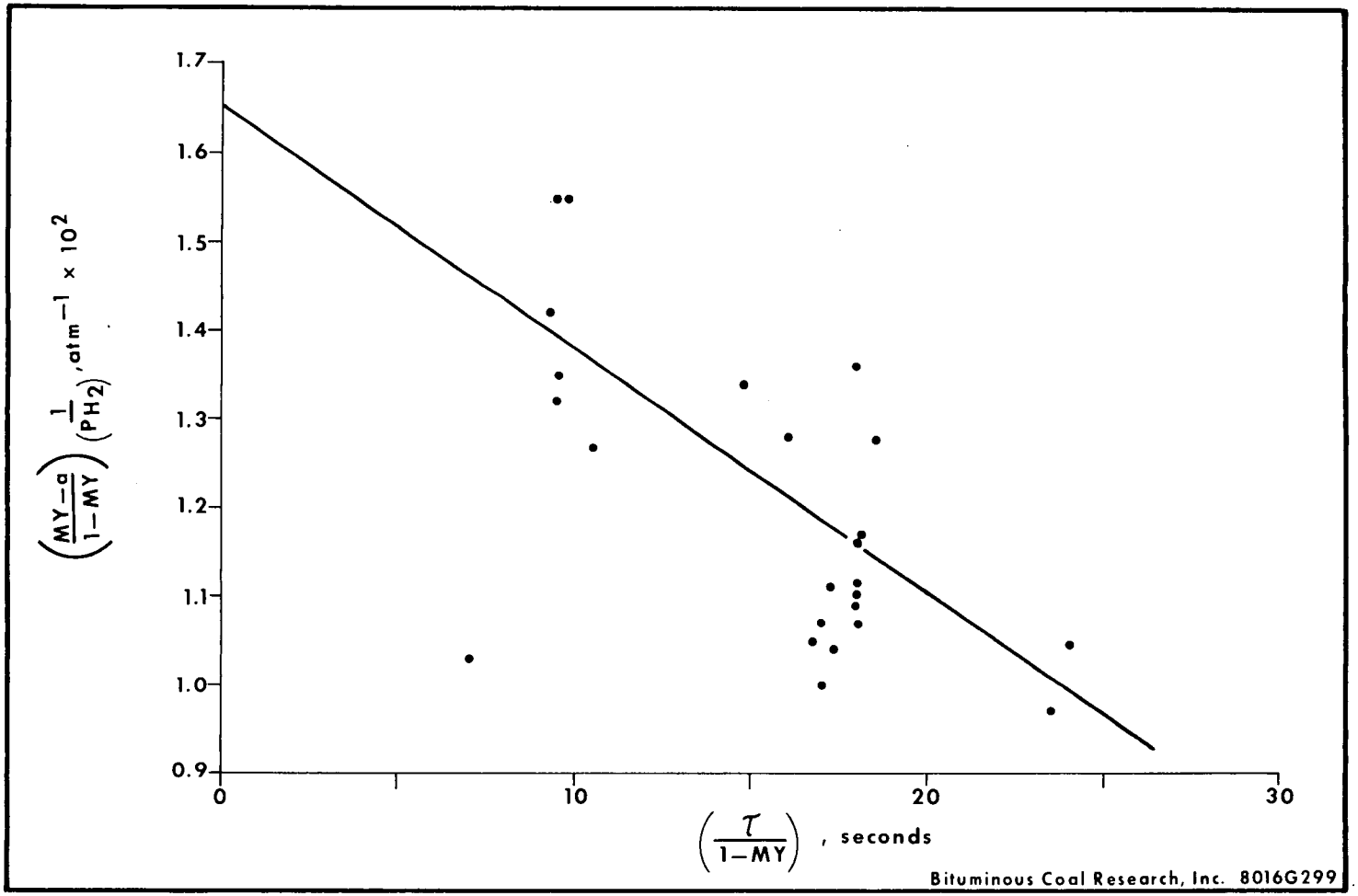

Figure 4. Methane Yield per Atmosphere of Hydrogen Partial Pressure vs. Residence Time for Pittsburgh Seam Coal

Equation (8) the slope of the correlating line of Figure 4 is

$$\text{slope} = k\left(\frac{a + b\,(P_{H_2})}{(P_{H_2})}\right)$$

The value of this slope is 0.000275. If b = 0.0165 and the average hydrogen partial pressure is 15 atm, the value of k can be calculated:

$$k = \frac{0.000275\ \text{sec}^{-1}}{\dfrac{0.08 + 0.0165\,(15)}{(15)}} = 0.0126\ \text{sec}^{-1}$$

This value, 0.0126 sec^{-1}, is remarkably close to the value of 0.0113 sec^{-1} at 2240 F estimated from the methane decomposition tests.

A complete and consistent model for methane production in the PEDU may now be given. The following equation can be written for any temperature and contact time:

$$\left(\frac{MY - a}{1 - MY}\right)\left(\frac{1}{(P_{H_2})}\right) = b - k\left(b + \frac{a}{(P_{H_2})}\right)\left(\frac{\tau}{1 - MY}\right) \qquad (8)$$

For a given reaction temperature, b can be estimated from the paper by Zahradnik and Glenn[15] and k from Figure 3 and Equation (5). Then a plot of reduced methane yield per atmosphere of hydrogen partial pressure as a function of reduced residence time can be constructed, as in Figure 5. Notice that as temperature increases, the decomposition rate increases, thereby reducing the contact time required to destroy the methane. Moreover, for a given residence time, there is a "best" temperature at which to operate, best in the sense of yielding the highest methane yield per atmosphere of hydrogen partial pressure. This "best" temperature is shown as a function of residence time in Figure 6.

The results shown in Figures 5 and 6 are specific to the PEDU operation and involve numerous assumptions. Moreover, the temperature values are estimated reaction temperatures which combine the total effect of temperature profiles and gas mixing patterns. As in all the correlations presented here, they should be regarded as phenomenological and suggestive--not as the consequences of strict mechanisms. Nonetheless, they do underscore the effect of residence time and temperature on the yield from Stage 2.

STEAM-CARBON REACTION

The yield of carbon oxides from coal in Stage 2 has been attributed to the steam-carbon reaction and water-gas shift.

$$C + H_2O \rightarrow CO + H_2$$

$$CO + H_2O \rightarrow CO_2 + H_2$$

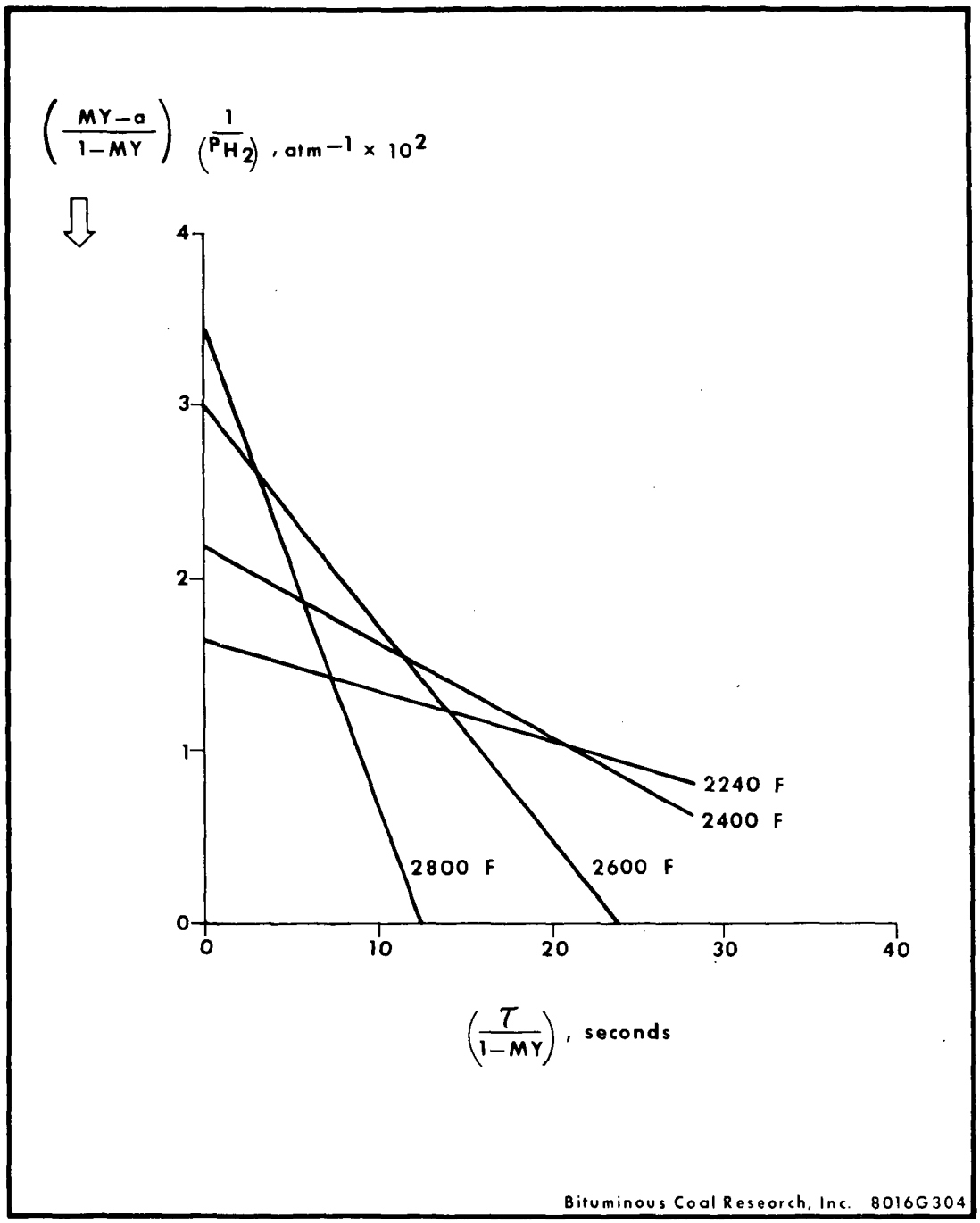

Figure 5. Residence Time and Temperature Effect on Methane Yield

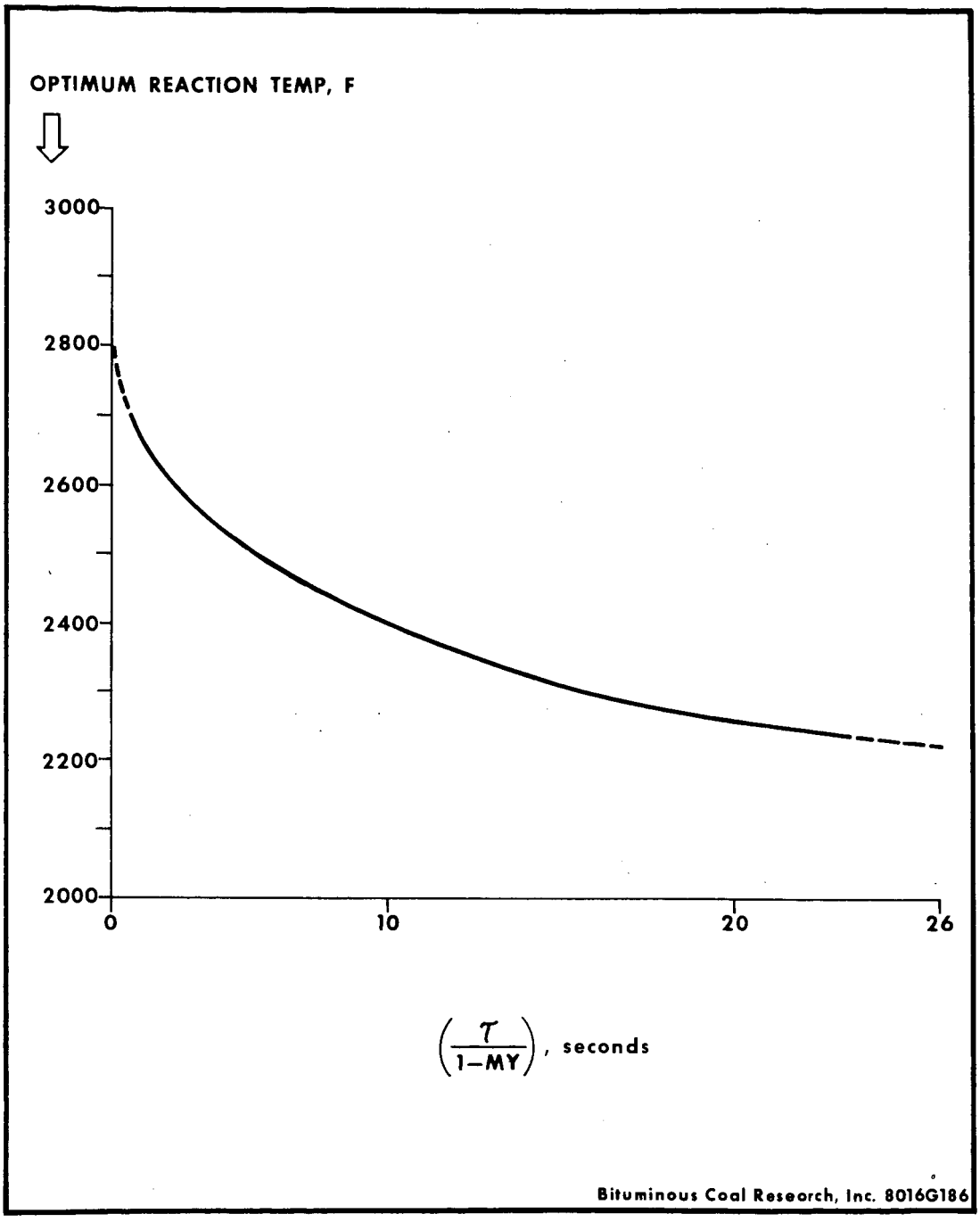

Figure 6. Optimum Temperature for Methane Production vs. Residence Time

The rate of production, under Stage 2 conditions, is to a first order approximation

$$\text{rate} = k' \frac{(P_{H_2O})}{(P_{H_2})}$$

where k' is an effective rate constant. Proper integration of this equation would have to take into account the temperature and composition paths, which are unknown. However, if outlet conditions are used to approximate the appropriate integrated equation, the following expression is obtained

$$\frac{CY}{\left(\frac{(P_{H_2O})}{(P_{H_2})}\right)_T} = k' \qquad (9)$$

where CY = fraction of carbon in coal gasified to carbon oxides.

Figure 7 is a plot of the natural logarithm of the carbon oxide yield expression from Equation (9) versus reciprocal outlet temperatures for all the data for Pittsburgh seam coal. The overall fit is fairly good, indicating that the various assumptions required to arrive at Equation (9) are not unreasonable.

GASIFICATION PHYSICS

The physical processes taking place during entrained gasification are as complex as the chemical ones. Complete modelling of the physics would have to include the expansion of the jet of coal into the hot synthesis gas, particle-particle collisions, particle heat up, etc. Many of these physical processes have been examined by BCR in an attempt to understand entrained gasification. However, in the light of the previous discussion concerning the recirculation reformers set up by the coal feed, the most significant physical process affecting methane yield is the mixing between the coal feed and hot Stage 1 gases.

Although it is not possible to predict or even infer the exact mixing patterns in Stage 2 of the PEDU, some insight into these flow patterns can be obtained by considering certain idealized conditions. If only the expansion of the coal feed jet into Stage 2 is considered, the fluid mechanics of turbulent jets predicts that the coal stream would strike the wall at a distance X_p[13,14], where

$$X_p = 5.85\ L$$

and 2 L is the Stage 2 diameter (ft). In the absence of reaction or other influence from the Stage 1 gases, the coal feed jet would strike the wall of the 8-inch diameter PEDU about 2 ft below its entrance.

As the coal feed jet slows down from its nozzle velocity, it entrains surrounding fluid in order to conserve its axial mementum and thereby sets up recirculation currents. The mass rate of material recirculated, m_r, per

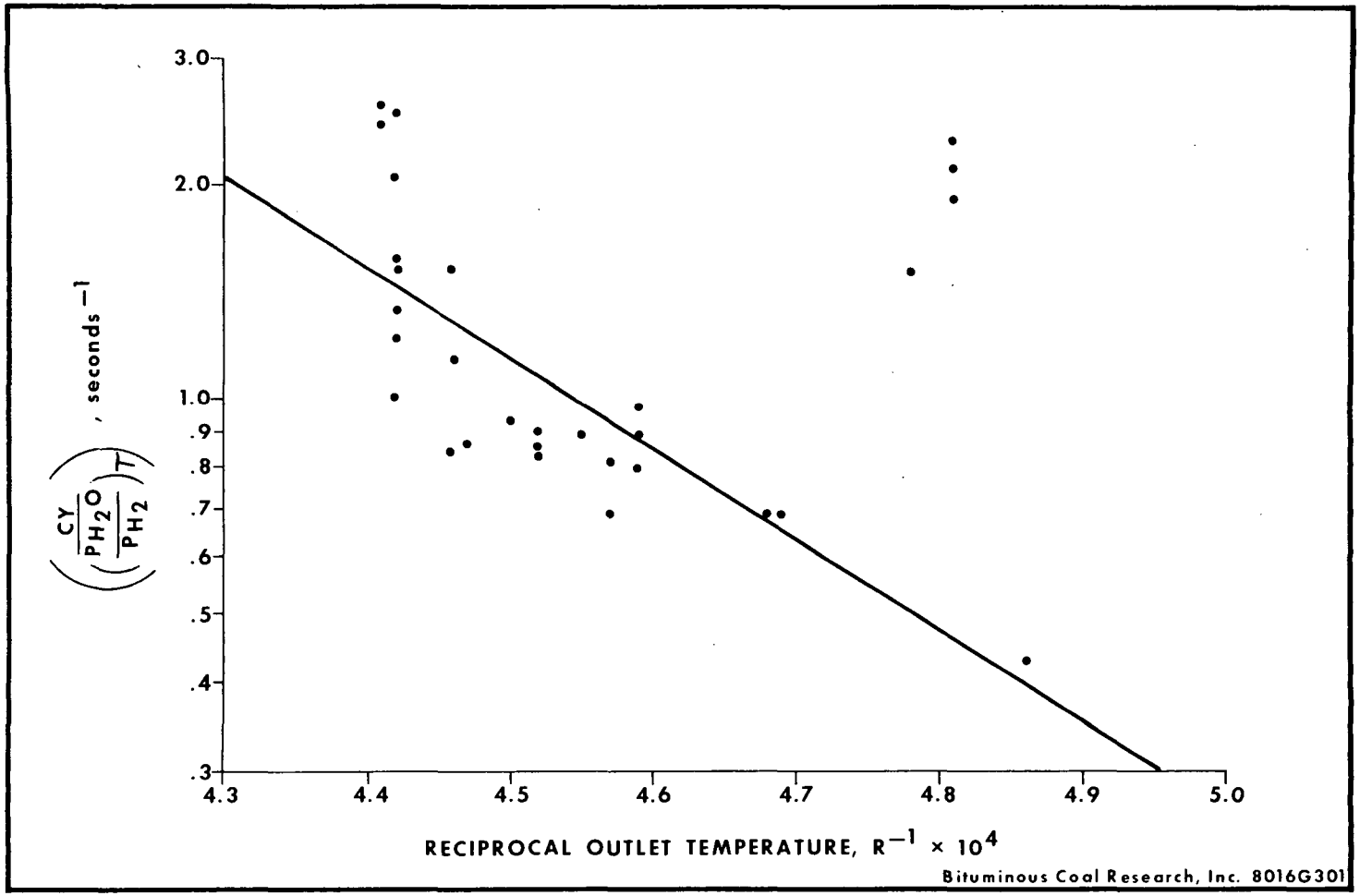

Figure 7. Carbon Oxides Yield Group vs. Reciprocal Outlet Temperature for Pittsburgh Seam Coal

mass rate of material fed, m_o, can be estimated from the following equation proposed by Thring[14].

$$\frac{m_r}{m_o} = \frac{0.47}{\theta} - 0.5 \qquad (10)$$

Where

$$\theta = \frac{m_o}{L(\pi \rho_a G)^{1/2}}$$

and ρ_a = density of surrounding fluid (lb/ft^3)

$G = m_o \times v_o$ = mass velocity at nozzle ($ft\ lb/sec^2$)

Typical values for PEDU operation are:

ρ_a = 0.6 lb/ft^3 (22 molecular weight gas, 1020 psia, 2700° R)

m_o = 100 lb/hr = $\frac{1}{36}$ lb/sec

v_o = 50 ft/sec

$G = \frac{50}{36}$ ft lb/sec^2

Hence

$$\theta = \frac{\frac{1}{36}}{\left[\frac{1}{3}\ \pi\ (0.6)\ \left(\frac{50}{36}\right)\right]^{1/2}} = \frac{1}{14.5}$$

And a typical recirculation ratio is:

$$\frac{m_r}{m_o} = \frac{0.470}{0.069} - 0.5 = 6.4$$

Operation at this ratio would result in the first two feet of Stage 2 being fairly well mixed. According to Thring, recirculation into the jet begins at a distance X_n,[14]

$$X_n = 6.25\ \theta\ L$$

which in this case is 1.7 inches. Entrainment into the jet continues until a distance X_1,

$$X_1 = 3.12\ (0.94 + \theta)\ L$$

which is about 13 inches. From this point onward disentrainment occurs, reaching a maximum at about 16 inches.

These dimensions are summarized on Figure 8, which is a schematic of the PEDU.

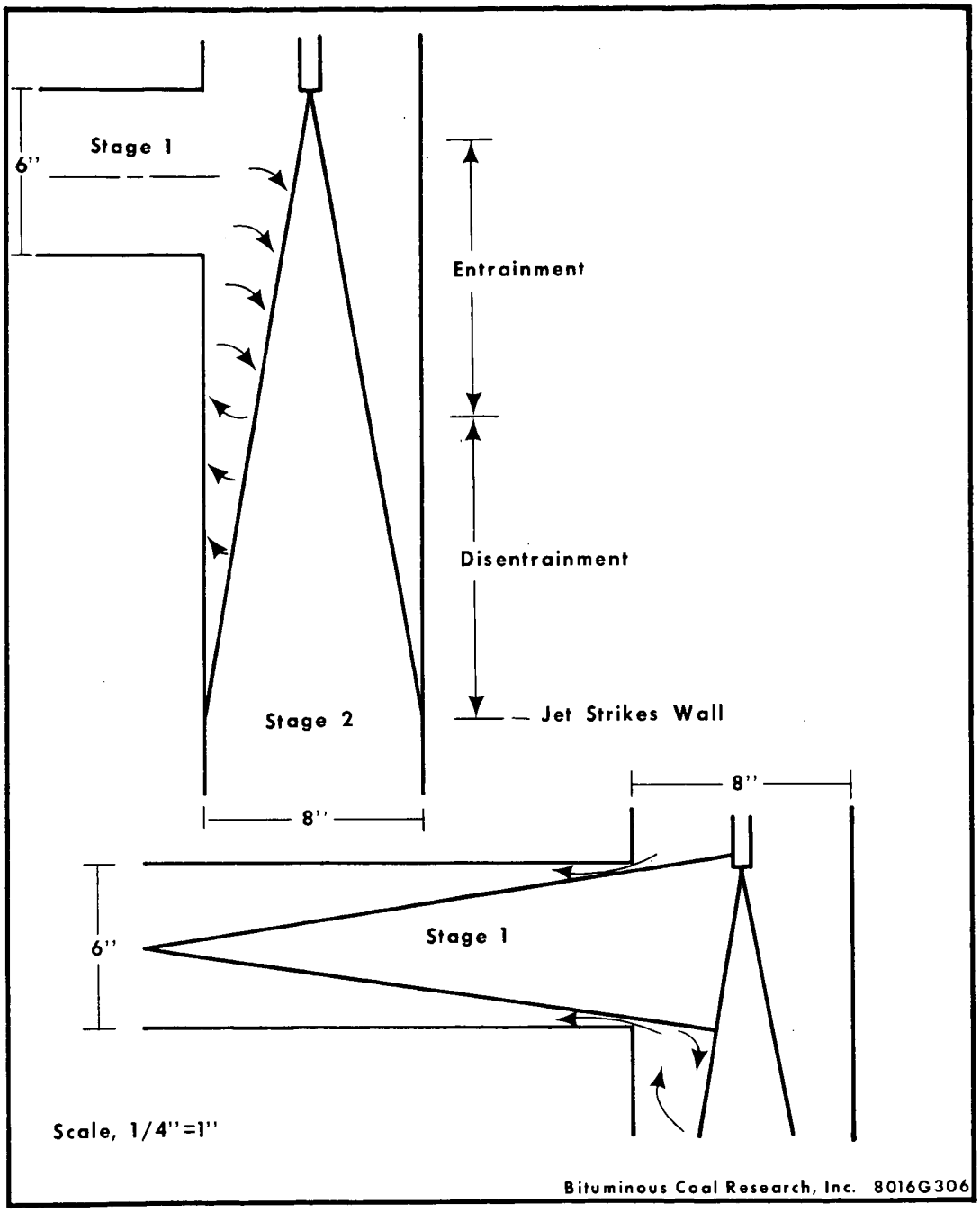

Figure 8. Typical Entrainment, Disentrainment Distances in the PEDU

The high recirculation rate and the fact that entrainment is taking place in the region where the hot Stage 1 gas enters Stage 2 indicate that product decomposition could occur in the PEDU. And as we have seen in the previous section, this does indeed occur.

When Stage 1 and Stage 2 are operating in concert, the mixing patterns are unquestionably more complicated. The Stage 1 zone is 18 inches long and its diameter is 6 inches. For these dimensions, it might be expected, on the basis of cold jet mixing, that the Stage 1 gases would strike the walls of the sidearm just prior to their entrance into Stage 2. However it has been reported that the jet half-angle in a furnace flame is about 4-1/4 degrees. At this angle the distance for the jet to strike the Stage 1 chamber walls, X_p, would be[4,14]

$$X_p = \cot\ (8.5°)\ (3") = 20"$$

Since this distance exceeds the length of the Stage 1 Zone, recirculation into Stage 1 from Stage 2 would be expected. From the previous arguments, it must be concluded that this would include both product gas and char. In actual fact, considerable insufflation into Stage 1 did occur, since extensive slag deposits were observed along the entire bottom of this zone. With this concept of PEDU circulation in mind, some tests were conducted in which hydrogen was used for coal transport. Low pressure operation was also employed. In these cases, nozzle velocities exceeded 100 ft/sec, and in some cases approached 300 ft/sec. Since θ is proportional to

$$(m_o/v_o)^{1/2}$$

and if all other variables were held constant, an increase in nozzle velocity to 200 ft/sec would decrease θ from the previously considered value by a factor of 1/2 to $\theta = 0.035$. Using this value, the mass recirculated ratio then would become

$$\frac{m_r}{m_o} = 12.9$$

The locations of the entrainment and disentrainment areas would remain relatively the same and, ideally, the jet would strike the Stage 2 chamber walls at about the same 2-ft level.

Under such operation, one would expect that a considerably higher degree of backmixing or recirculation would occur, although, of course, the average residence time of the gases in this part of the reactor would be dictated by overall flow rates. It is possible that the considerable backmixing leads to a higher inventory of char, particularly in the high temperature region exposed directly to Stage 1 input. This would lead to proportionately higher char gasification (to carbon oxides) than in less well-mixed tests.

Figure 9 presents the results of the high nozzle velocity tests for Pittsburgh seam coal. It can be seen that the carbon oxide yields are indeed higher than expected.

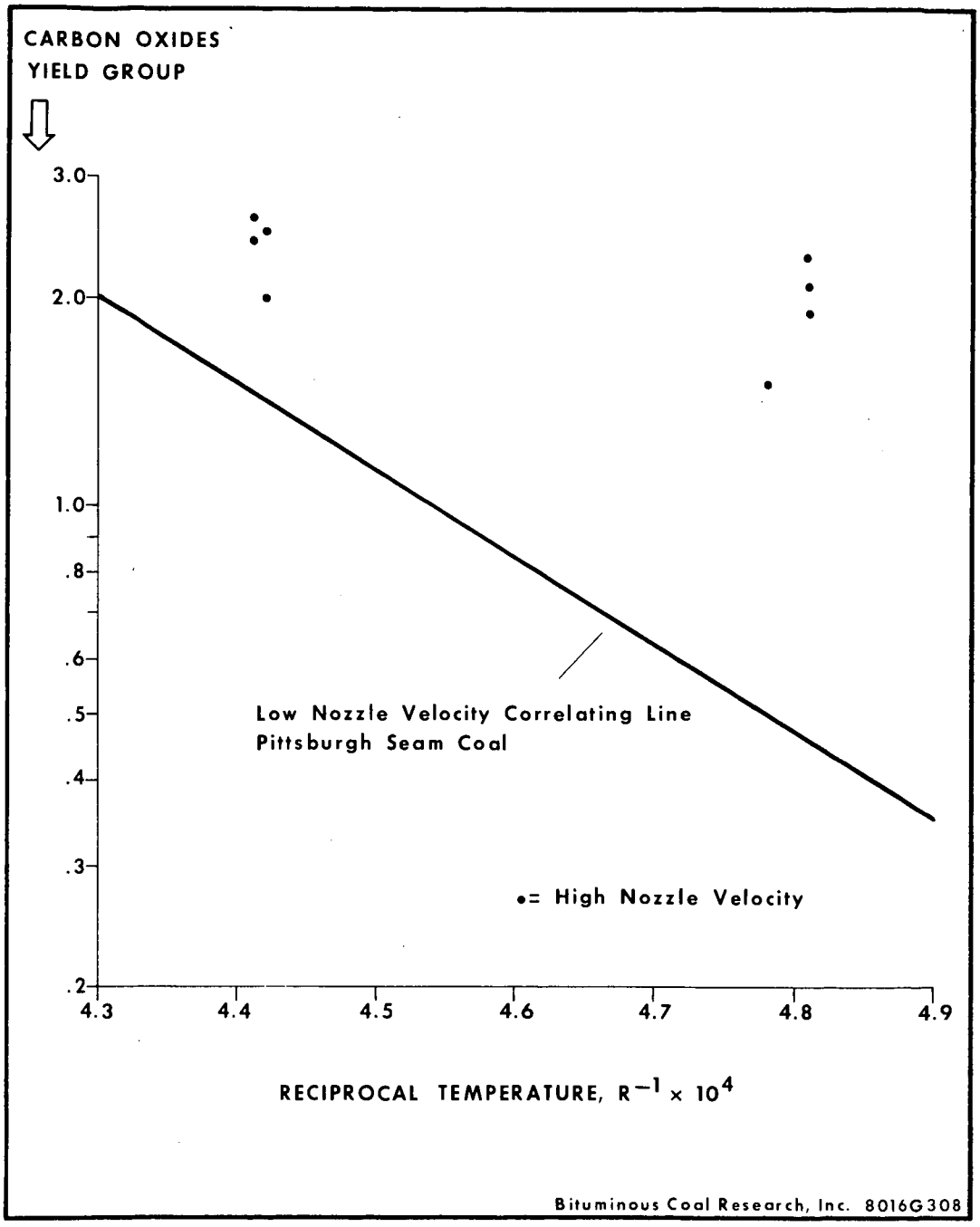

Figure 9. Effect of High Nozzle Velocity on Carbon Oxide Yield Group for Pittsburgh Seam Coal

The methane yields for these tests correlated in the same way as did those for the lower nozzle velocity tests and are included in Figure 4. This is as expected since the reactivity of char to direct methanation by hydrogen is considerably less than the active form of carbon produced in the initial heat-up of coal. Consequently, a higher char inventory, even in the high temperature region, would not produce higher methane yields.

DISCUSSION

It must be remembered that the results and correlations expressed in the previous sections are specific to the geometry and conditions of the PEDU. They do not represent fundamental limitations on the entrained gasification of coal, but are to be taken as guidelines to basic understanding of the process. Thus, if the flow patterns set up by the PEDU geometry result in destruction of a portion of the methane, it should be possible to alter this geometry to improve methane yields. For example, if the coal feed nozzle were lowered into Stage 2, the back mixing of coal and product gases into the hotter regions of the gasifier would be reduced.

In order to test this idea, arrangements were made to extend the coal feed nozzle to various lengths inside Stage 2. The best location of those tested occurred with the nozzle one inch below the Stage 1 center line. With Pittsburgh seam coal as feedstock and the nozzle in this position, a methane yield of 25 percent was obtained for an outlet hydrogen partial pressure of 16 atmospheres. This exceeds the correlation established for the original nozzle position shown in Figure 10 and emphasizes the importance of proper flow patterns in Stage 2.

Carbon oxides yield for this nozzle position was less than expected from earlier correlations, as shown in Figure 11. In this case, the product methane and char which were recirculated would have been exposed to less severe temperatures and hence contributed less to the yield of carbon oxides.

The correlations discussed in the previous sections can therefore be viewed as conservative. With proper design to avoid recirculation of product methane into zones of high temperature, the next generation two-stage gasifier can be expected to produce methane yields in excess of those obtained in the PEDU.

The PEDU tests discussed here have provided considerable information on the effects of temperature and residence time on the process. We have shown in this paper that simple ideas of gasification chemistry and physics can be combined into expressions adequate for correlating these data. Extrapolation of these expressions gives estimates for the methane yields which might be obtained from the entrained gasification of coal. For example, the extrapolations of Figure 6 indicate that if residence times could be limited to 2 seconds and effective temperatures of 2800 F were attained while maintaining 20 atmospheres of hydrogen partial pressure, methane yields of 38 percent could result. Even at effective temperatures of 2240 F, which we know we can achieve, methane yields in excess of 30 percent could be obtained if residence times could be kept to 1 or 2 seconds.

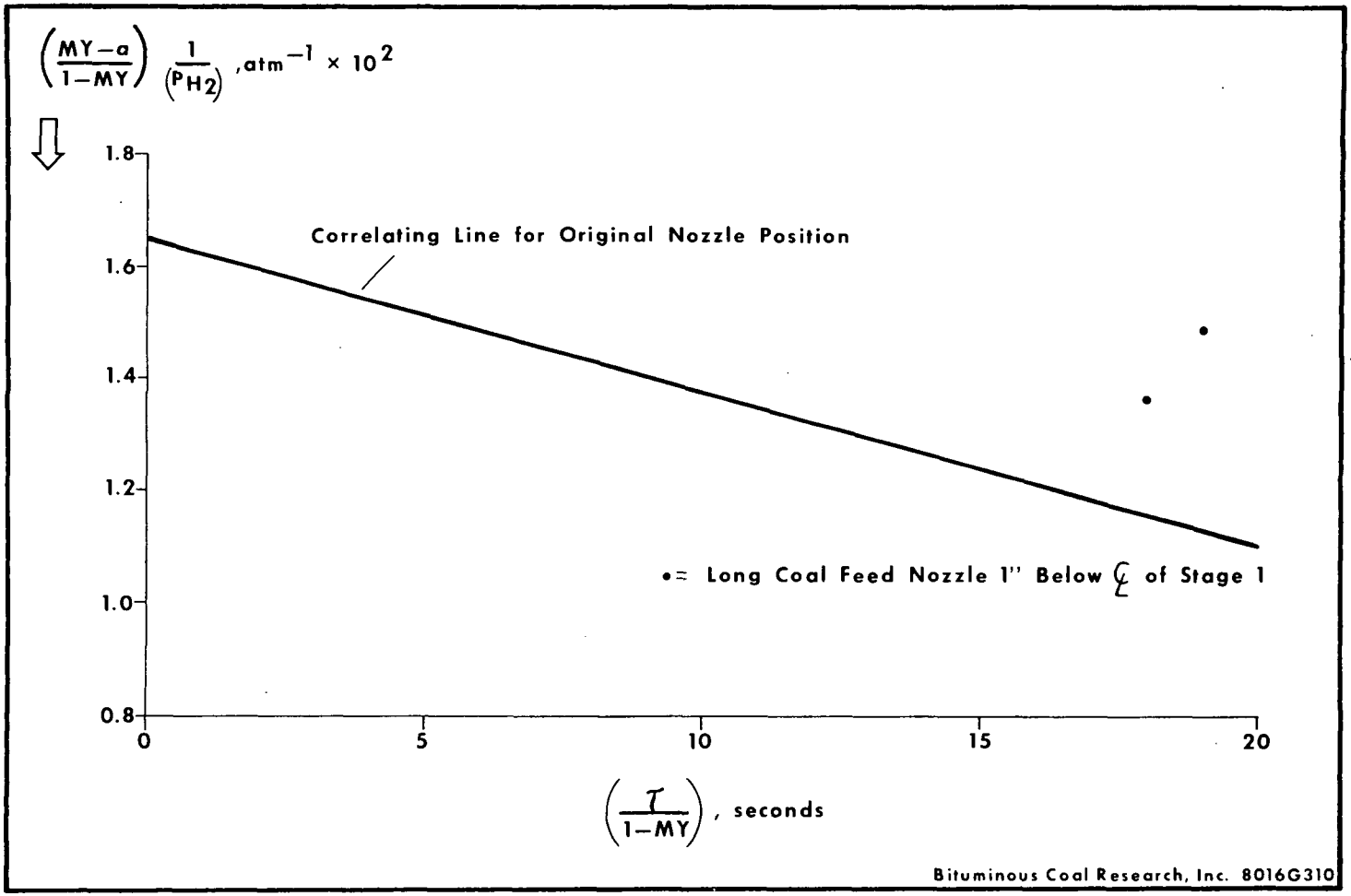

Figure 10. Effect of Location of Coal Feed Nozzle on Methane Yield Using Pittsburgh Seam Coal

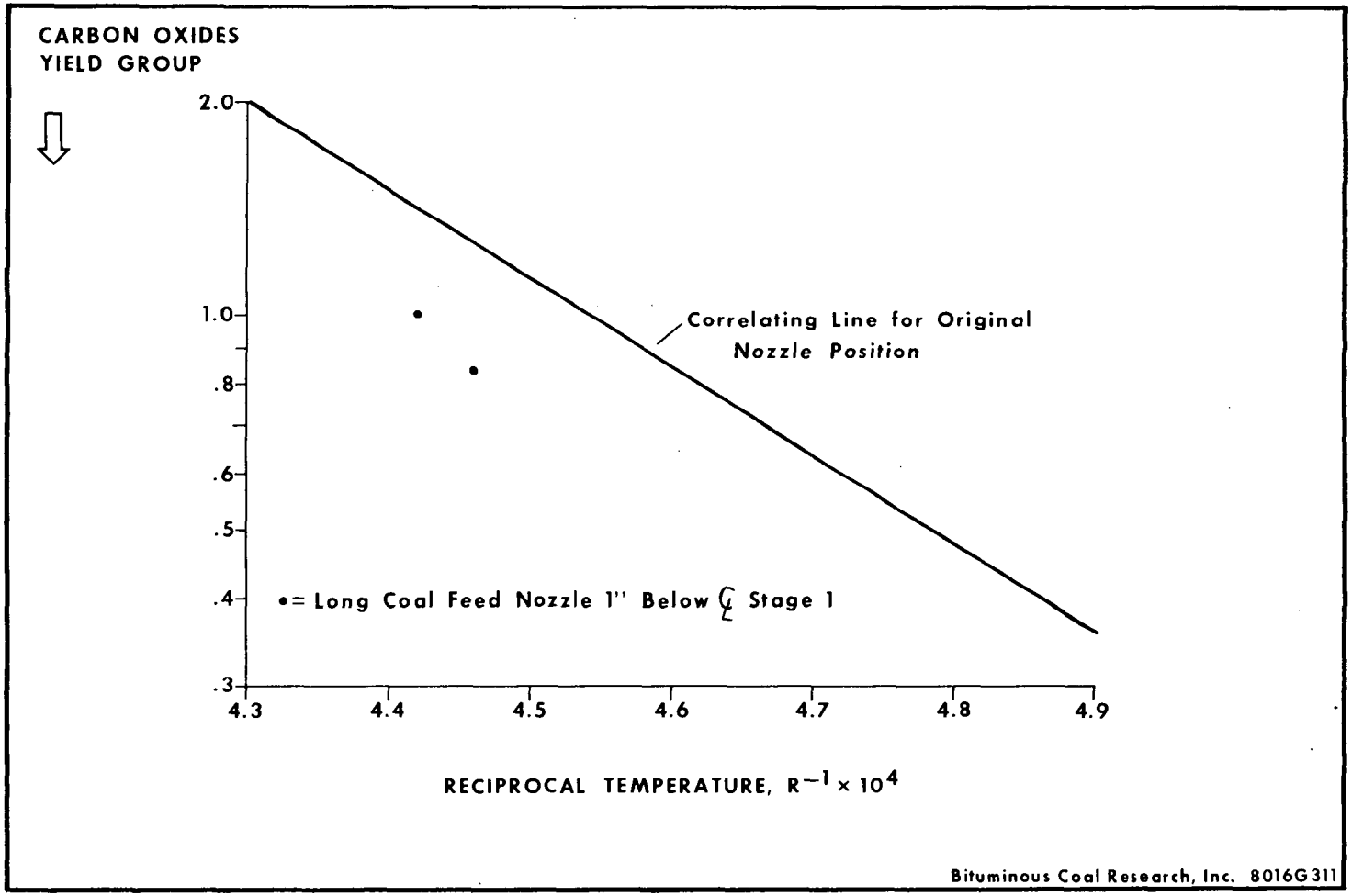

Figure 11. Effect of Location of Coal Feed Nozzle on Carbon Oxide Yield Group Using Pittsburgh Seam Coal

Whether the exact nature of the rapid, high temperature gasification of coal is properly captured by the correlations of this paper to allow such extrapolations to be validly made is of course open for discussion. Whether gasifiers with proper geometrics can be designed to attain these high yields remains to be seen. But on the basis of the analysis proposed in this paper, the promise is there.

ACKNOWLEDGEMENT

This paper is based on work carried out at Bituminous Coal Research, Inc. with support from the Office of Coal Research, U.S. Department of the Interior, under Contract No. 14-32-0001-1207, and the American Gas Association. The authors also acknowledge the advice and encouragement of Dr. Ernest Donath.

REFERENCES CITED

1. "Gas Generator Research and Development - Phase I. Survey and Evaluation," Bituminous Coal Research, Inc., Rept. to U.S. Office of Coal Res., R&D Rept. 20--Interim Rept. No. 1, Washington: U.S. Government Printing Office, 1965. 2 volumes.
(Out of print copies on file at OCR depository libraries.)

2. "Gas Generator Research and Development - Phase II. Process and Equipment Development," Bituminous Coal Research, Inc., Rept. to U.S. Office of Coal Res., R&D Rept. 20--Final Rept., Washington: U.S. Government Printing Office, 1971. (520 pp.)

3. Donath, E.E. and Glenn, R.A., "Pipeline gas from coal by two-stage entrained gasification," in "Operating Section Proceedings," New York: Am. Gas Assoc., 1965. pp 65P147-151.

4. Field, M. A., Gill, D. W., Morgan, B. B., and Hawksley, P. G. W., "Combustion of Pulverized Coal," Leatherhead, England: Brit. Coal Util. Res. Assoc., 1967.

5. Glenn, R. A., Donath, E. E., and Grace, R. J., "Gasification of coal under conditions simulating Stage 2 of the BCR two-stage super-pressure gasifier," in "Fuel Gasification," Advances in Chemistry Series 69, R. F. Gould, Ed., Washington: Am. Chem. Soc., 1967. pp 81-103.

6. Glenn, R. A. and Grace, R. J., "An internally-fired process development unit for gasification of coal under conditions simulating Stage Two of the BCR two-stage super-pressure process," Second Synthetic Pipeline Gas Symposium, Pittsburgh, Pa., Am. Gas Assoc., 1968. 17pp.

7. Glenn, R. A., "Status of the BCR two-stage super-pressure process," Third Synthetic Pipeline Gas Symposium, Pittsburgh, Pa., Am. Gas Assoc., 1970. 18pp.

8. Grace, R. J., Glenn, R. A., and Zahradnik, R. L., "Gasification of lignite by the BCR two-stage super-pressure process," Symposium on Synthetic Hydrocarbon Fuels from Western Coals, Denver, Colo., Am. Inst. Chem. Engrs., 1970. 23 pp.

9. Grace, R. J. and Zahradnik, R. L., "BI-GAS process enters pilot plant stage," Fourth Synthetic Pipeline Gas Symp., Chicago, Ill., Am. Gas Assoc., 1972. 22 pp.

10. Moseley, F. and Paterson, D., "The rapid high-temperature high-pressure hydrogenation of bituminous coal," J. Inst. Fuel 40 (322), 523-30 (1967).

11. Moseley, F. and Paterson, D., "The rapid high-temperature hydrogenation of coal chars - Part 1: Hydrogen pressures up to 100 atmospheres," J. Inst. Fuel 38 (288), 13-23 (1965).

12. Moseley, F. and Paterson, D., "The rapid high-temperature hydrogenation of coal chars - Part 2: Hydrogen pressures up to 1000 atmospheres," J. Inst. Fuel 38 (296), 378-91 (1965).

13. Narasimham, K. S., "Flame length calculation for furnace design," Erdol und Kohle 24 (7), 471-472 (1971).

14. Thring, M. W., "The Science of Flames and Furnaces," 2nd ed., New York: John Wiley & Sons, Inc., 1962. 625 pp.

15. Zahradnik, R. L. and Glenn, R. A., "Direct methanation of coal," Fuel 50 (1), 77-90 (1971).

KINETICS OF BITUMINOUS COAL CHAR GASIFICATION WITH GASES CONTAINING STEAM AND HYDROGEN

by

J. L. Johnson

Institute of Gas Technology
Chicago, Illinois 60616

INTRODUCTION

Correlations to quantitatively define the effects of pertinent intensive variables on the kinetics of coal or coal char gasification reactions are necessary for the rational design of commercial systems to convert coal to pipeline gas. The available information, which can be applied to the development of such correlations is relatively limited, particularly because the data reported from many studies conducted with integral contacting systems reflect, in part, undefined physical and chemical behavior peculiar to the specific experimental systems used. Although some differential rate data have been obtained with various carbonaceous materials, they cover only narrow ranges of the conditions potentially applicable to commercial gasification systems.

During the last several years, the Institute of Gas Technology (IGT) has been conducting a continuing study to obtain fundamental information on the gasification of coals and coal chars, which could be used, along with selected information in the literature, to develop engineering correlations which quantitatively define the effects of intensive variables on gasification rates over a wide range of conditions applicable to a variety of conceivable gasification processes. The models and correlations developed at the present time are primarily applicable to bituminous coal chars prepared at mild or severe conditions in either inert or oxidizing atmospheres. Although we have achieved some success in applying these correlations to the gasification of subbituminous and lignite coals for limited ranges of conditions, the gasification kinetics of such materials have shown wide deviations from predictions of the correlations at lower temperatures and during initial stages of gasification.

The objective of this paper is a) to discuss the models which have been developed; b) to present the correlations derived from these models; and c) to demonstrate the consistencies between predictions of these correlations and various experimental gasification data obtained primarily with bituminous coal chars. We obtained the experimental information used in developing the models from two main sources. Initial development of the model for application to the gasification of devolatilized coal char in hydrogen and steam-hydrogen mixtures was based both on data obtained in an extensive study conducted at IGT with a high-pressure thermobalance apparatus and on differential rate data obtained by investigators at the Consolidation Coal Company for the gasification of Disco char in a small-scale fluid bed.[9, 18, 19] Then, the model was extended to apply to the gasification of char containing volatile matter and to gasification with gases containing carbon monoxide, carbon dioxide, and methane, as well as steam and hydrogen, using data obtained primarily in the thermobalance study.

The thermobalance has been a particularly useful tool for obtaining fundamental gasification information, since with this type of apparatus, gasification rates can be measured at constant, well-defined, environmental conditions. Since a major amount of the information used in the formulation of the kinetic models developed, was based on data obtained in several hundred tests conducted with the thermobalance, a brief description of this apparatus is given below.

EXPERIMENTAL

The thermobalance is an apparatus capable of continuously weighing a coal sample which is undergoing reaction in a gaseous environment of desired composition at a constant pressure. The temperature can either be kept constant or varied. (10°F/min is the maximum rate for the apparatus used at IGT.) The nature of gas-solid contacting with the apparatus used in this study is shown in Figure 1. The coal sample is contained in the annular space of a wire-mesh basket bounded on the inside by a hollow, stainless-steel tube and on the outside by a wire mesh screen. To facilitate mass and heat transfer between the bed and its environment, the thickness of the bed is only 2-3 particle diameters when using −20+40 USS sieve-size particles. Gas flow rates used with this system are sufficiently large relative to gasification rates, that gas conversion is limited to less than 1% for devolatilized coal char.

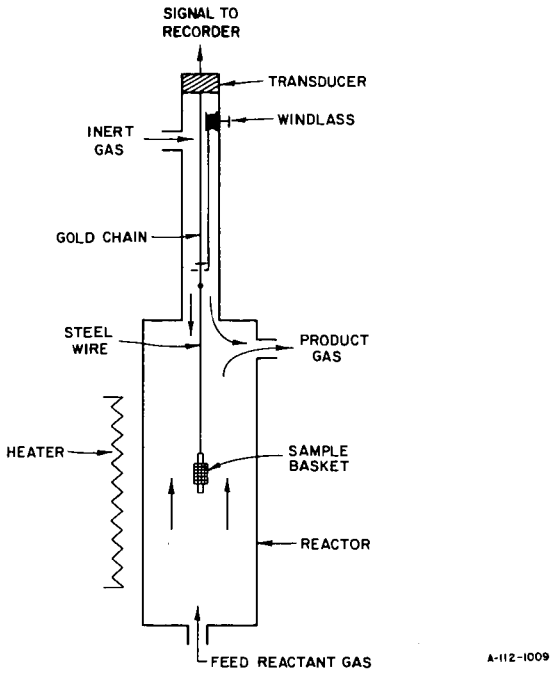

Figure 1. DIAGRAM OF THERMOBALANCE REACTOR

The following is a typical test procedure: The wire mesh basket is initially in an upper cooled portion of the reactor in which a downward, inert gas flow is maintained. During this time the desired temperature and pressure conditions are established in a lower heated portion of the reactor in the presence of a flowing gas. A test is initiated by lowering the basket into the heated reaction zone, a procedure which takes 5-6 seconds. Theoretical computation indicates that about 2 minutes are required for the sample to achieve reactor temperature, as measured by several thermocouples surrounding the basket in the reaction zone. This computation is reasonably corroborated by various kinetic indications and by the behavior of the thermocouples in reattaining their preset temperatures. The sample is kept in the heated portion of the reactor for the specified time while its weight is continuously recorded. The test is terminated by raising the basket back to the upper, cooled portion of the reactor.

During a test, the dry feed gas flow rates are measured by orifice meter and the dry product gas flow rates by a wet-test meter. Periodic samples of product gas are taken to determine the dry gas' composition by mass spectrograph. Feed and product steam flow rates are measured by gravimetric means, and the solids residues are analyzed for total carbon and hydrogen.

Figure 2 shows some typical, smoothed, weight loss-versus-time characteristics obtained using an air-pretreated hvAb Pittsburgh coal char from the Ireland mine. These curves are discussed in more detail in a subsequent

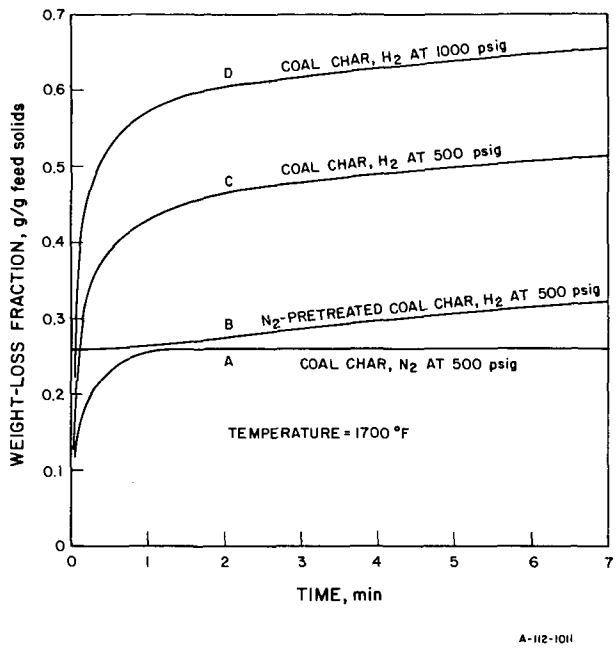

Figure 2. TYPICAL WEIGHT-LOSS CURVES OBTAINED WITH THE HIGH-PRESSURE THERMOBALANCE FOR GASIFICATION OF AIR-PRETREATED IRELAND MINE COAL CHAR IN HYDROGEN AND IN NITROGEN

section of this paper. The composition of the coal char, used extensively in the experimental study, is given in Table 1.

Table 1. COMPOSITION OF AIR-PRETREATED hvAb PITTSBURGH NO. 8 COAL CHAR (Ireland Mine)

Ultimate Analysis, dry	wt %
Carbon	71.1
Hydrogen	4.26
Oxygen	8.85
Nitrogen	1.26
Sulfur	3.64
Ash	10.89
Total	100.00

Proximate Analysis, ~~as received~~ dry	
Fixed Carbon	60.7
Volatile	28.4
Ash	10.9
Total	100.0

DESCRIPTION OF KINETIC MODELS

When a coal or coal char containing volatile matter is initially subjected to an elevated temperature, a series of complex physical and chemical changes occur in the coal's structure accompanied by thermal pyrolysis reactions, which result in devolatilization of certain coal components. The distribution of the evolved products of the reactions, which initiate at less than 700 °F and can be considered to occur almost instantaneously at temperatures greater than 1300 °F, is generally a function of the temperature, pressure, and gas composition existing during devolatilization and of the subsequent thermal and environmental history of the gaseous phase (including entrained liquids) prior to quenching.

When devolatilization occurs in the presence of a gas containing hydrogen at an elevated pressure, in addition to thermal pyrolysis reactions, coals or coal chars containing volatile matter also exhibit a high, although transient, reactivity for the formation of methane. Although some investigators have suggested that this process occurs concurrent with thermal pyrolysis reactions,

results of studies made with a greater time resolution indicated that this rapid-rate methane formation occurs at a rate which is at least an order of magnitude slower than devolatilization.[7, 17] In this sense it occurs consecutively to devolatilization.

The amount of carbon gasified to methane during the transient period of high reactivity increases significantly with increases in hydrogen partial pressure.[7, 13, 17] Experimental evidence indicates that, at sufficiently high hydrogen partial pressures, virtually all of the carbon not evolved during devolatilization can be gasified to methane during a very short time period by this process.[13] This is contrary to some proposed models, which assume that only a limited amount of carbon can be gasified in this reaction stage, regardless of the hydrogen partial pressure.[3, 16]

At temperatures greater than 1700°F, the transient reactivity for rapid-rate methane formation exists for a very short period of time. For coals, or coal chars prepared in inert atmospheres, this period lasts only seconds or less.[13] IGT's studies suggest that for air-pretreated coal chars, this period is more extended, although the total amounts of carbon which can be gasified by this process at a given temperature and hydrogen partial pressure, are comparable for coals and coal chars prepared at sufficiently low temperatures either in inert gas or in air.

After the devolatilization and rapid-rate methane formation stages are completed, char gasification occurs at a relatively slow rate, and various models to describe the gasification kinetics of this material for various limited ranges of conditions have been proposed. The differential rates of reaction of devolatilized coal chars are a function of temperature, pressure, gas composition, carbon conversion, and "prior history."

General Assumptions in the Development of Models

The models developed in this study for the quantitative description of coal char gasification kinetics assume that the overall gasification process occurs in three consecutive stages: 1) devolatilization, 2) rapid-rate methane formation, and 3) low-rate gasification. The reactions in these three stages are independent. Further, a feed coal char contains two types of carbon, volatile carbon and base carbon.

Volatile carbon can be evolved solely by thermal pyrolysis, independent of the gaseous medium. The distribution of evolved products derived from the volatile carbon fraction is not defined in the model. In any application of the model to an integral contacting system, the devolatilization products are estimated by extrapolation or interpolation of yields obtained in pilot-scale fluid or moving-bed systems. This procedure can be applied for narrow ranges of conditions and only for very similar contacting systems.

Base carbon remains in the coal char after devolatilization is complete. This carbon can be subsequently gasified either in the rapid-rate methane formation stage or in the low-rate gasification stage.

A quantitative estimation of the initial amounts of volatile and base carbon is made from standard analyses of the feed coal char. The following definition has been made:

$$C_v \text{ (volatile carbon), g/g of feed coal} = C_t^o \text{ (total carbon), g/g of feed coal} - C_b^o \text{ (base carbon), g/g of feed coal} \quad (1)$$

where C_t^o represents the total carbon in the feed coal char obtained from an ultimate analysis and C_b^o represents the carbon in the "fixed carbon" fraction of the feed coal as determined in a proximate analysis. It is emphasized that C_b^o does not equal the fixed carbon fraction, since the fixed carbon fraction includes, in addition to carbon, other organic coal components not evolved during standard devolatilization.

Experimental results from thermobalance or free-fall tests conducted at IGT indicate that the assumption of a constant volatile carbon fraction is valid for coal heat-up rates as high as 200 °F/s. However, other studies conducted with extremely rapid heat-up rates (10^4 to 10^7 °F/s) have shown that quantities of carbon evolved during thermal pyrolysis can exceed the volatile carbon fraction defined in this model.[6, 11] An allowance for the increase in evolved carbon would, therefore, have to be made in systems employing such high heating rates.

The base carbon conversion fraction, X, is defined as:

$$X = \frac{\text{base carbon gasified}}{\text{base carbon in feed coal char}} = \frac{C_b^o - C_b}{C_b^o} \quad (2)$$

where

C_b = base carbon in coal char at an intermediate level of gasification, g/g feed coal char

When making a kinetic analysis of the thermobalance data, it was necessary to relate the measured values of weight-loss fraction, $\Delta W/W_o$, to the base carbon conversion fraction, X. When devolatilization is complete, essentially all of the organic oxygen has been gasified. Thereafter, additional weight loss, which primarily results from gasification of the base carbon, is accompanied by the evolution of a constant fraction of noncarbon components in the coal such as nitrogen, hydrogen, and sulfur. Estimates of an average value of the fraction of noncarbon components gasified along with the base carbon for each type of coal char tested, have been based on analyses of char residues obtained in thermobalance and pilot-scale fluid-bed tests. With this simplifying assumption, the following relationships result:

$$C_b^o = (1 - V - A)(1 - \gamma) \tag{3}$$

and

$$C_b = C_b^o - \left[(\Delta W/W_o) - V\right] (1 - \gamma) \tag{4}$$

where

V = volatile matter in feed coal char (including moisture), g/g feed coal char

A = nongasifiable matter in feed coal char (including ash and some sulfur), g/g feed coal char

γ = noncarbon matter evolved along with base carbon, g/g base carbon evolved

Thus, from Equations 2, 3, and 4 —

$$X = \frac{(\Delta W/W_o) - V}{1 - V - A} \tag{5}$$

The results shown in Figure 2 can be interpreted by the three reaction stages defined above. Curve A corresponds to a test in which air-pretreated Ireland mine coal char was exposed to a nitrogen atmosphere at a pressure of 500 psig. During the first minute when the sample is heating up in the

thermobalance, the weight loss corresponds to the evolution of volatile matter. After this period, no further significant weight loss occurs. The total weight loss of approximately 26 % corresponds closely to the volatile matter in the feed coal char obtained by standard proximate analysis. Within the context of the three reaction stages defined, weight loss in this test occurs entirely in the devolatilization stage, where all of the volatile carbon has been gasified; all of the base carbon remains in the devolatilized coal char. When the char resulting from this test is then exposed to hydrogen at 500 psig (curve B), the reaction of the hydrogen with base carbon to form methane results in further weight loss. This reaction, which takes place at a much lower rate than devolatilization, occurs in the low-rate gasification stage. With this particular sample, there was no reaction in the rapid-rate methane formation stage because the reactivity of the coal char in this stage was destroyed during prolonged exposure to nitrogen.

Weight loss as a result of the reaction in the rapid-rate methane formation stage is illustrated by curve C, where a sample of the original coal char was exposed only to hydrogen at 500 psig with no initial exposure to nitrogen. There is a weight loss during the first minute of this test which is considerably greater than the corresponding weight loss obtained during this period when the coal char was exposed to nitrogen (curve A). The difference in the amount of weight loss between curves C and A during the first minute, or so, is caused by gasification of base carbon in the rapid-rate methane formation stage. Weight losses of the magnitude exhibited by curve B during this initial period are negligible. This is consistent with the assumption that base carbon gasification in the rapid-rate methane formation stage and in the low-rate gasification stage occur consecutively.

Curve D is qualitatively similar to curve C, except that there is a greater weight loss from rapid-rate methane formation resulting from the higher hydrogen pressure.

Correlations for Rapid-Rate Methane Formation Stage

The amount of base carbon gasified during the rapid-rate methane formation stage can be estimated by the base carbon conversion level, X_R, obtained from weight loss-versus-time characteristics 2 minutes after a sample is lowered into the reactor. As indicated previously, this corresponds to the time required for coal heat-up. During this period negligible conversion occurs in the low-rate gasification stage, although devolatilization and rapid-rate methane formation reactions should be complete at temperatures above approximately 1500 °F. Values of X_R have been correlated with hydrogen partial pressure, P_{H_2}, according to the following expression for data obtained in tests conducted at a variety of conditions:

$$M(X_R) = \int_0^{X_R} \frac{\exp(+\alpha X^2)\, dX}{(1-X)^{2/3}} = 0.0092\, f_R P_{H_2} \qquad (6)$$

where

P_{H_2} = hydrogen partial pressure, atm

f_R = relative reactivity factor for rapid-rate methane formation dependent on the particular carbonaceous solid. (Defined as unity for air-pretreated Ireland mine coal char.)

α = kinetic parameter dependent on gas composition and pressure

The value of α in the above expression is approximately 0.97 for tests conducted in pure hydrogen or in hydrogen-methane mixtures, and is approximately equal to 1.7 for a wide variety of gas compositions containing steam and hydrogen. This parameter will be discussed in greater detail in a later section on the low-rate gasification stage. It is of interest here, however, that for the case where $\alpha = 0.97$, then $M(X_R) \cong -\ln(1 - X_R)$.

In Figure 3, a plot of the function, $M(X_R)$, versus hydrogen partial pressure, P_{H_2}, for a number of tests conducted on the thermobalance with air-pretreated Ireland mine coal char, shows the good agreement between these data and the correlation form given in Equation 6. Equation 6 also appears to be reasonably applicable to the gasification of some coals, as well as to coal chars.

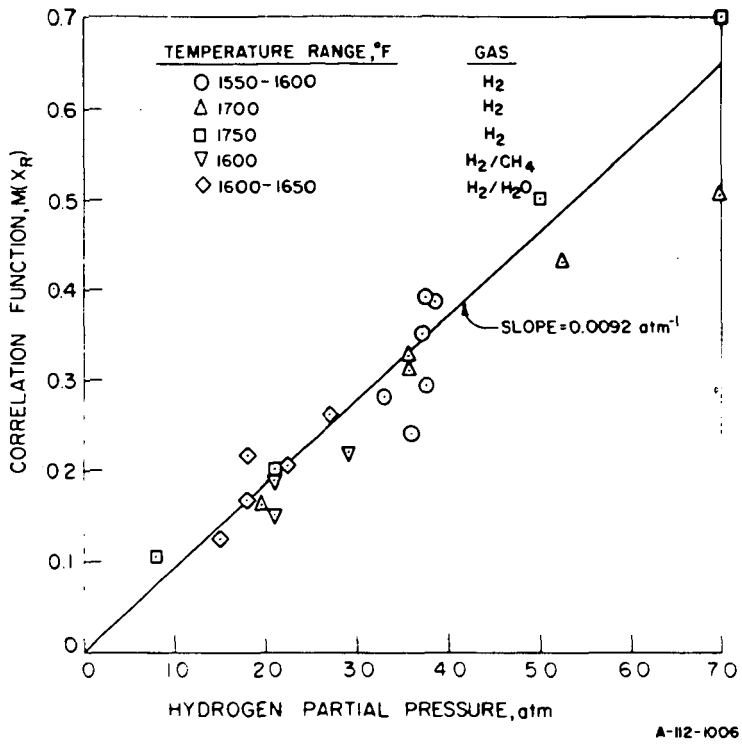

Figure 3. CORRELATION OF BASE CARBON CONVERSION FOR GASIFICATION OF AIR-PRETREATED IRELAND MINE COAL CHAR IN THE RAPID-RATE METHANE FORMATION STAGE

Data obtained by Birch, et al.,[1] for the hydrogenation of Brown coal in a fluid bed and by Hiteshue, et al.,[10] for the hydrogenation of a hvAb Pittsburgh coal in a fixed bed are given in Figures 4 and 5. Details of the procedures used in treating the data from these two investigations have been previously described.[14] It is of practical interest that relatively small variations in values of f_R are exhibited by the different materials considered. Similar small degrees of variation have also been noted for several other bituminous coal chars tested at IGT using the thermobalance.

The gasification of base carbon in the rapid-rate methane formation stage is apparently only dependent on hydrogen partial pressure and is not dependent on the partial pressures of other gaseous species normally present in gasifying atmospheres. This is partly indicated in Figure 3 for tests

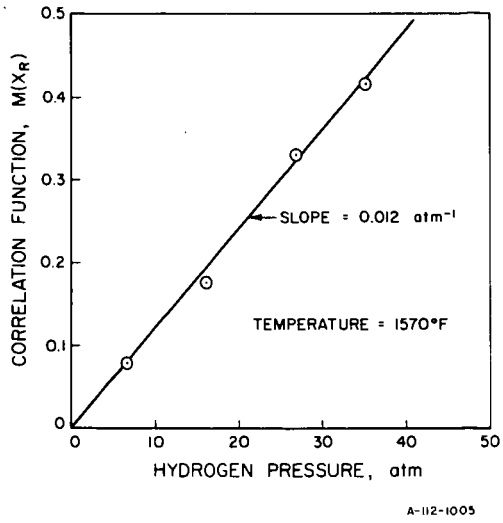

Figure 4. CORRELATION OF BASE CARBON CONVERSION FOR GASIFICATION OF BROWN COAL IN A FLUID BED IN THE RAPID-RATE METHANE FORMATION STAGE[1]

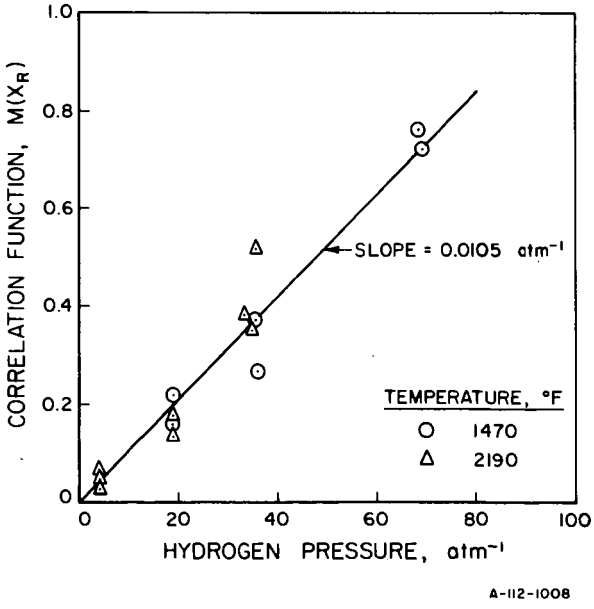

Figure 5. CORRELATION OF BASE CARBON CONVERSION FOR GASIFICATION OF hvAb PITTSBURGH COAL IN A FIXED BED IN THE RAPID-RATE METHANE FORMATION STAGE[10]

conducted with hydrogen-methane and hydrogen-steam mixtures, and has also been observed with synthesis-gas mixtures. In a system containing no hydrogen, no evolution of base carbon occurs except through gasification in the low-rate gasification stage. In Figure 6, this effect is illustrated for tests conducted with pure steam. After the first few minutes, there is no difference in the weight-loss traces for a sample of air-pretreated coal char initially lowered into a steam atmosphere, and one which was devolatilized in nitrogen prior to being exposed to the steam atmosphere. This behavior can be compared to results shown in Figure 2 for similar tests conducted in hydrogen.

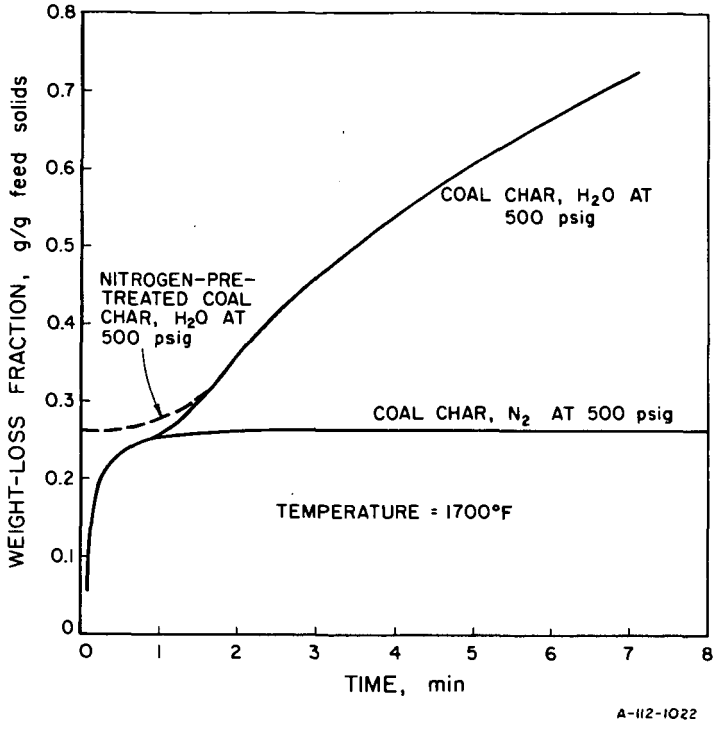

Figure 6. WEIGHT-LOSS CURVES OBTAINED IN HIGH-PRESSURE THERMOBALANCE FOR GASIFICATION OF AIR-PRETREATED IRELAND MINE COAL CHAR IN STEAM AND IN NITROGEN

Although the effects of pretreatment temperature on reactivity in the rapid-rate methane formation stage have not been systematically studied in this investigation, some indication is apparent from the results given in Figure 7. It shows total weight losses for materials subjected to different pretreatments in nitrogen obtained after gasification of air-pretreated coal char in hydrogen for 1 hour. Below 1000 °F, no effect of the nitrogen pretreatment is apparent on subsequent weight loss in hydrogen. Above this temperature, however, the total weight loss for materials initially exposed to nitrogen tends to decrease with increasing temperature, and above approximately 1500 °F, no rapid-rate methane formation occurs with these materials.

The correlation described by Equation 6 was developed based on data obtained from thermobalance tests conducted above 1500 °F, where coal char samples were submitted to rather specific heat-up rates characteristic of the experimental apparatus (approximately 30 °F/s). The fact that this correlation appears to apply for data obtained in other experimental systems where heat-up rates as high as 200 °F/s were employed, suggests that, within a limited range of heat-up rates, base carbon conversion in the rapid-rate methane formation stage is independent of heat-up rate for final temperatures greater than 1500 °F. This conclusion only applies for the case where reaction in the rapid-rate methane formation stage goes to completion. At sufficiently low temperatures, the amount of base carbon conversion which can be attributed to rapid-rate methane formation, is less than that which would be predicted by Equation 6, even for exposure to hydrogen for periods as long as 1 hour. This is apparent from the results shown for curve A in Figure 7.

Data obtained in a series of experiments conducted at lower temperatures, such as those illustrated in Figure 7, have been correlated using a more detailed model to describe the rapid-rate methane formation process prior to the completion of this reaction. This model is described in a previous publication.[14] It is of interest here, however, to point out certain characteristics of this model which rationalize the independence of total base

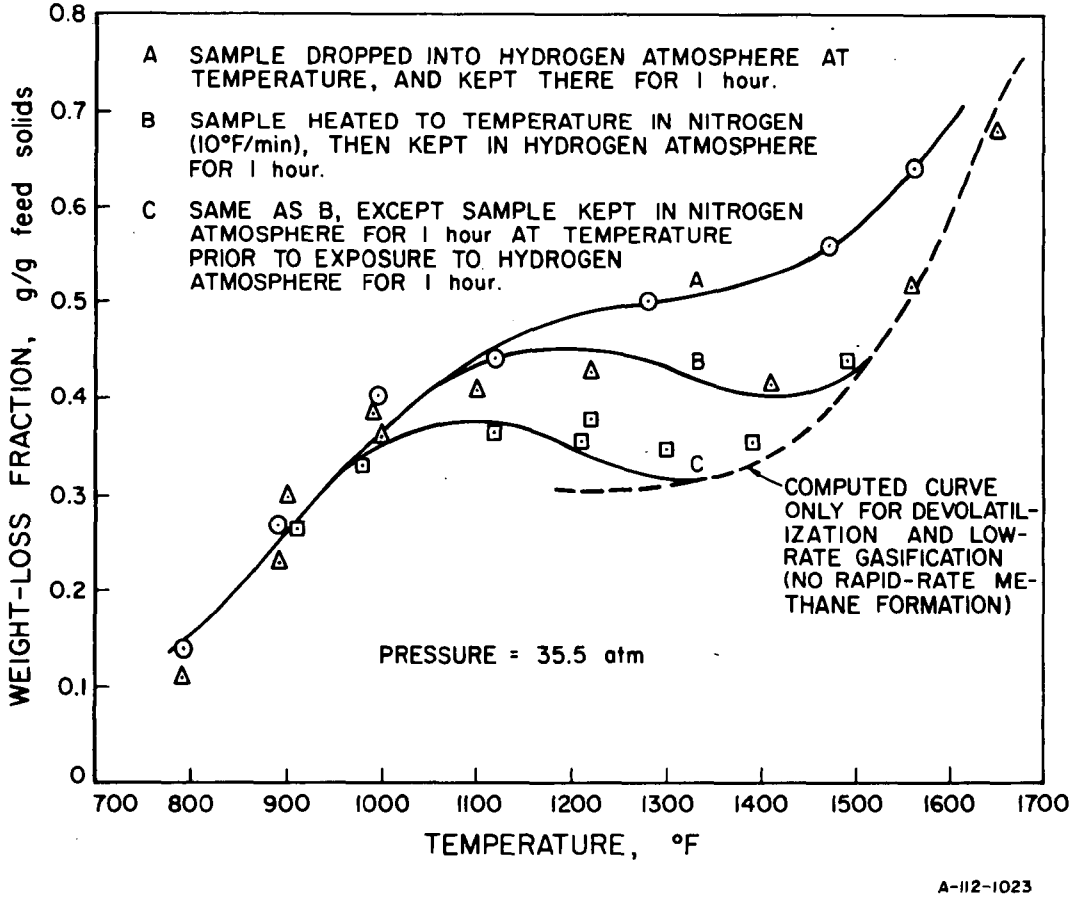

Figure 7. EFFECT OF PRIOR EXPOSURE TO NITROGEN ON GASIFICATION OF AIR-PRETREATED IRELAND MINE COAL CHAR IN THE RAPID-RATE METHANE FORMATION STAGE

carbon conversion in the rapid-rate methane formation stage from heating rate and final temperature for tests conducted above 1500 °F. The following critical steps assumed in the model relate to this range of conditions:

$$A_o \rightarrow A_* \tag{7}$$

$$A_* \rightarrow B \tag{8}$$

$$\text{base carbon} + \text{hydrogen} \xrightarrow{A_*} \text{methane} \tag{9}$$

This model, which is qualitatively similar to one proposed by Mosely and Patterson,[13] assumes that the coal char initially forms an active intermediate, A_*, (Equation 7) which catalyzes the reaction between base carbon and gaseous hydrogen to form methane (Equation 9). This reaction, however, competes with a reaction in which A_* deactivates to form the inactive species, B (Equation 8).

The following expression is assumed to describe the rate of reaction in Equation 9:

$$dX/dt = f_R k_3(T) P_{H_2} (1 - X)^{2/3} \exp(-\alpha X^2) N_{A_*} \tag{10}$$

where

$k_3(T)$ = rate constant dependent on temperature, T

N_{A_*} = concentration of species, A, mol /mol of base carbon

t = time

The rates of reactions in Equations 7 and 8 are assumed to be first order, leading to the expression —

$$d(N_{A_*} + N_{A_o})/dt = - k_2(T) \cdot N_{A_*} \tag{11}$$

where,

$k_2(T)$ = rate constant, dependent on temperature

N_{A_o} = concentration of species, A_o, mol /mol base carbon

Combining Equations 10 and 11 leads to the expression –

$$\frac{dX}{d(N_{A_*} + N_{A_o})} = -f_R \frac{k_3(T)}{k_2(T)} P_{H_2}(1-X)^{2/3} \exp(-\alpha X^2) \qquad (12)$$

If, then, it is assumed that the ratio $k_3(T)/k_2(T)$ is independent of temperature and is equal to β, then Equation 12 can be integrated to yield the following expression for the condition at which all of the species A_o has been converted to B.

$$M(X_R) = \int_0^{X_R} \frac{\exp(\alpha X^2)\, dX}{(1-X)^{2/3}} = f_R \beta \cdot N^o_{A_o} P_{H_2} \qquad (13)$$

Comparing this expression with Equation 6 indicates that $\beta N^o_{A_o} = 0.0092$ atm^{-1}. Since no definition of the temperature history was required in the development of Equation 13, the suggested model indicates that the amount of base carbon conversion to methane during the rapid-rate methane formation step is independent of heat-up rate or temperature level when the intermediate, A, has been completely deactivated.

Correlations for Low-Rate Gasification Stage

For practical purposes, coal chars undergo low-rate gasification only after the devolatilization and rapid-rate methane formation reactions are completed. Results obtained with the thermobalance indicate that, at temperatures greater than 1500 °F, char reactivity over a major range of carbon conversion in the low-rate stage is substantially the same whether devolatilization occurs in nitrogen, or in a gasifying atmosphere at the same conditions. Therefore, this study treats low-rate char gasification as a process essentially independent of devolatilization conditions, with one important exception: The temperature of devolatilization, since it has been shown in this study as well as by Blackwood[2] that the reactivity of a char at a given temperature, T, decreases with increasing pretreatment temperature, T_o, when $T_o > T$. This effect is quantitatively represented in the correlations presented below. However, the model adopted does not account for pretreatment effects on gasification during initial stages of char gasification, which

occur particularly at gasification temperatures less than 1600 °F. At these lower temperatures, specific pretreatment conditions such as gas atmosphere and time of pretreatment produce somewhat complex effects during subsequent gasification for base carbon conversions of less than 10 %.[8] These limitations have no practical significance in using the simplified model developed to describe coal char gasification kinetics at higher temperatures, or for base carbon conversion levels sufficiently greater than 10 %.

The gasification data of Zielke and Gorin[18,19] and Goring, et al.,[9] obtained for fluid-bed gasification of Disco char, as well as the bulk of data obtained in IGT's studies with the high-pressure thermobalance and pilot-scale fluid beds, were used to evaluate parameters in a quantitative model developed to describe coal char gasification kinetics over a wide range of conditions in the low-rate gasification stage. Three basic reactions were assumed to occur in gases containing steam and hydrogen:

Reaction I: $H_2O + C \rightleftarrows CO + H_2$

Reaction II: $2H_2 + C \rightleftarrows CH_4$

Reaction III: $H_2 + H_2O + 2C \rightleftarrows CO + CH_4$

Reaction I is the conventional steam-carbon reaction, which is the only one that occurs in pure steam at elevated pressures* or with gases containing steam at low pressure. Although, at elevated temperatures this reaction is affected by thermodynamic reversibility only for relatively high steam conversions, the reaction is severely inhibited by the poisoning effects of hydrogen and carbon monoxide at steam conversions far removed from equilibrium for this reaction. Some investigators have also noted inhibition by methane.

Reaction II, the only reaction that could occur in pure hydrogen or in hydrogen-methane mixtures, greatly depends on the hydrogen partial pressure. Many investigators have found that, at elevated pressures, the rate of this reaction is directly proportional to the hydrogen partial pressure.

---

* Although some methane has been detected in gaseous reaction products when gasification is conducted with pure steam, it is uncertain whether this methane results from the direct reaction of steam with carbon or from the secondary reaction of hydrogen, produced from the steam-carbon reaction, with the carbon in the char.

The stoichiometry of Reaction III limits its occurrence to systems in which both steam and hydrogen are present. Although this reaction is the stoichiometric sum of Reactions I and II, this model considers it to be a third independent gasification reaction. This reaction, arbitrarily assumed to occur in the development of this model to facilitate correlation of experimental data, has been suggested by Blackwood and McGrory[4] as being necessary in such a system. Curran and Gorin[5] also assumed this reaction to correlate kinetic data for gasification of lignite at 1500 °F in steam-hydrogen-containing gases.

The correlations developed in this study to describe kinetics in the low-rate gasification stage are summarized as follows:

$$dX/dt = f_L \, k_T (1 - X)^{2/3} \exp(-\alpha X^2) \tag{14}$$

where,

$$k_T = k_I + k_{II} + k_{III} \tag{15}$$

Here, k_I, k_{II}, and k_{III} are rate constants for the individual reactions considered. It is assumed that each of the three reactions occur independently, but that the rate of each is proportional to the same surface area and surface reactivity terms. The term $(1 - X)^{2/3}$ is proportional to the effective surface area undergoing gasification, and the term $\exp(-\alpha X^2)$ represents the relative reactivity of the effective surface area, which decreases with increasing conversion level for positive values of α.

Individual parameters in Equations 14 and 15 are defined as functions of temperature and pressure according to the following expressions:

$$f_L = f_o \exp(8467/T_o) \tag{16}$$

$$k_I = \frac{\exp(9.0201 - 31{,}705/T)\left(1 - \dfrac{P_{CO} P_{H_2}}{P_{H_2O} K_I^E}\right)}{\left[1 + \exp(-22.2160 + 44{,}787/T)\left(\dfrac{1}{P_{H_2O}} + 16.35 \dfrac{P_{H_2}}{P_{H_2O}} + 43.5 \dfrac{P_{CO}}{P_{H_2O}}\right)\right]^2} \tag{17}$$

$$k_{II} = \frac{P_{H_2}^2 \exp(2.6741 - 33{,}076/T)\left(1 - \frac{P_{CH_4}}{P_{H_2}^2 K_{II}^E}\right)}{\left[1 + P_{H_2} \exp(-10.4520 + 19{,}976/T)\right]} \tag{18}$$

$$k_{III} = \frac{P_{H_2}^{1/2} P_{H_2O} \exp(12.4463 - 44{,}544/T)\left(1 - \frac{P_{CH_4} P_{CO}}{P_{H_2} P_{H_2O} K_{III}^E}\right)}{\left[1 + \exp(-6.6696 + 15{,}198/T)\left(P_{H_2}^{1/2} + 0.85 P_{CO} + 18.62 \frac{P_{CH_4}}{P_{H_2}}\right)\right]^2} \tag{19}$$

$$\alpha = \frac{52.7 P_{H_2}}{1 + 54.3 P_{H_2}} + \frac{0.521 P_{H_2}^{1/2} P_{H_2O}}{10.707 P_{H_2O} + 0.50 P_{H_2}^{1/2} P_{H_2O}} \tag{20}$$

where,

K_I^E, K_{II}^E, K_{III}^E = equilibrium constants for reactions I, II, and III, considering carbon as graphite

T = reaction temperature, °R

T_o = maximum temperature to which char has been exposed prior to gasification, °R (if $T_o < T$, then a value of $T_o = T$ is used in Equation 16)

P_{H_2}, P_{H_2O}, P_{CO}, P_{CH_4} = partial pressures of H_2, H_2O, CO, and CH_4, atm

f_o = relative reactivity factor for low-rate gasification dependent on the particular carbonaceous solid

Values of f_o obtained in this study were based on the definition $f_o = 1.0$ for a specific batch of air-pretreated Ireland mine coal char. Samples of this coal char obtained from different air-pretreatment tests exhibited some variations in reactivity as determined by thermobalance tests conducted at standard conditions. The values of f_o so determined, ranged from approximately 0.88 to 1.05. Results of tests made with the thermobalance using a variety of coals and coal chars have indicated that the relative reactivity factor, f_o, generally tends to increase with decreasing rank, although

individual exceptions to this trend exist. Values have been obtained which range from 0.3 for a low-volatile bituminous coal char to about 10 for a North Dakota lignite. The reactivity of the Disco char used in gasification studies conducted by the Consolidation Coal Company[9, 18, 19] is $f_o = 0.488$.

An integrated form of Equation 14 was used to evaluate certain parameters in the above correlations, based on data obtained with the thermobalance.

$$M(X) = \int_0^X \frac{\exp(+\alpha X^2)\,dX}{(1-X)^{2/3}} = \int_0^{X_R} \frac{\exp(+\alpha X^2)\,dX}{(1-X)^{2/3}} + \int_{X_R}^X \frac{\exp(-\alpha X^2)\,dX}{(1-X)^{2/3}}$$

$$= \int_0^{X_R} \frac{\exp(+\alpha X^2)\,dX}{(1-X)^{2/3}} + f_L k_T t \qquad (21)$$

The term $\int_0^{X_R} \frac{\exp(+\alpha X^2)\,dX}{(1-X)^{2/3}}$ was evaluated from Equation 6 for tests in which no nitrogen pretreatment was used. For tests in which the feed coal char was initially devolatilized in nitrogen at the same temperature and pressure to be subsequently used for gasification in a gasifying atmosphere, reactivity for rapid-rate methane formation was destroyed above 1500 °F and $X_R = 0$. For this condition –

$$M(X) = \int_0^X \frac{\exp(+\alpha X^2)\,dX}{(1-X)^{2/3}} = f_L k_T t \qquad (22)$$

Typical plots of M(X) versus t are given in Figures 8, 9, and 10 for data obtained with air-pretreated Ireland mine coal char. The slopes of the lines drawn correspond to values of $f_L k_T$ characteristic of each test. Results of tests conducted with pure steam (Figure 8) were correlated using $\alpha = 0$ consistent with Equation 20 which corresponds to the situation in which specific gasification rates, $\frac{dX/dt}{(1-X)}$, increase with an increasing carbon conversion level. For gasification in hydrogen or steam-hydrogen mixtures (Figures 9 and 10), however, specific gasification rates generally decrease with increasing conversion level.

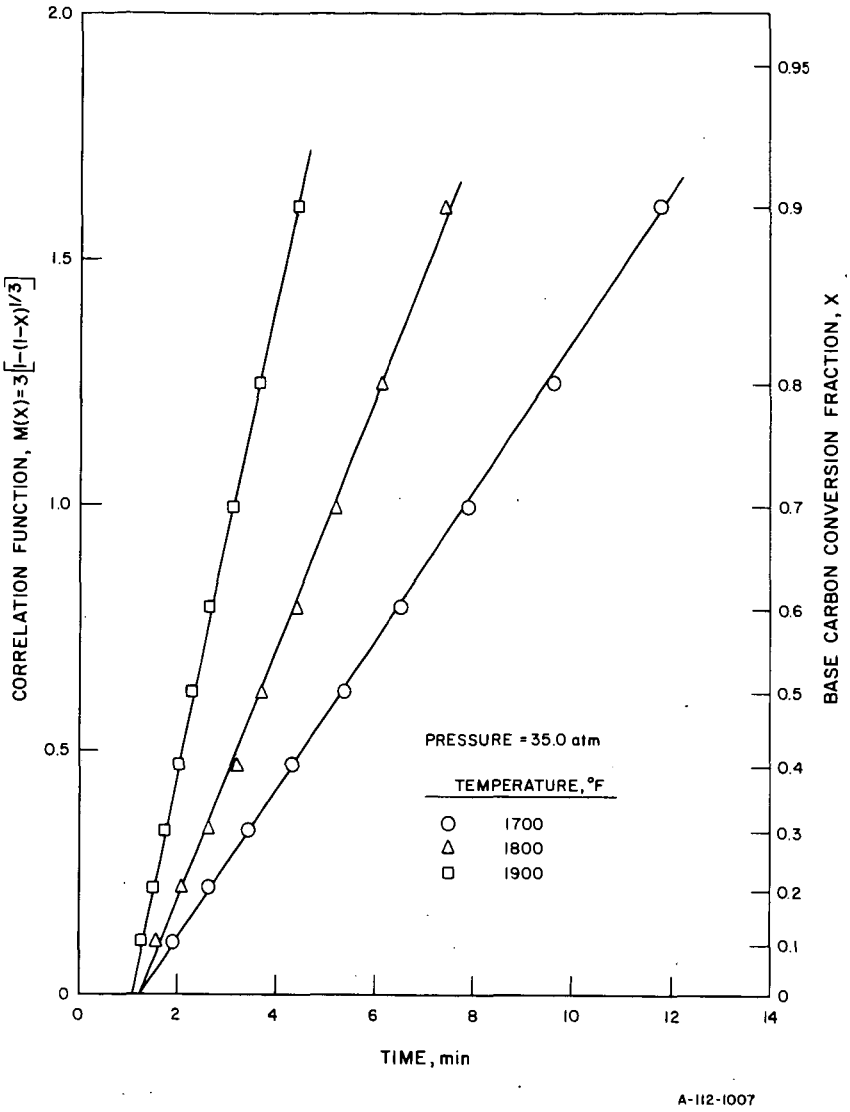

Figure 8. EFFECT OF TEMPERATURE ON LOW-RATE GASIFICATION OF AIR-PRETREATED IRELAND MINE COAL CHAR IN STEAM

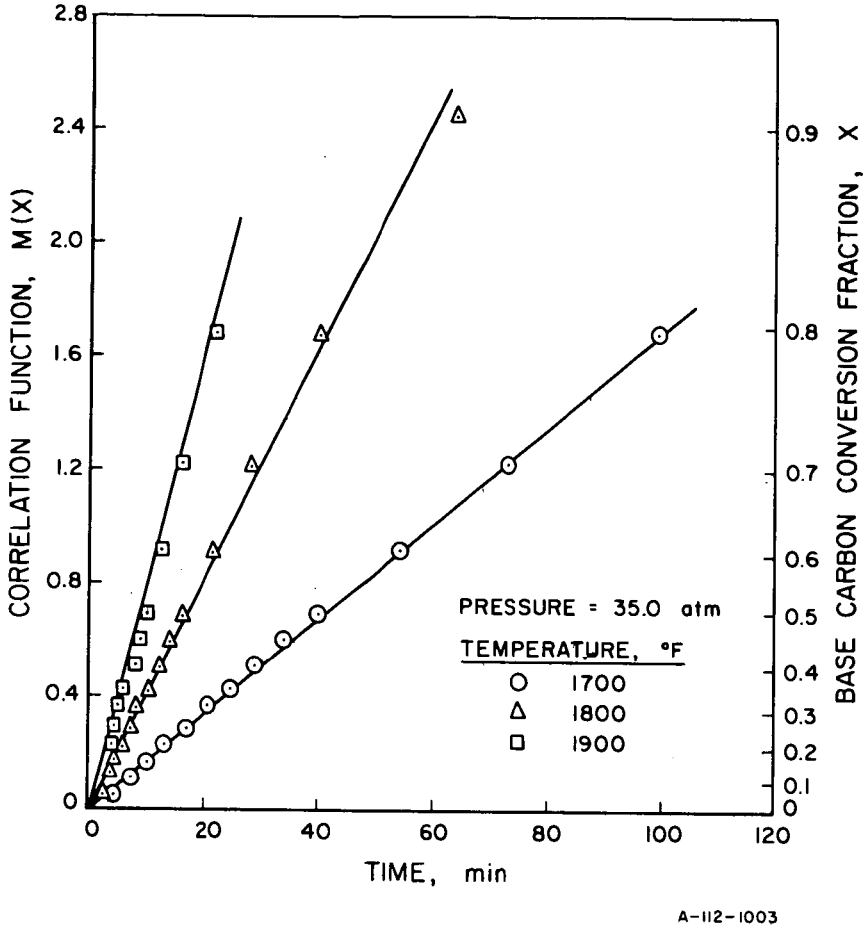

Figure 9. EFFECT OF TEMPERATURE ON LOW-RATE GASIFICATION OF AIR-PRETREATED IRELAND MINE COAL CHAR IN HYDROGEN

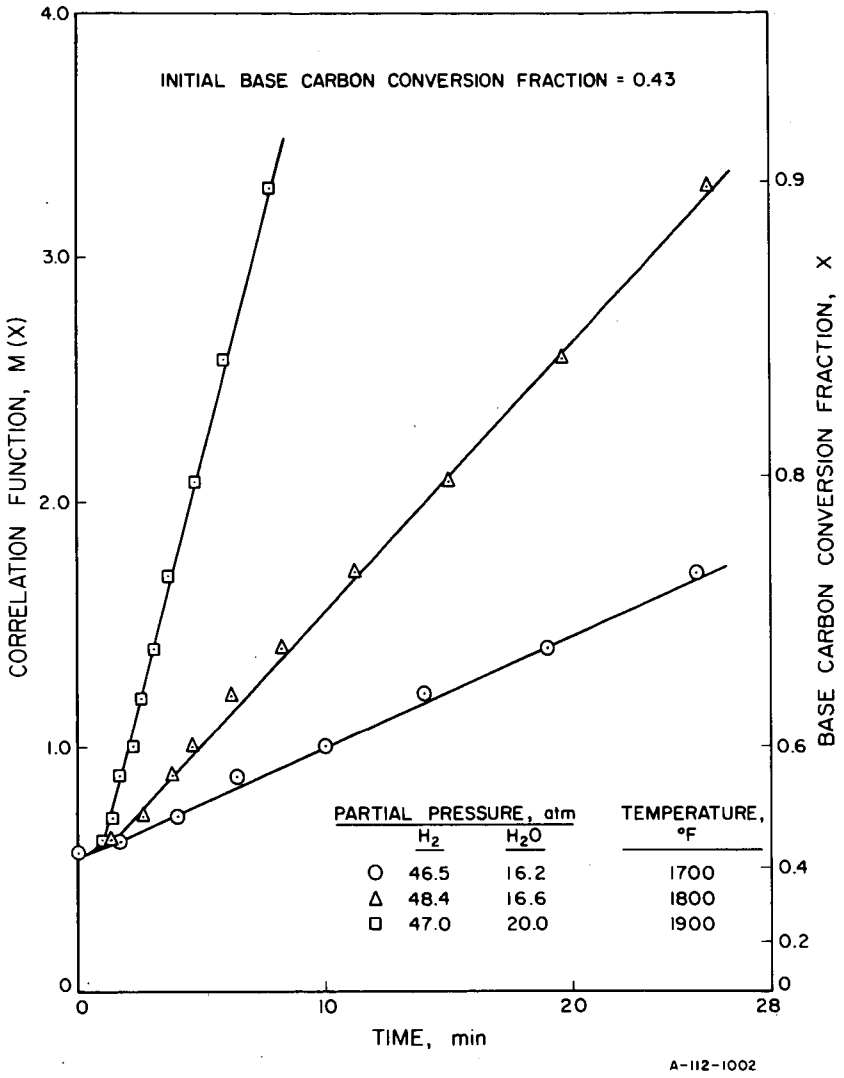

Figure 10. EFFECT OF TEMPERATURE ON LOW-RATE GASIFICATION OF AIR-PRETREATED IRELAND MINE COAL CHAR IN STEAM-HYDROGEN MIXTURES

Carbon gasification rates were directly measured in the fluid-bed tests conducted with Disco char,[9,18,19] and values of $f_L k_T$ and α can be obtained graphically by plotting values of $\ln \frac{dX/dt}{(1-X)^{2/3}}$ versus X^2. Such a plot is illustrated in Figure 11, where the value of $\ln \frac{dX/dt}{(1-X)^{2/3}}$ at X = 0 is equal to $f_L k_T$ and the slope of a given line is equal to α. Generally, the correlations presented are consistent with values of $f_L k_T$ and α obtained for the gasification of Disco char at temperatures of 1600° and 1700°F and pressures of 1, 6, and 30 atmospheres for gasification with pure hydrogen and with various steam-hydrogen mixtures. The correlations are also consistent with individual rates of methane and carbon oxide formation reported in the investigations conducted with Disco char for initial levels of carbon conversion. Although the relative rates of methane to carbon oxide formation were reported to increase somewhat with increasing conversion level, a trend not accounted for in the model developed in this study, investigators at the Consolidation Coal Company have suggested that this effect was caused by a catalytic reaction downstream of the fluid-bed reactor employed, in which some of the carbon monoxide produced in the reactor was converted to methane.[5]

The consistency between the calculated and experimental values of $f_L k_T$ for tests conducted at a variety of conditions with the thermobalance using air-pretreated Ireland mine coal char is demonstrated in Tables 2, 3, and 4 and in Figures 12, 13, and 14. The correlations developed have also been used to predict behavior in pilot-scale moving- and fluid-bed tests conducted at IGT and elsewhere. The assumptions made in characterizing the nature of gas-solids contacting in these integral systems have been previously described.[14] The most important assumptions made for fluid-bed systems are a) the gas in the fluid bed is perfectly mixed and b) when continuous solids flow is employed, the solids are in plug flow. For moving-bed systems, we assumed that both gas and solids were in plug flow. With these simplifying assumptions, the conditions of primary importance in

Table 2. COMPARISON OF EXPERIMENTAL AND CALCULATED RATE CONSTANTS FOR GASIFICATION OF AIR-PRETREATED IRELAND MINE COAL CHAR IN HYDROGEN

Temp, °F	Hydrogen Press., atm	Base Carbon Conversion Range, fraction	Rate Constant, $f_L k_T$, min^{-1} Experimental	Rate Constant, $f_L k_T$, min^{-1} Calculated
1600	36.5	0-0.314	0.0068	0.0069
1650	36.3	0-0.541	0.0117	0.0112
1650	36.7	0-0.592	0.0111	0.0113
1650	36.7	0-0.654	0.0097	0.0113
1700	19.3	0-0.197	0.0106	0.0090
1700	36.2	0-0.329	0.0167	0.0181
1700	53.2	0-0.449	0.0276	0.0273
1700	69.9	0-0.508	0.0292	0.0365
1700*	35.1	0-0.802	0.0175	0.0175
1750	35.4	0-0.348	0.0261	0.0277
1750	35.4	0-0.509	0.0274	0.0277
1750	36.1	0-0.640	0.0237	0.0283
1750	35.2	0-0.367	0.0272	0.0276
1770*	1.0	0	0	0.0002
1770*	18.1	0-0.069	0.0175	0.0152
1770*	36.6	0-0.134	0.0350	0.0341
1770*	36.1	0-0.570	0.0290	0.0335
1770*	52.9	0-0.180	0.0500	0.0510
1770*	69.9	0-0.250	0.0700	0.0686
1800	21.6	0-0.263	0.0222	0.0239
1800	49.9	0-0.263	0.0641	0.0617
1800*	36.0	0-0.910	0.0416	0.0414
1900*	35.3	0-0.850	0.0910	0.0920

* In these tests, the air-pretreated coal char was either initially devolatilized in nitrogen for 1 hour at the temperature subsequently used for gasification in a gasifying medium, or it was devolatilized and partially gasified in an integral fluid-bed test using a steam-hydrogen feed gas.

Table 3. COMPARISON OF EXPERIMENTAL AND CALCULATED RATE CONSTANTS FOR GASIFICATION OF AIR-PRETREATED IRELAND MINE COAL CHAR IN STEAM AND STEAM-HYDROGEN MIXTURES

Temp, °F	Partial Pressure, atm		Base Carbon Conversion Range, fraction	Rate Constant, $f_L k_T$	
	H_2	H_2O		Experimental	Calculated
				min^{-1}	
1700	--	35.0	0-0.941	0.1547	0.1736
1700	27.3	29.8	0-0.977	0.0598	0.0528
1700	12.8	23.6	0-0.327	0.0706	0.0566
1700	17.8	18.4	0-0.272	0.0365	0.0385
1700	19.2	17.5	0-0.651	0.0356	0.0361
1700	18.2	17.9	0-0.816	0.0344	0.0373
1700	23.3	12.4	0-0.300	0.0339	0.0274
1700	23.2	12.5	0-0.429	0.0262	0.0275
1700	23.8	11.9	0-0.511	0.0190	0.0267
1700	25.0	11.3	0-0.725	0.0224	0.0261
1700*	13.7	48.5	0.43-0.908	0.0831	0.1110
1700*	46.5	16.2	0.43-0.781	0.0446	0.0385
1700*	28.3	32.5	0.43-0.832	0.0425	0.0564
1750	17.6	18.5	0-0.801	0.0526	0.0763
1750	18.3	18.2	0-0.495	0.0613	0.0741
1750	17.6	18.5	0-0.702	0.0667	0.0763
1750	18.0	18.5	0-0.940	0.0917	0.0758
1750	5.3	30.8	0-0.573	0.1803	0.2162
1750	23.2	13.2	0-0.320	0.0441	0.0532
1750	26.9	9.2	0-0.334	0.0406	0.0422
1750	17.6	18.3	0-0.350	0.0670	0.0815
1800	--	35.0	0-0.990	0.2559	0.2815
1800	48.4	16.6	0-0.956	0.1115	0.1130
1800	32.4	27.6	0-0.981	0.1643	0.1710
1900	--	35.0	0-0.992	0.4795	0.4366
1900*	17.2	42.7	0.43-0.996	0.6570	0.8750
1900*	47.0	20.0	0.43-0.999	0.4000	0.3900
1900*	33.2	33.2	0.43-0.997	0.680	0.607

* In these tests, the air-pretreated coal char was either initially devolatilized in nitrogen for 1 hour at the temperature subsequently used for gasification in a gasifying medium, or it was devolatilized and partially gasified in an integral fluid-bed test using a steam-hydrogen feed gas.

Table 4. COMPARISON OF EXPERIMENTAL AND CALCULATED RATE CONSTANTS FOR GASIFICATION OF AIR-PRETREATED IRELAND MINE COAL CHAR IN SYNTHESIS GAS

Temp, °F	Partial Pressure, atm					Base Carbon Conversion Range, fraction	Rate Constant, $f_L k_T$	
	CO	CO_2	H_2	H_2O	CH_4		Experimental	Calculated
							min^{-1}	
1550	0.17	0.32	5.92	28.11	1.68	0-0.277	0.0045	0.0034
1600	0.95	0.28	14.46	11.07	10.73	0-0.130	0.0002	0.0006
1600	0.65	0.35	12.74	13.82	9.68	0-0.143	0.0007	0.0009
1600	0.65	0.38	14.49	11.33	10.29	0-0.159	0.0006	0.0006
1600	0.17	0.17	7.73	14.66	9.65	0-0.228	0.0022	0.0044
1600	0.10	0.33	6.41	26.58	2.18	0-0.571	0.0146	0.0093
1600	8.60	6.38	11.07	7.50	2.38	0-0.106	0.0001	0.0001
1600	7.57	1.70	18.87	6.84	1.04	0-0.258	0.0022	0.0033
1600	2.28	0.46	19.03	6.57	8.48	0-0.176	0.0004	0.0002
1650	0.55	0.26	11.76	14.66	9.65	0-0.228	0.0026	0.0036
1650	0.10	0.29	6.27	26.47	2.51	0-0.703	0.0234	0.0233
1650	2.24	3.25	6.00	23.02	1.29	0-0.426	0.0089	0.0099
1700	1.85	1.23	8.47	24.71	0.04	0-0.745	0.0272	0.0400
1700	6.05	1.64	15.81	12.91	0.16	0-0.550	0.0122	0.0122
1700	5.27	4.17	10.43	15.87	0.05	0-0.576	0.0143	0.0128
1700	4.52	3.79	9.54	18.11	0.12	0-0.619	0.0166	0.0161
1700	6.90	4.45	10.88	13.58	0.14	0-0.543	0.0125	0.0096
1700	2.26	3.12	3.49	28.07	0.11	0-0.817	0.0516	0.0481
1700	4.33	4.69	4.18	22.54	0.07	0-0.736	0.02680	0.0216
1700*	0.60	2.80	4.30	60.10	0.40	0.43-0.871	0.104	0.128
1700*	5.0	9.4	19.8	25.8	2.1	0.43-0.663	0.0200	0.0169
1700*	1.8	3.1	6.3	19.2	0.4	0.43-0.659	0.0188	0.0274
1700*	5.9	10.8	13.2	28.0	0.9	0.43-0.661	0.0136	0.0172
1700*	4.3	5.1	6.7	16.8	0.5	0.43-0.556	0.0110	0.0117
1750	6.07	4.62	9.69	13.47	2.34	0-0.452	0.0092	0.0095
1750	3.31	4.80	8.12	19.08	1.23	0-0.842	0.0404	0.0315
1750	2.49	3.94	4.99	24.18	0.94	0-0.952	0.0771	0.0588
1750	5.87	6.61	7.03	16.00	0.16	0-0.697	0.0230	0.0217
1750	6.6	4.9	10.6	13.9	0.3	0-0.623	0.0170	0.0175

Table 4, Cont. COMPARISON OF EXPERIMENTAL AND CALCULATED RATE CONSTANTS FOR GASIFICATION OF AIR-PRETREATED IRELAND MINE COAL CHAR IN SYNTHESIS GAS

Temp, °F	Partial Pressure, atm					Base Carbon Conversion Range, fraction	Rate Constant, $f_L k_T$	
	CO	CO_2	H_2	H_2O	CH_4		Experimental	Calculated
							min^{-1}	
1800*	6.2	7.4	18.1	31.6	0.3	0.43-0.933	0.0880	0.0880
1800*	1.8	4.9	11.6	47.7	0.2	0.43-0.979	0.236	0.248
1800*	10.7	6.7	17.7	19.1	1.5	0.43-0.776	0.043	0.0300
1800*	4.5	2.6	7.4	13.3	0.3	0.43-0.784	0.0395	0.0448
1800*	6.9	3.4	10.7	8.4	0.4	0.43-0.678	0.0229	0.0193
1800*	6.0	9.7	13.4	30.5	0.4	0.43-0.878	0.0736	0.0849
1800*	2.9	11.1	14.1	36.5	0.4	0.43-0.899	0.105	0.146
1800*	5.9	4.9	7.6	14.1	0.2	0.43-0.771	0.0431	0.0389
1800*	1.1	3.3	4.3	24.7	0.2	0.43-0.959	0.182	0.199
1800*	12.9	4.9	7.5	9.4	0.3	0.43-0.647	0.0111	0.0101
1800*	0.5	2.0	4.0	27.4	0.1	0.43-0.892	0.246	0.268
1800*	--	1.2	2.6	30.1	0.1	0.43-0.914	0.273	0.271
1900*	4.0	7.4	18.0	35.7	0.2	0.43-0.998	0.391	0.395
1900*	3.2	5.3	11.8	42.9	0.1	0.43-0.991	0.579	0.513
1900*	12.3	7.8	23.7	16.0	1.3	0.43-0.845	0.0820	0.0964
1900*	3.9	2.9	8.8	11.9	0.1	0.43-0.956	0.141	0.169
1900*	7.1	3.3	11.4	7.9	0.2	0.43-0.840	0.0638	0.0713
1900*	1.5	3.1	6.6	20.7	0.2	0.43-0.981	0.364	0.415
1900*	8.9	10.5	15.2	28.2	0.5	0.43-0.999	0.227	0.200
1900*	19.2	11.6	16.6	15.5	0.7	0.43-0.824	0.0721	0.0609
1900*	3.8	7.8	11.0	41.0	0.3	0.43-1.009	0.438	0.442
1900*	6.1	5.3	8.3	13.5	0.1	0.43-0.984	0.191	0.142
1900*	1.4	3.7	4.7	23.7	0.1	0.43-1.033	0.500	0.471
1900*	10.6	5.2	8.4	10.5	0.1	0.43-0.872	0.085	0.064
1900*	0.3	1.3	2.7	29.7	--	0.43-1.028	0.655	0.817
1900*	1.0	3.3	7.0	56.7	0.1	0.43-1.001	1.000	0.892
2000*	3.2	5.3	13.4	46.1	0.2	0.43-0.991	1.36	1.27
2000*	7.5	6.0	18.6	35.8	0.5	0.43-1.047	0.771	0.873
2000*	0.8	0.3	33.9	32.5	0.5	0.43-0.987	1.462	1.297

* In these tests, the air-pretreated coal char was either initially devolatilized in nitrogen for 1 hour at the temperature subsequently used for gasification in a gasifying medium, or it was devolatilized and partially gasified in an integral fluid-bed test using a steam-hydrogen feed gas.

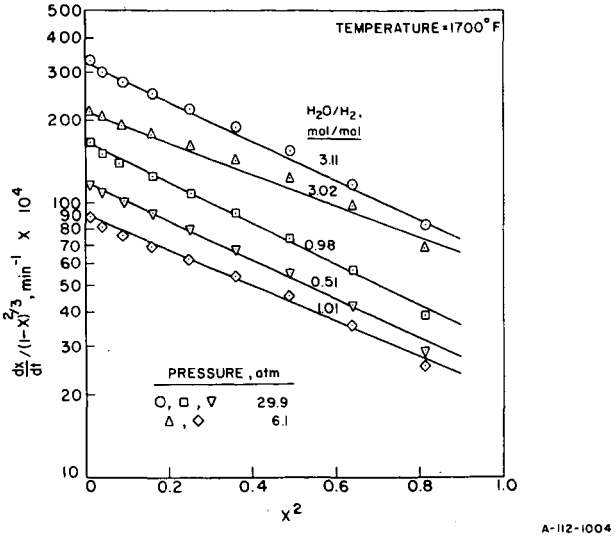

Figure 11. EFFECTS OF PRESSURE AND GAS COMPOSITION ON LOW-RATE GASIFICATION OF DISCO CHAR IN STEAM-HYDROGEN MIXTURES[9, 19]

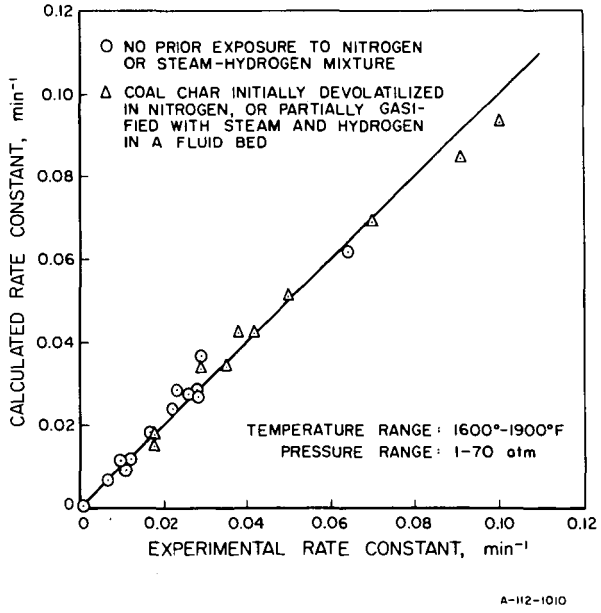

Figure 12. COMPARISON OF EXPERIMENTAL AND CALCULATED RATE CONSTANTS FOR LOW-RATE GASIFICATION OF AIR-PRETREATED IRELAND MINE COAL CHAR IN HYDROGEN

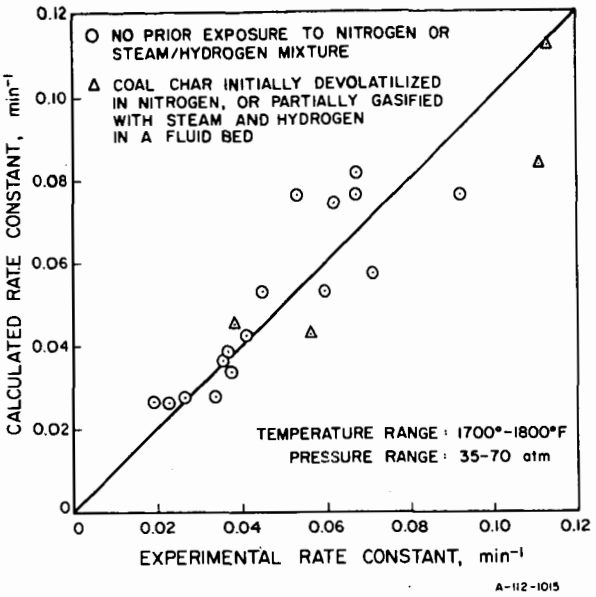

(a)

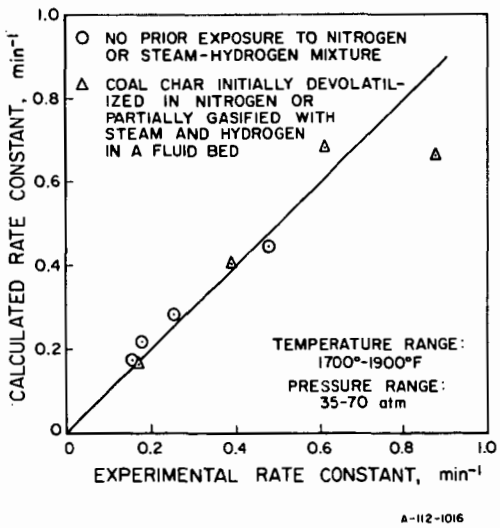

(b)

Figure 13. COMPARISON OF EXPERIMENTAL AND CALCULATED RATE CONSTANTS FOR LOW-RATE GASIFICATION OF AIR-PRETREATED IRELAND MINE COAL CHAR IN STEAM-HYDROGEN MIXTURES

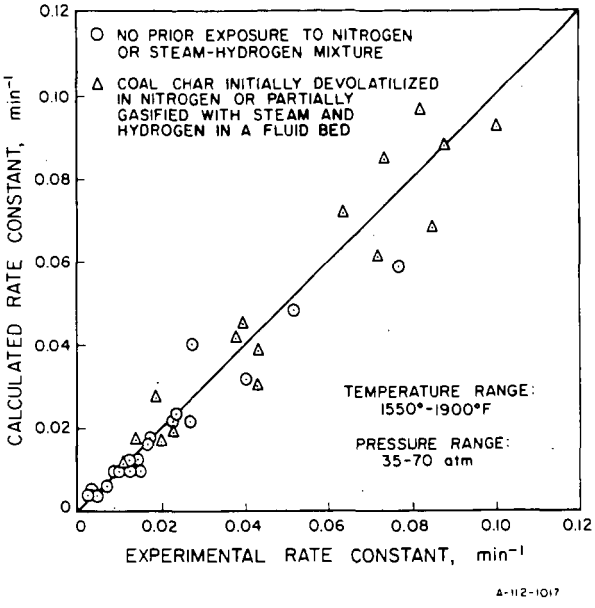

(a)

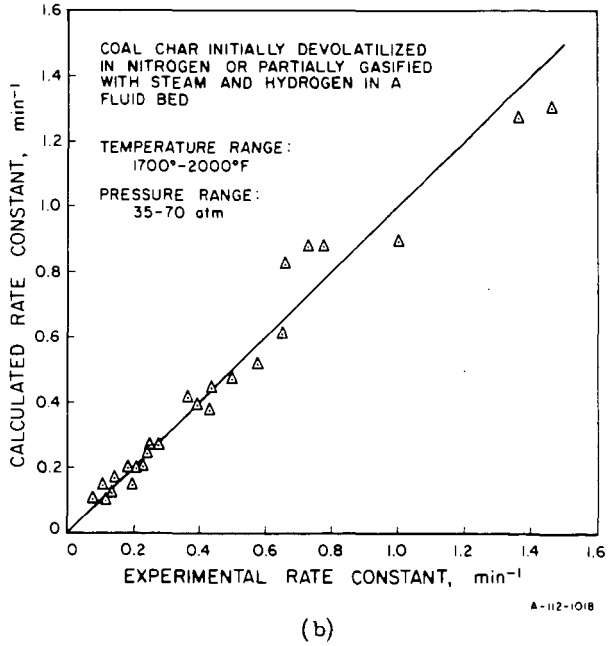

(b)

Figure 14. COMPARISON OF EXPERIMENTAL AND CALCULATED RATE CONSTANTS FOR LOW-RATE GASIFICATION OF AIR-PRETREATED IRELAND MINE COAL CHAR IN SYNTHESIS GASES

characterizing integral gasification behavior in individual tests include coal char feed rate and composition, particle residence times in the reactor, reactor temperature, pressure, feed gas composition, and flow rate. For cases where coal char containing volatile matter was used as a feed material, rapid-rate methane formation and devolatilization were assumed to occur in a free-fall space above the reaction beds employed in the systems. When devolatilized coal char was the feed material, no rapid-rate methane formation was considered to occur. Predicted and experimental integral rates of carbon oxides and methane formation are compared in Figures 15-19, which show good agreement for a wide range of experimental conditions.

Frequently, the $P_{CH_4}/P^2_{H_2}$ ratio in product gases from integral fluid-bed systems for the gasification of coal or coal char with steam-hydrogen containing gases is greater than the equilibrium constant for the graphite-hydrogen-methane system. This has often been interpreted as corresponding to a situation in which the coal or coal char has a thermodynamic activity greater than unity with respect to graphite. The models proposed in this paper offer two other explanations for this phenomenon: Rapid-rate methane formation occurs when coal or coal char containing volatile matter is used as a feed material. The methane yield resulting from this step is kinetically determined, independent of methane's partial pressure. Under certain conditions then, values of the ratio, $P_{CH_4}/P^2_{H_2}$, greater than that corresponding to the equilibrium for the graphite-hydrogen-methane system can result. Values of the $P_{CH_4}/P^2_{H_2}$ ratio greater than that corresponding to the equilibrium considered can also occur for low-rate gasification of coal char according to the model assumed in this study. This is illustrated in Figure 20, where the results shown were based on computations of gas yields in a hypothetical fluid-bed for char gasification with a pure steam feed gas, using the correlations described above. The reason for the behavior illustrated is that, at intermediate values of hydrogen partial pressure, the rate of Reaction III, which produces methane, is greater than the reverse rate of Reaction II in which methane is consumed when a potential for carbon deposition by this

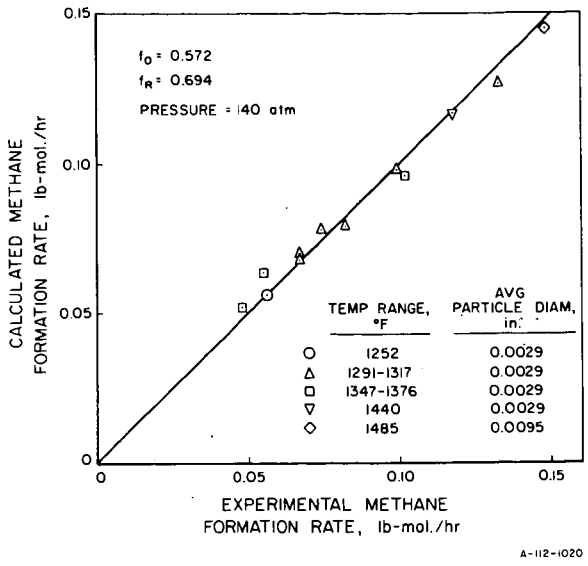

Figure 15. COMPARISON OF EXPERIMENTAL AND CALCULATED INTEGRAL RATES OF METHANE FORMATION FOR HYDROGENATION OF MONTOUR BITUMINOUS COAL CHAR (17% Volatile Matter) IN A MOVING-BED REACTOR (IGT Study)

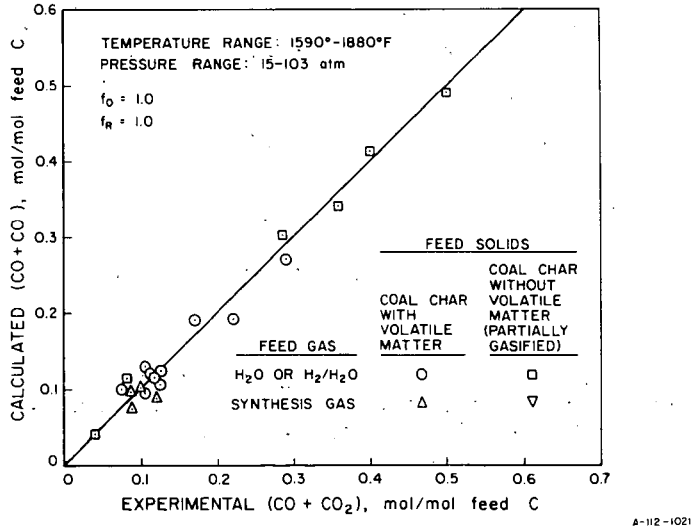

Figure 16. COMPARISON OF EXPERIMENTAL AND CALCULATED INTEGRAL RATES OF CARBON OXIDES FORMATION FOR GASIFICATION OF AIR-PRETREATED IRELAND MINE COAL CHAR IN 2-, 4-, AND 6-INCH-INSIDE-DIAMETER FLUID-BED REACTORS (IGT Studies)

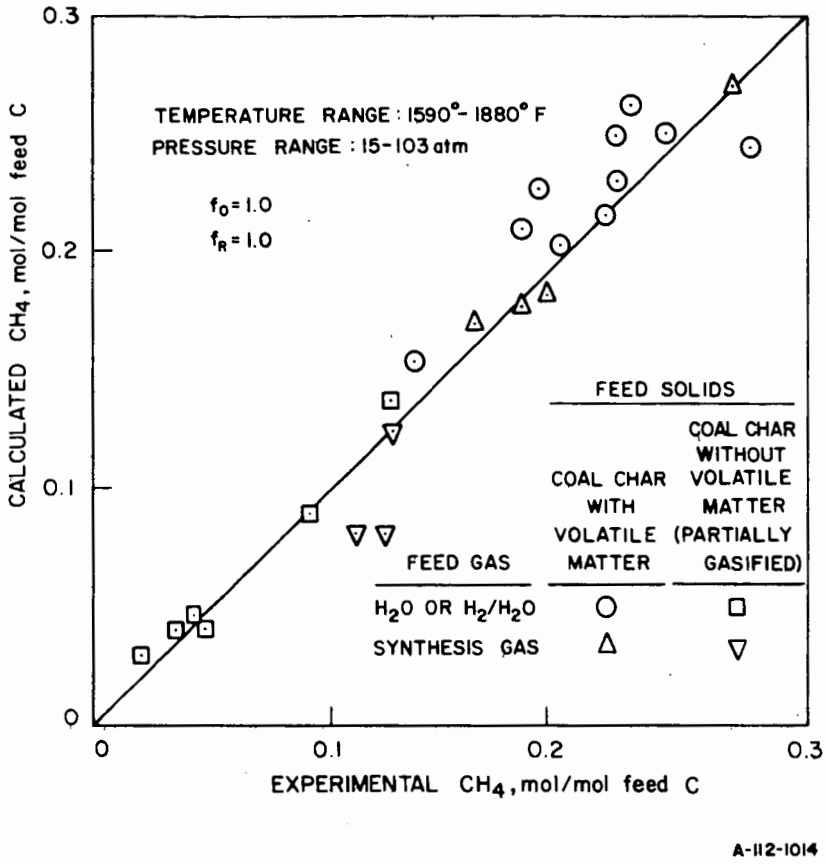

Figure 17. COMPARISON OF EXPERIMENTAL AND CALCULATED INTEGRAL RATES OF METHANE FORMATION FOR GASIFICATION OF AIR-PRETREATED IRELAND MINE COAL CHAR IN 2-, 4-, AND 6-INCH-INSIDE-DIAMETER FLUID-BED REACTORS (IGT Studies)

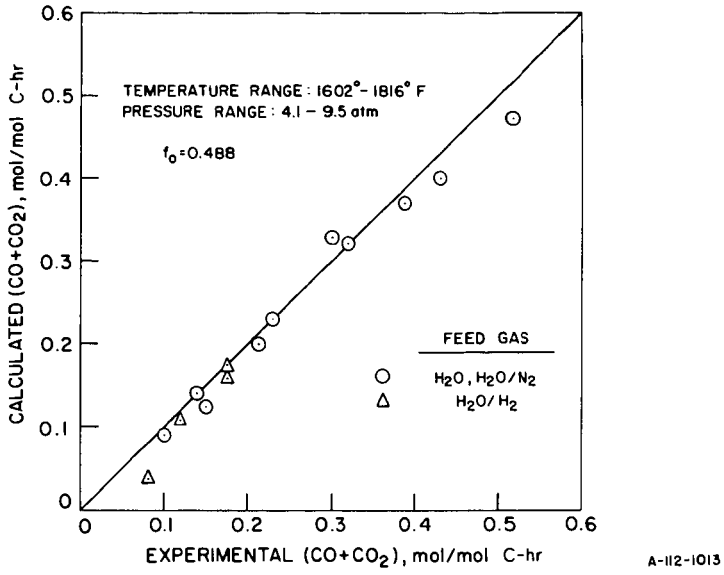

Figure 18. COMPARISON OF EXPERIMENTAL AND CALCULATED INTEGRAL RATES OF CARBON OXIDES FORMATION FOR GASIFICATION OF DISCO CHAR IN A FLUID-BED REACTOR[12]

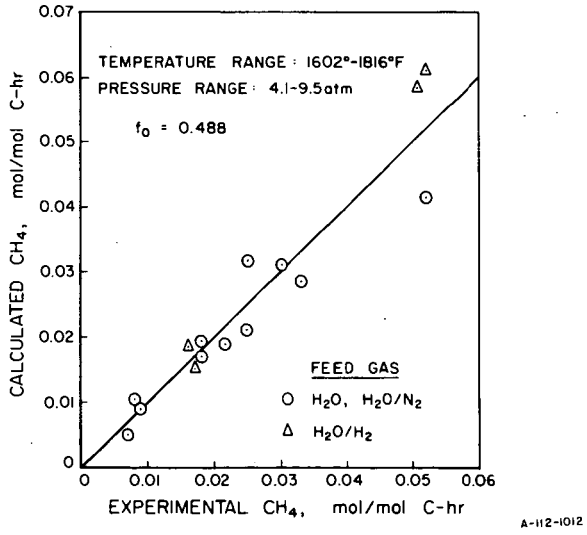

Figure 19. COMPARISON OF EXPERIMENTAL AND CALCULATED INTEGRAL RATES OF METHANE FORMATION FOR GASIFICATION OF DISCO CHAR IN A FLUID-BED REACTOR[12]

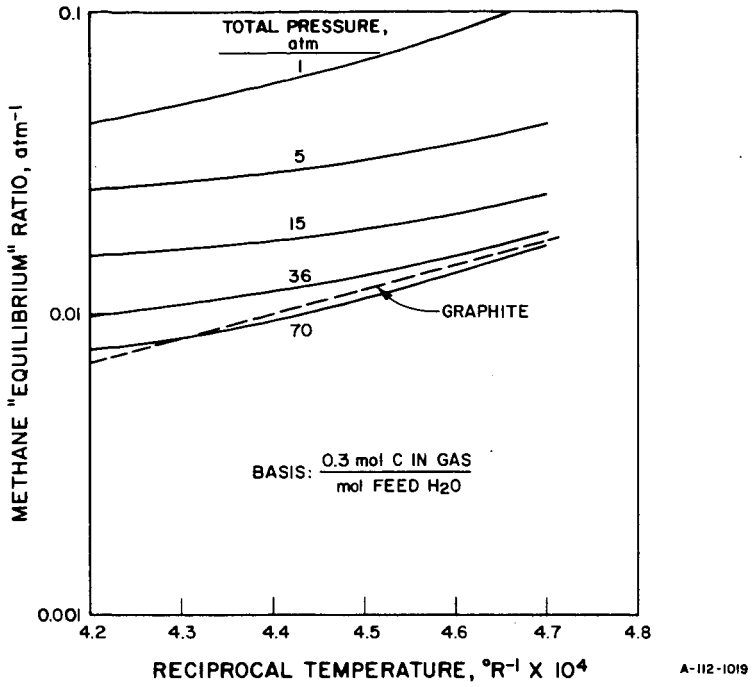

Figure 20. CALCULATED VARIATIONS OF THE METHANE "EQUILIBRIUM" RATIO ($P_{CH_4}/P^2_{H_2}$) FOR GASIFICATION OF CARBON WITH STEAM IN A BACKMIXED REACTOR

reaction exists. The partial pressure dependencies defined in the correlations developed are such, however, that, at sufficiently high hydrogen partial pressures, Reaction II dominates and equilibrium for this reaction is approached.

The qualitative trends exhibited in Figure 20 and even the magnitudes of these trends bear a striking resemblance to a similar plot given by Squires[15] to correlate the activities of coals and chars for equilibrium in the char-hydrogen-methane system with temperature and pressure.

SUMMARY OF NOTATION

A = nongasifiable matter in feed coal char (including ash and some sulfur), g/g feed coal char

C_b = base carbon in coal char at an intermediate gasification level, g/g feed coal char

C_b^o = carbon in the fixed carbon fraction of the feed coal char as determined by a proximate analysis, g/g feed coal char

C_t^o = total carbon in the feed coal char as determined by an ultimate analysis, g/g feed coal char

C_v = volatile carbon in feed coal, g/g feed coal char

f_o = relative reactivity factor for low-rate gasification dependent on the particular carbonaceous solid

f_L = relative reactivity factor for low-rate gasification dependent on the particular carbonaceous solid and pretreatment temperature

f_R = relative reactivity factor for rapid-rate methane formation, dependent on the particular carbonaceous solid

k_T = overall rate constant for low-rate gasification, min^{-1}

$k_{2(T)}$, $k_{3(T)}$ = rate constants, min^{-1}

k_I, k_{II}, k_{III} = rate constants for Reactions I, II, and III, min^{-1}

K_I^E, K_{II}^E, K_{III}^E = equilibrium constants for Reactions I, II, and III considering carbon as graphite

N_{A_o} = concentration of species A_o at any time, mol/mol base carbon

$N_{A_o}^o$ = initial concentration of species A_o, mol/mol base carbon

N_{A_*} = concentration of species A_* at any time, mol/mol base carbon

P_{H_2}, P_{H_2O}, P_{CO}, P_{CO_2}, P_{CH_4} = partial pressures of H_2, H_2O, CO, CO_2 and CH_4, atm

t = time, min

T = reaction temperature, °R

T_o = pretreatment temperature, °R

V = volatile matter in feed coal char (including moisture), g/g feed coal char

W_o = weight of feed coal char, g

ΔW = weight loss of coal char during gasification, g

X = total base carbon conversion fraction

X_R = base carbon conversion fraction after reaction in rapid-rate methane formation stage is completed

Greek Symbols

α = kinetic parameter, dependent on gas composition and pressure

β = $k_3(T)/k_2(T)$ ratio

γ = noncarbon matter evolved along with base carbon, g/g base carbon evolved

ACKNOWLEDGMENT

The work conducted in this study was sponsored by the American Gas Association, the U. S. Department of the Interior, Office of Coal Research, and the Fuel Gas Associates. The author wishes to express his appreciation for the permission of these groups to publish this paper.

REFERENCES CITED

1. Birch, T. J., Hall, K. R. and Urie, R. W., "Gasification of Brown Coal With Hydrogen in a Continuous Fluidized-Bed Reactor," J. Inst. Fuel 33, 422-35 (1960) September.

2. Blackwood, J. D., "The Reaction of Carbon With Hydrogen at High Pressure," Aust. J. Chem. 12, 14-28 (1959) February.

3. Blackwood, J. D. and McCarthy, D. J., "The Mechanism of Hydrogenation of Coal to Methane," Aust. J. Chem. 19, 797-813 (1966) May.

4. Blackwood, J. D. and McGrory, F., "The Carbon-Steam Reaction at High Pressure," Aust. J. Chem. 11, 16-33 (1958) February.

5. Curran, G. and Gorin, E., "Phase II, Bench-Scale Research on CSG Process — Laboratory Physicochemical Studies," U. S. Office of Coal Research R&D Report No. 16, Interim Report No. 3, Book 2, Washington, D.C.: U.S. Government Printing Office, 1970.

6. Eddinger, R. T., Freidman, L. D. and Rau, A., "Devolatilization of Coal in a Transport Reactor," Fuel 19, 245-52 (1966).

7. Feldmann, H. F., et al., "Reaction Model for Bituminous Coal Hydrogasification in a Dilute Phase." Paper presented at the 160th National Meeting of the American Chemical Society, Division of Petroleum Chemistry, Chicago, September 13-18, 1970.

8. Goring, G. E., et al., "Kinetics of Carbon Gasification by Steam: Effect of High-Temperature Pretreatment on Reactivity of Low-Temperature Char to Steam and Carbon Dioxide," Ind. Eng. Chem. 44, 1051-57 (1952) May.

9. Goring, G. E., et al., "Kinetics of Carbon Gasification by Steam: Mechanism of Interaction of Low-Temperature Char and Steam-Hydrogen Mixtures at 1600°F," Ind. Eng. Chem. 45, 2586-91 (1953) November.

10. Hiteshue, R. W., Friedman, S. and Madden, R., "Hydrogasification of a High-Volatile A Bituminous Coal," U.S. Bur. Mines Rep. Invest. No. 6376 (1964).

11. Kimber, G. M. and Gray, M. D., "Rapid Devolatilization of Small Coal Particles," J. Combust. Flame Inst. 2, 360-62 (1967) August.

12. May, W. G., Mueller, R. H. and Sweetser, S. B., "Carbon-Steam Reaction Kinetics From Pilot Plant Data," Ind. Eng. Chem. 50, 1289-96 (1958) September.

13. Mosely, F. and Patterson, D., "The Rapid High-Temperature Hydrogenation of Coal Chars. Part 2: Hydrogen Pressures up to 1000 Atmospheres," J. Inst. Fuel 38, 378-91 (1965) September.

14. Pyrcioch, E. J., Feldkirchner, H. L., Tsaros, C. L., Johnson, J. L., Bair, W. G., Lee, B. S., Schora, F. C., Huebler, J. and Linden, H. R., "Production of Pipeline Gas by Hydrogasification of Coal," IGT Res. Bull. No. 39. Chicago, November 1972.

15. Squires, A. M., "Steam-Oxygen Gasification of Fine Sizes of Coal in Fluidized Bed at Elevated Pressure. I. Reaction of Carbon With Hydrogen," Trans. Inst. Chem. Eng. 39, 3-9 (1961); II. "Reaction of Carbon With Steam," ibid., 10-15 (1961); III. "Relation of Integral to Differential Rates: Effect of Carbon Level on Gasification Rate and Role of the Shift Reaction," ibid., 16-21 (1961).

16. Wen, C. Y. and Huebler, J., "Kinetic Study of Coal-Char Hydrogasification — Rapid Initial Reaction," Ind. Eng. Chem. Process Des. Dev. 4, 147-54 (1965) April.

17. Zahradnick, R. I. and Glenn, R. A., "Direct Methanation of Coal." Paper presented at 158th National Meeting of the American Chemical Society, Division of Fuel Chemistry, New York, September 7-12, 1969.

18. Zielke, C. W. and Gorin, E., "Kinetics of Carbon Gasification. Interaction of Hydrogen With Low-Temperature Char at 1500° to 1700°F," Ind. Eng. Chem. 47, 820-25 (1955) April.

19. Zielke, C. W. and Gorin, E., "Kinetics of Carbon Gasification," Ind. Eng. Chem. 49, 396-403 (1957) March.